UNIVERSITÉ DE STRASBOURG

ÉCOLE DOCTORALE DES SCIENCES DE LA VIE ET DE LA SANTÉ

IGBMC - CNRS UMR 7104 - Inserm U 964

THÈSE présentée par :

Alexis HUBAUD

soutenue le : **27 juin 2016**

pour obtenir le grade de : **Docteur de l'université de Strasbourg**

Discipline/ Spécialité : Biologie du Développement

Dynamique de la signalisation cellulaire au cours de la segmentation des Vertébrés

THÈSE dirigée par :
   Mr. POURQUIÉ Olivier   Professeur, Université de Strasbourg

RAPPORTEURS :
   Mr. AULEHLA Alexander   Professeur, EMBL Heidelberg
   Mr. PAUL François   Professeur, McGill University

AUTRES MEMBRES DU JURY :
   Mme. GUEVORKIAN Karine   Chargée de Recherche, Université de Strasbourg
   Mr. GREGOR Thomas   Professeur, Princeton University

ACKNOWLEDGMENTS

TABLE OF CONTENTS

LIST OF FIGURES

Introduction

Chapter I

Chapter II

Chapter III

Chapter IV

INTRODUCTION

The general aim of this thesis is to understand how an embryonic tissue, the paraxial mesoderm, becomes patterned during development, and which mechanisms orchestrate its segmentation in units called somites. This introduction is thus organized as follows: first we give a general overview of the early Vertebrate development to put into context the patterning of the paraxial mesoderm; then, we present the process of somitogenesis, one of the major event organizing the paraxial mesoderm; we next examine how this segmental patterning is achieved by presenting the oscillatory dynamics and the signaling gradients at work in the paraxial mesoderm; we then present the molecular basis of this segmentation by introducing the mechanism that link these oscillations and signaling gradients to the formation of segments; last, we summarize the different models explaining the segmentation of the paraxial mesoderm.

# 1.	Overview of Vertebrate Development

The development of Vertebrates starts with the fertilization, where the female and male gametes fuse to give rise to a zygote. Following this event, the zygote undergoes a series of cell divisions leading to the formation of a morula, then blastula. The embryo geometry and type of cleavages depend on the species: in chicken (meroblastic cleavage), cells on top of the yolk actively divide and form a blastodisc, while in mice (holoblastic cleavage), the divisions are not impeded by the yolk and form an inner cell mass. This structure, analogous to the blastodisc, lies on a large fluid cavity called blastocoel and is surrounded by trophectodermal cells. The cleavage pattern, the disposition of the embryo and the distribution of maternal determinants contribute to its initial patterning and to the determination of the embryonic axes.

Later, complex morphogenetic movements reorganize the embryos and set the blueprint for the final organization of tissues. This event called gastrulation is central to the formation of the Vertebrate body plan. It ends with a multilayered organization of the embryo with three primary germ layers: the ectoderm outside of the embryo, the endoderm inside of the embryo, and the mesoderm in-between. In chicken and mice, cells involute at the level of the embryo midline in a furrow called the primitive streak to form the endoderm, and then the mesoderm. This process continues later at the level of a structure called the tailbud, which can be considered as the continuation of the primitive streak and which contains the progenitors forming the most posterior parts of the mesoderm and neurectoderm. Concomitantly to this involution process, the embryo elongates at its posterior end by a combination of mechanisms involving convergent extension and tissue reorganization.

At this stage, classically referred to as the neurulation, the germ layers start to become organized into different tissues and organs: the ectoderm gives rise to the central nervous system, epidermis, sense organs and neural crests; the endoderm differentiates into organs of the digestive and respiratory tracts; from the mesoderm arise notably the skeleton, muscles, blood vessels, heart and dermis.

The mesoderm lying on both sides of the neural tube, the paraxial mesoderm, first appears as a mesenchyme called the presomitic mesoderm (PSM), which becomes progressively segmented at its anterior end into epithelial blocks called somites. Somites give rise to a variety of tissues: vertebrae, back dermis, skeletal muscles (Christ et al., 2007), endothelial cells (Nguyen et al., 2014), tendons (Brent et al., 2003, Stephenson et al., 2012). As the elongation of the anteroposterior axis ends, the paraxial mesoderm becomes entirely segmented in somites (except the anterior head mesoderm and the very posterior part (Tenin et al., 2010)). This segmentation process is not only at the basis of the metamerism in Vertebrates, but also of the organization of other tissues, such as neural crests and blood vessels (Figure 1). Indeed, the patterning of the presomitic mesoderm provides positional

information organizing neural and vascular structures, e.g. blood vessels will be formed between segments. Therefore the patterning of the presomitic mesoderm is central to the organization of the body axis of Vertebrates.
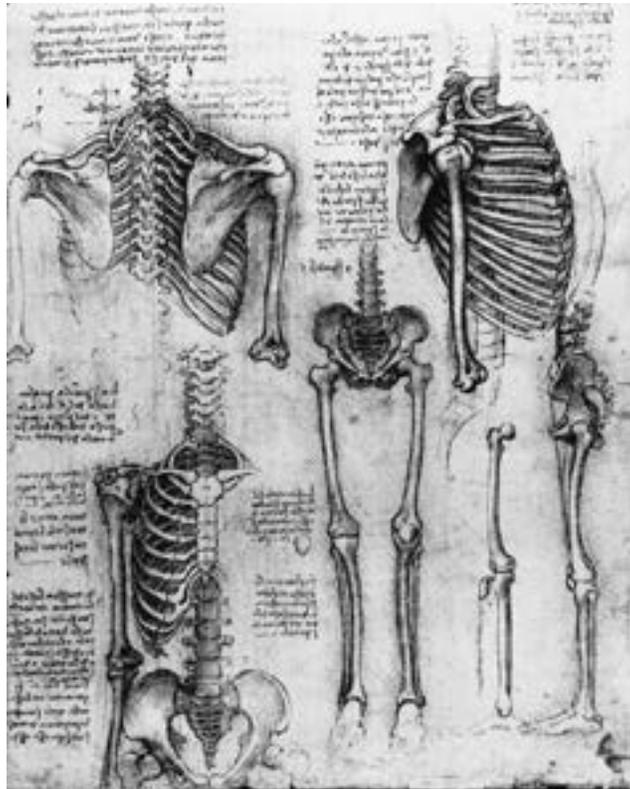
Figure 1 - Segmentation of the Vertebrate body
Leonardo Da Vinci

2. Development of the presomitic mesoderm

Early steps of mesoderm specification

The specification of the presomitic mesoderm occurs progressively during the first steps of Vertebrate development. We present these different events in the mice embryos, and while the earliest patterning events vary between Vertebrates, the main signaling pathways involved are presumably conserved between species.

The zygote is first specified into two cell types (16/32-cell stage): the inner cell mass (ICM) and the trophectoderm (TE) (Stephenson et al 2012) (Figure 2A). The former will give rise to the epiblast and primitive endoderm, while the latter will form precursors of the trophoblast, the extraembryonic ectoderm (ExE) and the ectoplacental cone. How this first cell decision is made is not fully understood, and different models have been proposed to account for this event (mechanical "inside-out" model, pre-patterning model, cell polarity model). Notably, a model of self-organization of the morula proposes that both physical cues (e.g. cell adhesion) and signaling pathways (e.g. cell polarity, maternal determinants) locally interact and control the symmetry-breaking of the embryo (Wennekamp et al., 2013).

The signaling circuit underlying this decision involves the Hippo pathway that biases the activation of antagonistic ICM or TE gene networks. Inhibition of the Hippo pathway in the TE leads to the expression of the TE determinant *Cdx2* through the Yap/Tead transcription factors, while the activation of this pathway in the ICM precludes the nuclear translocation of Yap. This results in the bifurcation of TE and ICM fates, respectively induced by the transcription factors Cdx2 and Oct4. As we will discuss later, cells from the inner cell mass can be derived and stably cultured *in vitro* into embryonic stem cells (mESC).

At stage E3.5-E4, ICM cells are further segregated in epiblast and primitive endoderm (PE - also known as hypoblast), which gives rise to the adult tissues, and the visceral and parietal yolk sacs respectively (Hermitte and Chazaud, 2014, Stephenson et al., 2012) (Figure 2A). First, cells in the ICM express a salt-and-pepper pattern of epiblast (Nanog) and PE (Gata6) markers; later on, PE cells become localized next to the blastocoel. How this cell segregation occurs is poorly understood, but the Fgf/ERK pathway is central to this cell fate decision, as it promotes the specification of the ICM cells into primitive endoderm. As for the ICM vs. TE decision, antagonistic loops between transcription factors (Gata6/Nanog) interacting with a signaling pathway (Fgf) seems to mediate this cell fate decision.

At the stage E5.5, the epiblast is patterned between the three germ layers: ectoderm, mesoderm, and endoderm (Arnold and Robertson, 2009). This is mainly mediated by the position of epiblast cells
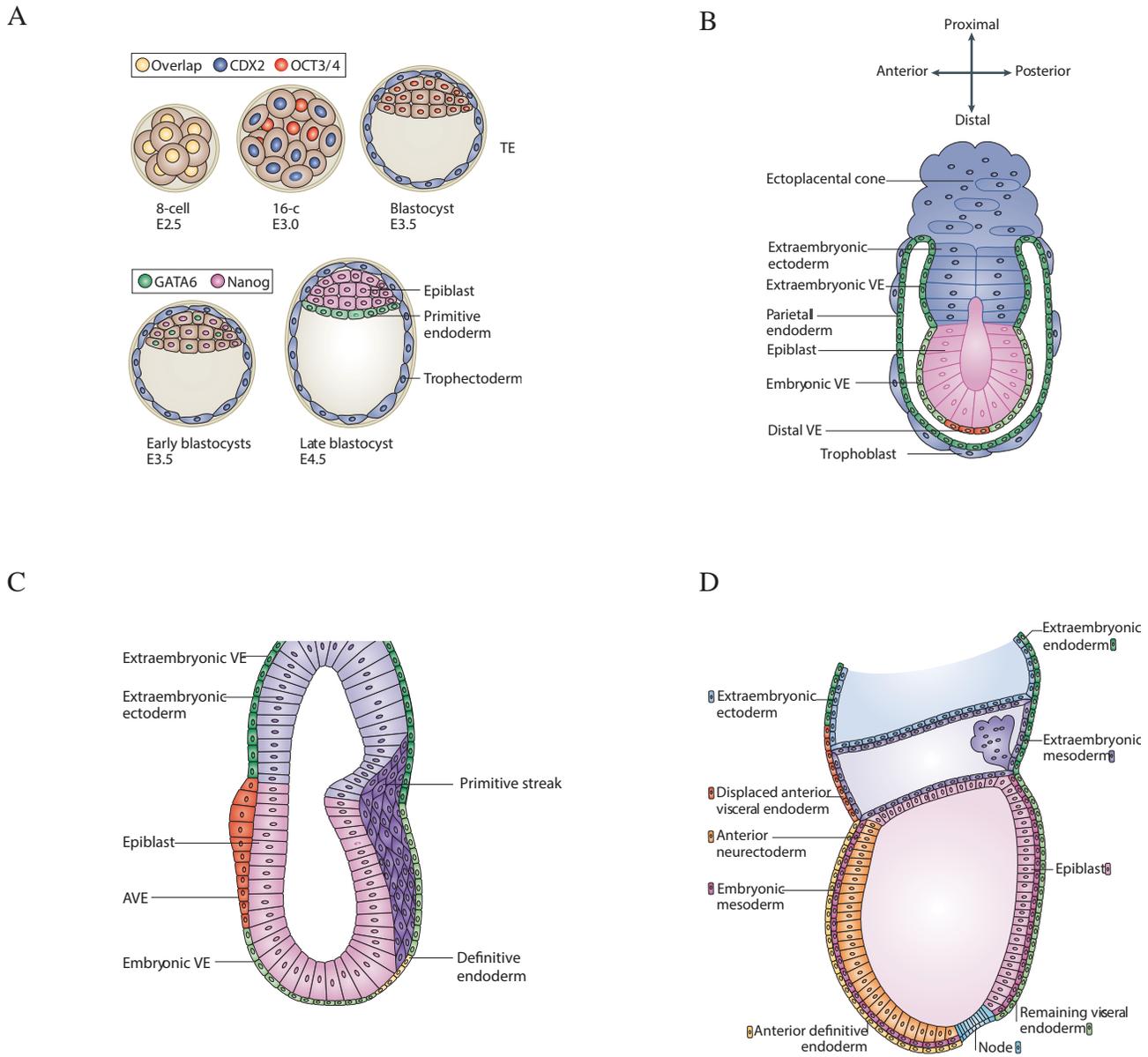
Figure 2 - Early steps of mouse development

A. The blastula is segregated between the inner cell mass and the trophectoderm (TE) under the respective control of Oct3/4 and Cdx2. Later, the inner cell mass is further divided between the epiblast and the primitive endoderm.

B. The epiblast is patterned through two feeedback loops leading to a gradient of Nodal signaling: the secretion of Wnt/Nodal inhibitors by the distal visceral endoderm (VE) and through the amplification of Nodal signaling by the extraembryonic ectoderm.

C. The asymmetries in Wnt and Nodal signaling, notably mediated by the migration of the anterior visceral endoderm (AVE), lead to the formation of the primitive streak and the specification of the germ layers.

D. During gastrulation, epiblast cells ingress and form three layers: the definitive endoderm, the embryonic mesoderm and the neurectoderm.

Modified from Arnold and Robertson, 2009

within the embryo: at this stage, the epiblast is located at the distal end of the embryo, while the ExE is located at its proximal end (with respect to the uterine mesometrium) (Figure 2B). A cavity elongates along the proximo-distal axis within the epiblast ("egg cylinder" stage), and the visceral endoderm, a derivative of the PE, surrounds both the epiblast and the ExE. At the distal tip of the PE, a specific group of cells is formed, called the distal visceral endoderm (DVE), which is crucial for the antero-posterior patterning of the embryo. How this population is induced is not clearly understood, but it could be mediated by a mechanical compression caused by the elongation of the cylinder (Hiramatsu et al., 2013). This region secretes inhibitors of the Nodal (Lefty1) and Wnt (Cer1, Dkk1) pathways. Conversely, at the proximal side of the epiblast, Nodal signaling is enhanced by the expression of furins in the ExE that are necessary for the full processing of the ligand (conversion of pro-Nodal in active Nodal), and by a secondary feedback loop involving BMP and Wnt3. This results in a gradient of Nodal and Wnt activities along the proximo-distal axis. The latter is converted into an antero-posterior polarity, when the DVE cells migrate to the prospective anterior side of the embryo. This migration leads to the formation of the AVE (Takaoka et al., 2011), which secretes Nodal and Wnt inhibitors. The epiblast cells next to the AVE will thus differentiate into the neurectoderm, while cells at the opposite side of the egg cylinder will form the primitive streak and become mesodermal and endodermal cells (Figure 2C).

Following the specification of the mesoderm and endoderm, the BMP and Nodal pathways will pattern the primitive streak and specify its different cell types at the stage E6.5 (Figure 2D). Whether a common mesendodermal progenitor population exists as proposed in *Xenopus* and *D.rerio (*Schier and Talbot, 2005) remains to be tested, but the early segregation of *T* and *FoxA2* domains (Burtscher and Lickert, 2009) and the low co-labeling of endoderm and mesoderm in lineage tracing experiments (Tzouanacou et al., 2009) would argue against such idea. It has been shown that the graded activity of the Nodal pathway controls the axial identity of the mesendoderm: high levels of Nodal signaling induce the definitive endoderm and the prechordal plate (head mesoderm), intermediate levels trigger the specification of the node, and low levels lead to the formation of the lateral, intermediate and paraxial mesoderm (Vincent et al., 2003, Dunn et al., 2004). BMP signaling is also involved in the mesoderm patterning, as the loss of BMP signaling in the epiblast leads to the expansion of the paraxial mesoderm at the expense of the lateral mesoderm (Miura et al., 2006).

In the primitive streak, cells undergo an epithelial-to-mesenchymal transition that leads to their delamination and their migration (Figure 3A). By this process, the paraxial mesoderm forms two bilateral stripes of mesenchymal cells on both sides of the neural tube. Later, as the primitive streak regresses, a new structure called the tailbud is formed at the posterior tip of the paraxial mesoderm. While an exact definition is lacking, it could be considered as the "*an anatomical protrusion becoming distinct at the posterior end of the embryo after the completion of gastrulation*" (Beck, 2015); functionally, this region contains the progenitors of the most posterior tissues. The formation

A
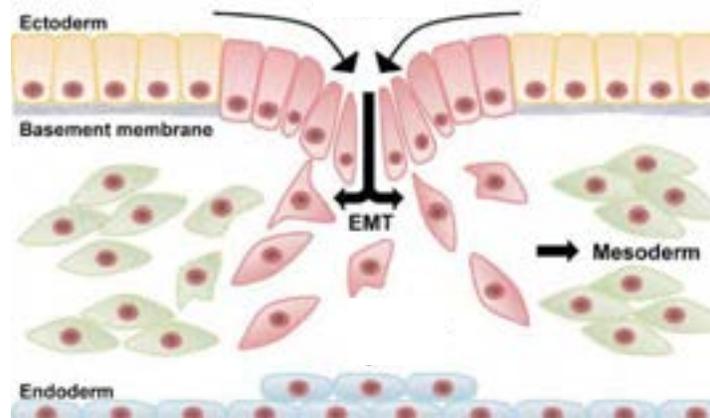
B
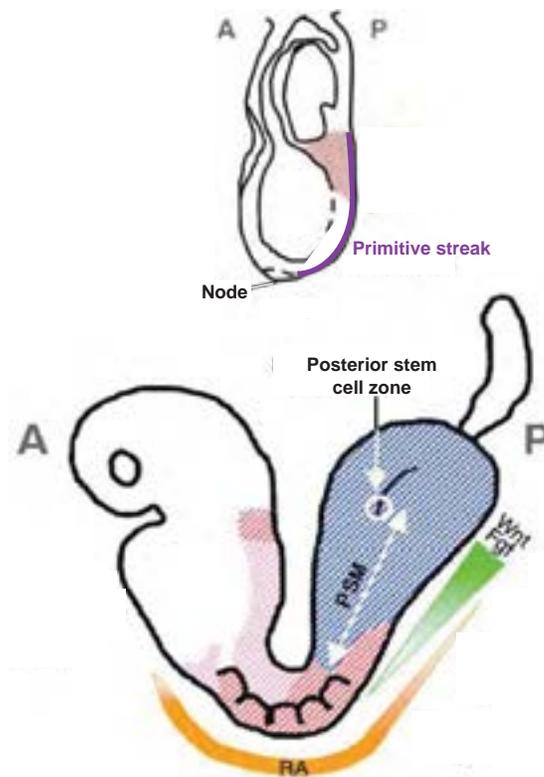
Figure 3 - PSM progenitors in the mouse embryo

A. Scheme of the epithelial-mesenchymal transition (EMT) occuring at the level of the primitive streak.

B. (*Top*) At early somite stages, the PSM is mainly fueled by the addition of cells (red region) at the primitive streak (purple). (*Bottom*) At later somite stages, the more posterior PSM tissues (in blue) come from a pool of stem cells located in the tailbud and maintained by Fgf/Wnt signaling.

Modified from Rangel et al. (2012); Deschamps and Van Nes (2005)

of the posterior tissues is considered as a continuation of the early gastrulation events because of the continuity in gene expression, in cell movements and the existence of discrete fates within the tailbud (similarly to the regionalization of the primitive streak and by opposition to a previous hypothesis postulating the existence of a blastema) (Gont et al., 1993, Catala et al., 1995, Wilson and Beddington, 1996, Knezevic et al., 1998). At stage E8.5, the progenitors at the midline primitive streak only differentiate into mesodermal tissues, while progenitors located at the node-streak border and caudal lateral epiblasts at E8.5 can give rise to both paraxial mesoderm and neural tube (neuromesodermal progenitors) (Figure 3B). At stage E10.5, this axial stem cell population is restricted to a specific region of the tailbud called the chordo-neural hinge (Figure 3B). Evidence for a neuromesodermal progenitor also comes from cell labeling experiments: Tzouanacou and colleagues showed the labeling of both mesodermal and neurectodermal cells, suggesting the existence of such multipotent progenitor (Tzouanacou et al., 2009). Conversely, the neural-restricted or mesodermal-restricted progenitors give rise to a shorter clonal population, indicating that those progenitors are transient and committed. By examining the contribution of the neuro-mesodermal progenitors at different axial levels, the authors proposed that this population is rearranged during development as the progenitors pool of early stages (until the anterior trunk) contributes less to more posterior tissues. This suggests that the modalities of paraxial mesoderm differentiation change during mouse development. Others have postulated the existence of a progenitor population common to the paraxial, intermediate and lateral mesoderms (Stern et al., 1988), but this likely reflects the labeling of mixed cells.

Regulators of the PSM fate

We now examine the different genetic determinants of this presomitic state.

T/Brachyury

T/Brachyury is a conserved T-box transcription factor marking the primitive streak in Vertebrates, and later expressed in the tailbud and in the notochord (Figure 4A). It is a central factor in the specification of the blastopore and in gastrulation in Animals (Sebe-Pedros et al., 2013). Mice mutants for the gene *T* (*short-tailed* mutant) have defects both in notochord and paraxial mesoderm formation starting at stage E8.5 (Chesley, 1935). Before this stage, mutant embryos are undistinguishable from their control littermate and still produce paraxial mesoderm (Chapman et al., 1996). The observed phenotype is likely caused by a misspecification of cells toward the neural lineage as the number of neurectodermal cells increase in the *short-tailed* mutant and ectopic neural structures are formed (Yanagisawa et al., 1981, Yamaguchi et al., 1999). This suggests that T is

involved in the balance between neural and mesodermal fates. Accordingly, the mouse line expressing the recombinase Cre using a T enhancer (T-Cre) shows labeling of both notochord, paraxial mesoderm and neural tube (Perantoni et al., 2005) starting at E9.0 suggesting that *T* is expressed in the neuro-mesodernal progenitors (Henrique et al., 2015). Interestingly, no labeling was observed in the neural tube before this stage, further indicating that the molecular control of the paraxial mesoderm state is remodeled during development. Defects in cell migration are also observed as mutant cells tend to stay in the primitive streak (Wilson et al., 1993). Indeed, the dose of T controls the exit of cell from the primitive streak: mutant for *T* have a short tail and stops elongation (Chesley, 1935, Herrmann et al., 1990), while increasing the dose of T induces a premature migration from the streak (Wilson and Beddington, 1997). How the defects in cell migration are related to the defects in patterning remain to be studied. However, the fact that the most anterior axial and paraxial mesoderm are still formed in *T* mutants (as evidenced by *Mox1* and *T* expression at early stages - (Herrmann, 1991, Conlon et al., 1995a)) suggests that T is not strictly required for the induction of the paraxial mesoderm fate, but is rather necessary for the maintenance of neuromesodermal progenitors and for their mesodermal differentiation.

Wnt signaling

The canonical Wnt pathway is one of the major pathways involved in mesoderm differentiation. Briefly, the binding of the ligand to the receptor Frizzled and its coreceptor LRP5/6 inactivates the β-catenin degradation complex. This leads to the stabilization and nuclear translocation of β-catenin, and ultimately to the induction of target genes through interactions with Tcf/Lef transcription factors. In the PSM, the ligand *Wnt3a* is restricted to the tailbud (Figure 4B) and *Wnt3a* mutants display a loss of paraxial mesoderm tissues and axis truncations. Indeed, deletion of *Wnt3a* biases the differentiation toward the neural lineage at the expense of the notochord and paraxial mesoderm, leading to the formation of three neural tubes, and depletes cells in the tailbud (Takada et al., 1994, Yoshikawa et al., 1997, Yamaguchi et al., 1999, Nowotschin et al., 2012, Greco et al., 1996). Loss of Wnt3a leads to the disappearance of neuromesodermal progenitors (marked by the co-expression of *T* and *Sox2*), suggesting that Wnt signaling does not induce mesodermal fate *per se*, but rather blocks the biased differentiation of neuromesodermal progenitors towards the neural fate (Garriock et al., 2015). Accordingly, overactivation of the canonical Wnt pathway by use of a non-degradable β-catenin is permissive for the specification and maintenance of neural tissues and rather increases the number of neural progenitors (Garriock et al., 2015).

Compound mutants for the downstream effectors of Wnt signaling Lef1 and Tcf1 leads to similar defects in paraxial mesoderm specification (depletion of mesodermal tissues, ectopic neural tubes) (Galceran et al., 1999) and expression of an active form of Lef1 can rescue the *Wnt3a* mutation (Galceran et al., 2001). Furthermore, it has been shown that *T* is a target of Wnt3a/Tcf1 (Yamaguchi
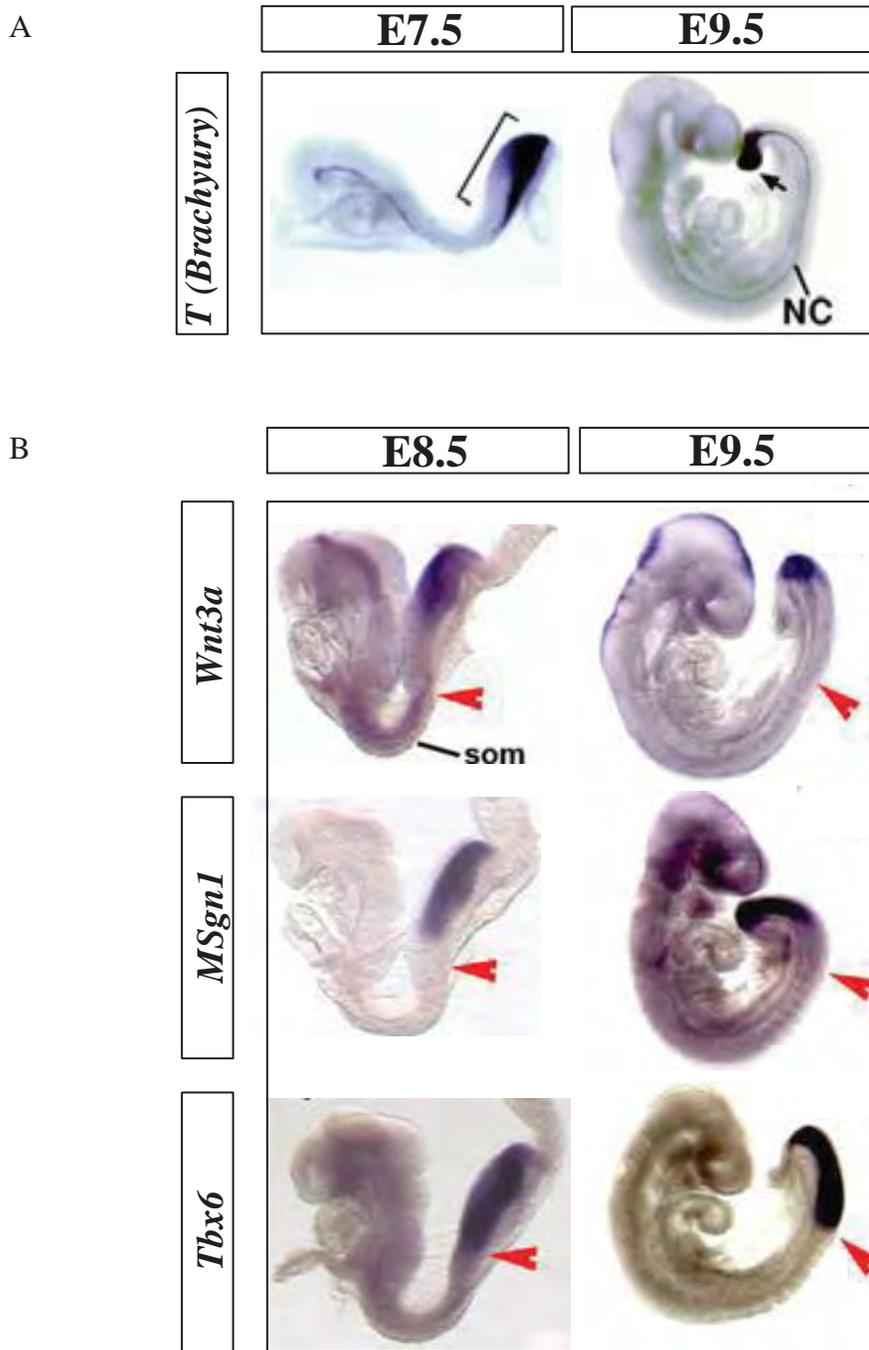
Figure 4 - Expression of the transcriptional regulators of the PSM state

A. *T (Brachyury)* is expressed in the primitive streak, in the nascent mesoderm and in the notochord (NC)

B. *Wnt3a* is expressed in the primitive streak and in the most posterior part of the paraxial mesoderm, while *Tbx6* and *Msgn1* are expressed in the paraxial mesoderm and extend more anteriorly. The red arrows mark the position of the last somite formed.

Modified from Galceran et al. (2001) and Nowotschin et al. (2012)

et al., 1999) and that Lef1 is required for the maintenance but not the initiation of *T* expression (Galceran et al., 2001). Wnt signaling also promotes the expression of neural determinants: in chicken and mouse, the regulatory region for *Sox2* contains an enhancer (N1 enhancer) with Lef1 binding sites (Takemoto et al., 2011, Takemoto et al., 2006); deletion of this enhancer in mouse leads to the loss of *Sox2* expression in the caudal epiblast where neuromesodermal progenitors reside (Takemoto et al., 2011). Together this points toward a signaling axis composed of Wnt3a/Tcf-Lef/T that is required for the maintenance of neuromesodermal progenitors and thus for the formation of paraxial mesoderm by maintaining a balance between neural and mesodermal fates. Interestingly, the presence of a posterior growth center expressing *Wnt* and *T* seems a common feature among Bilaterians (Martin and Kimelman, 2009, Petersen and Reddien, 2009).

Fgf signaling

Fgf signaling is another major pathway involved in the specification of the paraxial mesoderm. Briefly, binding of dimers of Fgf ligands to the Fgf receptor leads to the transphosphorylation of the receptor intracellular domain. This leads to the activation of several downstream pathways, such as the ERK (also known as MAPK) pathway, the PI3K pathway or the PLCγ pathway (Dorey and Amaya, 2010). In Vertebrates, loss of Fgf signaling affects the specification of the paraxial mesoderm and causes strong defects in gastrulation (Deng et al., 1994, Ciruna et al., 1997, Sun et al., 1999).

While the mesoderm is still specified, patterning defects are observed in Fgf mutants. This is partly due to its regulation of *T* (Naiche et al., 2011). Indeed, deletion of FgfR1 phenocopies the loss of T function with accumulation of cells in the primitive streak and with an excessive neural differentiation leading to the formation of ectopic neural tubes (Ciruna et al., 1997). Fgf signaling also induces expression of *Sox2* in the caudal epiblast through the N1 enhancer in synergy with Wnt signaling (Takemoto et al., 2006, Takemoto et al., 2011) suggesting that it maintains a balance between mesodermal and neural fates. Furthermore, Fgf signaling is required for the expression of other PSM regulators, such as *T, Tbx6* and *Msgn1* (Wahl et al., 2007, Naiche et al., 2011).

Tbx6

Tbx6 is a T-box transcription factor, first expressed in the primitive streak (Chapman et al., 1996), and then restricted to the posterior paraxial mesoderm and intermediate mesoderm (Figure 4B - J.Chal, M.Oginuma, personal communication). *Tbx6* is expressed in mesodermal cells that have already ingressed but not in the neuromesodermal progenitors (Garriock et al., 2015). Accordingly, expression of CreERT2 under the control of the regulatory sequences of *Tbx6* in mouse does not label the neural tube (Peter Lopez and Fan, 2012). Mutation of *Tbx6* leads to the loss of paraxial mesoderm and the formation of three neural tubes (Chapman et al., 1996, Nowotschin et al., 2012).

As for the *Wnt3a* and *T* mutants, the most anterior part of the paraxial mesoderm is still formed and segmented, but contrary to these mutants, the notochord is not affected and the tailbud is enlarged (Nowotschin et al., 2012). *Tbx6* expression is not affected by the loss of T at early stages, but disappears in E8.5 *T* mutants, suggesting that T is required for the maintenance of *Tbx6* expression (Chapman et al., 1996). The ectopic formation of neural tissues is rescued by the deletion of *Sox2* expression in the caudal epiblast (deletion of the enhancer N1 - (Takemoto et al., 2011)), further supporting the model of a balance between mesodermal and neurectodermal fate. However, upon suppression of *Sox2* and *Tbx6*, the fate of this paraxial tissue remains elusive as it does not express paraxial (*Pax3, Mox1*), intermediate (*Pax2*), lateral (*Foxf1*) mesoderm markers, nor endoderm marker (*Foxa2*), nor neural markers (*Sox1, Pax6, Pax3*) (Takemoto et al., 2011). As *Wnt3a* is upregulated in the paraxial mesoderm compartment of *Tbx6* mutants, Takemoto and colleagues proposed a model where the excess of Wnt signaling leads to an overactivation of *Sox2* and neural differentiation of the bipotent progenitors (Takemoto et al., 2011). Conversely, inhibition of BMP signaling in the neuromesodermal progenitors would dampen the expression of *Sox2* in the caudal epiblast and prevents neural differentiation. However, this model does not explain why overactivation of the Wnt pathway in the paraxial mesoderm does not induce a neural fate (Garriock et al., 2015) and why loss of Wnt signaling in *Wnt3a* or *Tcf1/Lef1* mutants leads to ectopic neural tubes and does not expand the mesodermal compartment (Yamaguchi et al., 1999, Galceran et al., 2001, Nowotschin et al., 2012). While the decision between neural and paraxial mesoderm is not fully understood, Tbx6 appears to have two effects in this process: repression of the neural specification by the indirect restriction of *Sox2* and induction of the paraxial mesoderm fate (Takemoto et al., 2011, Nowotschin et al., 2012). Evolutionary, expression of *Tbx6* in the posterior paraxial mesoderm is conserved in the cephalochordate amphioxus (*Branchiostoma lanceolatum*) (Belgacem et al., 2011), in the ascidians *Halocynthia roretzi* (Yasuo et al., 1996) and *Ciona intestinalis* (Kugler et al., 2010) suggesting a conserved role in the specification of paraxial tissues in Chordates.

Mesogenin1 (Msgn1)

Msgn1 is a bHLH transcription factor that is first expressed in the primitive streak, and then in the tailbud and paraxial mesoderm (Yoon and Wold, 2000, Nowotschin et al., 2012) (Figure 4B). *Msgn1* is a direct target of Tbx6 and of the Wnt signaling (Chalamalasetty et al., 2011, Wittler et al., 2007, Aulehla et al., 2008, Dunty et al., 2008). As the previous mutants, *Msgn1* mutants have a normal development for their most anterior tissues, and display a loss of paraxial mesoderm at later stages (Yoon and Wold, 2000, Nowotschin et al., 2012). However, they do not develop an ectopic neural tube and the expression of *Sox2* remains comparable to the wild-type level despite the loss of *Tbx6* expression (Nowotschin et al., 2012). The *Msgn1* mutant also displays an enlarged tailbud as the

Tbx6 mutant, likely resulting from a defect in cell migration. Indeed it was shown that Msgn1 regulates the epithelial-to-mesenchymal transition in the mouse tailbud (Chalamalasetty et al., 2014), and similar findings have been reported in zebrafish (Fior et al., 2012). Interestingly, forced expression of *Msgn1* using a T-Cre driver reduces the allocation of neuromesodermal progenitors toward the neural lineage and increases the number of paraxial mesoderm Tbx6-positive cells (Chalamalasetty et al., 2014). While the notochord is not affected in the *Msgn1* mutant (Nowotschin et al., 2012), forced expression of Msgn1 severely represses the notochord fate (Chalamalasetty et al., 2014). This indicates that Msgn1 is crucial to induce the paraxial mesoderm fate. Furthermore, the forced expression of Msgn1 partially rescues the defects of the *Wnt3a* mutation, as *Meox1* expression is observed in the posterior trunk tissues; however, it did not rescue the the formation of an ectopic neural tube, nor the defects in axis elongation (Chalamalasetty et al., 2014). The latter phenotype could be explained by a depletion of the progenitor pool. Accordingly, in zebrafish, it was proposed that Msgn1 represses the PSM progenitor state, and promotes the determination of the paraxial mesoderm by repressing the *T* homologue (Yabe and Takada, 2012, Fior et al., 2012). In mice, *T* and *Wnt3a* expressions are upregulated in the *Msgn1* mutant, and the tailbud is enlarged, further suggesting that Msgn1 triggers a transition from the progenitor to the paraxial mesoderm state (Nowotschin et al., 2012). The expression of *Msgn1* in the paraxial mesoderm appears to be a Vertebrate invention as its orthologue in *Ciona intestinalis* is only expressed in heart progenitors (Satou et al., 2004). This expression pattern is conserved for the mouse paralogues of *Msgn1- Mesp1* and *Mesp2-* (Kitajima et al., 2000), suggesting that Msgn1 has acquired functions specific to the paraxial mesoderm development in Vertebrates.

Paraxial mesoderm state

Given the multiple interactions between those different components, it is difficult to propose a simple model for the specification of the paraxial mesoderm state. A paramount question is to understand why the paraxial mesoderm mutants (*T*, *Tbx6*, *Wnt3a* and *Msgn1*) are still able to form anterior somites (as well as the double mutants *Wnt3a/Tbx6*, *Wnt3a/Msgn1* and *Msgn1/Tbx6* (Nowotschin et al., 2012)). It is possible that there is a differential regulation between the primitive streak and tailbud stages, which is consistent with the remodeling of the progenitor pools (Tzouanacou et al., 2009). The balance between neural and mesodermal states could evolve between early and late paraxial mesoderm formation, and one could imagine that a single T-box factor (T or Tbx6) is sufficient at early stages to counteract neural fates. At later stages, a clearer picture of paraxial mesoderm specification emerges, where bipotent progenitors are poised by expressing pro-neural (*Sox2*) and pro-mesodermal (*T, Tbx6*) factors in a Wnt-dependent state (Figure 5A). This

A

Epiblast

Non-neural ectoderm

NMP
T⁺Sox2⁺

Other mesodermal tissues; endoderm

Neural tube
Sox2⁺ Tbx6⁻

Paraxial mesoderm
Sox2⁻ Tbx6⁺

B
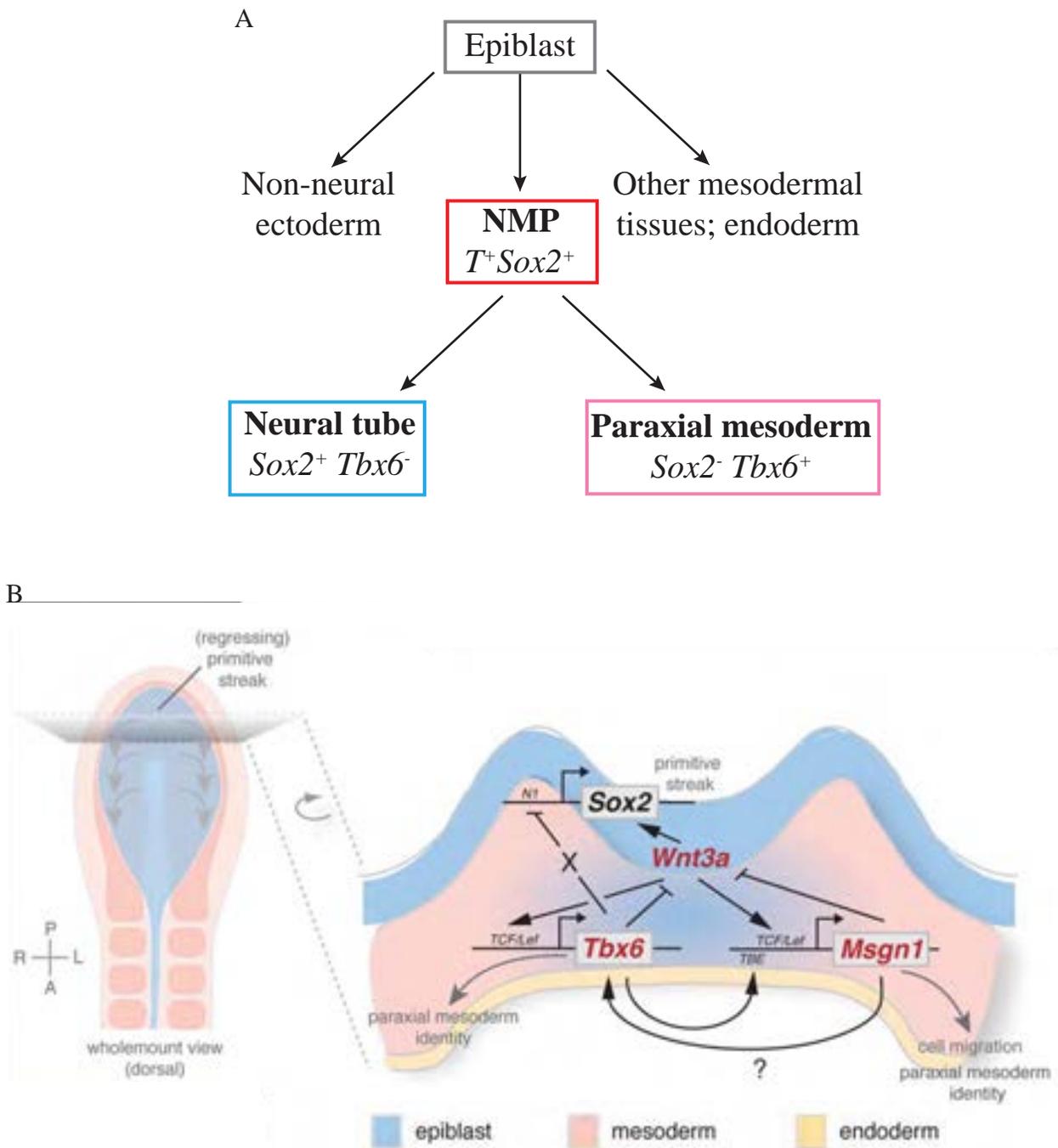
Figure 5 - Transcriptional control of the PSM state

A. At late somite stages, neuromesodermal progenitors (NMP) can give rise to either neurectoderm or paraxial mesoderm in function of a balance between neural (Sox2) and mesodermal (T,Tbx6) factors

B. Summary of the genetic interactions occuring at the tailbud

Modified from Nowotschin et al. (2012)

balance is then biased toward the mesodermal fate, where Msgn1 and Tbx6 counteract the neural fate (Figure 5B), but how this is achieved is not fully understood. Later, in the paraxial mesoderm, the Fgf and Wnt signaling pathways, which are organized in gradient along the PSM, maintain the presomitic fate by activating each other (Aulehla et al., 2008, Naiche et al., 2011) and maintaining high levels of *Msng1* and *Tbx6* (Wittler et al., 2007, Wahl et al., 2007, Naiche et al., 2011, Dunty et al., 2008, Chalamalasetty et al., 2011).

At early stages, the specification of the paraxial mesoderm state mainly involves a correct dosage of Wnt, Nodal and BMP signaling in epiblast cells along the primitive streak (Arnold and Robertson, 2009). At later stages, the specification of paraxial mesoderm appears to rely on the position of bipotent progenitors within the tailbud, as the differentiation of neuromesodermal progenitors could be biased toward the neural or mesodermal fates by graft in specific regions of the node-streak border (Wymeersch et al., 2016). The identity of these environmental cues remains to be determined. After having briefly examined how the PSM state is acquired *in vivo*, we focus on the specification of this fate occurs *in vitro* in embryonic stem cells.

Paraxial mesoderm state *in vitro*

Embryonic stem cells have emerged as an *in vitro* system to study the Vertebrate development. In addition to their interest for regenerative medicine and drug screening, they provide a tool in basic research to deconstruct the cell decisions occurring in the embryo. Compared to the embryo, embryonic stem cells present several advantages, such as the ease of genetic manipulation, the material quantity and the reduction of sacrificed animals.

Mouse embryonic stem cells (mESC) are traditionally derived by culturing blastocysts on embryonic fibroblast cells (known as feeders) under specific conditions (Nichols and Smith, 2012). While they originate from the ICM, transcriptome analysis reveals that mESCs resemble more to pre-implantation epiblast (Boroviak et al., 2014). They have the ability to self-renew and to differentiate into the three germ layers. This is achieved through a specific gene regulatory network, where pluripotency factors maintain each other and where differentiation genes for the germ layers are poised for a later activation or repression depending on the environmental context (Jaenisch and Young, 2008). *In vitro,* these pluripotent factors such as *Oct4*, *Sox2*, *Nanog*, are induced by the Leukemia Inhibitory Factor (LIF), while pro-differentiation factors are repressed by inhibition of Fgf/MAPK and by partial activation of Wnt (Nichols and Smith, 2012). This culture condition called "2i" (for two inhibitors) maintains mESC in a ground state of pluripotency, where the undifferentiated mESC state is stabilized and their spontaneous differentiation is reduced (Ying et al., 2008, Silva et al., 2008). This is likely achieved by the stabilization of the core pluripotency

network and by the repression of differentiation genes (Nichols and Smith, 2012). Inhibition of Fgf/MAPK induces a ground state notably by repressing the primitive endoderm specification (Nichols et al., 2009) and the epiblast differentiation into any of the three germ layers (Kunath et al., 2007). On the other hand, activation of the Wnt pathway is thought to repress the transition to a primed state corresponding to the post-implantation epiblast by modulating the activity of Tcf3 (Satou et al., 2004, Niwa, 2011). mESCs have the ability to form all the germ layers as shown by injection in blastula or adult (teratoma), by tetraploid complementation and by *in vitro* differentiation (Jaenisch and Young, 2008). Therefore, mESC provide an interesting tool to understand how different cell fates are acquired.

Specifically, mESC can be differentiated into a state resembling the *in vivo* paraxial mesoderm fate by transiting through a primed epiblast state. Removal of the pluripotent conditions leads to the priming of mESC into a state similar to the post-implantation epiblast, when they are able to differentiate into the three germ layers (Jackson et al., 2010, Thomson et al., 2011, Hayashi et al., 2011, Turner et al., 2014a). Interestingly, neuromesodermal progenitors have been observed at this stage, as evidenced by the coexpression of neurectodermal and mesodermal markers (Gouti et al., 2014, Turner et al., 2014a). Different protocols have shown that activation of the Wnt pathway and repression of the BMP pathway further direct their differentiation toward the presomitic mesoderm (Tanaka et al., 2009, Craft et al., 2013, Chal et al., 2015). Another study suggests that using high dose of Fgf in combination with an activator of the Wnt pathway promotes a posterior PSM state (Sudheer et al., 2016). Similar protocols based on Wnt activation and BMP repression have been established with human embryonic stem cells (Umeda et al., 2012, Craft et al., 2015). In mESC, Wnt signaling promotes mesodermal fates (Gadue et al., 2006); however a closer analysis reveals that it might be an indirect effect due to a delay of the pluripotency exit as premature differentiation is biased toward neurectodermal lineages (Turner et al., 2014b). On the other hand, BMP inhibition represses lateral mesoderm specification and promotes the paraxial mesoderm fate (Tanaka et al., 2009, Craft et al., 2013, Chal et al., 2015), as observed *in vivo* (Miura et al., 2006, Tonegawa et al., 1997, Tonegawa and Takahashi, 1998, James and Schultheiss, 2005, Stafford et al., 2014).

3. Segmentation and somitogenesis

After its specification, the paraxial mesoderm evolves from a mesenchymal tissue, called the presomitic mesoderm (PSM), to a series of epithelial units, called somites. In this section, we present the main morphogenetic events leading to the formation of such segments.

Somite formation

Morphogenetic events

After ingression, posterior PSM cells form a mesenchyme on both sides of the neural tube, and as new tissues are continuously added at the level of the primitive streak/tailbud, those cells have a relatively more anterior position in the PSM. This is concomitant with large and gradual changes in gene expression (Ozbudak et al., 2010), cell metabolism (Ozbudak et al., 2010)(M.Oginuma, personal communication), cell motility (Delfini et al., 2005, Benazeraf et al., 2010), and epithelialization (Chal and Pourquie, 2009), which culminate by the individualization of blocks of cells, called somites. This mesenchyme-to-epithelium transition occurs in the anterior PSM and involves a complex reorganization of cells and extra-cellular matrix (Martins et al., 2009). Somites are organized as a sphere with epithelial cells in an aster-like shape surrounding a cavity (somitocoel) filled with mesenchymal cells (Christ et al., 2007) (Figure 6A).

The formation of somite boundaries (intersomitic cleft) requires the regionalization of several adhesion molecules. Notably, the ephrin/Eph system appears to have a role in this process by modulating cell adhesion, tension and/or repulsion (Cayuso et al., 2015). In the anterior PSM, *EphA4* is expressed in the anterior part of the somite S-II, while its receptor *ephrinB2* is expressed in the posterior part of the somite S-I (S-I is the segment corresponding to the next somite to form, while S0 is the forming somite) (Durbin et al., 2000, Nakajima et al., 2006) (Figure 6B). In zebrafish and chicken, the juxtaposition of these regions is thought to play a role in the positioning of the intersomitic cleft as creation of an artificial EphA4/ephrinB2 interface by grafting *EphA4* expressing cells in the middle of the *ephrinb2* expressing region triggers the formation of an ectopic boundary at the interface between the grafted tissue and the host (Barrios et al., 2003, Watanabe et al., 2009). However, the complete molecular mechanism still remains to be understood, as mouse mutants for *EphA4* exhibit normal segmentation (Dottori et al., 1998) and as the *EphA4* boundary does not strictly correlate with the final boundary formation in chicken (Kulesa and Fraser, 2002).

In addition to the Eph/ephrin repulsion, other mechanisms contribute to the formation of the somitic cleft, such as the reorganization of the fibronectin net (Martins et al., 2009) or differential adhesion.
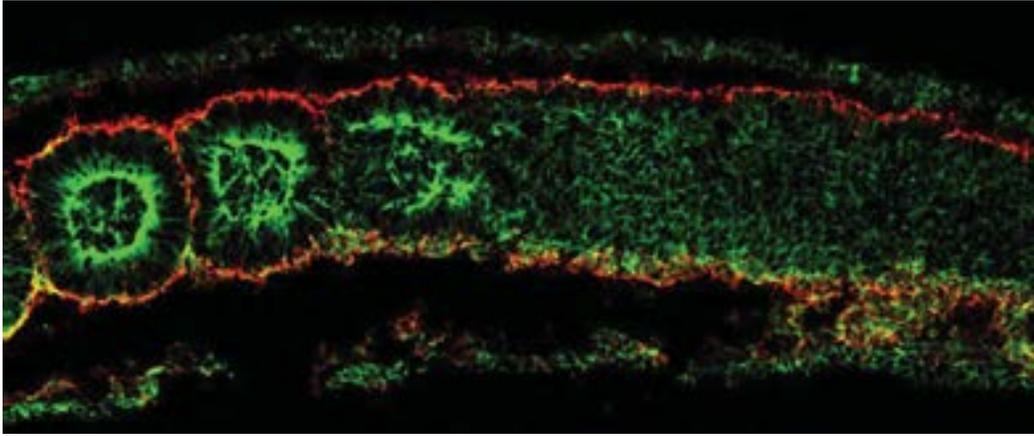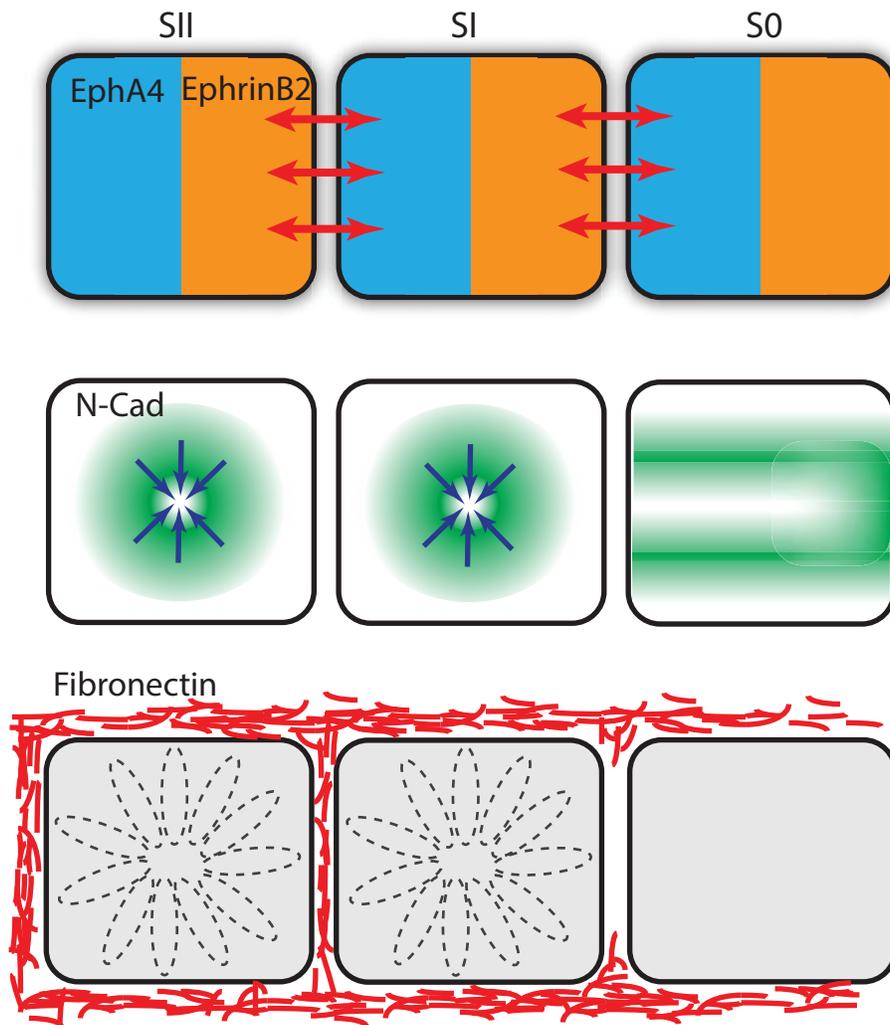
Figure 6 - Formation of a somite

A. Longitudinal section of a chicken paraxial mesoderm showing the rearrangement of the extracellular matrix (Fibronectin - red) and N-cadherin (green).
Modified from a figure of J.Chal (personal communication)

B. Scheme showing the different processes involved in the formation of a somite: creation of a EphA4/EphB2 boundary (*top*), polarization of N-cadherin (*middle*), assembly of fibronectin (*bottom*)

Notably, localized expression of the protocadherin *PAPC* (*Pcdh8*) in the anterior somite seems to play a role in preventing mixing between the anterior and posterior somite compartments (Yamamoto et al., 1998, Yamamoto et al., 2000, Kim et al., 2000, Rhee et al., 2003). However, a question remains: if the EphA4/ephrinB2 interface is crucial for boundary, why an additional boundary does not form in the middle of the segment where such an interface also exists? It was proposed that the localization of N-cadherin at the center of the somite provides homophilic adhesion between cells, and maintains both halves together (Figure 6B). This is required to maintain segment cohesion, as the mouse mutant for *N-cadherin* and compound mutants for the *N-cadherin* and *Cadherin-11* display smaller somites resulting from the separation of the anterior (*EphA4*-positive) and posterior (*ephrinB2*-positive) compartments (Radice et al., 1997, Linask et al., 1998, Horikawa et al., 1999). Accordingly, both Eph/ephrin repulsion and N-cadherin cohesion are sufficient to reproduce the segmentation pattern in simulations using a Cellular Potts Model (Glazier et al., 2008). In zebrafish, McMillen and colleagues observed that N-cadherin proteins become localized in a saw tooth pattern, with low levels of N-cadherin in the anterior part of the somites SI and SII and high levels in their posterior part (McMillen et al., 2016). They showed that a sharp boundary of N-cadherin induces the formation of a somatic cleft, while a gradient within the somite prevents the formation of an additional fissure. The mechanism seems to involve a modulation of tissue contractility and matrix assembly, as N-cadherin represses the activation of integrin-α5 that is required for the assembly of the fibronectin matrix (Julich et al., 2015); however, it should be noted that the somite organization differs between zebrafish and amniotes: in amniotes, N-cadherin is first observed in a U-shape with low levels in the anterior part of the somite, and then restricted to the apical side of somite cells (Chal and Pourquie, 2009).

Transcriptional control

The formation of somite boundaries requires a complex rearrangement of cell adhesion and extracellular matrix; how is this process controlled at the genetic level? Two main classes of factors regulate the epithelialization and the formation of boundary in Vertebrates: Paraxis and Mesp1/2. Paraxis is a bHLH transcription factors expressed in a gradient along the PSM (Burgess et al., 1995), whose loss abolishes the formation of the somitic epithelium and the formation of *bona fide* somites (Burgess et al., 1996). However, the somitic cleft is still observed and several genes are clearly expressed in a segmental manner. Microarray analysis of *Paraxis* mutants shows that it regulates the expression of genes associated with extracellular matrix reorganization, cell adhesion and cytoskeleton (Rowton et al., 2013). Paraxis seems therefore necessary for the epithelialization of the presomitic mesoderm, but not for its segmentation *per se*. On the other hand, Mesp1 and Mesp2 are bHLH transcription factors, whose loss leads to segment defects (Saga et al., 1997). *Mesp2* mutants still display somitic clefts for the most anterior somites; however, this is thought to occur because of

a partial redundancy with *Mesp1* as further reduction of *Mesp1* dose correlates with a stronger phenotype (Takahashi et al., 2000, Oginuma et al., 2008a). Alternatively, anterior somites could be segmented in a Mesp-independent manner. Mesp factors are cyclically expressed in a band in the anterior PSM, first of the size of an entire somite and then of a half-somite at its presumptive anterior part (Morimoto et al., 2005). They induce the expression of the adhesion molecules, EphA4 and PAPC (Rhee et al., 2003, Nakajima et al., 2006), which contributes to the periodic formation of segment boundaries. Accordingly, in chimera comprising wild-type and *Mesp1-/-;Mesp2-/-* cells, *Mesp*-deficient cells are excluded from the somites and do not form boundary (Takahashi et al., 2005).

Antero-posterior polarity of the somites

Somites are further specified into anterior and posterior compartments (also known as rostro-caudal polarity) (Figure 7A). This is mainly due to the anterior restriction of the Mesp factors and a partition in Notch signaling, which is repressed in the anterior half and activated in the posterior half (Saga and Takeda, 2001).

Segments are still formed in mouse mutants with defects in antero-posterior somite polarity (Nakajima et al., 2006, Feller et al., 2008). Similarly, somites without antero-posterior polarity can be artificially produced in chicken by treating the posterior primitive streak with a BMP inhibitor (Dias et al., 2014). This suggests that the somite polarity is not strictly necessary for the formation of somites. However, it is likely required for the correct organization of the segments along the embryo axis, as we will discuss in the next section. Furthermore, the antero-posterior polarity is crucial for the specification of the somite derivatives, as evidenced by the phenotype of *Tbx18* and *Uncx4*.1 mutants. Those two transcription factors are respectively expressed in the rostral and caudal half of the somites, and regulate the fate of the somite derivatives. In mouse, loss of those genes leads to major spine defects due to a misspecification of the sclerotome (Leitges et al., 2000, Mansouri et al., 2000, Bussen et al., 2004).

Somitogenesis and segmentation

It is important to distinguish three processes: the molecular segmentation (*i.e.* the expression of a subset of factors in stripes along the antero-posterior axis), the somitogenesis (*i.e.* formation of epithelial blocks), and the antero-posterior somite polarity (Figure 7B). While those three processes occur concomitantly and are molecularly interconnected, they are distinct modules and can be uncoupled. As mentioned above, molecular segmentation can occur without formation of an epithelial block in *Paraxis* mutant (Burgess et al., 1996). Similarly, Palmeirim and colleagues showed that isolation of chicken PSM from surrounding tissues blocks the formation of somites, while stripes of segmental genes are still observed (Palmeirim et al., 1998). Somite and segments can

A
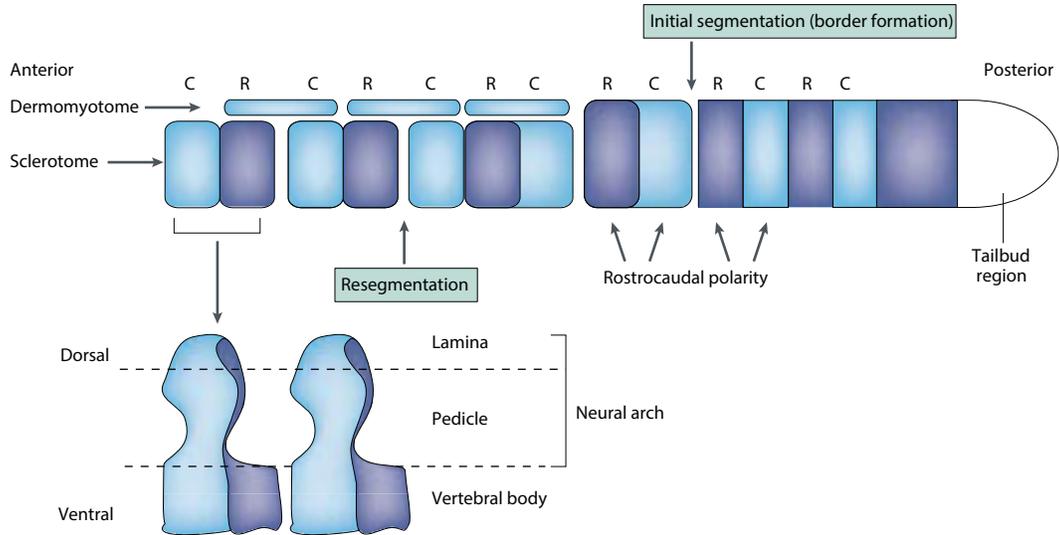
B
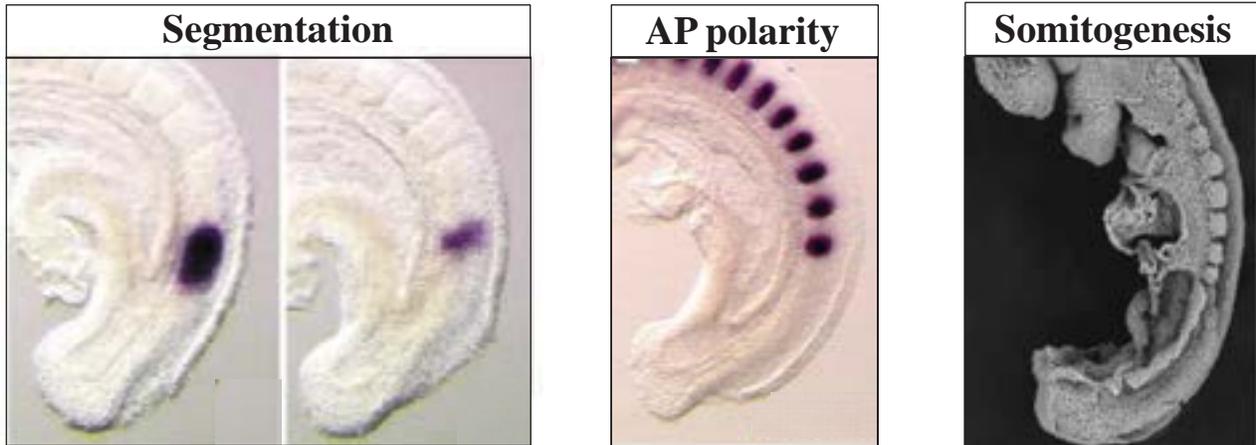
Figure 7 - Different patterning events shaping a segment

A. Scheme showing the somite polarity and the resegmentation process: a newly formed segment acquired an antero-posterior polarity (also known as rostrocaudal) that is the basis for the ulterior polarity of the vertebrae

B. Three different patterning processes: i) segmentation: the specification of metameres along the axis; ii) antero-posterior patterning; iii) somitogenesis: the morphogenetic process leading to the differentiation of a segment and the formation of epithelial units.
(*Left*) Expression pattern of *Mesp2* in mouse that is first expressed in the whole presumptive segment and subsequently restricted to its anterior compartment. (*Middle*) Expression pattern of the caudal marker *Uncx4.1* in mouse. (*Right*) Scanning electron microscopy of a mouse embryo

Modified from Saga and Takeda (2001), Takahashi et al. (2000), Takahashi et al. (2008) and Aulehla et al. (2008)

be formed without their final antero-posterior polarity as suggested by mutants of the Notch pathway (Saga and Takeda, 2001). Moreover, in chicken, ectopic formation of paraxial mesoderm by inhibiting BMP signaling in an explant of posterior primitive streak results in the formation of epithelial blocks without antero-posterior polarity and without apparent expression of the segmental marker *Mesp2* (Dias et al., 2014).

The term "segmentation" designs the process leading to the "*repetition along the anterior–posterior axis of a structural unit that comprises a suite of characters involving the entire body*" (Davis and Patel, 1999). It is however not clear which process in the PSM is at the origin of the metamerism. Mutants displaying defects in the antero-posterior polarity of somite, such as *Uncx4.1, Tbx18, Ripply1/2* (Takahashi et al., 2010), still show signs of segmentation of the spine suggesting that it is not strictly required for the final segmentation of the body axis. Furthermore, *Paraxis* mutants have a clear segmentation of the axial skeleton (Burgess et al., 1996), arguing against the strict necessity of somitogenesis for the final metamerism. Similarly, the serial organization of the myotome is conserved in those mutants (Leitges et al., 2000, Mansouri et al., 2000, Bussen et al., 2004, Burgess et al., 1996). Which process could thus account for the segmentation in Vertebrates? One hypothesis is that those mutants show only a partial loss of polarity and/or somitogenesis (e.g. the *Paraxis* mutant still displays a tissue boundary). Alternatively, the patterning of the paraxial mesoderm could have some degree of self-organization due to cell sorting or local interactions, which would explain the residual metamerism in these mutants (Takahashi et al., 2013). In other words, while the serial differentiation of paraxial mesoderm in these mutants might be the consequence of a local self-organization, the molecular segmentation in a wild-type PSM assures its proper deployment along the antero-posterior axis. Genetic studies in mouse point toward a central role of Mesp factors in this regard. Indeed Mesp factors regulate several adhesion molecules as discussed above, and specify the rostral compartment of the somite. They are also necessary for the further differentiation of somites in myotome and sclerotome (Saga et al., 1997, Takahashi et al., 2007). Similar findings were found in zebrafish, where mesp-b factors are involved in the differentiation of a somite derivative, the dermomyotome (Sawada et al., 2000, Windner et al., 2015). While the complete loss of Mesp factors have been difficult to achieve, the correlation between the dose of Mesp factors and the severity of segmentation defects suggests that their segmental expression is key to the final metamerism of Vertebrates (Saga et al., 1997, Takahashi et al., 2000, Oginuma et al., 2008a). Double *Mesp1*-null, *Mesp2*-null mutants lack paraxial mesoderm precluding the study of their segmentation (Kitajima et al., 2000). However, in the chimera experiment of Takahashi and colleagues previously mentioned, double-null cells cluster without any sign of boundary but retain markers of the paraxial mesoderm (*Uncx4.1, Paraxis*) (Takahashi et al., 2005). The central role of Mesp factors is further indicated by the phenotype of the *Ripply1/2* double mutants, where *Mesp2* is no more expressed in stripes in the anterior PSM and where strong defects in the axial skeleton are observed (Takahashi et al., 2010).

Because Mesp factors are involved in the molecular segmentation, the formation of boundaries, and the somite antero-posterior polarity, this could assure the coupling of these three processes *in vivo*.

Somite derivatives

After their formation, somites are further specified in different compartments that give rise to a variety of cell types (Christ et al., 2007, Christ and Scaal, 2008) (Figure 8). This is mainly achieved by signaling clues from neighboring tissues, and thus from the position of the cells within the somite. The five main compartments derived from the somites are:

- the sclerotome containing the precursors of the chondrocytes and osteocytes of the vertebrae, ribs and intervertebral discs;
- the myotome containing the precursors of the skeletal muscle cells, smooth muscle and adipocytes (brown fat);
- the dermatome containing the precursors of the fibrocytes of connective tissues and back dermis;
- the endotome containing the precursors of endothelial cells and pericytes;
- the syndetome containing the precursors of fibrocytes of the tendons

The segmentation of the sclerotome is central to the formation of the future axial skeleton. Indeed, the ventral sclerotome undergoes a process called resegmentation during vertebrae morphogenesis (Figure 7A) (Christ and Scaal, 2008). A vertebra is composed of a vertebral body articulated by intervertebral discs, and neural arches that provide attachment sites for the ligaments. The vertebral body comes from the medial sclerotome of a pair of somites, after their migration towards the ventral midline. Then, the sclerotome coming from the caudal half of a somite joins the sclerotome arising from the rostral half of the adjacent somite. In other words, the boundary between the rostral and caudal somitic compartments becomes the boundary between adjacent vertebrae. At this boundary, cells from the somitocoel along with notochord cells form the intervertebral discs. Other mechanisms might play a role in skeleton segmentation, such as self-organization (Takahashi et al., 2013) or input from the notochord (Fleming et al., 2004). However, genetic mutants with somite defects strongly support a central role of somite formation in the future segmentation of the adult body.
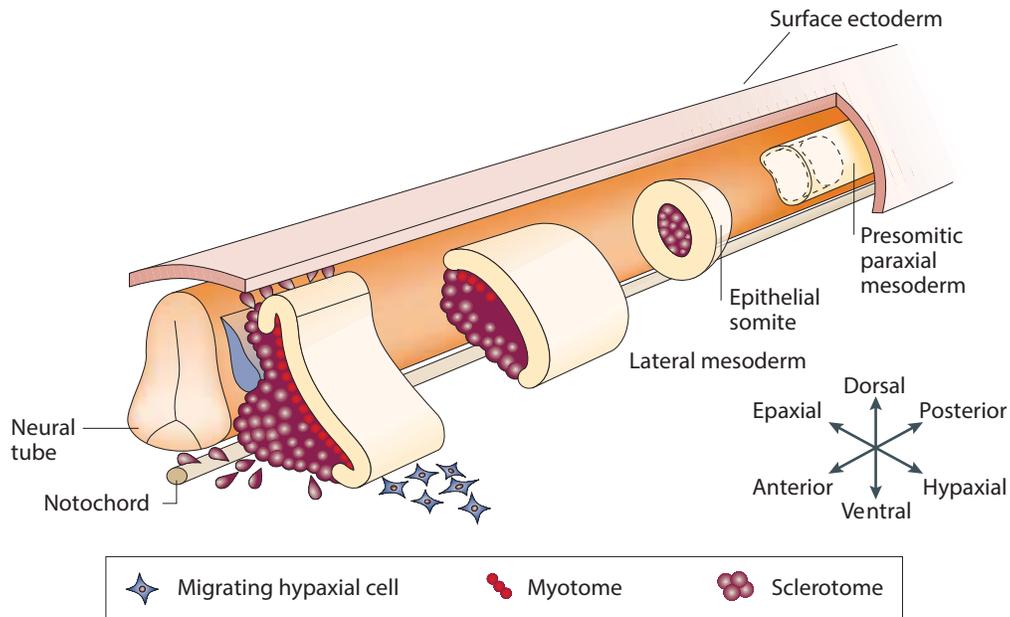
Figure 8 -Somite derivatives

Scheme showing the determination of the somite along the antero-posterior axis.

After the formation of an epithelial unit, the somite is further specified into different compartments depending on the signals sent by neighboring tissues. Notably, the dermomyotome will give rise to the muscle and the back dermis, while the sclerotome will be resegmented to form the axial skeleton.

Modified from Saga and Takeda (2001).

4. The segmentation clock

We have previously discussed that the segmentation in Vertebrates is mainly the result of the cyclic expression of segmental genes such as the Mesp factors in the anterior PSM. We now examine how this molecular segmentation occurs. In this section, we introduce the segmentation clock, a gene regulatory network underlying the oscillatory activity of cellular processes during segmentation.

Cyclic genes

How to account for the periodic formation of segments in the paraxial mesoderm? A very natural hypothesis is to postulate the existence of a mechanism translating the temporal periodicity of a molecular oscillator into the spatial periodicity of somites. A seminal discovery was made by Palmeirim and colleagues when analyzing the gene expression of *Hairy1* in chicken embryo, whose homologue in the fly *D.melanogaster* was a known factor involved in the body segmentation (Palmeirim et al., 1997). They observed that *Hairy1* was cyclically expressed in the PSM with a period (in the posterior PSM) equivalent to the period of somitogenesis (Figure 9A); furthermore the authors postulated the existence of traveling waves of gene expression along the tissue. Modeling by J.Lewis suggested that this characteristic wave (large band of *Hairy1* in the posterior PSM that becomes restricted in the anterior PSM) is produced by a slowing-down of individual oscillators in the anterior PSM (Palmeirim et al., 1997). Subsequently, other genes were identified as cyclic genes in different Vertebrate studies; in all cases, the repetition of the expression pattern was consistent with the period of somitogenesis. This provided strong evidence in favor of a molecular oscillator that would control the pace of segmentation, the so-called segmentation clock.

Among studied Vertebrates species, at least one member of the Hes/Her transcription factors family undergoes oscillatory expression in the PSM, which suggests that this class is at the heart of the Vertebrate clock (Bessho et al., 2001, Oates and Ho, 2002, Holley et al., 2002, Kusumi et al., 2013). Oscillations in the Notch pathway components also arise as a common theme in Vertebrates. The ligand Delta has been shown to oscillate in mouse, chicken and marsupials (Dll1 - (Maruhashi et al., 2005, Keyte and Smith, 2012, Bone et al., 2014, Shimojo and Kageyama, 2016) and in zebrafish (*Dllc* - (Jiang et al., 2000)). This leads to the periodic activation of the pathway as evidenced by the oscillation of the Notch intracellular domain (NICD) (Huppert et al., 2005). In mouse, oscillations of genes of the Wnt and Fgf pathways have been convincingly shown (Dequeant et al., 2006, Aulehla et al., 2003, Niwa et al., 2007, Niwa et al., 2011). Microarrays analysis in chicken and zebrafish also

suggest the cyclic expression of a subset of Wnt and Fgf targets (Krol et al., 2011); however, this remains to be firmly demonstrated.

While most of the oscillations have been described at the level of the transcription, it is important to emphasize that post-transcriptional and post-translational oscillations occur in the PSM. For instance, *hes6* mRNA is not oscillating in zebrafish, but its protein is cycling (Schröter et al., 2012). Recent work suggests that the level of mRNAs and protein poorly correlate during Xenopus development (Peshkin et al., 2015), suggesting that another layer of regulation could underlie the architecture and function of the segmentation clock. Similarly, oscillations of post-translational modifications have been observed in the PSM, such as for the Fgf effector ERK (Niwa et al., 2007, Niwa et al., 2011) or for the phosphorylation of CREB (Lopez and Fan, 2013). Identifying post-transcriptional oscillations is further justified by studies of another oscillator, the circadian rhythm, showing the importance of protein modifications to regulate the stability or activity of clock proteins (Gallego and Virshup, 2007). Accordingly, the circadian clock operates in systems without transcription, such as human red blood cells that lack nucleus (O'Neill and Reddy, 2011) or photosynthetic alga in the dark (O'Neill et al., 2011). Interestingly, other cellular processes occur in a periodic manner along the day, such as ribosome and protein synthesis (Huang et al., 2013, Jouffe et al., 2013) or cell metabolism (Milev and Reddy, 2015). The relevance of such non-transcriptional events in the mechanism of the segmentation clock remains to be studied.

Molecular mechanisms of oscillations

We now examine how these oscillations are created in the PSM. A fundamental feature of biological oscillators is the existence of a negative feedback loop with specific properties to avoid a steady state, notably time delay and non-linearity (Lewis, 2003, Monk, 2003, Alon, 2007, Novak and Tyson, 2008) (Figure 9B).

Negative feedback loops with delay

Negative feedback loops are frequent in biological systems, and often contribute to the cell homeostasis by adjusting the levels of signaling or metabolites (Kitano, 2004). In the PSM, many cyclic genes are transcriptional or signaling repressors involved in such negative feedback loops. For instance, Hes/Her factors are transcriptional repressors that are activated by Notch signaling and repress their own transcription (Sasai et al., 1992, Takebayashi et al., 1994, Bessho et al., 2001, Hirata et al., 2002, Chen et al., 2005, Kageyama et al., 2007, Giudicelli et al., 2007). Similarly, in mouse, the Fgf, Notch, and Wnt pathways cyclically induce the expression of their own repressors, such as *Dusp4* (Niwa et al., 2007, Niwa et al., 2011), *Sprouty2* (Dequeant et al., 2006), *Sprouty4*

(Hayashi et al., 2009), *Snail* (Dale et al., 2006) for Fgf signaling ; *Axin2* (Aulehla et al., 2003), *Dkk1* (Dequeant et al., 2006, Aulehla et al., 2008), *Dact1* (Dequeant et al., 2006, Suriben et al., 2006), *Nkd2* (William et al., 2007) for Wnt signaling; and *Lfng* (Aulehla and Johnson, 1999), *Nrarp* (Wright et al., 2009) for Notch signaling.

In addition to the existence of negative feedback loops, a time delay is necessary to obtain sustained oscillations (Lewis, 2003, Monk, 2003); intuitively, this allows the system to alternate between activation and repression rather than to stall in a steady state. An analogy is useful here: in a seesaw game, kids alternatively hit the ground to go in the air; if they were trying to elevate at the same time without time delay, they will be both poised. This time delay in the gene network can be explicit through the time required for the formation of the repressor or activator (e.g. RNA splicing, RNA transport, translation, post-translational modification, etc. – Figure 9B) or implicit through indirect activation or repression.

Theoretical work showed that the duration of the time delay influences the period of oscillations (Lewis, 2003). In the PSM, it has been proposed that the delay originates from the time that is required to transcribe the *Hes/Her* or *Lfng* genes, or from their splicing or nuclear export. However, measuring the transcription elongation rate in the PSM suggests that the delay due to this step is not sufficient and is thus unlikely to be responsible for the generation of oscillations (Hoyle and Ish-Horowicz, 2013); similar findings have been found in zebrafish (Hanisch et al., 2013). Consistently, increasing the length of one intron of *Lfng* in mouse, which is expected to increase the delay between transcription and translation, has no effect on mouse segmentation (Stauber et al., 2012). Other studies rather suggest that RNA splicing has an important role in imposing a delay between activation of *Hes7* in mouse and its auto-inhibition. Deletion of all *Hes7* introns abolishes oscillations and leads to major defects in the segmentation of the axial skeleton (Takashima et al., 2011). Removing two of the three introns of this gene, and thus reducing the delay imposed by splicing, changes the period of *Hes7* oscillations by 11 minutes (Harima et al., 2013). This results in an increase in the number of anterior somites, and later, to a dampening and an arrest of the oscillations. The genetic modifications of the locus required to remove the introns might affect *Hes7* expression (Stauber et al., 2012, Takashima et al., 2011), but even so, these studies support a role for the specific delay caused by splicing in the generation of oscillations. In addition, kinetic analysis of *Lfng* and *Hes7* mRNA maturation shows that nuclear export also contributes to the time delay (Hoyle and Ish-Horowicz, 2013). Interestingly, the durations of splicing and nuclear export in the control of oscillations seem to vary in zebrafish, mouse and chicken, which potentially provides an explanation for the interspecies difference in clock period and somitogenesis.

Non-linear interactions

Moreover, theoretical work indicates that non-linearity through cooperativity or positive feedback loops is also important to generate sustained oscillations (Goldbeter, 2002, Alon, 2007, Novak and Tyson, 2008). Such non-linearity can originate from multimerization of factors: it was shown in zebrafish that dimerization of Hes/Her factors is essential to generate oscillations (Schröter et al., 2012, Trofka et al., 2012, Ay et al., 2013) and modeling further suggests that such molecular interactions have to be non-linear to reproduce the oscillations observed *in vivo* (Schröter et al., 2012). In the same line, a study in chicken embryos postulates the existence of a positive feedback loop between the level of the Notch effector NICD and its half-life potentially leading to non-linear effects (Wiedermann et al., 2015).

Clearance of mRNAs and proteins

In addition, mathematical modeling predicts that sustained oscillations require rapid degradation of the cyclic mRNAs and proteins to allow the alternation of pathway activation and repression (Lewis, 2003, Ay et al., 2013). Experimental work confirms such prompt clearance of cyclic factors: for instance, the half-lives of *Hes1* mRNA and HES1 protein are 24 and 22 minutes, respectively (Hirata et al., 2002). The short half-life of proteins relies on their ubiquitination and rapid degradation by the proteasome (Hirata et al., 2002, Bessho et al., 2003, Hirata et al., 2004). It was possible to increase the stability of the protein HES7 by mutating lysine residues involved in the proteasome-dependent degradation: this leads to an increase of the protein half-life from 22 to 30 minutes, while the repressive activity remains unaffected (Hirata et al., 2004). In mice expressing this less degradable form of HES7, oscillations are progressively lost during somitogenesis, consistent with mathematical simulations of a negative-feedback loop with delay. Similarly, inhibition of the E3 ubiquitin ligase complex SCF in chicken increases the stability of the Notch intracellular domain and is thought to delay the oscillations of *Lfng* (Wiedermann et al., 2015). Last, it was also proposed that secretion of some proteins, such as for LFNG in mouse, contributes to reducing their intracellular half-life (Williams et al., 2016).

Little is known about the degradation of cyclic mRNAs in the PSM. Differences in stability between mRNAs are partly explained by their 3′untranslated region (UTR) (Chen et al., 2005, Hilgers et al., 2005, Nitanda et al., 2013). A role for microRNAs in the cyclic mRNA degradation has been proposed in chicken: *miR-125a-5p* was shown to induce the destabilization of *Lfng* mRNA in chicken embryos (Riley et al., 2013). In this work, alleviating *miR-125a-5p*-mediated repression of *Lfng* arrests the oscillations of Lfng, and leads to segmentation defects. Whether this mechanism is conserved in other species is unclear. However, zebrafish and conditional mouse mutants for *Dicer*, an enzyme necessary for microRNAs biogenesis, have no obvious defects in somitogenesis arguing for a minor role of microRNAs in the clearance of cyclic mRNAs (Giraldez et al., 2005, Zhang et al.,

2011)(S.D.Vincent, personal communication). Interestingly, stabilization of the *Hes7* transcript was observed in a gain-of-function mutant for *Lfng*, suggesting that the degradation of cyclic mRNAs could be regulated by the segmentation clock itself (Williams et al., 2016).

Cell state and oscillatory regime

We have seen that the existence of oscillations requires a specific set of parameters: time delay, non-linearity, fast degradation, but it remains to be determined how those parameters are tuned at the cellular level during development. In other words: what makes a cell state permissive for oscillations of cyclic genes? Genetic oscillations are not restricted to the PSM state: *Hes1* is oscillating in the mouse PSM as well as in fibroblasts (Masamizu et al., 2006), neural progenitors in the telencephalon (Shimojo et al., 2008), mESC (Kobayashi et al., 2009), but not in another subset of neural cells (e.g. isthmus, interrhombomeric boundaries, zona limitans intrathalamica, roof plate, the floor plate) (Baek et al., 2006). This disparity between cell types can be explained by different gene regulatory networks or by specific cellular parameters leading to a proper time delay or mRNA/proteins clearance. Supporting the former hypothesis, a link between the PSM state and the segmentation clock has been identified in mouse, where the master regulators Msgn1 and Tbx6 bind to the promoter of cyclic genes (Chalamalasetty et al., 2011, González et al., 2013). Accordingly, Msgn1 regulates the expression of the cyclic gene *Lfng* and mutant for *Msgn1* appears to lose its oscillations (Chalamalasetty et al., 2011), while Tbx6 controls the expression of the cyclic gene *Hes7* (González et al., 2013). Whether there is an additional regulation of cellular parameters, such as protein degradation or expression rate, in specific cell states remains to be answered.

The mouse segmentation clock

After having examined how single oscillatory loops can arise by negative feedback loop with delay, we discussed what they are integrated. In other words, how these multiple loops interact in the mouse PSM?

Dequeant and colleagues performed a series of microarrays of the posterior PSM and identified two main clusters of cyclic genes based on their phase: Hes/Notch/Fgf genes and Wnt genes (Dequeant et al., 2006). The former oscillate in-phase between each others, while they oscillate out-of-phase with the latter. However, subsequent studies showed that this phase relation changes along the axial level, as Hes/Notch and Fgf oscillations become out-of-phase in the anterior PSM (Niwa et al., 2011) and the phase difference between Wnt and Notch oscillators also evolves along the antero-posterior level of an *ex vivo* system recapitulating PSM differentiation (Lauschke, 2013). Based on genetic analyses,
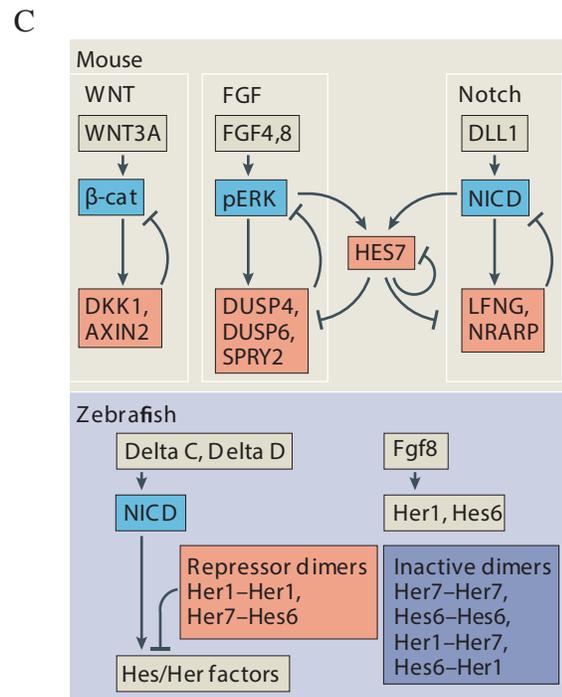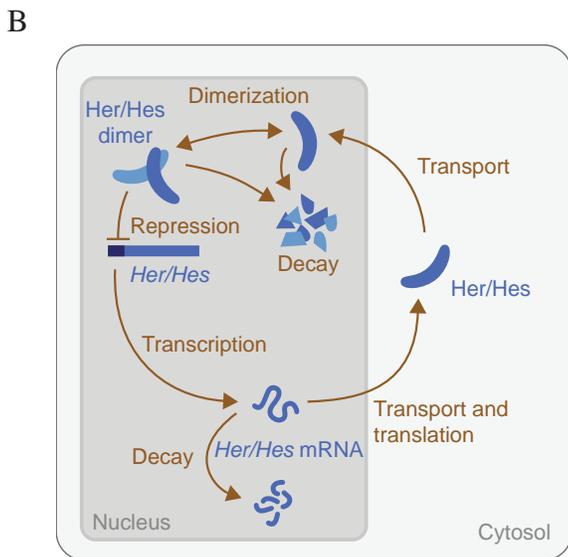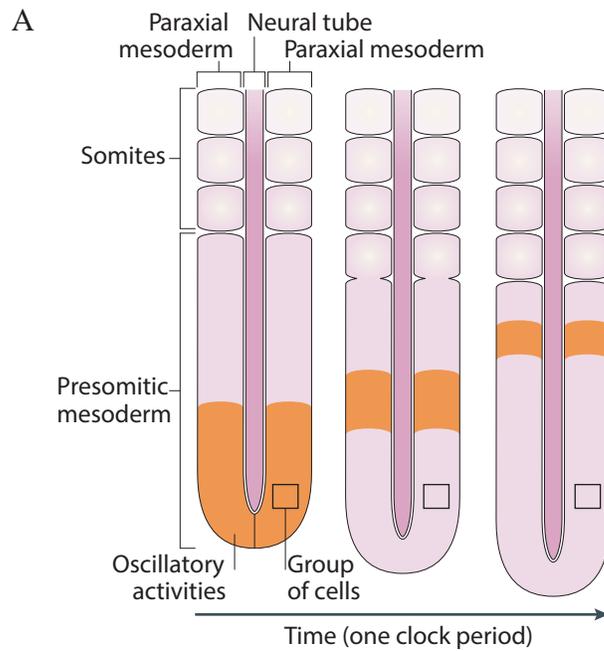
Figure 9 - The segmentation clock

A. Scheme showing the expression pattern of cyclic gene like *Lunatic Fringe* (orange); in a group of cells (square), this expression is oscillatory, and thus, the wave of expression is not due to cell movement.

B. Scheme showing the different cellular processes potentially accouting for the creation of a time delay in a negative feedback loop.

C. Schematic representation of the gene regulatory networks generating oscillations in mouse and zebrafish

Modified from Hubaud and Pourquié (2014), Oates et al. (2012)

we propose to divide the segmentation clock in four connected modules: Hes, Notch, Wnt and Fgf (Figure 9C).

Hes7 module

As mentioned above, oscillations of Hes/Her factors are a conserved feature of the segmentation clock among Vertebrates. In mouse, the *Hes7* mutant shows strong defects in segmentation (Bessho et al., 2001), probably due to the loss of *Mesp2* cycling and its expression as a single band moving steadily (Niwa et al., 2011). *Hes1*, *Hes5* and the Hes-related *Hey2* also oscillate in the PSM (Leimeister et al., 1999, Jouve et al., 2000, Kageyama et al., 2007); however, their mutation do not lead to any discernible segmentation defect (Ishibashi et al., 1995, Ohtsuka et al., 1999, Donovan et al., 2002, Gessler et al., 2002).

Genetic studies suggest that the Hes7 module is independent from the Wnt module and interacts with the Fgf and Notch modules depending on the axial level. Indeed, *Hes7* oscillations seem independent from Wnt oscillations, as *Axin2* cycling is still observed in *Hes7* mutants (Hirata et al., 2004, Ferjentsik et al., 2009). By contrast, *Hes7* mutants lose the cyclic expression of Notch targets, such as *Lfng* (Hirata et al., 2004, Ferjentsik et al., 2009, Niwa et al., 2007, Niwa et al., 2011) as well as the cyclic production of NICD (Niwa et al., 2011). In the posterior PSM, *Hes7* oscillations do not strictly require Notch signaling as evidenced by *Rbpκj* and *Dll1* mutants (Niwa et al., 2007) - even if the loss of *Hes7* cycling in Psen1/2 double mutants prompts further examination (Ferjentsik et al., 2009). However, Fgf signaling is necessary for the oscillations of *Hes7* in the posterior PSM and loss of Hes7 oscillations leads to a loss of pERK and *Dusp4* oscillations suggesting that the Hes7 module controls the oscillations of Fgf signaling (Niwa et al., 2007, Niwa et al., 2011). It remains to be determined whether oscillations of Fgf targets *per se* are necessary for Hes7 oscillations or whether Fgf signaling is only permissive for its cycling. This contrasts with the situation in the anterior PSM, where the loss of Notch oscillations but not Fgf signaling leads to a drastic loss of *Hes7* oscillations (Niwa et al., 2007). Hes7 could thus couple the oscillations of Fgf and Notch modules between the posterior and anterior PSM (Harima and Kageyama, 2013). Importantly, *Hes7* mutants where only the oscillations are lost but the protein remain expressed at a steady level similarly display a loss of Notch oscillations suggesting that Hes7 is not only a permissive signal, but that its oscillatory activity is required (Hirata et al., 2004, Takashima et al., 2011, Harima et al., 2013).

As mentioned earlier, the period of *Hes7* oscillations can be modulated by removal of one intron. Interestingly, this leads to an alteration of the somites number and length suggesting that Hes7 oscillations are central to the mouse segmentation (Harima et al., 2013). While Hes7 does not act as an independent oscillator, this suggests that Hes7 is part of the mouse pacemaker. The central evolutionary role of Hes/Her factors and the fact that *Hes6* mutant zebrafish have a similar phenotype (Schroter and Oates, 2010) would confirm such hypothesis. The persistence of Wnt

oscillations in *Hes7* mutants, however, raises the question of the existence of several pacemaker mechanisms and of the identity of the actual somitogenesis pacemaker.

Notch module

Several Notch mutants have defects in segmentation (Barrantes et al., 1999): *Notch1* (Swiatek et al., 1994, Conlon et al., 1995b), *Dll1* (Hrabe de Angelis et al., 1997), *RBPJ-κ* (Oka et al., 1995), *Lfng* (Evrard et al., 1998, Zhang and Gridley, 1998), *Dll3* (Dunwoodie et al., 1997), *Psen1*/2 (Donoviel et al., 1999), *Nrarp* (Kim et al., 2011), *Pofut1*(Shi and Stanley, 2003, Schuster-Gossler et al., 2009), *ADAM10* (Hartmann et al., 2002), *Mind-bomb1*(Barsi et al., 2005, Koo et al., 2005), *Mastermind-like 1/3* (Oyama et al., 2011), *Nicastrin* (Li et al., 2003), *APH1A* (Serneels et al., 2005) as well as mutant overexpressing NICD (Feller et al., 2008).

Dll1 acts as a ligand in the PSM that triggers a first extracellular cleavage of Notch1 by the metalloprotease ADAM, and then a second cleavage of the intracellular domain by the γ-secretase complex containing the presenilins Psen1 and Psen2, and the proteins Nicastrin and APH1A. In the nucleus, this intracellular domain (NICD) interacts with RBPJ-κ and the Mastermind-like factors to activate the transcription of several genes; it can also interact with the repressor Nrarp that promotes its clearance (Lamar et al., 2001). Several proteins tune the interactions between Notch and its ligand, such as POFUT1 that mediates the O-fucosylation of Notch1, and the glycosyltransferase Lunatic fringe (Lfng) that could post-translationally modify Notch1 or Dll1 (Okubo et al., 2012). The E3 ubiquitin ligase Mind-bomb 1 is thought to regulate the internalization of the Dll1 ligand that facilitates the intracellular cleavage of Notch (Itoh et al., 2003, Koo et al., 2005). Of note, the receptor *Jagged1* is also expressed in the PSM (Barrantes et al., 1999), but its mutant does not present obvious segmentation phenotype (Xue et al., 1999). Furthermore, the ligand Dll3 is not exposed at the plasma membrane, but presumably represses Notch1 at the Golgi apparatus (Geffers et al., 2007, Chapman et al., 2011).

Those mutants for the Notch pathways have often defects in both segmentation and antero-posterior somite polarity, but problems in their vascularization make the analysis more difficult. In addition to the repressors described earlier, both the ligand and receptor are oscillating in the PSM: Dll1 (Maruhashi et al., 2005, Bone et al., 2014, Shimojo et al., 2016), and Notch1 (Bone et al., 2014, Shimojo et al., 2016). As mentioned above, oscillations of Hes7 are required for the oscillations of Notch targets, and the loss of Notch signaling leads to a loss of *Hes7* cycling in the anterior PSM. However, it is not clear whether Notch signaling is permissive or whether its oscillations are required for the cycling of Hes7. Work from the Kageyama lab where mutants for Dll1 lose their oscillations still display oscillations of *Hes7* (a closer examination of the data indicates that Hes7 might still be oscillating - see Fig.4E) (Shimojo et al., 2016) and in the *Lfng* mutant, *Hes7* oscillations still occur (Ferjentsik et al., 2009), while coordinated oscillations of the Notch pathway are lost (Ferjentsik et

al., 2009, Niwa et al., 2011). This could indicate that Notch signaling is permissive to Hes7 oscillations, even at a steady state.

The Wnt and Notch modules can operate independently: in the *Dll1* mutant, oscillations of *Axin2* are still observed arguing that the Wnt module is independent from the Notch module (Aulehla et al., 2003). However, both pathways remain connected as the amplitude of *Axin2* oscillations is perturbed in this mutant and a Wnt agonist Nkd1 was shown to be part of the Notch module (Ishikawa et al., 2004). Last, as mentioned above, the Fgf and Notch modules appear to be coupled through their cross-regulation with Hes7.

Wnt module

Besides the repressors mentioned earlier, oscillations of the Wnt pathway have been described for the activator *Sp5* (Dequeant et al., 2006, Kennedy et al., 2016) and *β-catenin* (Fongang and Kudlicki, 2013). Wnt signaling is required for the specification of the PSM; therefore loss of oscillations is difficult to interpret in these mutants. Conversely, expression of a non-degradable β-catenin that activates Wnt signaling changes the amplitude of Wnt cyclic targets but does not disrupt their oscillations (Aulehla et al., 2008). This suggests that the periodicity of the Wnt module is not controlled at the level of the degradation of β-catenin but rather at a downstream level (e.g. cofactor regulation). Mutations of the cyclic genes *Sp5, Axin2, Dact1* or *Dkk1* do not lead to significant phenotype in segmentation (*Dact1* mutants present axis truncation) (Harrison et al., 2000, MacDonald et al., 2004, Yu et al., 2005, Suriben et al., 2009). As mentioned above, the Wnt module appears independent from the Notch and Hes7 modules. While it is possible that the Wnt oscillator lies upstream of all oscillators in the PSM, no genetic data is available to support this hypothesis. Changing the level of Wnt signaling by use of a chemical inhibitor leads to a change in the *Hes7* oscillation period (González et al., 2013), but this has to be further clarified given the discrepancy with other reports (Aulehla et al., 2008, Gibb et al., 2009). The precise role of the Wnt oscillator in the clock mechanism remains therefore elusive.

Fgf module

In mouse, the Fgf/ERK pathway is periodically activated as evidenced by the cycling of its targets (Dequeant et al., 2006) and by the phosphorylation of ERK (Niwa et al., 2007, Niwa et al., 2011). Similarly to the Wnt module, a clear function for the Fgf oscillator is difficult to study given the role of Fgf signaling in the PSM determination and no mutant has been described where a specific loss of the Fgf oscillator affects segmentation in mouse. Losses of *Sprouty2* (Taketomi et al., 2005), *Sprouty4* (Taniguchi et al., 2007), *Dusp4* (Al-Mutairi et al., 2010) or *Dusp6* (Li et al., 2007) do not lead to detectable defects in segmentation, while mutants for *Snail1* present a strong gastrulation phenotype (Carver et al., 2001). Even if there might be some level of redundancy, genetic analysis

rather suggests that the Fgf module is downstream of the Hes7 module. Interestingly, this appears conserved in zebrafish, where square oscillations of pERK are downstream of Hes/Her oscillations (Akiyama et al., 2014).

The segmentation clock in other Vertebrates

Among other Vertebrates, the segmentation clock of zebrafish has been extensively described. The core circuit of the segmentation clock differs from mice: in fish, only the Hes/Her factors and the Notch pathway have been functionally implicated in the oscillator. It has been proposed that the Hes/Her negative-feedback loops act as a pacemaker for the segmentation clock (Lewis, 2003, Oates and Ho, 2002) based on diverse combinations and activities of Hes–Her dimers (Figure 9C) (Schröter et al., 2012, Trofka et al., 2012, Hanisch et al., 2013). Specifically, Her1, Hes6 and Her7 can form homodimers and heterodimers, but only Her1–Her1 and Hes6–Her7 dimers have a strong and redundant DNA-binding affinity. These dimers ("dimer cloud") were proposed to regulate the clock period depending on their availability and stability (Schröter et al., 2012). Nevertheless, it remains to be understood why the *Her1;Hes6* double mutants, in which none of the active dimers should form and where no oscillations of *Her1* or *Her7* are detected, retain some form of segmental organization (Schröter et al., 2012). Other Hes/Her factors are cyclically expressed in the zebrafish PSM (*Her11*, *Her12* and *Her15*) and could regulate the segmentation clock, but their precise role remains to be clarified (Gajewski et al., 2006, Shankaran et al., 2007, Trofka et al., 2012). Alternatively, the notochord also contributes to the axial skeleton and could have a role in this remaining segmentation (A.Oates, personal communication). Oscillations of the Wnt and Fgf targets in zebrafish have been proposed based on microarray or qPCR (Krol et al., 2011, Schwendinger-Schreck et al., 2014), but this remains to be firmly demonstrated.

In addition to *Hairy1*, oscillations of the Notch pathway have been clearly described in chicken, and appear to involve a negative feedback loop with Lfng (Dale et al., 2003, Wiedermann et al., 2015), but the segmentation clock has not been described as thoroughly as in mouse and zebrafish.

Oscillators synchronization

A striking feature of oscillations in the PSM is their local synchronization between neighboring cells. That is, oscillators are locally in a similar phase. We now examine the biological basis for this synchronization. At the tissue level, such coordination ultimately underlies the concerted changes in cell adhesion necessary for segment formation.

Synchronization of cellular oscillator has been well described in zebrafish, where it was proposed that Notch signaling is required for the clock synchrony between neighbors. Loss of Notch signaling
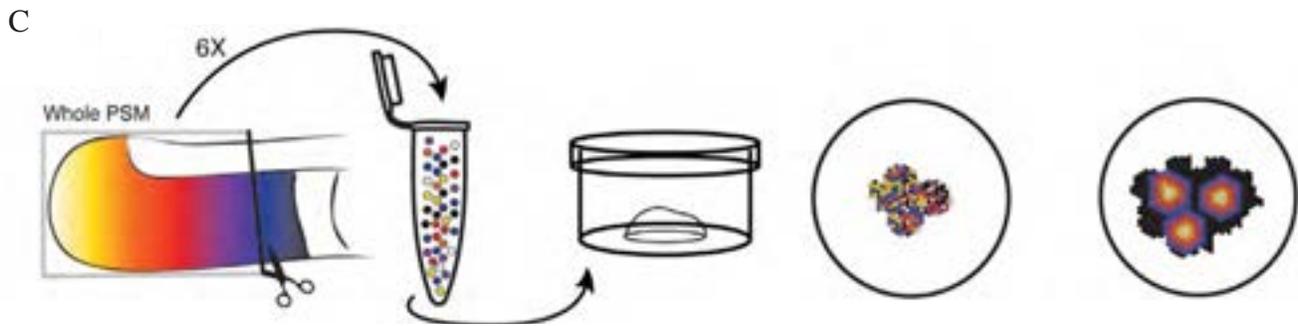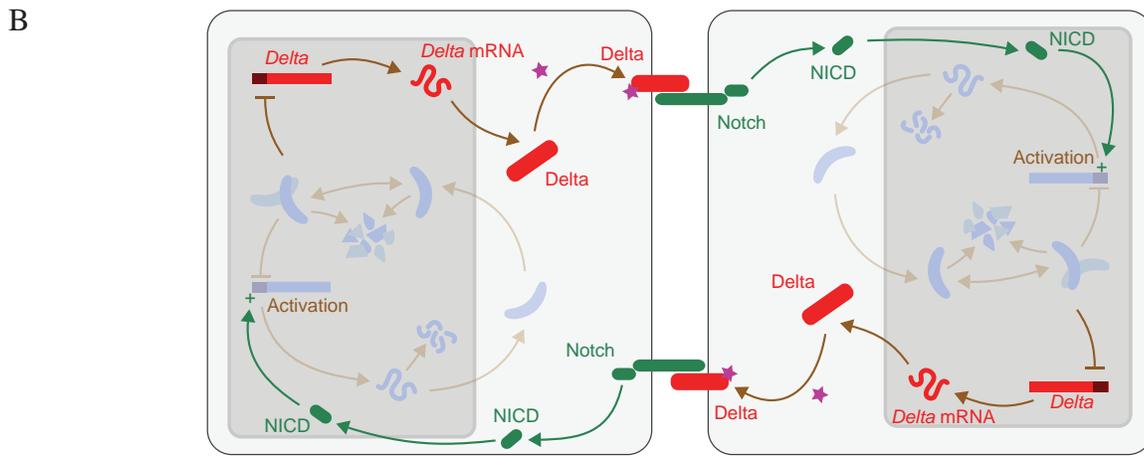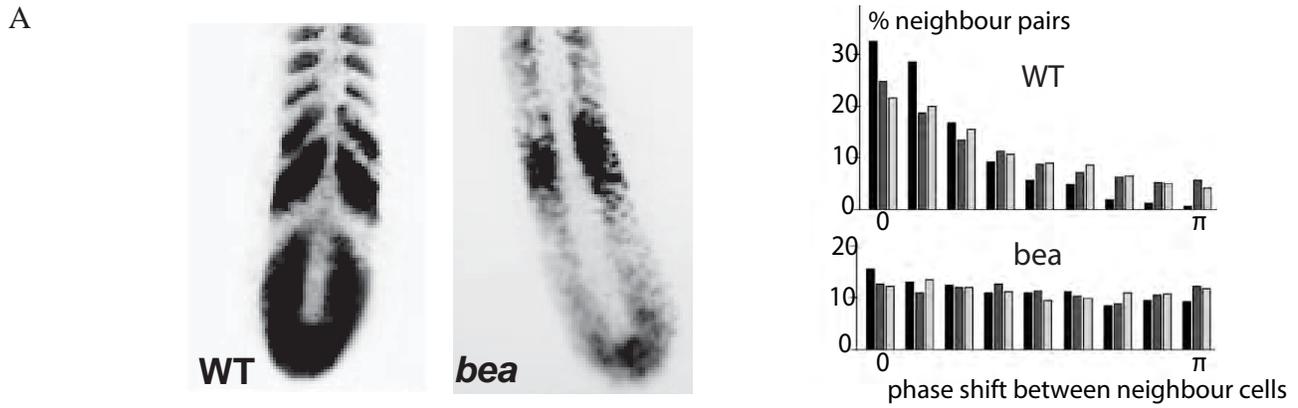
Figure 10 - Synchronization of oscillators

A. Effet of Notch inhibition in zebrafish. (*Left*) *In situ* hybridization for *DllC* in a wild-type (WT) and the *bea* mutant defective for *DllC*. (*Right*) Graph showing the distribution of phase shift of *Her1* between neighboring cells in wild-type and *bea* mutant embryos

B. Scheme illustrating the mechanism of synchronization through the Delta/Notch pathway in zebrafish

C. Scheme showing the experimental procedure used by Tsiaris and Aulehla: mouse PSM are dissociated and reaggregating by spinning; the aggregates are plated and show self-organized oscillations from several foci.

Modified from Jiang et al. (2000), Delaune et al. (2012), Oates et al. (2012), Tsiairis and Aulehla (2016)

in mutants or in embryos treated with the γ-secretase inhibitor DAPT leads to a salt-and-pepper pattern of the cyclic genes, *Her1* and *Delta-C* (Jiang et al., 2000, Horikawa et al., 2006, Riedel-Kruse et al., 2007, Ozbudak and Lewis, 2008) (Figure 10A), suggesting that oscillations persist but are not coordinated in the PSM. Use of a live reporter for Her1 confirms that neighboring cells do not harbor the same phase (Delaune et al., 2012). A model was thus proposed where *Delta-C* activates *Her* genes in the neighboring cells, leading to the synchronization of oscillators (Lewis, 2003, Mara and Holley, 2007) and where Notch signaling is required for the synchronization but not the emergence itself of oscillations (Figure 10B). However, tracking of individual cells shows that the period of oscillation drastically change upon Notch inhibition and it is not clear whether this is due to fluctuations in gene expression or *bona fide* oscillations with noise (Delaune et al., 2012).

This noise could arise from cell division, stochasticity in gene expression or random cell movements (Horikawa et al., 2006, Uriu et al., 2010). Webb and colleagues described a system of isolated cells where Her1 oscillations exist and have a regular profile - albeit with a longer period that *in vivo* (Webb et al., 2014, Webb et al., 2016). As oscillations are more regular than in embryos lacking Notch activity, it is difficult to reconcile these observations with the leading hypothesis that Notch signaling is only required for the synchronization of oscillations and for the buffering against noise.

In mouse, Notch signaling was also proposed to locally synchronize oscillators (Okubo et al., 2012). Okubo and colleagues used chimeras of *Dll1* mutant cells and wild-type cells to address this question: the authors made the assumption that *Dll1*-null cells could still be activated by wild-type cells, and therefore if Notch signaling is only required for the emergence of oscillations, chimera embryo would display synchronized oscillation. However, they observed that oscillations were not fully synchronized in those chimeras, suggesting that Notch signaling is also required for the clock synchronization. A caveat of this study is that the authors did not show that individual cells, both wild-type and *Dll1*-null, did oscillate in the chimera, even if they displayed heterogeneous levels of *Lfng*. They proposed a model where Lfng inhibits Dll1 cell-autonomously, and thus, controls and synchronizes Notch signaling in the neighboring cell. Accordingly, *Lfng* mutant displays a salt-and-pepper pattern for NICD (Ferjentsik et al., 2009, Niwa et al., 2011). Further evidence of oscillators synchronization by Notch signaling comes from an *ex vivo* study, where several mouse PSM with a live reporter for *Lunatic fringe* oscillations ("*LuVeLu*") are dissociated in single cells, and then reaggregated into a two-dimensional explant (Tsiairis and Aulehla, 2016) (Figure 10C). In normal conditions, oscillators tend to synchronize together and display self-organized traveling waves, while in conditions where Notch signaling is chemically inhibited, individual cells display unsynchronized oscillations.

The existence of single-cell oscillations in mouse has been poorly studied. Using a *Hes1* live reporter, Kageyama and colleagues showed short-term "oscillations" for three cells but with a variable period and amplitude (Masamizu et al., 2006). The authors modeled this behavior using an

excitable system (see below), where noise in gene expression intermittently causes spikes of *Hes1* leading to a noisy oscillatory pattern.

Additionally, synchronization appears to have a role in setting the oscillations period. Modeling of the segmentation clock predicts that the collective period of synchronized oscillators can differ from the individual period of isolated cells: changing the coupling strength or the time delay imposed by intercellular signaling can change the collective period of gene oscillations and thus the somitogenesis period (Morelli et al., 2009). These predictions concur with the lengthening of the somitogenesis period after partial inhibition of the Notch pathway in zebrafish (Herrgen et al., 2010). Similarly, forced entrainment through periodic pulses of DeltaC using a heat-shock system can entrain cellular oscillators and likely modify their collective period (Soza-Ried et al., 2014). In mice, using the reaggregation assay described earlier, Tsiairis and Aulehla showed that mixing cells with different initial periods leads to a synchronization of their period (Tsiairis and Aulehla, 2016). This further indicates that the collective period of a population of oscillators can be tuned by local synchronization even if one cannot exclude that other secreted factors are also averaged in this experiment. As Notch mutants display a strong phenotype in mouse, a role of this pathway in setting the collective period has remained elusive. Maternal administration of the Notch inhibitor DAPT also appears to alter the somitogenesis period (Kim et al., 2011), but the direct effect of Notch inhibition on clock synchronization has not been formally tested.

Little is known about the synchronization of the Wnt and Fgf oscillations in mouse, especially in the context of Notch mutants. It is possible that extracellular cyclic factors such as Dkk1 locally synchronize the oscillations, in a manner similar to the reaction-diffusion process described for the patterning of hair follicles (Sick et al., 2006). Alternatively, the oscillations could be triggered by a simultaneous signal among neighbors (e.g. PSM specification, cell ingression), and remain synchronized in the PSM.

Traveling waves

We have seen that how oscillations can arise at the cellular level and how they can be synchronized between neighbors. We now examine the mechanisms underlying the traveling waves of gene expression initially observed by Palmeirim and colleagues. These waves do not imply the propagation of a signal as separation of the PSM into two pieces does not block their anterior progression (Palmeirim et al., 1997, Masamizu et al., 2006, Lauschke et al., 2013). In mice, existence of such waves was formally confirmed using live reporters for *Hes1* (Masamizu et al., 2006), *Lfng* (Aulehla et al., 2008), *Hes7* (Takashima et al., 2011), *Axin2* (Lauschke, 2013), *Dusp4* (Niwa et al., 2011) (Figure11). However, the traveling waves differ in their pattern: for instance, *Hes1*, *Hes7* and
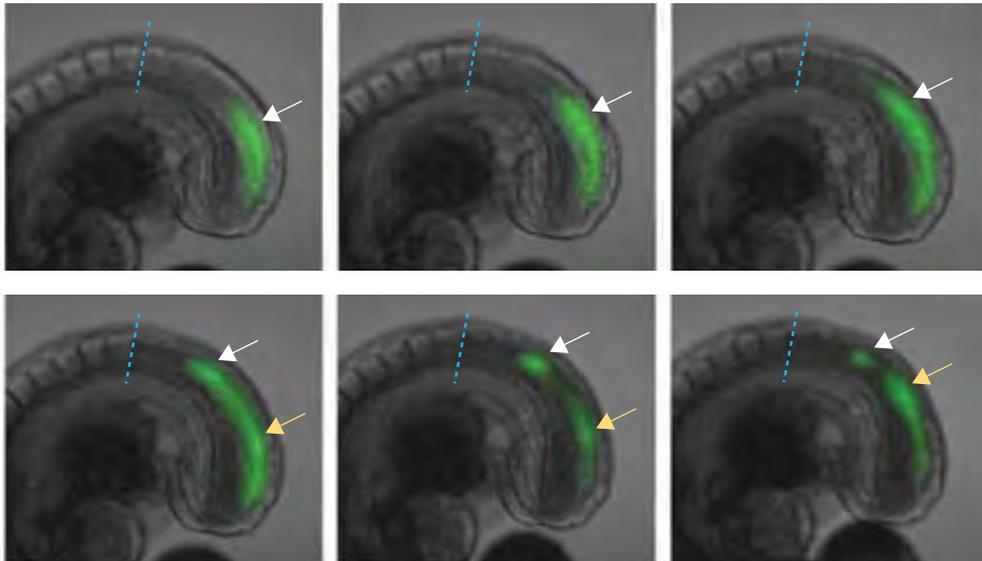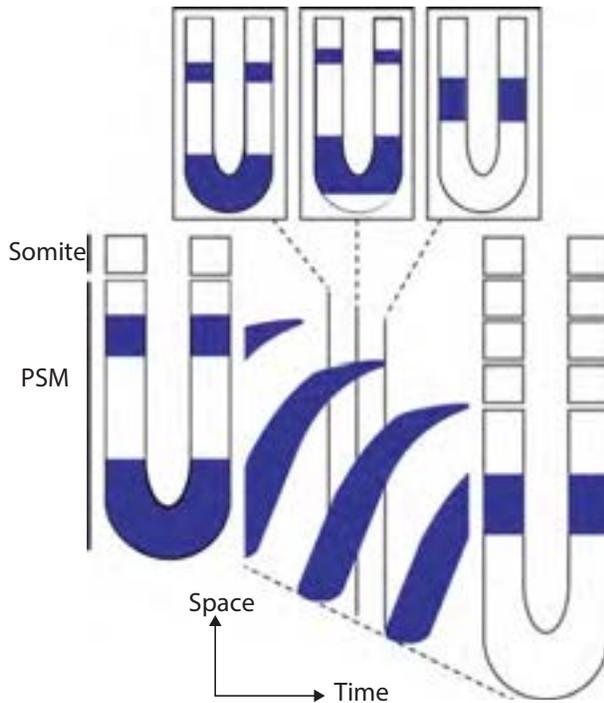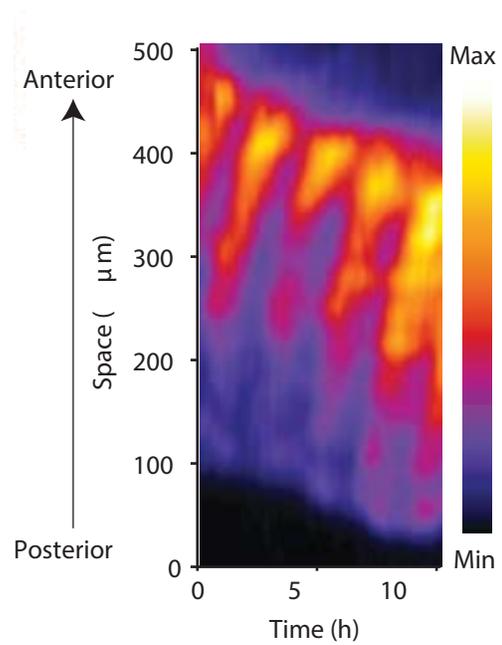
Figure 11 - Traveling waves in the PSM

A. Snapshots of the fluorescent reporter *LuVeLu* for the cyclic gene *Lunatic Fringe* (every 0.5h) ; the white arrow marks the traveling and arrest of a first wave, while the yellow arrow shows the propagation of a second wave along the PSM

B. Scheme explaining the generation of kymographs

C. Kymograph along the PSM of a LuVeLu embryo (E10.5)

Modified from Aulehla et al., (2008), Harima and Kageyama (2013), Lauschke et al. (2013)

Lfng waves are characterized by the traveling of a sharper stripe, while *Dusp4* and *Axin2* travel as larger bands. Indeed, Lauschke and colleagues showed that *Lfng* and *Axin2* have distinct slowing down profile: while *Lfng* oscillations slows-down along an *ex vivo* model recapitulating the PSM maturation, *Axin2* oscillates in an on-off fashion and then abruptly slows-down after the segment determination (Lauschke, 2013).

Mathematical models proposed that the slowing-down of the clock in the anterior PSM is sufficient for the formation of waves (Palmeirim et al., 1997, Kaern et al., 2000, Jaeger and Goodwin, 2001, Morelli et al., 2009, Ares et al., 2012, Jorg et al., 2014). Accordingly, such slowing-down was measured for *Lfng* oscillation in mouse (Tsiairis and Aulehla, 2016) and Her1 oscillations in zebrafish (Shih et al., 2015). The molecular mechanism underlying this slowing-down has not yet been elucidated. A common hypothesis is that the gradients of Fgf and Wnt activity in the PSM (that will be discussed later) control the period of the oscillations (Morelli et al., 2009). This could be mediated by a reorganization of the gene regulatory network along the antero-posterior level under the control of signaling gradients (much as described by Balaskas and colleagues for the neural tube patterning (Balaskas et al., 2012)). This is consistent with the differential regulation of *Hes7* by Fgf signaling in the posterior PSM and by Notch signaling in the anterior PSM (Niwa et al., 2007). Similarly, oscillations of phosphorylated CREB are only observed in the anterior PSM, suggesting that the segmentation clock is rewired in the anterior PSM (Lopez and Fan, 2013). Accordingly, cyclic genes in mouse and zebrafish are targets of Fgf and Wnt signaling (*Hes7* in mouse, *Hes6* in zebrafish) and it was proposed in zebrafish that the Hes/Her dimers evolve along the PSM (Trofka et al., 2012, Schröter et al., 2012).

As discussed earlier, some reports point to a regulation of the clock period by Wnt signaling (Gibb et al., 2009, González et al., 2013, Wiedermann et al., 2015). However, in the mutant with a non-degradable β-catenin, slowing-down of the *Lfng* oscillations is still observed despite a loss of the Wnt gradient arguing against this hypothesis (Dunty et al., 2008, Aulehla et al., 2008). A role for the Fgf gradient seems more likely: in chicken and zebrafish, gain-of-function for Fgf signaling was performed using a bead soaked in a ligand solution and then implanted in the PSM (Dubrulle et al., 2001, Sawada et al., 2001, Ishimatsu et al., 2010); in these embryos, the Fgf gradient was anteriorly expanded and the stripes of *Hairy2* and *Her1* were anteriorly expanded suggesting a dampened slowing-down of the clock. Furthermore, implantation of a FGF8-bead induces somitic defects that expand up to 6-7 somites (~600μm) anterior to the bead (Dubrulle et al., 2001), which are likely caused by an effect on the clock since the spreading of FGF8 should be less ~100μm (in other words, the modification of the determination front by diffusion of the morphogen from the beads cannot explain alone the effect on somites) (Toyoda et al., 2010, Muller et al., 2013). Conversely, treatment with the Fgf inhibitor SU5402 leads to a posterior shift of the *Hairy2* stripes in chicken and of the first *Her1* stripe in zebrafish consistent with a sharper slow-down (Dubrulle et al., 2001, Ishimatsu et

al., 2010). Using their reaggregation assay, Tsiairis and Aulehla observed that traveling waves with a frequency gradient spontaneously emerged in the newly formed explant (Tsiairis and Aulehla, 2016). Importantly, this was not due to cell sorting but rather to a self-organization of PSM cells. The authors also observed that a progressive cell determination was formed in parallel with a gradient of Wnt activity, further arguing that signaling gradients control the traveling of waves in the PSM. This experiment also reveals a high level of self-organization and a tight interplay (likely reciprocal) between the spatial organization of the signaling gradients and the segmentation clock.

Clock and segmentation

As discussed above, several studies link the segmentation clock to the formation of somites:

- the segmentation defects in *Hes7* and Notch mutants;
- the *Hes7* intronic mutant with a shortened period;
- the *Nrarp* (mouse) and *Hes6* (zebrafish) mutants with a longer period;

Moreover, the strong correlation between the somitogenesis period and the period of genetic oscillations further argues for a control of segmentation by the clock. This was formally demonstrated in zebrafish, where the period of Her1 oscillations in the anterior PSM corresponds to the period of somitogenesis (Soroldoni et al., 2014).

However, such role for the segmentation clock was disputed by Dias and colleagues (Dias et al., 2014). Using a system of ectopic PSM in chicken (posterior primitive streak treated with the BMP inhibitor Noggin and implanted in the extraembryonic area), they observed the formation of grapes of epithelial blocks with a similar organization as the somites, expressing *Paraxis* and able of myogenic differentiation after a secondary graft at the level of a somite. As they did not observe clear oscillations of cyclic genes, nor *Mesp2* expression by *in situ* hybridization, they concluded that the clock was not required for segmentation in Vertebrates, but only necessary to the establishment of the antero-posterior somite polarity. However, there are important limitations to this study. First, it is difficult to affirm the absence of oscillations without the use of live reporter. Second, the system is poorly characterized: the authors did not discuss whether the ectopic PSM has the same molecular signature as the PSM (e.g. expression of the markers *Tbx6*, *Msgn1* or formation of gradients within the grapes), nor whether known regulators of the segmentation clock in chicken (e.g. γ-secretase inhibitor, overexpression of *Lfng*) disrupt the formation of ectopic segment, nor whether the ectopic segments formed in line recreates the segmentation clock. Last, Dias and colleagues do not make the distinction between segmentation and somitogenesis; as discussed above, both processes can be uncoupled and the fundamental question of Vertebrate segmentation is to understand how those metameres are regularly organized along the antero-posterior axis. The formation of somite alone is

only a differentiation process and epithelium are known to self-organize in rosettes or tubes, while segmentation relates to the positioning of somite along the body axis (as an analogy, the chaotic cell determination in teratoma is fundamentally different from the elegantly orchestrated patterning occurring in the embryo). It is likely that the phenomenon observed by Dias and colleagues results from the simultaneous epithelialization of ectopic PSM cells to minimize the tissue surface tension. Nevertheless, these findings raise interesting questions about the importance of local cellular interactions during somitogenesis. This process could be at work *in vivo* as the oscillatory process described above would determine the position of determined cells which would ultimately self-organize to form a somite (Kondo, 2014). Such local organization could provide robustness to somitogenesis, but it remains to be understood how the mechanical properties of cells are tuned during development to explain the important variations of somite size within a species (~2-fold change in mouse (Gomez et al., 2008)).

5. Signaling gradients and determination of the PSM

In the previous section, we have shown that oscillations in gene expression and signaling pathways underlie the segmentation of Vertebrates and provide the molecular basis for its periodicity. What controls the spatial distribution of segmental genes? We now examine how the signal from the clock is translated into the activation of segmental genes and how signaling gradients can provide positional information.

Morphogen gradients during development

We first present some general principles about the formation and interpretation of signaling gradients during embryogenesis (Figure 12).

Interpretation of morphogen gradients

The idea that the distribution of diffusive signals control the genetic patterning of the embryo has emerged after three main advances: i) the discovery by T.Boveri (1901) and T.H. Morgan (1901) that neighboring tissues can influence the cell fate during sea urchin blastomeres differentiation and regeneration of planarians respectively; ii) the hypothesis of signaling threshold from J.Rünnstrom and S.Hörstadius, while studying the dorso-ventral patterning of sea urchin; iii) the molecular framework linking those signaling thresholds to the expression of different subset of genes by L.von Ubish (1953) to explain the classical experiment of H.Speeman and H.Mangold (1924). Last, in 1969, L.Wolpert gathered these findings to propose a theory of position information during development with the "French Flag" model (Wolpert, 1969). Accordingly, cells compute their position along the embryo in function of the concentration of a morphogen; in other words, their fate is specified by specific ranges of morphogen concentrations.

Work on Bicoid provided the first direct evidence for such morphogen, as the mRNA of the transcription factor *Bicoid* was shown to diffuse within the fly syncitium and specify different antero-posterior fates depending on its dose (Driever and Nusslein-Volhard, 1988a, Driever and Nusslein-Volhard, 1988b). Notably, this was correlated with the expression of different genes, e.g. the activation of one of its target, *hunchback*, was directly linked to the binding sites at the target enhancer. Since then, the canonical model of patterning involved the gradual distribution of a factor (generally an extracellular factor) inducing a subset of discrete responses in a dose-dependent manner.
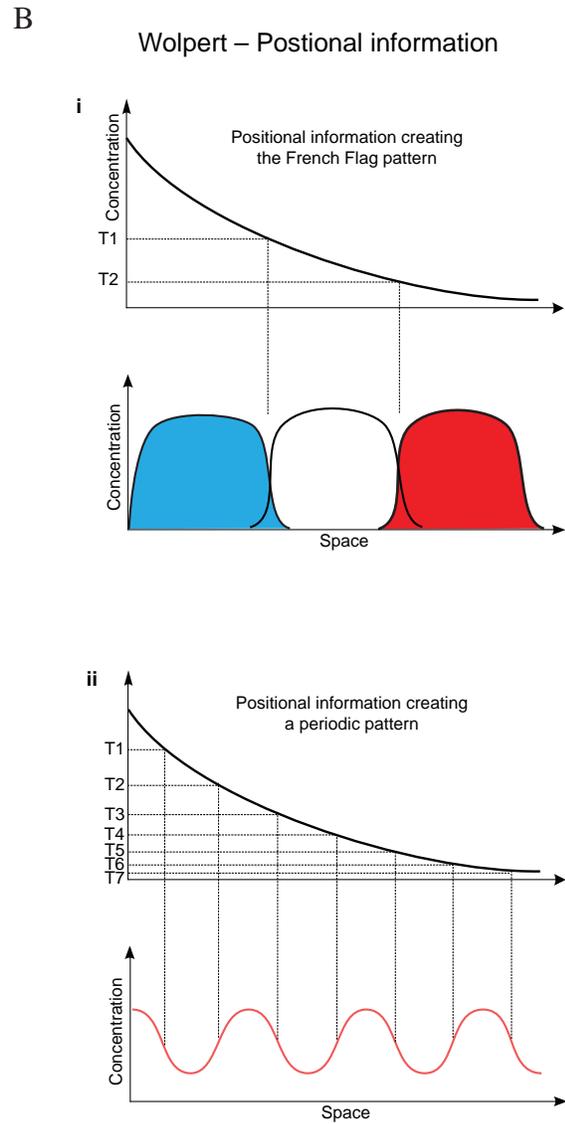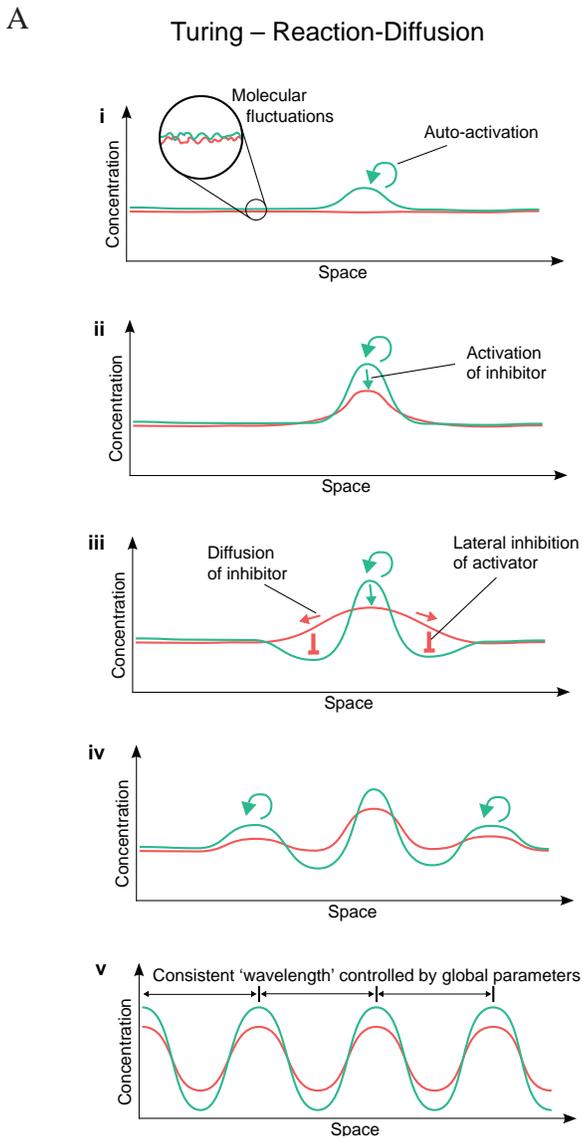
Figure 12 - Segmental patterning

A. Segmental patterning can be achieved by a reaction-diffusion mechanism through the interaction of a slow-diffusing activator and a fast-diffusing inhibitor. Random fluctuations trigger a first peak of activator, which induces a repressor that diffuses laterally around the peak. At the end, these local interactions generate a segmental pattern of the activator and repressor.

B. A morphogen gradient can specify positional information (French flag model) and create a segmental pattern based on threshold (T_i)

Modified from Green and Sharpe (2015)

Another layer of complexity was later discovered, notably in the field of Sonic Hedgehog (Shh) signaling. Shh was previously considered as a classical morphogen specifying diverse embryonic structures, such as the digits identity and the neural fate within the spinal cord in Vertebrates or the wing disc in Drosophila. However, several groups showed that the cell fate was not strictly correlated to the dose of Shh, but rather to its overall dynamics (Ahn and Joyner, 2004, Harfe et al., 2004, Dessaud et al., 2007, Nahmad and Stathopoulos, 2009, Dessaud et al., 2010). Indeed, a negative feedback loop with the inhibitor Patched represses Shh signaling, leading to the model where cells integrate the signal over time to drive the expression of different targets. However, the idea persisted that the absolute level of signaling (yet integrated over time) was specifying distinct target genes expression and cell fates.

Later, the concept of morphogen gradient was further refined by proposing that gradients do not instruct specific targets *per se*, but rather control the deployment of a specific gene regulatory network (Briscoe and Small, 2015). That is, the interpretation of the morphogen gradient occurs at the level of the network, and not at the level of each target. This view comes from works disputing the strict correlation between the level of a morphogen and the cell fate, e.g. Shh in the neural tube patterning (Balaskas et al., 2012) or the level of Bicoid in the fly (Chen et al., 2012b).

As put by Balaskas and colleagues, "*morphogen interpretation is an emergent property of the architecture of a transcriptional network*". This view reminds the self-organization at work in reaction-diffusion, another class of processes proposed to explain the patterning of embryos. Such mechanism was first proposed by A.Turing and relies on local interactions of diffusing morphogens reacting with each other; notably, it was shown that a model of short-range activator and long-range inhibitor could generate a variety of patterns (Turing, 1952). This model has been classically and wrongly opposed to Wolpert's view of patterning: while the former proposed that patterning results from self-organization and local interactions, the later suggested an instructive process imposed by large-scale gradients (Green and Sharpe, 2015). However, reaction-diffusion mechanisms can generate patterns by interacting with signaling gradients (Meinhardt, 1986, Glimm et al., 2012, Sheth et al., 2012, Raspopovic et al., 2014, Hiscock and Megason, 2015). In these models, morphogen gradients fine-tune parameters of the reaction-diffusion process, but the final pattern is the result of the downstream interactions between activators and repressors. One can argue that there is also a degree of self-organization with traditional morphogen gradients, since the interactions of downstream targets give rise to the final pattern. While reaction-diffusion mechanisms insist on the spatial dynamics of the activator and repressor at the tissue level, the later focuses more on the temporal dynamics of targets at the cellular level, but in both cases morphogen gradients only bias cellular processes that are later refined.

Formation of morphogen gradients

After having considered how morphogen gradients are interpreted, we briefly turn to the mechanisms of gradient formation in the embryo.

Morphogen gradients have been first proposed to arise from a source and sink mechanism (Crick, 1970), where the molecules are secreted at one extremity of the tissue and degraded at the other end. This model results in a linear distribution of the morphogen along the tissue; however, measurements of the profile for different gradients revealed an exponential gradient, indicative of an additional clearance over the entire tissue (Wartlick et al., 2009); this led to model of synthesis-diffusion-clearance. While this can be modeled as a diffusive process, morphogen rarely diffuse *in vivo* as in a Brownian motion and the precise mechanism can vary between gradients. Notably, morphogens diffusion can be "hindered" by the tissue geometry or by extracellular components, or occur by shuttling or cell protrusions (cytonemes) (Rogers and Schier, 2011, Muller et al., 2013).

The actual distribution of the morphogen gradient could result from the progressive differentiation of the tissue, as the polarity of an embryonic stage will lay out the polarity of the next embryonic stage (e.g. maternal determinants in Xenopus bias the formation of the BMP gradient patterning the dorso-ventral axis of the embryo). However, recent findings on tridimensional aggregates from differentiated embryonic stem cells ("organoids") reveal that such polarity can also result from self-organization (Turner et al., 2016). That is, relatively homogenous populations of differentiated stem cells are able to generate patterns and polarized structures, such as the retina cup (Eiraku et al., 2011) or the brain (Lancaster et al., 2013). Interestingly, a system of neuroepithelial organoids can recapitulate the formation of the Shh gradient involved in the dorso-ventral patterning of the neural tube (Meinhardt et al., 2014). This suggests that developmental programs do not simply unfold with cells passively reading gradients, but rather that cells actively shape their interactions to generate patterns. However, this might rather reflect a self-regulation of the system by opposition to the pure self-organization occurring in non-biological systems as other factors (e.g. strong heterogeneities, mechanical factors) likely provide positional clues to orient and amplify the patterning.

In the PSM, several morphogen gradients have been functionally involved in the PSM, notably the gradients Fgf4, Fgf8 (in a redundant manner) and Wnt3a (Aulehla and Pourquie, 2010) (Figure 13). Their polarity (high levels of Fgf/Wnt in the posterior PSM and low levels in the anterior PSM) was proposed to be acquired by a mechanism of RNA decay, where a gradient of mRNA imposes a gradient of protein and downstream signaling. This is markedly different from the synthesis-diffusion-clearance model described earlier: the protein gradient is mainly formed by transport of its mRNA, not by diffusion. Indeed, it was shown that cells leaving the primitive streak (or tailbud) stop the transcription of *Fgf8*, leading to the progressive degradation of the mRNA and the formation of a protein gradient (Dubrulle and Pourquié, 2004). Specifically, Dubrulle and Pourquié showed that *Fgf8* is only transcribed in the tailbud using an intronic probe and that its distribution along the PSM

is not affected by actinomycinD, an inhibitor of transcription. It is likely that the gradients of *Fgf4* and *Wnt3a* are formed by a similar mechanism. While this explains the global formation of the gradient at the level of the entire PSM, other mechanism could locally refine the diffusion of the ligands as it has been described in other developmental contexts.

The formation of the Fgf8 gradient has been well described in zebrafish, where it is thought to occur by "hindered diffusion" (Muller et al., 2013). Yu and colleagues used a fluorescent fusion of FGF8 in zebrafish gastrula to show that it diffuses as a single-molecule (53 $\mu m^2.s^{-1}$) and that its clearance is controlled by endocytosis (Yu et al., 2009). However, this measure of diffusion by FCS mainly addresses the local "jiggling" of the proteins; later studies using FRAP showed that its effective diffusion is much lower (2 $\mu m^2.s^{-1}$), mainly because of the interactions between FGF8 and the heparan sulfate proteoglycans (HSPG) (Muller et al., 2013). Little is known about the diffusion of the FGF8 ligand in the PSM; however, experiment from Delfini and colleagues would suggest a directional diffusion of the ligand, as implantation of a FGF8-soaked bead results in an increase of pERK staining only anteriorly to the bead (Delfini et al., 2005) (alternatively, downstream signaling could account for that observation). This also leads to asymmetric defects in the position of somite boundaries (only the segments anterior to the beads are affected) (Dubrulle et al., 2001). FGF4-soaked beads induce symmetric defects in chicken, indicating a possible difference in the diffusion of both ligands (Dubrulle et al., 2001); however, this likely reflects a technical issue as *Fgf4* and *Fgf8* are redundant in the mouse PSM (Naiche et al., 2011).

The regulation of Wnt3a gradients in Vertebrate embryos remains less studied; however, it was shown in other developmental systems that Wnt ligands are lipid-modified (palmitoylation) and travel through lipoproteins particles associated to the plasma membrane ("argosomes" – (Greco et al., 2001)) (Mikels and Nusse, 2006). Conversely, in an *in vitro* model of the intestinal crypt, it was proposed that WNT3 proteins do not travel at all, but only spread through cell divisions in a cell-bound manner (Farin et al., 2016).

Signaling gradients in the PSM

Several signaling gradients have been described in the PSM and implicated in somitogenesis and segmentation. We now examine their function in these different processes: the apparition of segments (as seen with the stripes of Mesp factors) and the progressive differentiation of the PSM (as seen with the progressive changes in gene expression). The posterior boundary delimitating the last segment specified by a stripe of Mesp2 is classically defined as the "determination front".
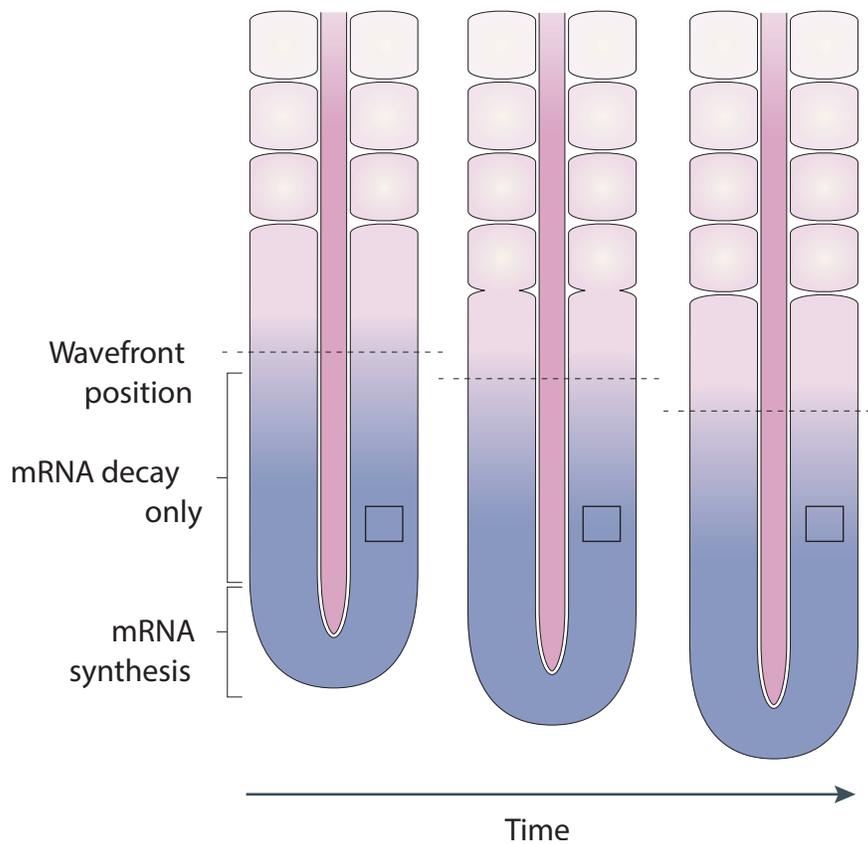
Figure 13 - Gradients in the PSM

Scheme showing the mechanism of gradients formation in the PSM by RNA decay.

The production of ligands transcripts stops when cells leave the tailbud leading to the formation of a gradient of mRNA. This gradient is later converted into a gradient of protein and signaling. A threshold of signaling is thought to position the wavefront (or determination front), and thus the position of the last determined segment.

Modified from Hubaud and Pourquié (2014)

A gradient of Fgf signaling exists along the PSM with a strong activity in its posterior part as evidenced by the phosphorylation of ERK and by the expression of its downstream targets (Sawada et al., 2001, Delfini et al., 2005, Niwa et al., 2007). Early studies in chicken demonstrated that Fgf signaling promotes a posterior, unsegmented state, as overexpression of Fgf8 delays somite formation, activation of the myogenic program and PSM differentiation (as evidenced by a shift in *Paraxis*), and prolongs the expression of posterior, undifferentiated PSM markers such as *Brachyury* (Dubrulle et al., 2001). Gain-of-function experiments using a constitutively-active Mkk1 show that electroporated cells are not incorporated in the somites and do not express *Mesp2* or *Paraxis* while maintaining *Tbx6* and *T* expression (Delfini et al., 2005). Last, Fgf signaling contributes to the positioning of somite boundaries, as ectopic activation or repression of the pathway leads to smaller and larger somites respectively (Dubrulle et al., 2001, Sawada et al., 2001) (Figure 14A). In mouse, a similar role was shown using a conditional mutant for the receptor *FgfR1* and double mutants for the ligands *Fgf4* and *Fgf8* (Figure 14B). In the *Fgf4/8* mutant, where both genes are inactivated by a T-Cre driver, there is a posterior shift of *Mesp2*, as well a shift in the PSM differentiation as evidenced by the gain of *Mox1* expression and the lost of posterior markers *Tbx6*, *Wnt3a* or *T* (Naiche et al., 2011). While these findings confirmed a model where the Fgf gradient controls both the segmentation and the determination of the PSM, other genetic mutants offered contradictory phenotypes.

Boulet and Capecchi used a different Cre driver (HoxB1) to inactivate both *Fgf4* and *Fgf8* (Boulet and Capecchi, 2012). This Cre driver starts to be active in the caudal primitive streak at E7 and effects on Fgf targets such as *Etv4* (also known as *Pea3*) are discernible starting at E8.5. While posterior PSM markers such as *Tbx6* or *Msgn1* are downregulated at this stage, there is no clear posterior shift in *Mesp2* expression at E8.5, nor posterior shift of somite formation as suggested by the normal antero-posterior pattern of *Uncx4*.1 at E9.5. In the *TCre;FgfR1* mutant, a similar phenotype is observed: the decrease in Fgf signaling is less pronounced than in the *TCre;Fgf4/8* mutant (as evidenced by the remaining *Sprouty2* expression at E8.75 compared to its complete loss in the *TCre;Fgf4/8* mutant at E7). However, microarray analysis reveals that other Fgf receptors are expressed in the mouse posterior PSM; *FgfR2* (low level) and *FgfR3* (low level) (Chal et al., 2015). Also, the actual protein distribution of FgfR1 has not been examined in wild-type or mutant, especially considering that its mRNA is more expressed in the anterior PSM and almost absent in the posterior PSM (Wahl et al., 2007). This could explain why the posterior shift in PSM differentiation is not clearly observed (no posterior shift of *Paraxis*, *Raldh2*, *T*), even if some posterior markers are downregulated (*Cyp26a1*, *Msgn1*). The position of *Mesp2* appears to be shifted

A

Addition of Fgf inhibitor   **Addition of FGF bead**

B

	T-Cre; FgfRI^{f/f}	*T-Cre; Fgf4^{f/Δ}; Fgf8^{f/Δ} (NA)*	*Hoxb1-Cre; Fgf4^{f/Δ}; Fgf8^{f/Δ} (B)*	*T-Cre; Ctnnb1^{lox(ex3)/+}; Fgf4^{f/Δ}; Fgf8^{f/Δ} (NA)*	*T-Cre; Ctnnb1^{lox(ex3)/+} FgfRI^{f/f} (A)*
Sprouty2	Progressively downregulated (W)	Absent			
Sprouty4	Absent (N)	Absent			
Dusp4	Absent (N)				Absent
Etv4 (Pea3)	Progressively downregulated (W)	Absent	Progressively downregulated		
T	Normal (W)	Downregulated	Progressively downregulated	Partial rescue	
Tbx6		Absent	Severely downregulated	Partial rescue	
Msgn1	Posteriorly shifted (W)		Severely downregulated		
Hes7	Absent (N)	Absent			
Lfng	Weakly and steadily expressed in the PSM (except its anterior band) (W) ; Steadily expressed through the PSM (N)	Expanded through the PSM; weakly expressed	Expanded through the PSM; weakly expressed	Expanded through the PSM; weakly expressed	Weakly expressed in several stripes - as in the *T-Cre;Ctnnb1^{lox(ex3)/+} FgfRI^{f/+}*
Raldh2	Normal (W)		Normal		
Meox1		Posteriorly shifted		Posteriorly shifted	
Paraxis	Downregulated, no shift (W)				
Mesp2	Downregulated, no shift (W) ; posteriorly shifted (O)	Posteriorly shifted	Downregulated, no shift		Anteriorly shifted; partial rescue of the anterior shift observed in *T-Cre; Ctnnb1^{lox(ex3)/+} FgfRI^{f/+}*

Figure 14 - Role of the Fgf and Wnt pathways in setting the determination front

A. Scheme showing the effects of Fgf/Wnt signaling on somitogenesis. (*Left*) Inhibition of the Fgf pathway by a FgfRI inhibitor (SU5402) leads to a posterior shift of the somite boundary and larger somites. (*Right*) A local increase of Fgf (or Wnt) signaling by addition of a bead leads to an anterior shift of the boundary and smaller somites.

B. Summary of the phenotypes of the Fgf and Wnt mutants W: (Wahl et al., 2007); N: (Niwa et al., 2007); O: (Oginuma et al., 2008); NA: (Naiche et al., 2011); B: (Boulet and Capecchi, 2013); A: (Aulehla et al., 2008)

Modified from Saga and Takeda (2001)

posteriorly (Wahl et al., 2007, Oginuma et al., 2008b), but in a lesser extent as for the *T-Cre;Fgf4/8* mutant.

Based on these experiments, it was argued that Fgf signaling does not act as a determination front, but rather on the specification of the mesoderm (Mallo, 2015). Alternatively, Fgf signaling could provide such positional information in the wild-type position, but the PSM maturation and segmentation could also require Fgf signaling. In other words, in these mutants, the paraxial mesoderm could lose the gene regulatory network that would normally respond to the inhibition of Fgf signaling. Accordingly, the segmentation clock is severely affected in the *HoxB1-Cre;Fgf4/8* and *T-Cre;Fgf4/8* mutants and cyclic genes such as *Lfng* become expressed at a low level, as well as *Mesp2* (Wahl et al., 2007, Boulet and Capecchi, 2012). Similarly, there is no expansion of the retinoic acid gradient (as we will discuss later, there is an inverse gradient of RA activity in the PSM) in those mutants despite the loss of the RA inhibitor *Cyp26a1* ((Wahl et al., 2007, Boulet and Capecchi, 2012), while the mutant for *Cyp26a1* exhibits a clear shift in RA activity until the tail tip (Sakai et al., 2001). This could be explained by a requirement of Fgf for the activation of factors promoting the maturation and segmentation of the PSM, such as the segmentation clock or positive factors of retinoic acid signaling (e.g. *RARgamma* that is expressed in a posterior gradient (Abu-Abed et al., 2003)). The discrepancy between early and late stages seen in *TCre;Fgf4/8* (where *Mesp2* and retinoic acid signaling do expand) vs. *HoxB1;Fgf4/8* could be explained either by different dynamics to clear Fgf signaling or by a difference in the patterning of anterior somites, consistently with the phenotype of mesodermal mutants discussed earlier. Further evidence for the role of Fgf signaling in the positioning of segments comes from treatment of embryos in the FgfR inhibitor SU5402 and the Fgf activator BCI (Dusp6 inhibitor), which display a posterior and anterior shift respectively in the posterior limit of *Mesp2* expression in mice (Niwa et al., 2011). As there is a clear boundary between the posterior limit of *Mesp2* and the anterior limit of Fgf signaling (as evidenced by *Dusp4* expression or pERK staining (Oginuma et al., 2008b, Niwa et al., 2011)), it was suggested that Fgf signaling directly represses the activation of the segmental program. However, this is not conserved in zebrafish or chicken as there is a clear separation between the anterior limit of pERK and the posterior limit of *Mesp* factors (Delfini et al., 2005, Akiyama et al., 2014, Bajard et al., 2014), raising the possibility that downstream targets of Fgf/ERK rather mediate these effects on the determination front. Taken together, these findings suggest that Fgf signaling opposes the differentiation of the PSM and promotes a posterior state, while it appears to indirectly position the determination front.

Wnt signaling

Similarly to Fgf signaling, the Wnt pathway displays an activity gradient along the antero-posterior PSM, as evidenced by the distribution of nuclear β-catenin (Aulehla et al., 2008), by the activity of

the transcriptional reporter *BAT-GAL* (Aulehla et al., 2003) or by the pattern of targets like *Axin2*, whose oscillation amplitude is stronger in the posterior PSM (Aulehla et al., 2003). The mechanism responsible for the gradient formation has not been studied; however, it is likely that a similar RNA decay mechanism is at work, as *Wnt3a* mRNA is distributed in a gradient along the PSM.

Loss of Wnt signaling by conditional ablation of β-catenin leads to a loss of PSM markers, and is difficult to interpret because of the loss of the tissue (Dunty et al., 2008). Mutants for *Wnt3a* also have defects in paraxial mesoderm formation; Dunty and colleagues observed that young embryos (0-4 somites) mutant for *Wnt3a* shows a slight posterior shift of *Mesp2* suggesting that Wnt signaling also contributes to the positioning of segments along the PSM (Dunty et al., 2008). However, genetic loss of Wnt activity is hard to interpret given the loss of mesoderm. Conversely, the loss of Wnt signaling in zebrafish has been studied in more details by Bajard and colleagues. Indeed, the authors used a heat-shock inducible system for the Wnt inhibitor Dkk1 and examined the position of Mesp factors (*mesp-b*), as well as the position of Wnt activity (Bajard et al., 2014). Interestingly, they showed that there is a shift of nuclear β-catenin one hour after the heat shock, but the posterior shift in *mesp-b* position is only observed after three hours. This suggests that the level of β-catenin does not directly control the position of the segment in zebrafish. The authors rather proposed that the position of the determination front is controlled by the activity of downstream Wnt targets, such as Msgn1.

However, gain-of-function experiments in mouse only partially support this model. Forced expression of *Msgn1* or of a non-degradable β-catenin using a condition *T-Cre* driver blocks somite formation (Dunty et al., 2008, Aulehla et al., 2008, Chalamalasetty et al., 2014). Local addition of Wnt3a through beads of NIH-3T3 cells expressing Wnt3a also shifts anteriorly the position of somites (Aulehla et al., 2003). However, even if *Mesp2* is anteriorly shifted in the β-catenin gain-of-function mutant (Dunty et al., 2008, Aulehla et al., 2008), forced activation of the Wnt pathway does not preclude its activation suggesting that Wnt does not control *per se* the position of the determination front. Similarly, forced expression of *Msgn1* does not fully extend the Tbx6-positive domain (Chalamalasetty et al., 2014). Differentiation of the PSM also takes place in the β-catenin gain-of-function mutant, as evidenced by the expression *Paraxis*, *Raldh2* or *Mox1*; however, not all differentiation markers are expressed in this context, as *Tbx18* and *Uncx4*.1 are strongly downregulated (Dunty et al., 2008, Aulehla et al., 2008). Therefore, Wnt signaling does not seem to control the position of segments, but rather blocks some aspects of the PSM differentiation. The observed effects on segment position could be explained by its regulation of the Fgf pathways, as we will now discuss.

Interaction Fgf/Wnt

Studies of the relative contribution of the Fgf and Wnt pathways are limited by the crosstalk between the two pathways. Indeed, activation of the Wnt pathway by a non-degradable β-catenin induces an up-regulation of *Fgf8*, while loss of Wnt signaling in the Wnt3a or β-catenin mutant leads to a decrease of *Fgf8* (Dunty et al., 2008, Aulehla et al., 2008). Conversely, loss of Fgf signaling in both double *Fgf4/8* mutants leads to a decrease in the expression of *Wnt3a* (Naiche et al., 2011, Boulet and Capecchi, 2012), even if this effect is not seen in the *TCre;FgfR1* mutant (Wahl et al., 2007). Naiche and colleagues tried to narrow down the specific effects of Fgf signaling, by using a combination of *Fgf4/8* loss-of-function and non-degradable β-catenin expression driven by *T-Cre*. Interestingly, Wnt overactivation rescues the loss of paraxial mesoderm as seen by the expression of *Tbx6* but a posterior shift of the PSM differentiation (*Mox1*) and likely segmentation (*Lfng*) is still observed (Naiche et al., 2011). Aulehla and colleagues reported contradictory results when using a compound mutant for *FgfR1* and the non-degradable β-catenin. They observed a posterior shift in Fgf activity; however *Mesp2* expression is still anteriorly shifted (albeit in a less pronounced manner than in the single non-degradable β-catenin mutant) (Aulehla et al., 2008). Even if reservations could be made over the use of the *FgfR1* mutant as discussed earlier, these results would argue against a direct role for Fgf in the positioning of the determination front as proposed by Naiche and colleagues and rather point toward a complex epistasis between the two pathways.

Together, these findings do not lead to a clear model of the determination front. While it was previously proposed that Fgf and/or Wnt signaling provide threshold of activity defining such front, it is more likely that dampening of their activity is only necessary for the determination of the PSM and its segmentation. In other words, the position of the segmental genes seems to not be determined by a single level of Fgf and/or Wnt, but rather by the gene regulatory network downstream of Fgf and Wnt. It also prompts the use of *ex vivo* methods, where these signaling pathways can be carefully manipulated and quantitatively monitored.

Retinoic acid

A gradient of retinoic acid (RA) activity exists along the paraxial mesoderm, with a strong activity in the somites that gradually decreases in the anterior PSM and is absent in the posterior PSM (Rossant et al., 1991, Shimozono et al., 2013). Contrarily to the Fgf and Wnt gradients, this gradient is formed by a source and sin" mechanism, with synthesis of RA in the somites through the localized expression of the enzyme *Raldh2* (source) and with a degradation of the retinoic acid by *Cyp26a1* in the tailbud (sink) (Niederreither et al., 1997, Niederreither et al., 2002).

Reducing RA anteriorly shifts the Fgf gradient, and thus, leads to smaller somites (Diez del Corral et al., 2003, Kawakami et al., 2005, Sirbu and Duester, 2006, Vermot and Pourquié, 2005, Vermot et al., 2005). In Xenopus, it was proposed that RA signaling directly activates the expression of the

Mesp2 homologue, *Thylacine1* (Moreno and Kintner, 2004, Moreno et al., 2008). However, this direct effect seems limited to the frog as RA is not strictly required for *Mesp2* expression in mouse. Indeed in the *Cyp26a1* mutant, no posterior shift of *Mesp2* is observed (Morimoto et al., 2005) and *Raldh2* mutants are still able to form anterior somites (Vermot et al., 2005, Sirbu and Duester, 2006). Furthermore, at later stages (>10 somites), *Mesp2* is expressed posteriorly to the domain of RA activity (as evidenced by the *RARE-LacZ* reporter) and its activation does not require RA activity in *Raldh2* mutant whose early RA-dependent defects were rescued by administration of exogenous RA (Sirbu and Duester, 2006).

The gradient of RA signaling in the paraxial mesoderm is therefore unlikely to position the determination front. It was rather shown that RA is important for the bilateral symmetry of segmentation in Vertebrates. Indeed loss-of-function and gain-of-function experiments lead to an asymmetry of somite formation between the left and right PSM at specific embryonic stages (Kawakami et al., 2005, Vermot and Pourquié, 2005, Vermot et al., 2005, Echeverri and Oates, 2007, Vilhais-Neto et al., 2010). Loss of RA signaling contributes to the expansion of the gradient of *Fgf8* mRNA on the right PSM and leads to fewer segments on this side (Vermot et al., 2005). This is accompanied by an asymmetry in the segmentation clock as revealed by the asynchrony for *Lfng* and *Hes7* oscillations in mouse (Vermot and Pourquié, 2005, Vermot et al., 2005, Vilhais-Neto et al., 2010). Vermot and Pourquié identified a genetic interaction between the *Raldh2* mutation and the *iv* mutation (mutation for a dynein involved in the left-right symmetry) (Vermot and Pourquié, 2005): while the asymmetry is one-sided in the *Raldh2* mutant, it becomes random in the *Raldh2-/-;iv-/-* double mutant. This suggests that RA signaling buffers the asymmetrical distribution of signals linked to the lateralization of other tissues such as the lateral mesoderm (Hornstein and Tabin, 2005, Brent, 2005). That is, in the *Raldh2* mutant, the left-right asymmetry of these neighboring tissues is unaffected and the signal imbalance is one-sided, leading to a consistent lateral bias in somitogenesis, while in the double mutant, this asymmetry becomes randomized, and induces random, two-sided defects in somitogenesis.

Other roles of retinoic acid signaling have been reported and remain to be studied in more details, such as the control of the head-to-trunk transition in zebrafish (Retnoaji et al., 2014) and the somitogenesis period in chicken (Resende et al., 2010).

Regulation of Mesp factors expression

Formation of segments

As Mesp2 is central to the segmentation of the PSM, we now present how its expression is controlled in mouse and how it integrates signals from both the segmentation clock and signaling gradients. *In*

situ hybridization and live imaging showed that *Mesp2* is first expressed as a large band of a size equivalent to a somite, and then becomes restricted to the anterior half of the segment (Takahashi et al., 2000, Morimoto et al., 2005). Mesp2 requires Notch signaling as its expression is reduced in Notch mutants (Barrantes et al., 1999, Takahashi et al., 2003). Additionally, enhancer analysis of *Mesp2* revealed that Tbx6 is an activator of *Mesp2*: the enhancer contains T-Box binding sites (Yasuhiko et al., 2006), which are bound by Tbx6 *in vivo* and whose mutation in mouse leads to a loss of *Mesp2* expression (Yasuhiko et al., 2008). Moreover, a transcriptional reporter for *Mesp2* is activated *in vitro* by ectopic expression of Tbx6 (Yasuhiko et al., 2006). While the *Mesp2* enhancer also contains RBPJ-κ binding sites, overactivation of the pathway by expression of RBPJ-κ::VP16 (fusion of RBPJ-κ with the transcriptional activation domain VP16) does not induce the reporter activation (Yasuhiko et al., 2006). In the mice overexpressing NICD, ectopic expression of *Mesp2* is not detected, suggesting that Notch alone cannot activate *Mesp2 in vivo* (Feller et al., 2008). Interestingly, Yasuhiko and colleagues showed that Notch signaling potentiates the effect of Tbx6, as co-expression of these activators with Tbx6 leads to a strong expression of the reporter (Yasuhiko et al., 2008). Furthermore, detailed examination of the dynamics of *Mesp2* activation shows a tight correlation between the traveling of the Notch wave (NICD) and the activation of this gene, as well as between the anterior boundary of both Tbx6 and *Mesp2*. This further suggests that Notch induces *Mesp2* in a Tbx6-dependent manner (Oginuma et al., 2008b). Together, this provides a molecular link between the segmentation clock and the segmentation program, as pulses of Notch activate *Mesp2*.

Despite the presence of Notch signaling and Tbx6 in the posterior PSM, *Mesp2* is not expressed suggesting the existence of a repressive mechanism. Fgf/ERK was proposed to mediate this effect in mouse, since there is a clear separation between the posterior boundary of *Mesp2* and the anterior boundary of pERK in mouse and since changes in Fgf/ERK are correlated with a shift in *Mesp2* expression. However, as previously discussed, this does not explain the phenotype of the compound mutant harboring Fgf loss-of-function and Wnt gain-of-function. Therefore, the inhibitory mechanism restricting the expression of Mesp2 in the posterior PSM remains to be elucidated.

The mechanism defining the anterior boundary of *Mesp2* has been studied in details by Oginuma and colleagues. They identified a negative feedback mechanism regulating the expression of *Mesp2*, where Mesp2 induces the degradation of Tbx6 by the proteasome pathway (Oginuma et al., 2008b). Therefore, as Mesp2 specifies the segment N, the degradation of Tbx6 assures that the anterior boundary of the next stripe of *Mesp2*, and thus the anterior boundary of the segment N+1, corresponds to the posterior boundary of the segment N (Figure 15A). It was later shown that the degradation of Tbx6 is mediated by Ripply2, a Mesp2 target (Morimoto et al., 2007, Takahashi et al., 2010), and a similar mechanism has been described in zebrafish (Wanglar et al., 2014).
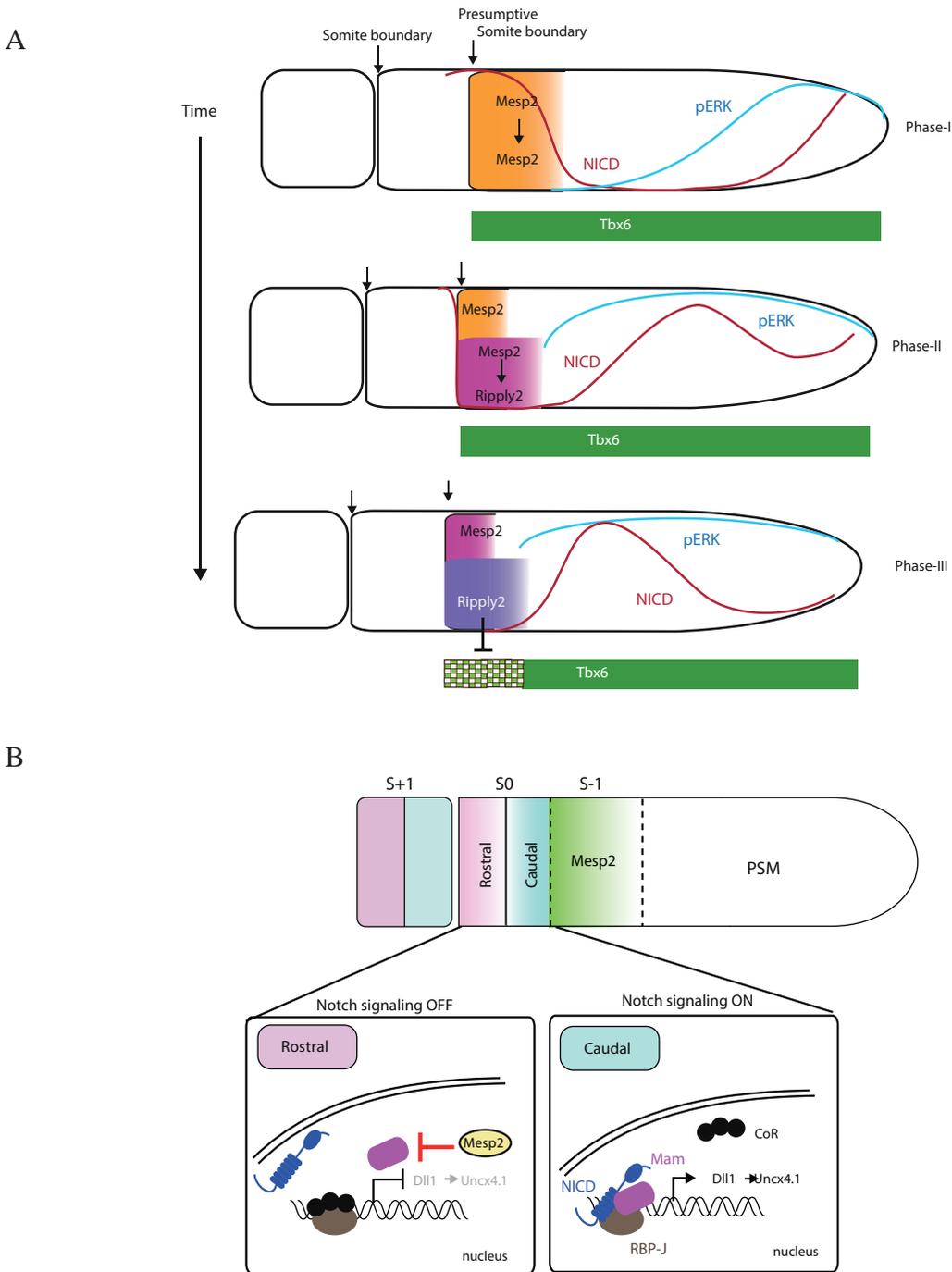
Figure 15 - Specification of intersegmental and intrasegmental boundaries by Mesp2

A. Scheme showing the interplay between Mesp2, Tbx6 and Ripply2 to assure the consecutive specification of somite boundaries (see text for detail)

B. Scheme showing the molecular control of the rostro-caudal polarity (also known as antero-posterior polarity): the restriction of Mesp2 in the anterior compartment leads to the partition of Notch signaling within the forming segment. The Notch pathway becomes inactive in the anterior half and active in the posterior half.

Modified from Saga (2012)

Formation of half-segments

In addition to its role in segment and somite formation, Mesp factors control the antero-posterior polarity of the somite. *Mesp2* mutants have defects in antero-posterior somite polarity, as the remaining paraxial mesoderm is caudalized (Takahashi et al., 2000). Several genetic studies have demonstrated that Mesp2 directs the rostrocaudal polarity of the newly formed segment by repressing Notch signaling in the rostral compartment, while activation of this pathway confers a caudal identity to the somites (Figure 15B). Accordingly, a partial loss of Notch signaling in the *Psen1* mutants blocks the specification of the caudal compartment (Koizumi et al., 2001), while overexpression of NICD leads to a uniform expression of caudal markers (Feller et al., 2008). Furthermore, activation of Notch signaling in the rostral compartment by expression of RBPJ-κ-VP16 under the control of the *Mesp2* enhancer leads to a caudalization of the somites, but blocking Notch signaling in this region with a dominant-negative RBPJ-κ rescues the phenotype of the *Mesp2* mutant (Sasaki et al., 2011). It was first proposed that the repression of Notch by Mesp2 was mediated by its induction of the repressor Lfng in the rostral compartment (Morimoto et al., 2005). However, the expression of *Lfng* in the rostral compartment is not necessary for a correct rostro-caudal polarity as Oginuma and colleagues showed using a mutant rescuing the oscillations of *Lfng* in the PSM but not its anterior expression induced by Mesp2 (Oginuma et al., 2010). Its forced expression under the control of the *Mesp2* promoter also does not rescue the loss of polarity in the *Mesp2* mutant (Oginuma et al., 2010). The effect of Mesp2 on Notch signaling was rather proposed to be mediated by the destabilization of the co-activator Mastermind-like 1 (Sasaki et al., 2011).

If the restriction of Notch signaling by Mesp2 is crucial to the acquisition of the somite polarity, what controls the restriction of Mesp2 in the rostral compartment? Oginuma and colleagues proposed that the traveling wave of NICD is sufficient to reproduce the antero-posterior polarity of *Mesp2* using mathematical simulations (Oginuma et al., 2010). Their model is essentially based on the restriction of the Notch wave in the anterior compartment, enabling the accumulation of *Mesp2* and the specification of the rostral identity. Clearance of Mesp2 in the caudal compartment is compatible with its short half-life due to its degradation by the proteasome (Morimoto et al., 2006). Accordingly, failure of restricting Mesp2 in the anterior compartment leads to defects in the somite polarity as evidenced by the *Ripply1/2* mutants. In the *Ripply1/2* mutants, Mesp2 mRNA and protein are ectopically expressed in single- or double-striped bands encompassing the entire segment, likely due to an anterior expansion of the Tbx6 domain that prolongs the activation of *Mesp2* (Morimoto et al., 2007, Takahashi et al., 2010). Lack of Mesp2 contraction in the anterior PSM in these mutants leads to a rostralized paraxial mesoderm, and later, to the absence of segments.

Together, these studies provide a molecular explanation on how the segmentation clock controls the formation of segments in Vertebrates, as pulses of Notch signaling periodically activate Mesp factors, which in turn organizes the creation of intersomitic boundaries and the rostro-caudal polarity

of the somites. However, it remains to be determined which mechanism represses *Mesp2* expression in the posterior PSM; this question is crucial to capture the molecular basis of the determination front.

6. Somitogenesis models

In the previous sections, we have showed that an oscillatory mechanism, collectively designed as the segmentation clock, is responsible for the periodicity of somitogenesis, and that a system of gradients spatially control the deployment of the segmental program. We now examine the different models of segmentation, after briefly presenting the theoretical basis of oscillations, synchronization, and traveling waves.

Models of oscillators

Excitable vs. Self-oscillatory oscillators

We can distinguish two models of oscillators: excitable and self-oscillatory (Winfree, 2001) (Figure 16). The first one ("hourglass" according to A.Winfree) is characterized by an attracting equilibrium, from which a strong stimulus should be applied to make a large excursion before coming back to the initial state. If this stimulus is repeated, such device becomes an oscillator. In other words, oscillations become spontaneous as the system is constantly above an excitability threshold. By contrast, a self-oscillatory system ("clock" according to A.Winfree) does not have such equilibrium, and is constantly running along its limit cycle.

Neurons are a classical example of excitable system: cells are naturally in a steady state with a defined membrane potential. A small stimulus induces a transient depolarization, but the neuron returns to its equilibrium state, while a strong stimulus (*i.e.* above the excitability threshold) leads to the formation of a potential action, where the neuron is strongly depolarized. Following this action potential, a neuron cannot be excited again; this state called "refractory period" is a general feature of excitable systems. Several mathematical models capture this idea of excitability, such as the FitzHugh-Nagumo model (Fitzhugh, 1961, Nagumo et al., 1962) (a reduction of the Hodgkin and Huxley model) or the theta model (Ermentrout and Kopell, 1986).

Synchronization

When a population of coupled oscillators interact each other, they can synchronize and oscillate in phase. This can be achieved by two ways: entrainment of non-interacting oscillators by periodic forcing or mutual synchronization of interacting oscillators.

Entrainment means that one oscillator ("master oscillator") controls the cycling of another oscillator ("slave oscillator"); for instance, the day-night cycles entrain the circadian clock. However, synchronization is not certain, but generally occurs when the slave oscillator cycles at a period which
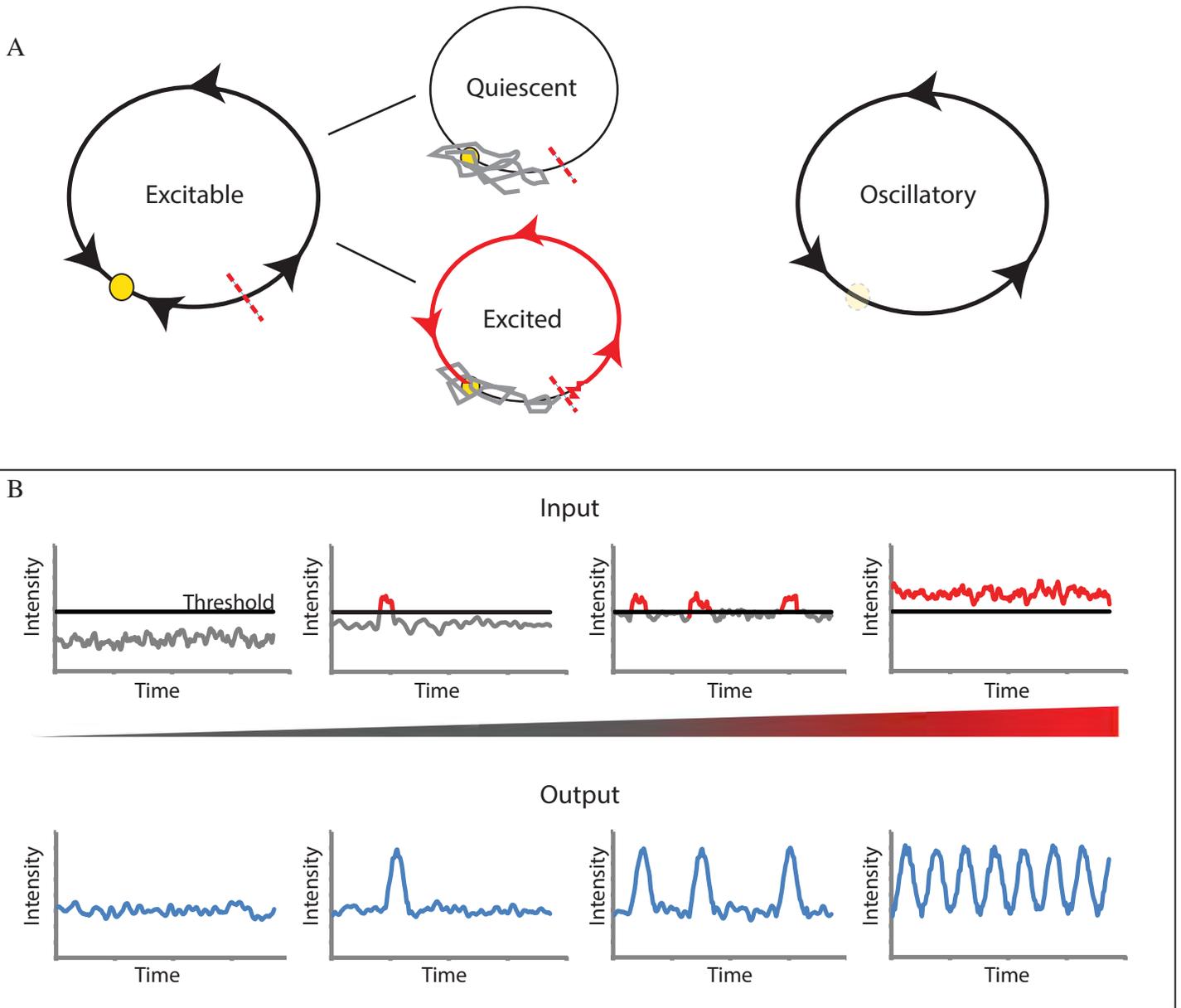
Figure 16 - Oscillatory vs. Excitable Dynamics

A. Schemes showing the phase portrait for excitable and oscillatory systems.
(*Left*) An excitable system is characterized by a stable fixed point (yellow circle) and a bifurcation point, the excitability threshold (red dashed line). When the system is below the excitability threshold, it fluctuates around the fixed point (quiescent - grey); when it crosses this threshold (excited), it undergoes a large excursion (red) before coming back to its initial state.
(*Right*) In an oscillatory regime, the fixed point is no longer stable and a limit cycle appears so that the system is constantly oscillating.

B. Graphs showing the dynamics of input and output signals (e.g. factor concentrations) for an excitable system. An excitable system can switch from a fully quiescent state (*left*) to an oscillatory state (*right*) by progressively increasing an input parameter. When this parameter is far below the excitability threshold, the system does not oscillate. As the system gets closer to the threshold, noise can trigger spikes. When this parameter is constitutively above the excitability threshold, the system becomes oscillatory and regular oscillations are observed.

is a rational multiple of the master oscillator (e.g. $T_{slave}=2xT_{master}$ or $T_{slave} = 3/2 \ xT_{master}$). This region of synchronization ("Arnold tongue") can vary depending on the coupling strength between the two oscillators. Entrainment can also occurs in mechanisms involving a pacemaker and an excitable medium; in that case the self-oscillatory pacemaker make the excitable cells cross their excitability threshold so that they follow the pacemaker oscillations and adopt its frequency (as we will see later, this can also give rise to traveling waves) (Mehta and Gregor, 2010).

Mutual synchronization has been notably formalized with the Kuramoto model (Figure 17A). This model presumes the existence of intrinsic oscillators (self-oscillatory) and supposes that their angular velocity is influenced by the phase difference with their neighbors. In other words, cells slow down or speed up their cycling depending on the phase difference with their neighbors (as an analogy, we can compare this synchronization to the rhythmic applause at the end of a concert, as spectators adjust their applause period to their neighbors (Neda et al., 2000)). This results in a phase-locking of oscillators (Kuramoto transition).

A special case of Kuramoto synchronization occurs when oscillators do not directly synchronize but interact through secreted factors in their environment (Schwab et al., 2012). This produces new properties, such as density-dependent birth and synchronization of oscillations, also known as "dynamic quorum sensing" (Figure 17B). In this model, cells secrete a factor that triggers oscillations at high concentrations. At low density cells are excitable and do not oscillate, while at high density, they secrete enough factors, so that cells become excited and simultaneously start to oscillate. This is a qualitatively distinct transition compared to the phase-locking of the original Kuramoto model, as the synchrony is intermingled with the emergence of oscillations (Mehta and Gregor, 2010). Dynamic quorum sensing has been proposed to occur in yeast glycolytic oscillations (De Monte et al., 2007) or in social amoebae (*Dictyostelium discoideum*) cAMP oscillations (Gregor et al., 2010, Sgro et al., 2015). Indeed, using a live reporter for cAMP, Gregor and colleagues showed that *Dictyostelium* cells display stochastic pulsing below a threshold of cAMP, while above this concentration they start oscillating (Gregor et al., 2010, Sgro et al., 2015). Importantly, as cells secrete cAMP, it enables a density-depend transition from quiescence to synchronized oscillatory behavior at the population level (Mehta and Gregor, 2010).

Traveling waves

Under certain conditions, synchronized oscillators can form traveling waves in a spatial setting. There are two main classes of waves, kinematic waves and trigger waves (Figure 18).

Kinematic waves are also called pseudowaves, as there is no matter transport, nor propagation of a signal across the system. Accordingly, placing a barrier along a kinematic wave does not block its traveling along the system. The oscillators are self-autonomous but coordinated often through a gradient of period that creates the visual illusion of a wave.

A

Kuramoto transition
Progressive synchronization by adjusting the phase shift

Oscillator A

Oscillator B

Oscillator C

Oscillator D

Time

B

Dynamic Quorum Sensing transition
Sharp synchronization by simultaneously switching to the oscillatory mode

Oscillator A

Oscillator B

Quiescent

Oscillator C

Oscillator D

Time
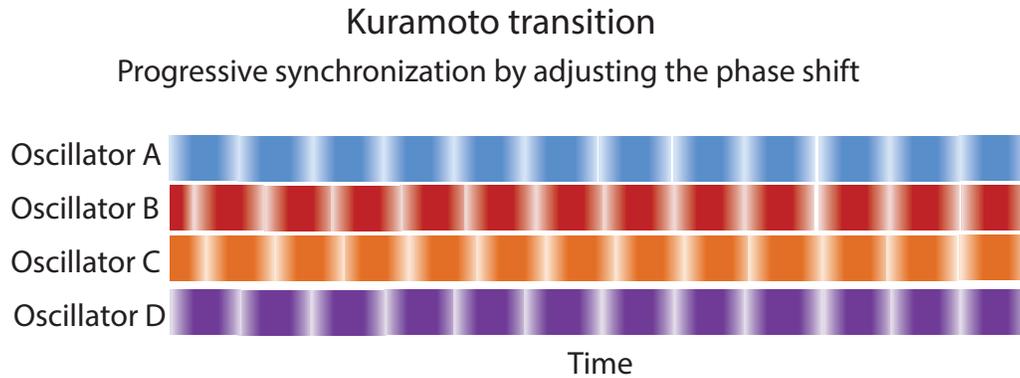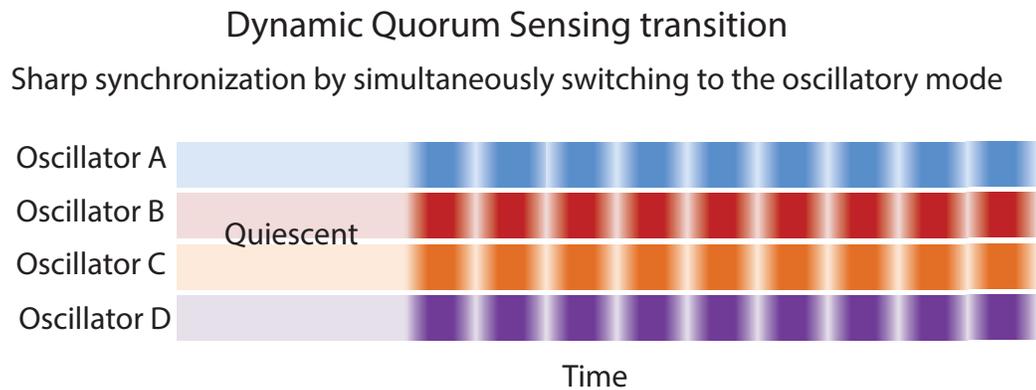
Figure 17 - Synchronization of excitable and oscillatory systems

Schemes showing the different transitions to synchronized oscillations

A. Oscillatory systems can progressively synchronized by locally sensing their phase difference and modulating their frequency depending on this shift.

B. Excitable systems can become synchronized by transiting from the excitable to the oscillatory state at the same time. When this bifurcation is density-dependent, it gives rise to the simultaneous emergence of oscillations both at the individual and collective levels, while in the former case, individual oscillations precede the apparition of collective oscillations.

A **Propagation of an excitation**

— Excitable region — | Pacemaker | —Excitable region—

B **Effect of a boundary**

Excitable
(trigger wave)

Self-oscillatory
(kinematic wave)

C
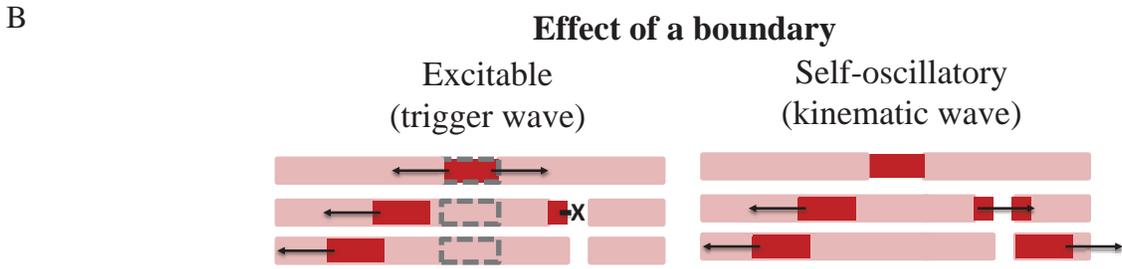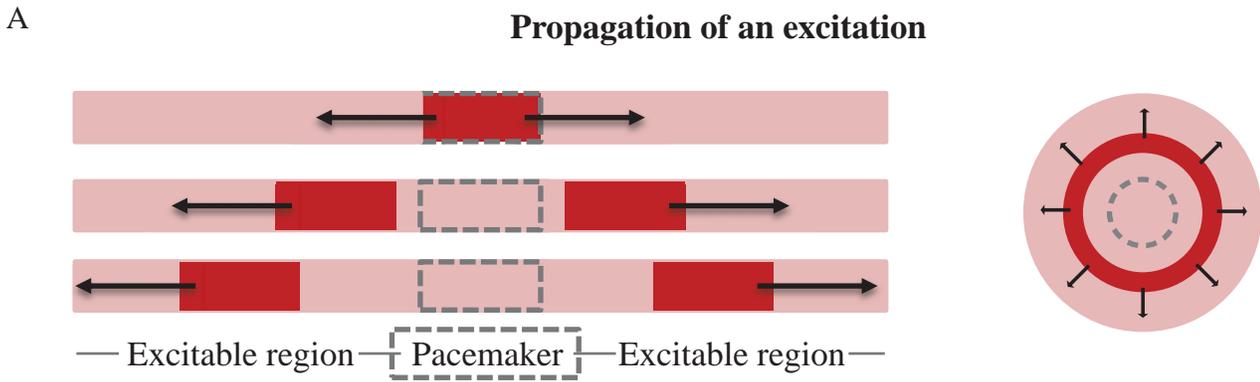
Figure 18 - Traveling waves

A. Scheme showing the signal propagation in an excitable medium. Target patterns can be created by the propagation of an excitation from a pacemaker (dashed rectangle at the center).
(*Left*) One-dimension. (*Right*) Two-dimensions

B. A trigger wave is blocked by a boundary as the excitation can no longer propagate, while a kinematic wave can "spread" across the boundary.

C. Photography of a Belousov-Zhabotinsky reaction, an example of excitable medium able to generate target patterns and spirals

Trigger waves occur in excitable media, as a stimulus propagates along the system. Those waves are blocked by a physical barrier and do not penetrate each other. This phenomenon (called annihilation) is a direct consequence of the refractory period of excitable systems. Such waves have been notably described for calcium waves in Xenopus eggs (Gelens, 2015), cAMP waves in *Dictyostelium* (Sager, 1996), potential action along a neuron or actin polymerization (Allard and Mogilner, 2013). A classical example of excitable media is the Belousov-Zhabotinsky reaction (a mixture of citric acid and bromate ions in a solution of sulfuric acid in the presence of a cerium catalyst) (Strogatz, 2003). Under specific conditions, this reaction is in the excitable regime and waves can be observed either in a target or in a spiral pattern. The former often necessitates the existence of a (self-oscillatory) pacemaker surrounded by excitable elements, so that the excitation from the pacemaker propagates concentrically in the medium. Such pacemaker can also be the result of heterogeneities in the medium, or of self-organization due to long-range interactions (Stich, 2003). By contrast, the spiral pattern does not necessitate a pacemaker, as the wave regenerates itself by chasing its own tail (that is, the wave rotates around the center of the spiral and re-excites itself). We now examine the different theoretical models of somitogenesis.

Cell cycle model

C. Stern and colleagues proposed a model where the cell cycle controls the competency to respond to a determination signal secreted by anterior cells already determined (Primmett et al., 1988, Primmett et al., 1989, Collier et al., 2000) (Figure 19A). This supposes a spatial order in cell cycle position along the PSM and a specific time window of the cell cycle when cells are competent, so that only a discrete population of PSM cells becomes determined upon exposure to the secreted signal. This model follows observations that heat-shock of chicken embryos produces segmental defects only after the formation of 6-7 segments (Primmett et al., 1988). The fact that this duration corresponds to the cell cycle and that drugs inhibiting the cell division similarly affects segmentation led Stern and colleagues to propose the cell cycle model.

Several arguments argue against such model: i) there is no obvious synchrony of the cell cycle in the zebrafish tailbud or along the chicken PSM (Kanki and Ho, 1997, Benazeraf et al., 2010); ii) there is a strong correlation between the periodicity of the segmentation clock and the periodicity of somitogenesis supported by live-imaging in zebrafish and zebrafish *Hes6* mutant (Schroter and Oates, 2010, Soroldoni et al., 2014). By contrast, a cell cycle mutant in zebrafish (*emi1*) does not have a strong segmentation phenotype (Zhang et al., 2008). Furthermore, in zebrafish, a heat-shock similarly produces segmentation defects after ~5 somites (Roy et al., 1999); however, this is shorter than the duration of the cell cycle (2.5h vs. 4h), which is difficult to interpret in the cell cycle model.

A

Cell cycle model

Last boundary

Incompetent phase — Competent Inducer

Time

New boundary
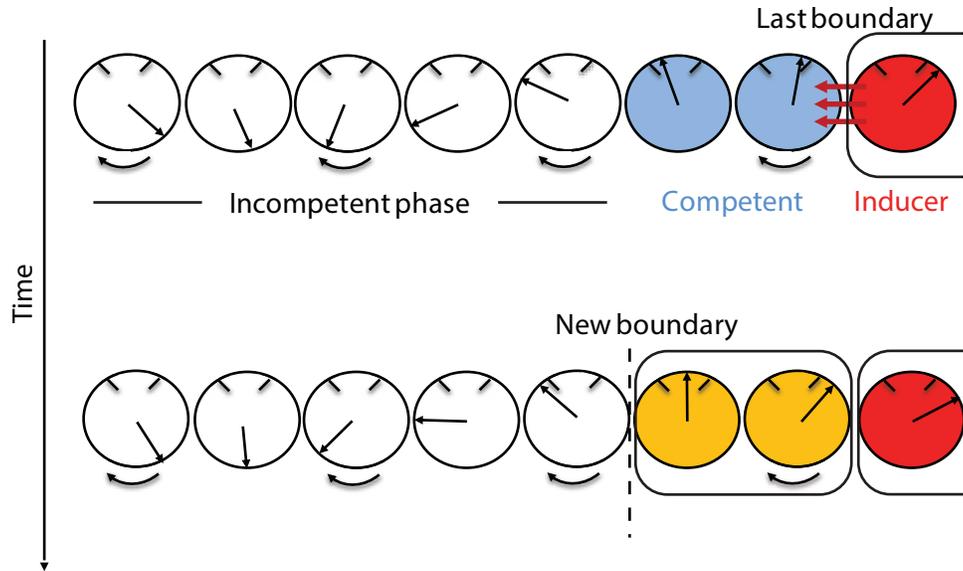
B

Mechanical model

Time
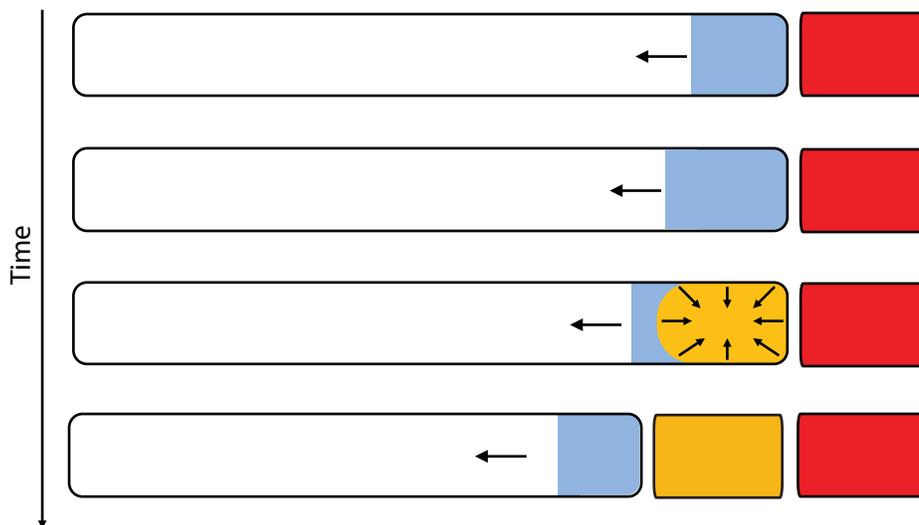
Figure 19 - Cell Cycle and Mechanical Models

A. Scheme showing the formation of a segment in the cell cycle model. According to this model, there is a synchrony among the cell cycles in the PSM. Depending on their position along the cell cycle, presomitic cells can either be in a refractory or competent state, while the last somitic cells produce a diffusing signal. A stripe of cells concomitantly form a segment (yellow) when they are in the competent phase (blue) and receive this signal from anterior inducer cells (red).

B. Scheme showing the formation of a segment in a "mechanical model". According to this model, a wave of cell determination progresses posteriorly and modifies the mechanical properties of the cells. To minimize the tissue surface tension, epithelial units are formed (yellow). It is worthwhile noting that, contrary to other models, a moving front is sufficient to create segments (without the necessary impulse of an oscillator).

Mechanical models

The formation of periodic structures based on local adhesive properties has been proposed by Oster and colleagues to explain the periodicity of the cartilage condensation in the limb and the feather germs, but serves as a more general alternative to chemical models (Oster et al., 1983). In a manner similar to the reaction-diffusion models ("mechanical instability" (Harris et al., 1984)), they proposed a short-range autocatalytic process (cells move toward regions of higher density) and a long-range inhibition (elastic response of the matrix) resulting in periodic condensation of mesenchymal cells. Interestingly, the authors imagined that this aggregation could become periodic if coupled to a maturity gradient, and that the sequential formation of a mechanical instability could drive somitogenesis (Oster et al., 1983, Harris et al., 1984) (Figure 19B).

This is very similar to the idea of "somites without clock" proposed by Stern and colleagues, where local interactions based on cell adhesion and interaction with the matrix can generate somites (Dias et al., 2014). While the authors boldly argued that somitogenesis could occur without clock, a more nuanced view could integrate this mechanism into the system of clock and gradients, as the traveling of a front would cause the progressive apparition of a mechanical instability leading to the formation of somites (Grima and Schnell, 2007). That is, the clock and gradients would globally instruct the position of somite within the PSM, while their formation would be controlled by a local mechanism based on cell-cell interactions (Kondo, 2014). As an analogy, we could imagine the formation of oil drops in water: the situation of Stern and colleagues would mirror a simple emulsion, where oil and water are stirred leading to a disorganized pattern of oil droplets (Swiecicki et al., 2014); the situation in the PSM would rather be a microfluidic device, where oil is progressively injected into a channel leading to a succession of oil droplets.

As for the cell cycle models, mechanical theories do not address the conclusive correlation between the clock periodicity and the somitogenesis periodicity. However, it remains to be studied how this mechanical organization is integrated within the system of oscillations, and what are the relative contributions of each mechanism in the final segment size.

Reaction-Diffusion models

Several models based on reaction-diffusion have been proposed, they generally share three features:

- a stable oscillatory state in the posterior PSM (limit cycle);

- a transition from an oscillatory state to a bistable state in the anterior PSM; each state represents either the rostral or caudal somite fate (using a coin toss as an analogy, it would be the transition from a coin spinning in the air to a coin laying on the ground either on its tail or head side);

- a morphogen gradient that controls the transition from oscillatory to bistable;

These models suppose that the pattern of oscillations arrest determines the segmental pattern.

Turing models

As mentioned earlier, Turing reaction-diffusion models constitute a group of models, where diffusive substances are locally interacting, but where diffusion makes a homogenous solution unstable ("Turing instability") leading to the creation of stable patterns like stripes or dots (Turing, 1952, Kondo and Miura, 2010). H.Meinhardt proposed such reaction-diffusion model to explain the periodic formation of somites (Meinhardt, 1986) (Figure 20A): he postulated the existence of two substances A and P specifying either the anterior part or the posterior part of the somite. Those substances activate themselves and locally repress each other, but mutually activate each other on a long range; such interactions can give rise to oscillations between A-positive and P-positive states. Meinhardt then showed that an AP segment will lead to the crystallization of the remaining tissue and forms additional AP segments AP-AP-AP, but he rightfully noticed that it does not explain why AP segments (AP-AP-AP-) and not PA segments (PA-PA-PA-) are formed. To explain how the first AP segment is formed and how segmentation occurs progressively from one end of the tissue, Meinhardt supposed the existence of a morphogen gradient that sets the threshold to switch between A and P states; that is, below a concentration, cells stop oscillating and create the first segment. Such model is able to recapitulate the formation of segments with an antero-posterior polarity.

Non-Turing mechanisms

In a Turing mechanism, both species diffuse and the difference in their diffusion will enable the emergence of oscillations. In non-Turing mechanisms of somitogenesis, only one substance diffuses; oscillations are rather generated by different time scales in the reactions between those substances (e.g. fast activation and slow repression found in several excitable systems). Alternatively, different thresholds for the activator or repressor can generate oscillations. Importantly, in non-Turing reaction-diffusion models, oscillations can occur at the single-cell level, as the diffusion couples the oscillators but is not strictly required the emergence of oscillations as for a Turing instability.

Such reaction-diffusion model (progressive oscillatory reaction-diffusion - "PORD") has been proposed by Cotterell and colleagues based on an activator-repressor model: using *in silico* evolution, they identified one class of mechanism with an activator and a diffusible repressor, the activator being activated by itself and by a gradient (Cotterell et al., 2015). Like in the Meinhardt model, segment formation occurs, when the morphogen concentration decreases so that oscillations are no longer sustained and a "domino-effect" propagates the formation of polarized segment. The authors proposed that the Fgf gradient could act as a morphogen gradient inducing the activator, and could control the transition from an oscillatory to a bistable state. Accordingly, they showed that

A **Meinhardt model**
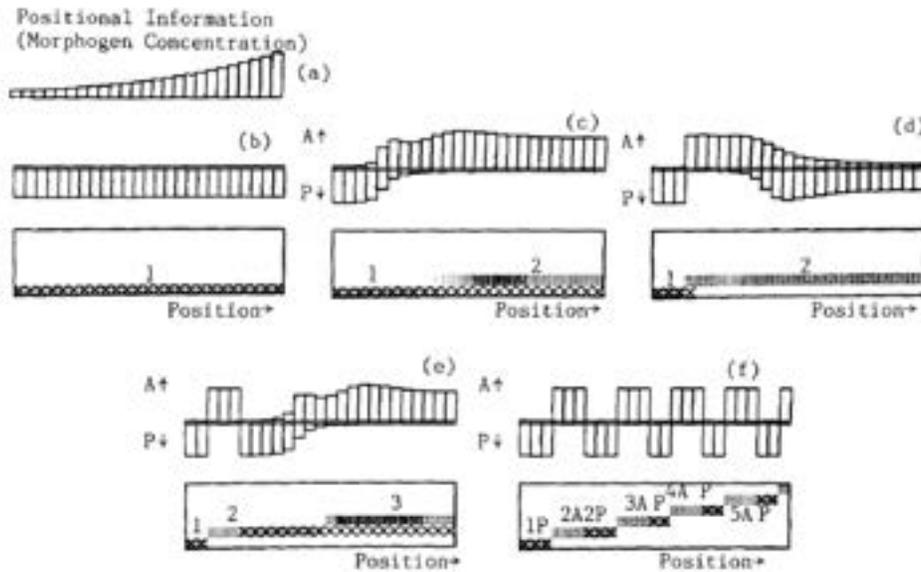
B **Cooke and Zeeman model**
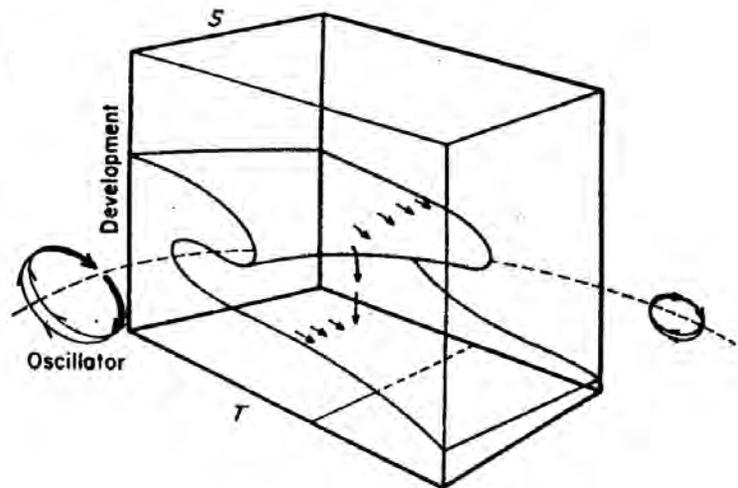
Figure 20 - Cooke and Zeeman model & Meinhardt model

A. Scheme showing the patterns of A and P substances in the Meinhardt model: a stable pattern of half-segments is formed as cells on the left side cannot switch between A and P states below a certain level of morphogen. After the creation of this fixed pattern, the alternation of A-P states propagates along the tissue.

B. Topological representation of segment determinaiton in the Cooke and Zeeman model: a segment is formed through the interaction of an oscillator and a moving determination front. There is an abrupt change in cell properties (intracellular variable "Development") triggered by the oscillator as the front make the cells progress along the developmental time (T).

Modified from Meinhardt (1986), Cooke and Zeeman (1976)

inhibition of Fgf signaling by means of a chemical inhibitor leads to the formation of several longer segments arguing against the existence of single threshold (like in the clock-and-wavefront model discussed below), while fitting with their PORD model.

Nagahara and colleagues proposed another non-Turing reaction-diffusion model, using the FitzHugh-Nagumo formalism (Nagahara et al., 2009). Here, the authors postulate the existence of a diffusible, self-activating activator and a non-diffusible repressor. As for previous models, a morphogen gradient dictates the directionality and arrest of traveling waves by controlling the transition between an oscillatory state and a bistable state (either activator-dominant or repressor-dominant).

Murray and colleagues used a phase model, where they reduced the oscillatory mechanism to the oscillator phase. They considered an autonomous oscillator with both attractive and repulsive coupling, which can be interpreted as the short-range activation and long-range inhibition of previous models (Murray et al., 2011). While the nature of this repulsive coupling remains to be determined, this model recapitulates the traveling and arrest of waves.

Clock-and-wavefront models

In 1976, J.Cooke and C.Zeeman proposed a model called "clock-and-wavefront" (Cooke and Zeeman, 1976) (Figure 20B). The authors propose the existence of two elements that jointly determine the segmental pattern:

- a wavefront, "*a front of rapid cell change moving slowly down the long axis of the embryo; cells enter a phase of rapid alteration in locomotory and/or adhesive properties*"; such changes were thought to lead to the formation of segment;

- a clock, "*a smooth cellular oscillator, for which cells throughout the embryo are assumed to be phase-linked*" that controls the progression of these changes in locomotory and/or adhesive properties ;

According to their model, there is a saltatory progression of these cellular properties at each clock cycle (either by a saltatory progression of the wavefront or by a saltatory activation of downstream processes when cells are passed by the wavefront), meaning that discrete bands of cells simultaneously change their properties to form a segment. The segment size is thus equal to the product of the wavefront velocity and the clock period. This model, however, does not account for the subsequent antero-posterior polarity of the somite.

Mathematical simulations of the clock-and-wavefront model mainly include molecular mechanisms, where *Mesp2* is activated when Fgf is below a defined threshold (wavefront) and Notch is active (clock) (Oginuma et al., 2010, Tiedemann et al., 2014, Hester et al., 2011) (Figure 21A). Based on
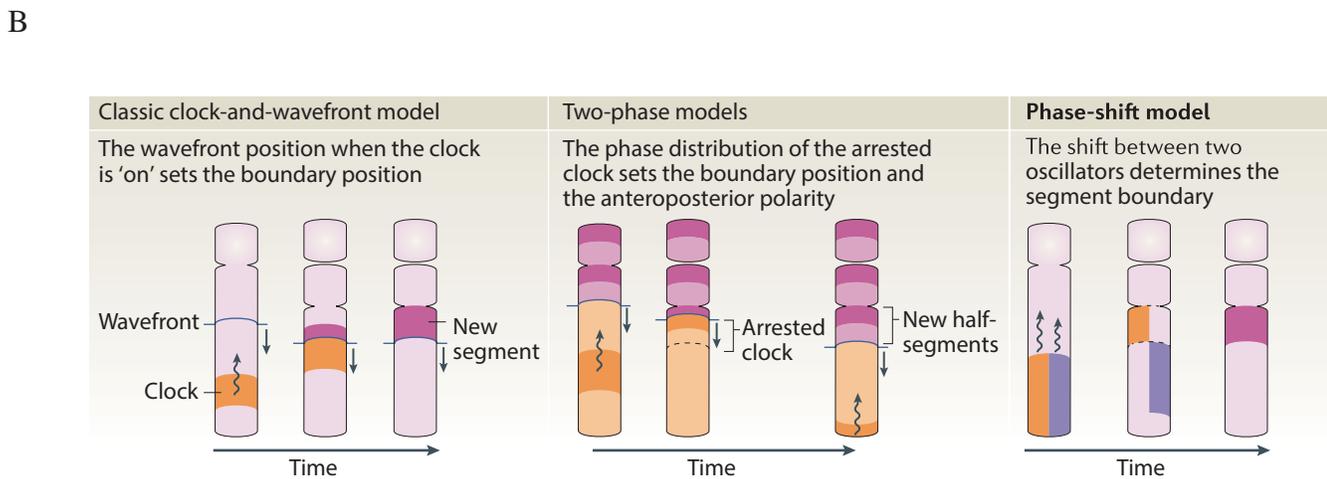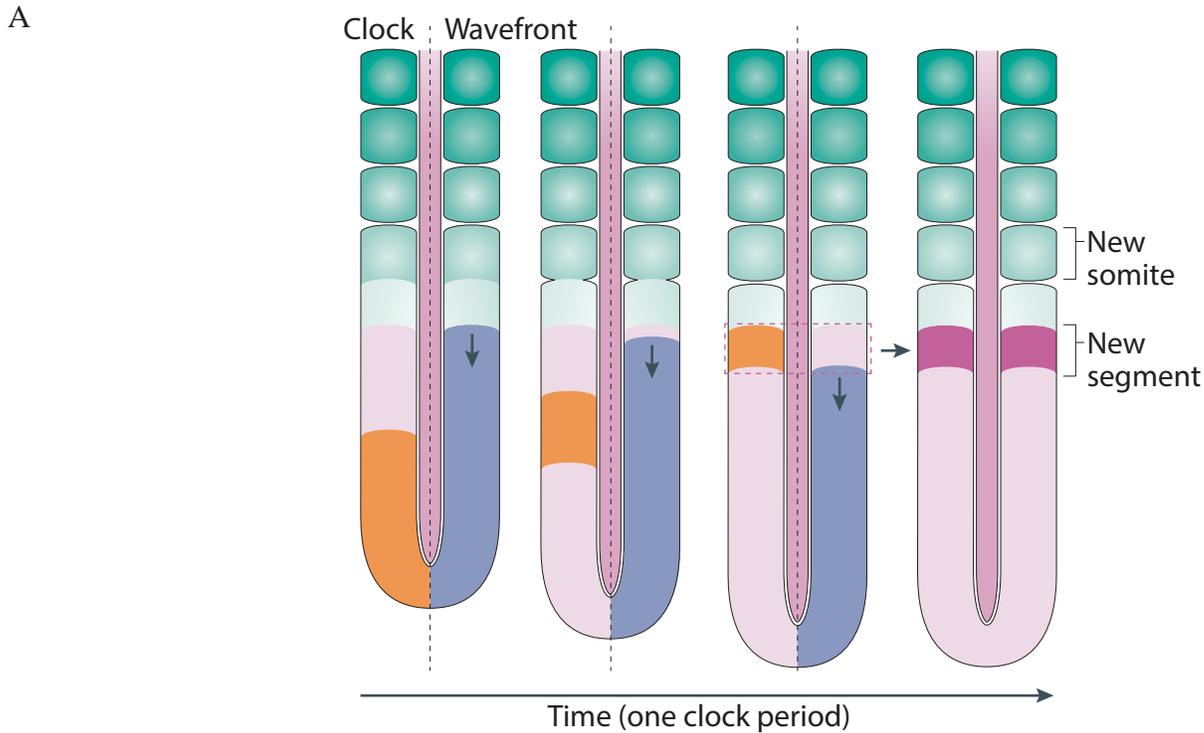
Figure 21 - Clock and wavefront models

A. Scheme illustrating the molecular interpretation of the Cooke and Zeeman model: PSM cells form a segment (purple), when they are passed by the determination front (anterior boundary of the blue domain) and hit by the signal of the clock (orange). It was proposed that the wavefront corresponds to a threshold of Fgf/Wnt signaling and the clock, to a Notch signal.

B. Schemes of the variants of the clock-and-wavefront model (see text for details)

Modified from Hubaud and Pourquié (2014)

live-imaging data, a variation of this model was proposed by Niwa and colleagues, where they assumed that the Fgf wavefront is also cyclic, and that the shift between the Notch and Fgf oscillators leads to the activation of *Mesp2* in the anterior PSM (Niwa et al., 2011) (Figure 21B).

Goldbeter et al. proposed a model of bistability to explain the transition from undetermined (Mesp2-negative) to determined (Mesp2-positive) PSM based on the antagonism between Fgf and RA gradients (Goldbeter et al., 2007). According to this model, below a threshold of Fgf, undetermined cells are in a bistable window, and the segmentation clock causes them to swing into the determined state. This is very similar to the "catastrophe" view of Cooke and Zeeman, where a signal provokes the switch in cell properties.

Biphasic models

Biphasic models with arrest front

Another class of models uses the pattern of arrested oscillations to determine the final segmental pattern. However, contrary to the reaction-diffusion models, no diffusion is required to generate this pattern (Figure 21B). Weak coupling can be included to synchronize the oscillators and counteract the effect of noise, but the final determination is essentially cell-autonomous.

Early models did not explicitly include the diffusion but just considerer the travelling and arrest of waves in a continuous manner. J.Lewis first proposed such model to explain the oscillations pattern of *Hairy1* (Palmeirim et al., 1997): he suggested that the period of oscillations becomes infinite as cells mature in the anterior PSM. Similar models have been proposed (Kaern et al., 2000, Jaeger and Goodwin, 2001, Giudicelli et al., 2007, Gomez et al., 2008, Ares et al., 2012, Jorg et al., 2014). The segment size corresponds thus to the wavelength of the arrested oscillations. Using *in silico* evolution, François and colleagues proposed a similar model based on an activator-repressor couple under the control of a morphogen gradient (Francois et al., 2007). Below a certain level of morphogen, there is a transition from the oscillatory state to a bistable state. While this transition is similar to the reaction-diffusion models, their model is cell-autonomous and is conceptually closer to the model of J.Lewis but with the addition of a bistability transition that sharpens the final arrest of the clock.

Morelli and colleagues extended this theory by using a discrete formalism (Morelli et al., 2009). Cells are modeled as coupled oscillators with single-cells behaving like autonomous oscillators. The authors also showed that introducing a delay in the coupling between cells can generate new properties, such as varying the number of stripes in the PSM. Continuous forms of this model has been derived (Ares et al., 2012, Jorg et al., 2014) and include both reaction and diffusion terms, but the diffusion term has only a limited effect on the overall pattern (Jorg et al., 2014).

In all these models, the wavelength is essentially determined by the oscillator period when cells enter the PSM, and is thus equal to the product of the period and elongation speed (Kaern et al., 2000, Jaeger and Goodwin, 2001, Morelli et al., 2009). Therefore, they are the mathematical versions of the "clock-and-trail" model initially proposed by M.Kerszberg and L.Wolpert, where the authors proposed the existence of a pre-pattern imposed by the oscillatory phase when cells leave the tailbud (Kerszberg and Wolpert, 2000). The underlying idea is that the final wavelength corresponds to the length of cells incorporated in the PSM through tissue growth over one oscillator period, independently of the phase gradient (providing a steady state with equal velocity for the tissue growth and the front of oscillations arrest). A more elaborate phase model has been proposed to take into account variations in the growth rate by adding an advection term and by arresting the oscillations at a finite period (Jorg et al., 2014).

We note that in the clock-and-wavefront models, only one phase of the oscillator signals triggers the catastrophe and the determination of cells, while in the previous models both the rostral and caudal parts are specified by the clock; therefore the biphasic models are not strictly clock-and-wavefront models. Oginuma and colleagues proposed a hybrid model, where the initial segment is determined by a pulse of Notch in a region freed from Fgf, but the antero-posterior polarity is then specified by the restriction of *Mesp2* due to the slowing-down of the clock (Oginuma et al., 2010).

Biphasic model without arrest-front

Lauschke, Tsiairis and colleagues developed an *ex vivo*, two-dimensional system of mouse PSM, where the PSM differentiation is recapitulated as segments are progressively formed at the periphery of the explant (Lauschke et al., 2013). Using the fluorescent reporter for *Lfng* (*LuVeLu*), the authors showed that the phase-gradient predicts the segment size and that the size of segment scales with the size of the undetermined tissue. Furthermore, the phase amplitude between the center of their explant (equivalent to the most-posterior PSM) and the periphery (anterior PSM) is constant and equal to 2π. These findings suggest that the segmentation clock alone contain all the information to specify the segment position. Their mathematical model is in some extent similar to previous biphasic models, as the final pattern of oscillations determines the segmental pattern; however, the difference lies in the absence of arrest front. That is, they postulate the existence of a mechanism that measures the phase-gradient so that the clock stops itself. This is in stark difference with previous models where a front imposes the arrest of the clock. In addition, the phase gradient is key in the model of Aulehla and colleagues, while the phase profile in previous biphasic models do not influence the final pattern, but is rather an *ad hoc* feature to reproduce the traveling wave (in other words, the final pattern is independent of the actual shape of the phase profile providing that the arrest front progresses at the same velocity of the axis growth). Nevertheless, this constant phase difference is not observed in zebrafish (Soroldoni et al., 2014). Similarly, in the mouse mutant expressing a constitutively active

form of β-catenin, the same 2π difference does not lead to segment determination as several stripes are observed in the PSM (Dunty et al., 2008, Aulehla et al., 2008). Therefore, this argues against a simple model of absolute measure of the phase gradient of a single oscillator, but rather points to an additional mechanism providing positional information. The latter could be encoded by a second oscillator, as suggested by the numerous interactions between oscillators in the PSM. Notably, Kageyama and colleagues put in evidence a cross-regulation between the Notch and Fgf oscillators (Harima and Kageyama, 2013). Furthermore, work in zebrafish indicates that the regression of the Fgf/ERK gradient is dependent on the Hes/Her oscillations (Akiyama et al., 2014). In that sense, it would be an extension of the clock-and-wavefront model, where both entities closely interact.

Aulehla and colleagues formalized these observations by postulating a mechanism measuring the phase shift between the Notch oscillator and the Wnt oscillator (Lauschke, 2013). This is in continuation of a general theory of Goodwin and Cohen (Goodwin and Cohen, 1969), where the positional information is determined by the phase difference between a slowing-down oscillator (e.g. Notch) and a fast-travelling oscillator (e.g. Wnt or Fgf). An additional mechanism was proposed by Goodwin and Cohen to adapt the phase difference with the tissue size providing scaling to the patterning.

Testing the models

We now examine the differences and the predictions between these models. First, the "clock-and-wavefront model" postulates that a segment is defined though the interaction of an oscillator and a traveling front of determination. Variants of this model ("phase shift models") involve a cyclic wavefront potentially interacting with the clock (Niwa et al., 2011, Lauschke et al., 2013). There is no assumption about the somite polarity, the mechanism generating the wave or the arrest of the oscillator. Second, the biphasic models (Palmeirim et al., 1997, Kaern et al., 2000, Jaeger and Goodwin, 2001, Francois et al., 2007, Morelli et al., 2009) depart from this original view by supposing that the segment is defined by the arrest of the clock and that the phase of the "frozen" oscillator determines the antero-posterior polarity of the somite. A variant of this model postulates that the oscillations arrest is not controlled by an independent front but rather by some intrinsic properties of the clock (Lauschke et al., 2013). Third, reaction-diffusion models are similarly based on the arrest of oscillations; contrarily to the biphasic models that are essentially cell-autonomous, the mechanism relies here on the diffusion of reactive substances (Meinhardt, 1986, Nagahara et al., 2009, Cotterell et al., 2015).

Biphasic models

A prediction of these models is that the phase pattern of arrested oscillations sets the segment rostro-caudal polarity. However, it is clear that the formation of a segment precedes its rostro-caudal polarization; this is notably evidenced by the dynamics of the Mesp2 factor. In other words, the determination precedes the arrest of oscillations. Therefore, there must be an additional mechanism providing such positional information to place the posterior segmental boundary.

Besides it is not clear in these models how the smooth phase pattern of arrested oscillators is converted into the sharp intra- and intersegmental boundaries (except for the model of Francois and colleagues that incorporates a bistable transition), especially since no infinite period bifurcation is observed *in vivo* (Shih et al., 2015).

Reaction-diffusion models

As mentioned earlier, Turing models seem unlikely as they cannot account for oscillations observed at the single-cell level (Webb et al., 2016). Non-Turing reaction-diffusion models are based on the diffusion of at least one species, thus a cut in the PSM should strongly disturb the oscillations. Cotterrel and colleagues observed a modification of the oscillations pattern after performing a cut in the chicken PSM (however, they need to assume some secondary effects on the Fgf gradient because of the wound effect). Such perturbations have not been observed using more reliable methods with live-imaging in mouse (Masamizu et al., 2006, Lauschke et al., 2013). Christ and colleagues also performed inversion experiments of the chicken PSM and showed that inversing the PSM *in situ* or at the location of the neural tube did not perturb its segmentation (Christ et al., 1974), while a reaction-diffusion model would predict a strong perturbation due to the presence of a new boundary or an adjacent "buffer zone".

However, recent work from Tsiairis and Aulehla argues in favor of a mechanism with some features of a reaction-diffusion system. By reaggregating cells from different PSM, they observed the formation of several oscillations foci, from which traveling waves originate (Tsiairis and Aulehla, 2016). The fact that oscillations with a frequency gradient can self-organize after mixing is reminiscent of reaction-diffusion models. Importantly, the distance between those centers is not random suggesting the existence of a typical wavelength commonly seen in reaction-diffusion. How to reconcile these observations with the relative insensitivity to ectopic boundaries? Theoretical work suggests that using mixed boundary conditions (more complex conditions where the tissue adapts to a new boundary contrary to a "zero-flux" boundary) can increase the robustness of reaction-diffusion mechanisms (Arcuri and Murray, 1986). Alternatively, the self-organization observed by Tsiairis and Aulehla could operate at the level of the spatial organization of the PSM, such as the graded distribution of Fgf/Wnt activities (that would not be affected by a cut in the embryo). This self-organization of PSM determination could act upstream of the Notch oscillations, which would thus

not be themselves generated by a reaction-diffusion mechanism. Accordingly, inhibiting Notch signaling does not block the formation of foci and does not change their characteristic inter-distance. Interestingly, while Lauschke and colleagues previously postulated a tight interdependency between the determination front and the segmentation clock, this observation rather suggests that both entities can be uncoupled – or, at least, that the Notch-dependent waves do not control all the aspects of the PSM determination. The work from Tsiairis and Aulehla raises important questions: what is the nature of the diffusive signal (diffusible proteins, mechanical, metabolic, etc.)? Is there a Notch-independent master oscillator controlling the foci distribution? What controls the wavelength between foci? How does this self-organizing mechanism translate *in vivo*?

Clock-and-wavefront model

Several issues have been raised against the clock-and-wavefront model:

- the elusive nature of the determination front: Cotterell and colleagues showed that the inhibition of Fgf in chicken leads to the formation of several larger somites, while the clock-and-wavefront model would predict the formation of only one large segment (Cotterell et al., 2015). Furthermore, the Fgf/ERK or nuclear β-catenin boundaries in zebrafish do not correlate with the segment boundary (Akiyama et al., 2014, Bajard et al., 2014), arguing against the existence of a discrete threshold. However, these observations are still compatible with the clock-and-wavefront model providing that the determination front lies in the downstream regulatory network of the Fgf and Wnt pathways, but not a discrete threshold of Fgf or Wnt activity. It should be noted that Cotterrel and colleagues addressed this question by simulating a downstream factor of Fgf with a longer decay rate to "spread" the effect of the wavefront on several clock cycles. They were not able to reproduce the *in vivo* observations with such topology, suggesting the existence of a more elaborate mechanism. The existence of a discrete threshold of Fgf/Wnt signaling was also criticized as this mechanism would not be robust given the slope of the gradient (Kondo, 2014) or the extensive cell mixing occurring in the PSM (Stern and Piatkowska, 2015).

- the formation of occipital somites: Stern and colleagues point that the most anterior somites are formed almost simultaneously, which is difficult to explain with the clock-and-wavefront model (Stern and Piatkowska, 2015). However, this could be specific to the most anterior somites (it could also explain why Dias and colleagues observed the simultaneous formation of segments using their ectopic graft). This is not conserved in zebrafish (Retnoaji et al., 2014), and thus requires further examination using live imaging.

- the lack of waves and antero-posterior patterning: the clock-and-wavefront model does not explain how the rostro-caudal polarity is acquired, nor how the traveling waves are formed.

- the prediction of somite size: Lauschke, Tsiairis and colleagues showed that in their *ex vivo* system of PSM, the spatial properties of the clock are sufficient to predict the segment size. This led

the authors to challenge the idea of a traditional wavefront, which is independent from the segmentation clock in the original Cook and Zeeman model (Lauschke et al., 2013). They rather proposed a model of somitogenesis based on the phase difference between oscillators, where the clock dynamics provide positional information (Sonnen and Aulehla, 2014).

Toward a synthetic model

While all mechanisms present some caveats, they are not fully exclusive and a synthetic model can be proposed. Accordingly, the initial segment determination would be specified by a mechanism similar to the clock-and-wavefront. The position of the determination front is likely not determined by a threshold of Fgf/Wnt activities as previously thought, but by downstream targets of their gene regulatory network that can oscillate in the PSM and interact with the Notch oscillator (Niwa et al., 2011, Lauschke et al., 2013, Akiyama et al., 2014, Bajard et al., 2014). After the specification of the segment, the slow-down of oscillations could provide the positional information -as proposed in the biphasic models- to specify the rostral and caudal halves of the somites through the restriction of Mesp2 and Notch signaling (Oginuma et al., 2010, Shih et al., 2015).

7. Integrated view of PSM development

In this section, we briefly discuss how the patterning of the PSM is integrated with other processes of embryonic development, such as the elongation of the body axis or its antero-posterior patterning, and how it compares to other mechanisms of segmental patterning.

Onset and arrest of somitogenesis

We now examine how the oscillations are created and arrested during Vertebrate development.

Onset of the segmentation clock
Jouve and colleagues studied the expression pattern of the cyclic genes *Hairy2* and *Lfng* in chicken (Jouve et al., 2002). They observed a dynamic pattern of those genes in the PSM progenitors located in the primitive streak (stage HH3-4) indicating that the onset of oscillations correlates with their ingression. Similarly, in zebrafish, Riedel-Kruse and colleagues showed that the cyclic expression of *Her7* starts in the presumptive mesoderm at the margin (epiboly stage - 5-6 hours post-fertilization) (Riedel-Kruse et al., 2007). Interestingly, the first expression of *Her7* appears to be synchronized suggesting that cells simultaneously enter in an oscillatory state. The expansion of Fgf signaling in the mesoderm could mediate such bursting phenomenon: in zebrafish the elevation of Fgf signaling in the mesoderm correlates with the initiation of *Her1* expression, and chemical inhibition or ectopic activation of the pathway modify the timing of its expression onset (Ishimatsu et al., 2010). In mouse, Oginuma and colleagues observe that the initiation of NICD oscillations correlates with the onset of *Tbx6* expression (Oginuma et al., 2008b). Since Tbx6 and Msgn1 can directly activate some cyclic genes (Chalamalasetty et al., 2011, González et al., 2013), the onset of the segmentation clock could be directly linked to the acquisition of the PSM state.

Arrest of the segmentation clock
The arrest of the segmentation clock is likely due to the regression of the PSM at late stages. As mentioned above, both in chicken and mouse, late somitogenesis is characterized by an increase of retinoic signaling and a decrease of Fgf/Wnt signaling, which divert cells from the mesodermal lineage and promote the neural differentiation of bipotent progenitors (Cambray and Wilson, 2007, Tenin et al., 2010, Olivera-Martinez et al., 2012).

The rate of somitogenesis progressively diminishes: while the first somites in mice are formed about every hour, the last somites appear with a 3h period (Tam, 1981), and similar observations have been

reported in zebrafish (Schröter et al., 2008) and chicken (Tenin et al., 2010). Genetic analysis of the segmentation clock in mice also revealed that the gene regulatory network evolves during development, as *Lfng* and *Hes7* oscillations seem required for segmentation of anterior (thoracic, lumbar) regions but not the sacral and tail regions (Shifley et al., 2008, Stauber et al., 2009). The progressive dampening of Fgf/Wnt signals could cause this differential axial requirements and the rearrangement of the clock machinery.

Control of somites number and identity

The number and length of segments are important features of the adult body; for instance, they influence the locomotion mode of fishes and reptiles (Ward and Mehta, 2010).

The axial identity of segments plays a role in the final organization of the Vertebrate body, as the final differentiation of somites varies depending on their axial position. This is evidenced by the variation in vertebrae that can become cervical, thoracic, lumbar or sacral. The axial identity is conferred by a group of transcription factors, the *Hox* family (Mallo et al., 2010): these genes are organized in four clusters (a-d) of thirteen paralogues groups in Vertebrates, which are progressively expressed in an antero-posterior sequence during development ("colinearity") (Figure 22A). For instance, the transition from cervical to thoracic segments is marked by the transition from *Hoxa-d5* to *Hoxa-c6* (Burke et al., 1995). It was first proposed that the number of oscillations could set the axial identity of segments: the head mesoderm in chicken would experience 1-2 oscillations, then the cervical somites 3 and more, etc. (Jouve et al., 2002). However, it is difficult to reconcile this hypothesis with the different phases of Hox expression (Deschamps and Wijgerde, 1993) and the plasticity of the Hox code in the tailbud (McGrew et al., 2008). An alternative hypothesis proposed that the axial identity was conferred at the time of segmentation. Accordingly, altering the Fgf gradient affects both somitogenesis and the *Hox* code (Dubrulle et al., 2001), and some *Hox* genes display a cyclic expression in stripes similar to *Mesp2* stripes (Zákány et al., 2001), potentially linking the clock and the *Hox* code. However, the *Hes6* zebrafish mutant displays a different somite number without homeotic transformation (Schroter and Oates, 2010), and the ectopic expression of *Hoxa10* in the PSM, not the somites, has an effect on the axial identity (Carapuco et al., 2005). Last, somitogenesis appears to be uncoupled from other developmental process, e.g. Burke and colleagues showed that the position forelimb is conserved and located anterior of the *Hoxc6* boundary (Burke et al., 1995), but the number of somites at this position considerably varies between species (Richardson et al., 1998). This plasticity argues against a strict correlation of axial identity and segmentation. Such dissociation of somitogenesis and *Hox* patterning rather explains how different species could have evolved distinct vertebrae formula depending on the environmental pressure they
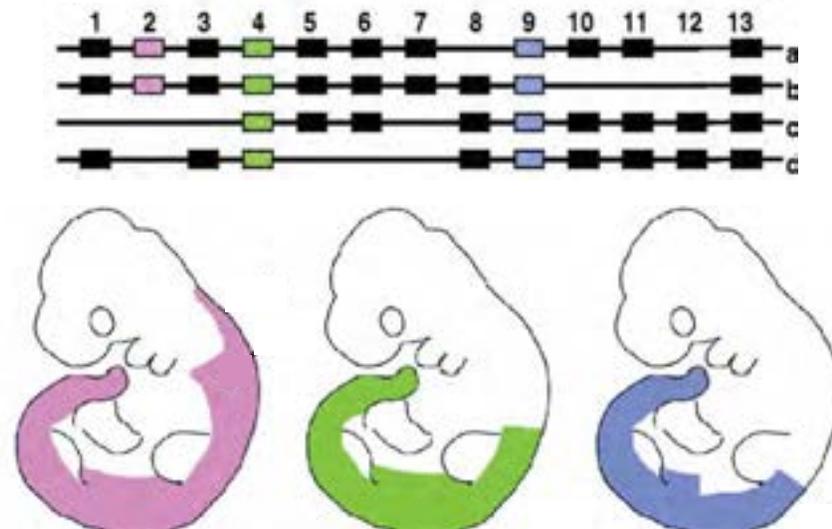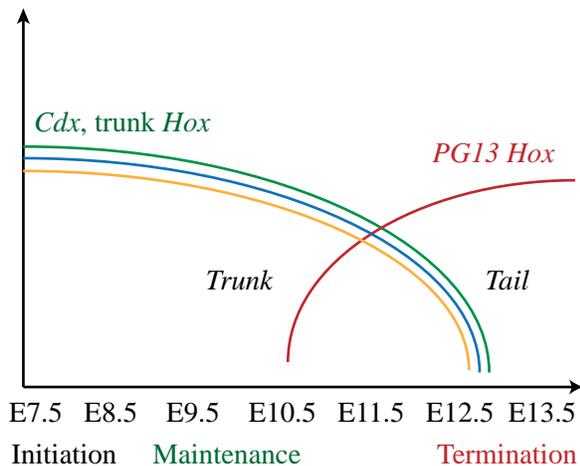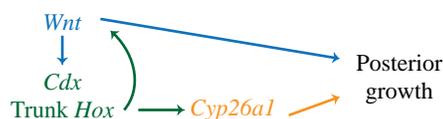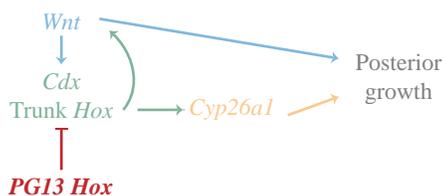
Figure 22 - Antero-posterior patterning of the body axis

A. (*Top*) Scheme showing the genomic organization of the four clusters of *Hox* genes (a,b,c,d). (*Bottom*) Expression pattern for different Hox genes. Anterior Hox genes (e.g. *Hoxa2* - pink) are only expressed in the most anterior tissues, while posterior Hox genes (e.g. *Hoxa9* - blue) are later expressed and have a dominant effect on the more anterior *Hox* genes.

B. Model of arrest of axis elongation in mouse. The paralogue group (PG) of *Hox13* genes orchestrates the arrest of axis elongation by repressing *Cdx* and trunk *Hox* genes leading to the upregulation of retinoic acid in the tailbud.

Modified from Deschamps and Van Nes (2005), Young et al. (2009)

faced (e.g. the swan has a long neck with 25 cervical vertebrae putatively allowing a better foraging of benthic vegetation)

While the number of somites is relatively fixed within a species, examples of intraspecific variability exist. This is markedly evidenced in teleosts, where the final vertebrae count can change depending on the temperature or other environmental factors (Fowler, 1970). Indeed it was suggested that the "developmental rate" affects the final number of segments, e.g. a higher developmental rate in trout caused by a larger yolk or a higher temperature is correlated with a smaller number of somites (Garside and Fry, 1959, Garside, 1966). The intraspecific variation of vertebrae number in fishes also depends on heritable characters (Alho et al., 2011) that can be selected depending on their geographical location.

The link between developmental rate and segment number was further suggested by Gomez and colleagues. They studied different Vertebrate species and proposed that a faster segmentation clock compared to the developmental rate (approximated by the cell cycle length) could explain the large segment numbers of species like the corn snake (Gomez et al., 2008). The latter has a slower developmental rate compared to its somitogenesis rate, enabling the addition of large number of somites before the arrest of axis formation. Interestingly, in corn snakes, the expression of *Hoxa13* and *Hoxd13* appear comparatively delayed compared to other Vertebrates, probably due to the addition of transposable elements in their regulatory regions (Di-Poi et al., 2010). This delay could prolong the time window of elongation and somitogenesis in the paraxial mesoderm by postponing the increase of RA signaling, and thus, the disappearance of the tailbud and PSM, as we will now discuss.

Elongation of the PSM

Mechanism of axis elongation

The segmentation of the PSM occurs concomitantly with an important elongation of the antero-posterior axis. It appears that there are two main mechanisms: an early elongation based on convergent-extension movements, and a later elongation based on addition of new motile tissues in the tailbud (Figure 23).

The early steps of development involve a complex reorganization of cells leading to the elongation of the most anterior tissues. This process has been extensively studied in the frog and in chicken, and is likely conserved among Vertebrates (Bénazéraf and Pourquié, 2013). Epiblast cells converge to the midline and undergo medio-lateral intercalation under the control of the non-canonical Wnt pathway (Wnt/PCP), leading to an elongation of the embryo along its antero-posterior axis (convergent extension).
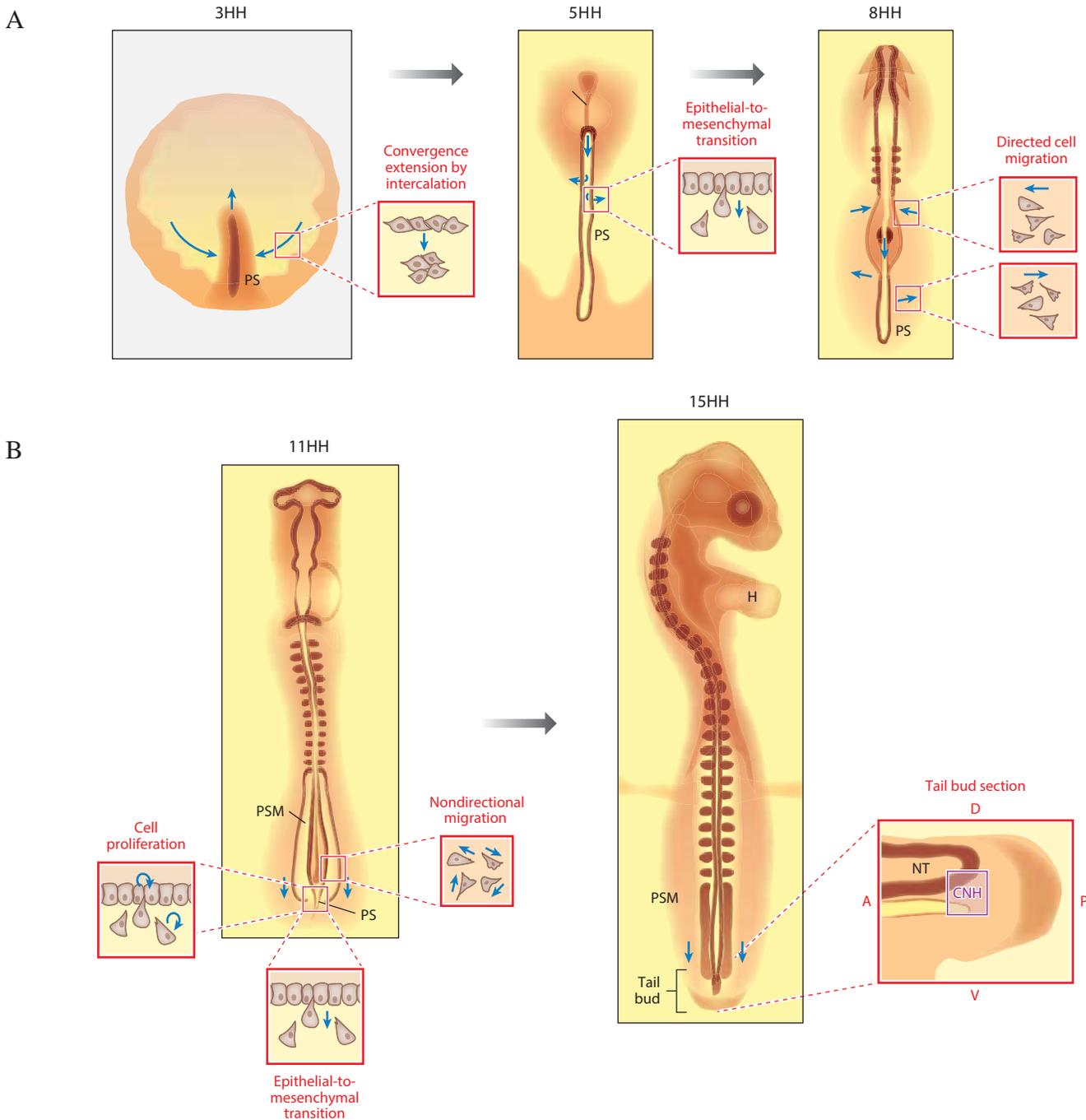
Figure 23 - Elongation of the body axis in chicken embryo

Schemes of a chicken embryo at different embryonic stages.

A. At early stages, the elongation of the axis is mainly driven by convergence extension and injection of cells by ingression (epithelial-to-mesenchymal transition) at the primitive streak (PS).

B. At later stages, the elongation is caused by non-directional movements of cells and by injection of cells at the level of the tailbud. Axial stem cells are located at the chordo-neural hinge (CNH) and give rise to the neural tube (NT) and PSM.

Modified from Bénazéraf and Pourquié (2013)

The elongation of the most posterior tissues appears to be mainly driven by the addition of cells at the tailbud that is itself propelled posteriorly by the PSM (Bénazéraf and Pourquié, 2013). Indeed Bénazéraf and colleagues studied this process in the chicken embryo, and showed that ablating the PSM severely reduced the elongation speed, while other tissues had a lesser contribution (on a short-term basis) (Benazeraf et al., 2010). By manipulating Fgf signaling, they showed that the gradient of Fgf imposed a gradient of random cell motility that is thought to drive elongation by displacing posteriorly the tailbud (Delfini et al., 2005, Benazeraf et al., 2010). On a long-term basis, the elongation is fueled by the addition of new PSM cells in the tailbud. Accordingly, mutants for the Wnt pathway display axis truncation, which is correlated with a loss of neuromesodermal progenitors and of PSM (Takada et al., 1994, Greco et al., 1996, Yamaguchi et al., 1999, Garriock et al., 2015). This dampening of Wnt signaling is associated with the arrest of axis elongation. Indeed, an allelic series for the gene *Wnt3a* performed by Greco and colleagues revealed that reducing the dose of *Wnt3a* correlates with more severe axis truncation (Greco et al., 1996). Furthermore, it was shown that the levels of posterior PSM transcripts (*Fgf8*, *Wnt3a*, *T*) progressively decreased during mouse somitogenesis, mirroring the arrest of elongation (Cambray and Wilson, 2007). The posterior *Hox* appear to control this transition by repressing *Cdx2*/4 as their precocious expression can prematurely arrest elongation (Young et al., 2009). Young and colleagues showed that the loss of *Cdx2/4* was associated with a loss of Wnt signaling and an increase of RA signaling due to a loss of *Cyp26a1* (Figure 22B). Accordingly, during the phase of elongation arrest in chicken embryos, the loss of Fgf/Wnt signaling and the rise of RA signaling cause the loss of neuromesodermal progenitors and an increase of neural progenitors at the expense of mesodermal progenitors (Olivera-Martinez et al., 2012). Posterior *Hox* can also act on the rate of cell ingression and thus reduce the elongation speed during the trunk-tail transition (Denans et al., 2015).

Interplay between axis elongation and somitogenesis

During somitogenesis, the PSM length considerably changes: at early stage (1-10 somites), the mouse PSM is ~0.5mm long, while it reaches ~1.3mm at later stages (15-25) somites before its shortening at later stages (Tam, 1981). How does it affect the process of somite formation? Measurements of the somite length revealed that it follows a similar dynamics in mouse embryo (Tam, 1981), as well as in chicken and snakes (Gomez et al., 2008) but with a delay compared to the PSM length: while the PSM length peaks at ~20 somites in mice, the somite size peaks at ~30 somites. Interestingly P.Tam treated E7.0 embryos with the cell cycle inhibitor mitomycin c and observed a correlation between the PSM length and the body length, as well as between PSM length and the somite length (until the recovery of the embryo at the trunk-tail transition) (Tam, 1981). The existence of regulatory process linking the PSM size with the somite length is further evidenced by two mice mutants showing a reduction of both PSM and somites lengths: the *AIF* mutant (Apoptosis-

inducing factor) (Brown et al., 2006) and the *amputated* mutant (Flint et al., 1978) that is supposedly defective for *Foxc2* (Kaestner et al., 1996). J.Cooke showed a similar regulation by removing tissues from a frog blastula, which leads to the development of smaller embryos with a correct number of smaller somites (Cooke, 1975). Historically, this observation served as a basis for the clock-and-wavefront model, as Cooke and Zeeman argued that the wavefront could adapt to a restriction of embryo size, while a reaction-diffusion mechanism would have a fixed wavelength determined by the diffusion parameters of the activator and repressor (Cooke and Zeeman, 1976). However, more elaborate reaction-diffusion mechanisms, where the wavelength depends on a gradient that scales with the tissue size, can similarly reproduce the scaling of somitogenesis (Cotterell et al., 2015).

How to account for such scaling of somite length to the PSM size? The gradients of Fgf and Wnt signaling in the PSM could link segmentation and elongation, as they are involved in both processes. For instance, such coupling of patterning and morphogenesis has been extensively described for the Dpp gradient, which controls both the elongation and the patterning of the fly wing disk (Wartlick et al., 2011).

Regarding somitogenesis, scaling can also be a natural consequence of the biphasic models presented earlier as the segment length is directly determined by the elongation speed (Kaern et al., 2000). While this feature is essentially a passive effect of laying down oscillators, Lauschke, Tsiairis and colleagues suggested that an additional mechanism could directly sense the PSM length to account for the scaling of segment length in their *ex vivo* system (Lauschke et al., 2013). A morphogen gradient scaling with the tissue or an adjusting phase-shift mechanism as proposed by Goodwin and Cohen could explain such scaling (Lauschke et al., 2013).

Clock mechanisms in other developmental contexts

In this last section, we briefly compare the segmentation of Vertebrates with other segmentation mechanisms.

Evolution of animal segmentation

Segmentation is a widespread feature of Animals; whether this indicates a common segmented ancestor ("Urbilateria") has been a long-standing question (De Robertis, 2008). The mechanisms of segmentation, however, differ between phylogenetic groups, and thus, it has been lost or acquired at multiple branches of the Animal tree. In insects, there are three main modes of segmentation: long-germ band insects (e.g. the fly *Drosophila melanogaster*) with a simultaneous formation of segments; short-germ band insects (e.g. the beetle *Tribolium castaneum*) with a progressive addition
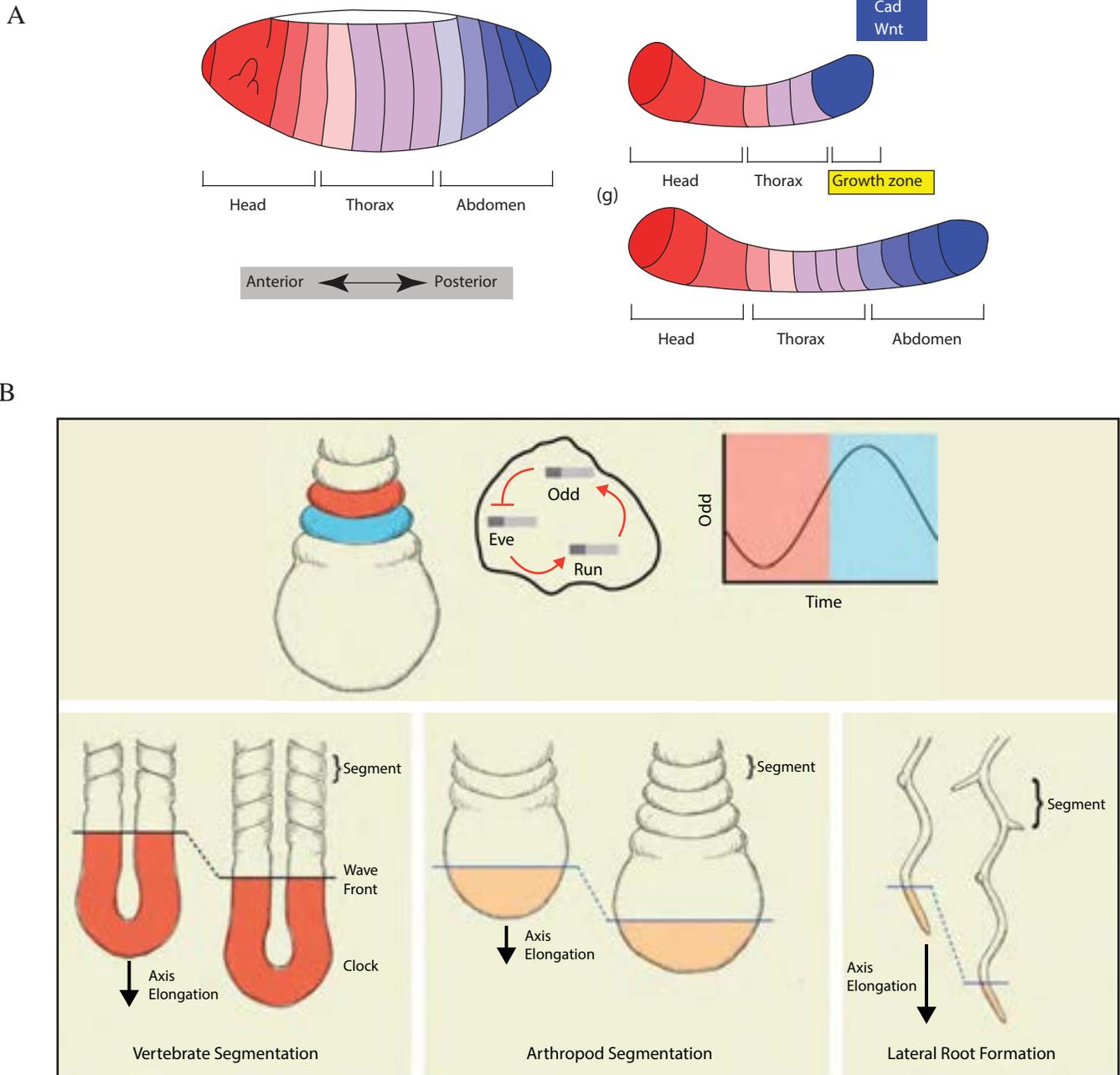
Figure 24 - Clock-mechanisms as developmental rulers

A. Scheme of *Drosophila (left)* and *Tribolium (right)* embryos. Long-germ band insects (*left*) undergo a simultaneous segmentation of their body axis, while short-germ band insects (*right*) experience a progressive segmentation of tissues at the posterior end of the embryo (growth zone)

B. Schemes of different elongating structures patterned by an oscillator.(*Top*) In short-germ band arthropods like *Tribolium*, there is a two-segment periodicity imposed by the oscillations of pair-rule genes.
(*Bottom*) Mechanisms of segmentation by a transcriptional oscillator have been identified in Vertebrate somitogenesis (*left*), in the segmentation of short-germ band insects (*middle*), and in the branching of *Arabidopsis* root (*right*).

Modified from Kimelman and Martin (2012), Valentin and Oates (2013)

Figure 25 - Evolution of the body axis development in Bilaterians

A. Table showing the characteristics of axis elongation and segmentation among the phylogenetic tree of Bilaterians.

B. Phylogenetic tree showing three scenarios for the evolution of segmentation in Bilaterians: i) (*Left*) the segmentation was independently acquired in three different phyla (black boxes); ii) (*Middle*) the common Protostome ancestor was segmented and its mechanism was lost in some phyla (white boxes), while the segmentation was acquired in Chordates; iii) (*Right*) the common ancestor was segmented, and this mechanism was lost several times in different phyla.

Modified from Valentin and Oates (2013), Davis and Patel (1999)

of segments at the level of a growth zone (Figures 24-25); intermediate germ-band insects that combine both modes of segmentation.

The long-germ band segmentation relies on a complex gene regulatory network based on the progressive specification of gap genes, pair-rule genes and segment polarity genes (Peel et al., 2005). By contrast, the segmentation of short-germ band insects resembles the clock-based segmentation of Vertebrates. Indeed, studies of various Arthropods point to an oscillatory mechanism based on cycling of pair-rule genes, such as *odd-skipped* (Chipman et al., 2004, Sarrazin et al., 2012) or *Hairy* (Pueyo et al., 2008). This clock might rely on negative feedback circuits between pair-rule genes as described in Tribolium (Choe et al., 2006). By contrast to the Vertebrate segmentation, the clock of short-germ band insects runs with various segment periodicity, mostly single-segment and double-segments periodicities (Valentin and Oates, 2013). Intriguingly, this periodicity can change during the development stage, such as for *S.maritima* that evolves from a double-segment to a single-segment periodicity (Valentin and Oates, 2013) or *Tribolium castaneum,* whose period of segment addition abruptly changes from 1h to 4h (Nakamoto et al., 2015). It is debated whether Notch signaling is cycling in these insect models as in Vertebrates and whether it has a conserved role in animal segmentation (Stollewerk et al., 2003, Chipman and Akam, 2008, Kainz et al., 2011, Eriksson et al., 2013). Conversely, there is a striking conservation of the posterior growth process (Martin and Kimelman, 2009), which depends on Wnt signaling and *Caudal/Cdx* genes (Copf et al., 2004, de Rosa et al., 2005, McGregor et al., 2009, Young et al., 2009, Chesebro et al., 2013).

Invertebrate Chordates also display progressive segmentation of their antero-posterior axis. For instance, the cephalochordate amphioxus (*Branchiostoma lanceolatum*) adds segments directly from its growing zone (with the exception of its most anterior segments) in an asymmetric way. Expression patterns suggest a gene regulatory network similar to the one operating in Vertebrate somitogenesis making likely the existence of a clock in the common ancestor of Chordates (Beaster-Jones et al., 2008). Interestingly, amphioxus segmentation does not require Fgf signaling (except for the most anterior somites that form synchronously) (Bertrand et al., 2011), suggesting that the Fgf-based determination front and the existence of a presomitic mesenchyme have been specifically acquired by Vertebrates. Bertrand and colleagues proposed that the apparition of the Fgf wavefront is a Vertebrate invention to separate the tailbud from the RA-producing mesoderm (Bertrand et al., 2015). Hypothetically, this could have enabled the symmetry of somitogenesis, and potentially, the acquisition of lateral locomotor structures (limbs, fins) in Vertebrates. This segmental mechanism was lost in the chordate *Ciona intestinalis* (Pasini et al., 2012), which correlates with its minor axis growth and further supports the relationship between clock mechanisms and elongation already seen in insects. Together this indicates a common segmentation principle for embryos with an elongating antero-posterior axis. Whether these similarities are the consequence of an inherited segmentation mechanism from their common ancestor remains unanswered.

Clock-based segmentation

Other segmented structures rely on molecular oscillators, indicating that clock-based segmentation is a more general mechanism to pattern elongating structures (Figure 24B). As previously discussed, the segmentation of short-germ band insects is controlled by the oscillations of pair-rule genes (Sarrazin et al., 2012). Moreover, it was shown that genetic oscillations mark the position of lateral roots along the elongating primary root axis in plants (Moreno-Risueno et al., 2010). This is also consistent with *in silico* evolution studies, where selection for a sequential segmentation inevitably leads to the apparition of clock-based mechanisms (Francois et al., 2007, Fujimoto et al., 2008, ten Tusscher and Hogeweg, 2011, Ten Tusscher, 2013). Interestingly, modeling work revealed that changing the repressor strengths of a gene regulatory network is sufficient to make the system switch from an oscillatory state to a hierarchical patterning (Panovska-Griffiths et al., 2013), providing a potential explanation to the transition between short-germ and long-germ band development. The generality of clock-based mechanism might be a consequence of their robustness and evolvability: *in silico* simulations suggest that clock-based mechanisms are more robust and evolvable than the hierarchical patterning mechanisms (Fujimoto et al., 2008, ten Tusscher and Hogeweg, 2011), while the latter could have been selected when a rapid development provided a competitive advantage (Fujimoto et al., 2008).

Nevertheless, other systems display stripes patterning without the involvement of an oscillator, but are rather based on a Turing mechanism: digit patterning in the limb bud (Sheth et al., 2012), pigment stripes in fishes (Kondo and Asai, 1995) and palate rugae (Economou et al., 2012).

Other roles of oscillators

Last, we must note that the role of oscillators is not restricted to "developmental ruler" (Webb and Oates, 2016) at the origin of segmental pattern in elongating structures. Oscillators can also control biological rhythms or encode information in other contexts.

For instance, the circadian clock enables to coordinate the biological rhythms to the daylight cycles or the cell cycle orders a sequence of events to assure the right proceedings of cell division. Other oscillators serve to compartmentalize activities either at the cellular level (e.g. metabolic oscillations are coupled to the cell cycle and alternate phases of growth, energy production and biomass degradation (Tu and McKnight, 2006)) or at the population level (e.g. metabolic oscillations in bacterial biofilms solve a trade-off between growth and nutrient availability (Liu et al., 2015)). Furthermore, at the level of the whole population, desynchronized oscillations could generate diversity to differentially respond to a unique signal in a similar manner as the bet-hedging strategy in bacteria. For instance, *Hes1* is oscillating in mouse embryonic stem cells; upon differentiation, *Hes1*-high cells tend to differentiate into mesoderm while *Hes1*-low cells follow the neural lineage (Kobayashi et al., 2009).

Last, signaling oscillations can expand the repertoire of cellular responses by encoding information through the dynamics rather than the absolute signal level (Levine et al., 2013, Sonnen and Aulehla, 2014). This is evidenced by the oscillations of NF-κB, whose frequency determines the activation of different subsets of genes (Nelson et al., 2004, Ashall et al., 2009). Similarly, neural differentiation in mouse is controlled by the dynamics, and not the overall expression, of the transcription factor Ascl1: Imayoshi and colleagues elegantly showed that oscillatory *Ascl1* expression maintains the pool of proliferating neuronal precursors, while its sustained expression triggers their differentiation (Imayoshi et al., 2013).

CHAPTER I

Transcriptional regulation of Mesp factors

In the introduction, we showed that the transcriptional regulation of the Mesp factors is fundamental to the segmentation of the PSM. It controls both the formation of segmental boundaries and the antero-posterior polarity of the segment. While it is commonly accepted that Notch signaling and Tbx6 trigger the expression of *Mesp2*, little is known about its repression in the posterior PSM. This is nevertheless a crucial question to understand the regulation of somitogenesis. Identifying the molecular basis of the determination front will also provide a better framework to theoretical models and genetic studies trying to decipher the contribution of each pathway. Therefore, we studied the mechanism by which *Mesp2* is repressed in the PSM. For that purpose, we used chicken embryos because of their ease of manipulation and *ex vivo* culture. We showed that overexpression of Tbx6 is sufficient to induce *Mesp2* in the posterior PSM. Furthermore, we tried to identify the downstream targets of the Fgf/ERK pathway, which was proposed to repress *Mesp2* in the PSM. Last, we present tools developed to study the formation and interpretation of the Fgf8 gradient in chicken. This addressed the spatial regulation of the determination front. Indeed, as previously mentioned, there is a tight link between the elongation and the segmentation of the PSM, as both processes are controlled by the gradient of Fgf signaling. Such joint regulation could underlie the size adaptation of somites to the variations in PSM length. The rationale of this project was thus to quantify the Fgf8 gradient and test the hypothesis that the scaling observed by several groups was a natural consequence of the scaling of the Fgf8 gradient.

1. Regulation of Mesp2 expression

1.1 Construction of a Mesp2 reporter

We first developed a fluorescent reporter to monitor the activation of *Meso2*, the chicken homologue of *Mesp2*. For this purpose, we constructed a plasmid containing a 3kb-genomic sequence upstream of the start codon of *Meso2* in front of the coding sequence of the fluorescent protein Venus (Figure 26A) (as previously done in other species - (Haraguchi et al., 2001, Wang and Ding, 2006, Moreno et al., 2008)). We then electroporated this construct in the progenitors of the PSM around stage HH5 (Hamburger and Hamilton, 1951), and examined the fluorescence one day after (around HH10). We observed the expression of the reporter starting at the level of somite S0/S-I in the entire forming segment (that is, both rostral and caudal compartments) (Figure 26B). Contrary to the endogenous protein in mouse, the fluorescence persists in the anterior somites (from S0 to at least SV). To validate the periodic activation of the reporter, we took advantage of a time-lapse station set up by B. Bénazéraf and the group of C.Little, where the development of chicken embryos can be followed for a long period (until day 2) (Benazeraf et al., 2010). Using this system, we observed the periodic

A

cMeso2 upstream region (3kb) | Venus | SV40pA

B

| Brightfield | *Meso2 Venus* |
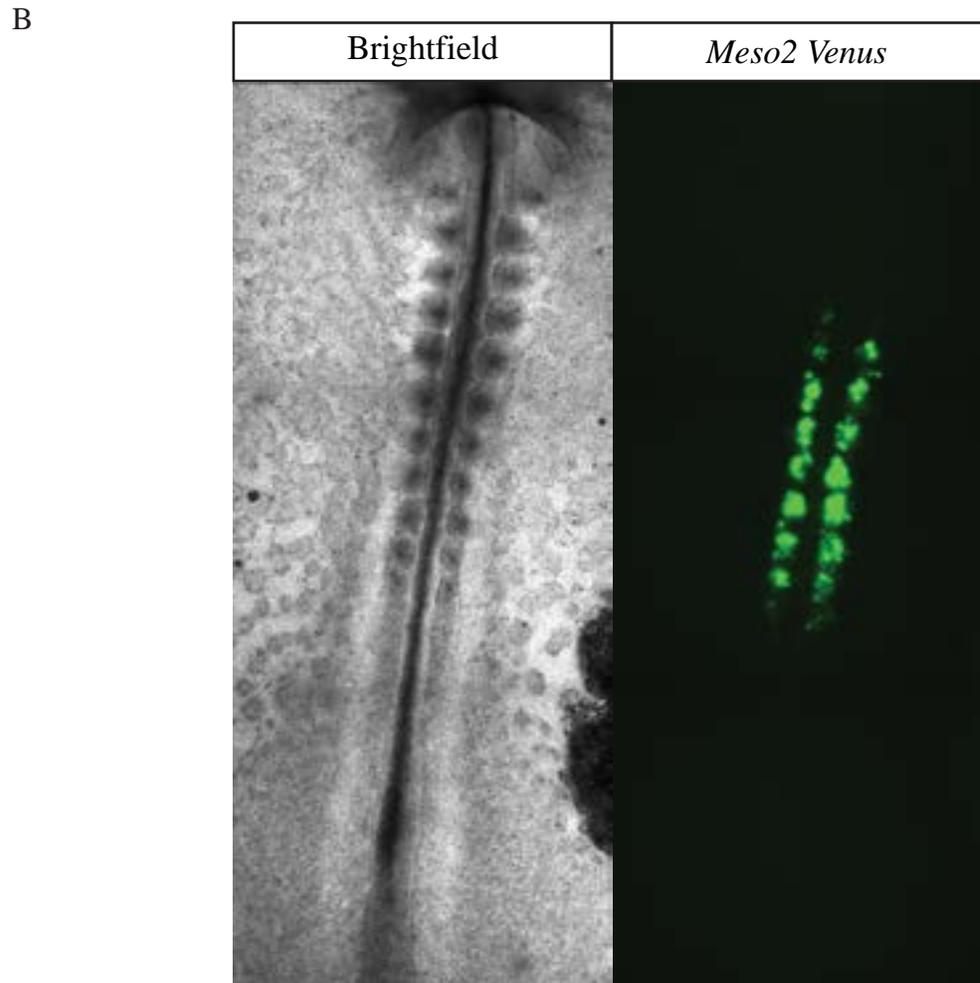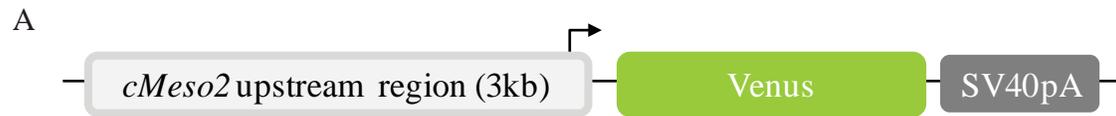
Figure 26 - Construction of a *Meso2* reporter

A. Construct design of the ***Meso2-Venus*** reporter

B. Representative pictures of a day 2 chicken embryo showing the morphology (*left* - brigthfield) and the reporter expression (*right* - Venus fluorescence)

A

T=0 min

T=+90 min

B

Brightfield

Endogenous *Meso2*

Venus mRNA
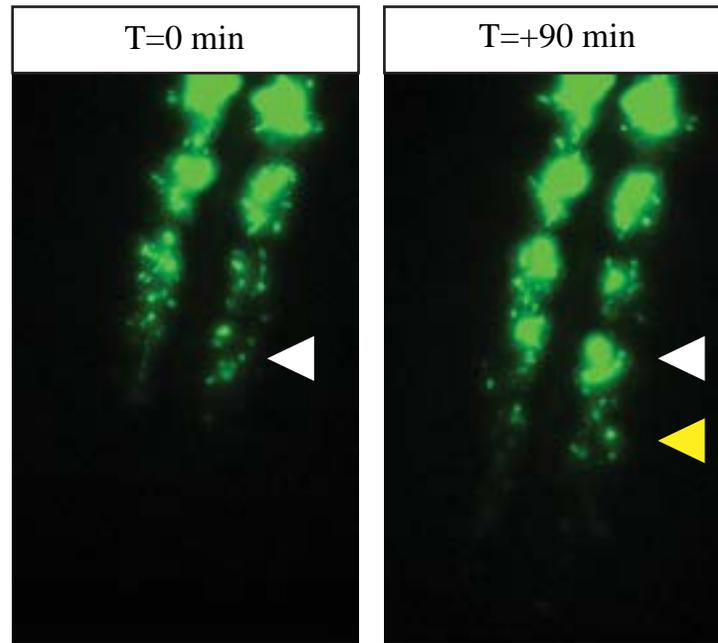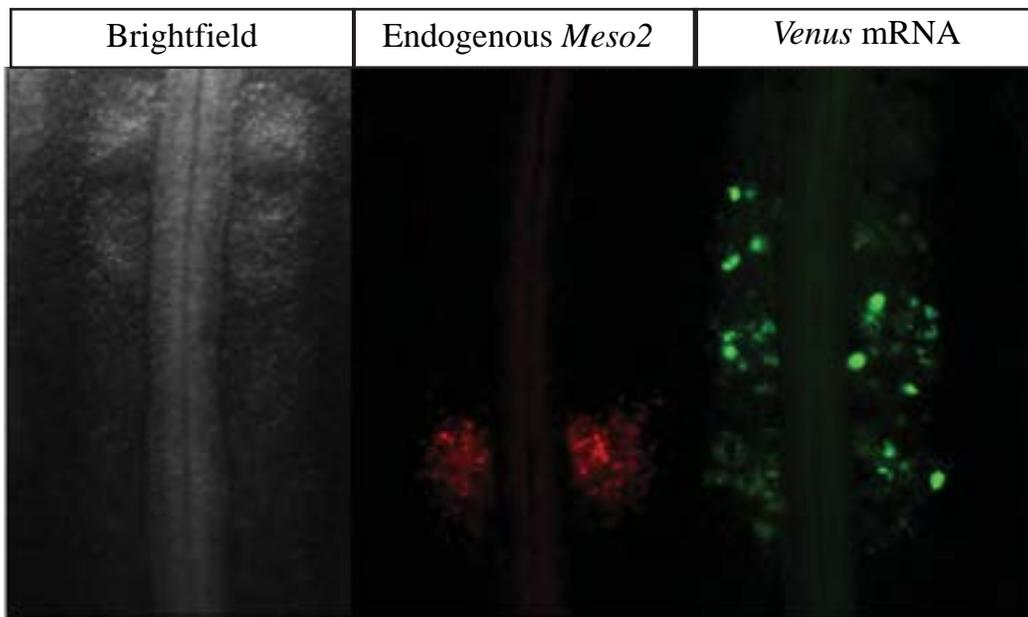
Figure 27 - Validation of the *Meso2* reporter

A. Expression pattern of the *Meso2-Venus* reporter (Venus fluorescence) at T=0min and T=+90min. The white arrow marks the same stripe of Meso2 between the two pictures, the yellow arrow marks the new stripe.

B. Fluorescent *in situ* hybridization of the endogenous *Meso2* mRNA and the *Venus* mRNA of the *Meso2* reporter

A.

| Brightfield | *Meso2-Venus* | *CAGGS-mCherry* |

cMeso2 - 500bp — Venus — pA

cMeso2-250bp — Venus — pA

B.

cMeso2– 3kb (-TBSE) — Venus — SV40pA

| Brightfield | *Meso2-Venus* | *CAGGS-mCherry* |
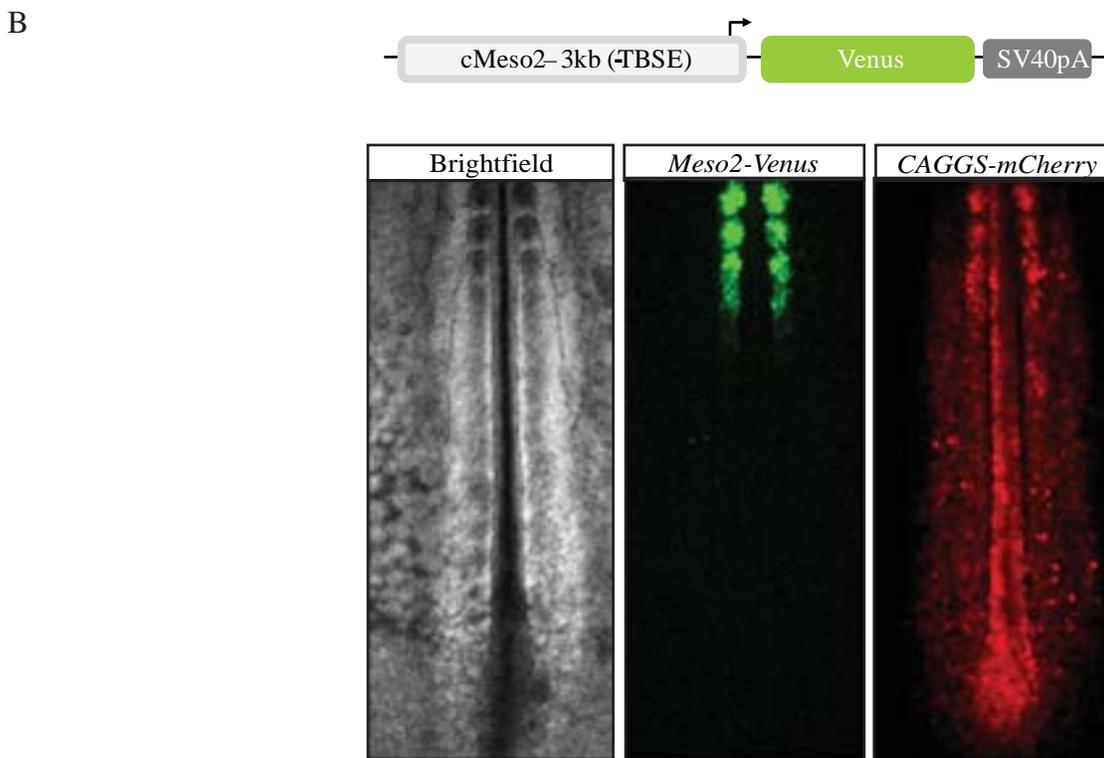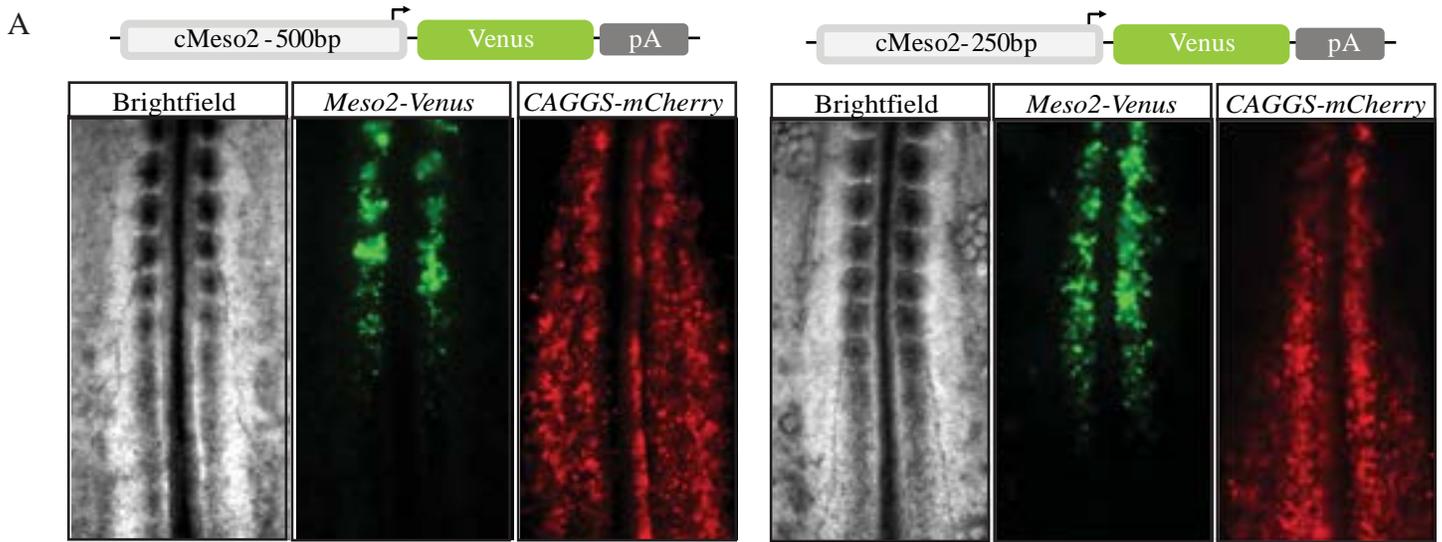
Figure 28 - Analysis of the *Meso2* enhancer

A. Expression pattern for a reporter containing 500bp (*left*) and 250bp (*right*) of the upstream regulatory sequence - a construct ubiquitously expressing mCherry was co-electroporated to validate the specificity of expression in the paraxial mesoderm

B. Expression pattern for a construct containing the 3kb enhancer without the putative tailbud suppressing element hypothesized by Haraguchi et al. (2001)

activation of the reporter every 90 minutes, confirming that it faithfully reports the activation of *Meso2* (Figure 27A). Last we performed double fluorescent *in situ* hybridization for the endogenous *Meso2* and for *Venus*; this revealed that both genes are activated at the same axial level (Figure 27B).

We further narrowed down the sequences required for the segmental activation of the reporter and found that only the first 250bp upstream of the start codon are sufficient to reproduce the stripe pattern (Figure 28A).

We tried to destabilize the fluorescent construct to better follow the dynamics of *Meso2* by fusing the Venus to a degradation domain (PESTd1) and the mRNA to AU-rich elements (Voon et al., 2005). We also fused Venus to the C-terminal sequence of Meso2 that supposedly target Mesp2 to the proteasome in mouse (Morimoto et al., 2006). However, in both cases, we could not reproduce the endogenous pattern of Mesp2 in mouse as the fluorescence perdures in the anterior somites.

1.2 Analysis of the enhancer sequence

As we were interested in identifying the molecular factor of the determination front, we tried to find the regulatory sequence that mediates the repression of *Meso2*. A strong candidate was the region between the position -185 and -160 for the mouse homologue *Mesp2*. Indeed, Haraguchi and colleagues showed that reporter constructs with an enhancer larger than 185 bp are able to reproduce the segmental activation of *Mesp2*, while a reporter with only 160bp upstream of the start codon showed ectopic expression in the tailbud (Haraguchi et al., 2001). This region could thus contain binding sites for a repressor. Accordingly, this region is well conserved in chicken (20/25bp). However, deletion of the homologue sequence in the fluorescent reporter comprising the 3kb enhancer region has no effect and no ectopic expression in the tailbud was observed (Figure 28B). Last, analyzing the putative binding sites for transcription factors in this region (using the Vista tool) did not reveal known regulators of mesoderm development.

1.3 Effect of Tbx6 overexpression

To identify this putative repressor, we turned to an unbiased approach by trying to pull-down the enhancer region. The rationale was to purify the enhancer region and identify proteins bound to the DNA. To preserve the natural interactions between DNA and proteins, we adopt the following strategy: DNA-binding sites *UAS* were introduced in front of the 250bp *Meso2* enhancer, and the fluorescent reporter was electroporated along with a construct overexpressing Gal4-Flag (that binds to *UAS*). Therefore, this fusion should bind to the reporter through Gal4, and then, be purified through the Flag tag to pulldown the enhancer and the proteins bound to it. As a control, we
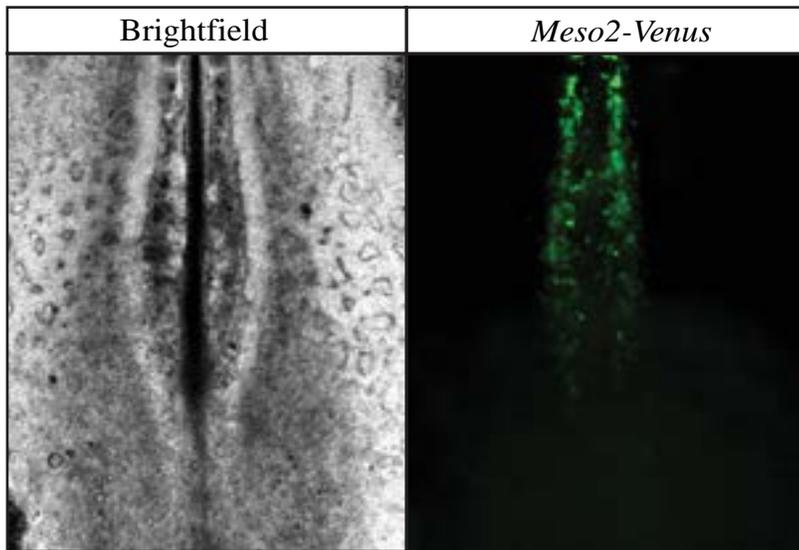
Figure 29 - Activation of *Meso2* by overexpression of Tbx6

A. Expression pattern of the *Meso2-Venus* reporter following overexpression of Tbx6 (Venus fluorescence)

B. *In situ* hybridization for the endogenous *Meso2* following overexpression of Tbx6.

electroporated a construct overexpressing Tbx6-Flag (CAGGS-Tbx6). Surprisingly, we observed ectopic expression of the fluorescent *Meso2* reporter in the posterior PSM. This also led to an epithelialization of the tissue as evidenced by compaction of cells, and in some cases, to the formation of epithelial blocks (Figure 29A). We also confirmed this finding using the original 3kb fluorescent reporter. We then expressed Tbx6 using a weaker driver (CMV promoter without the *β-globin* intron) to approach physiological levels; in this condition, we still observed the ectopic activation of the fluorescent reporter albeit in much smaller number of cells. Furthermore, this effect is likely a direct effect of Tbx6 overexpression as embryos electroporated at stage HH5 show the first sign of reporter activation at stage HH6 (after ~4h). Last, to validate that overexpression of Tbx6 leads to the ectopic activation of *Meso2*, we confirmed this phenotype by examining the endogenous transcript by *in situ* hybridization (Figure 29B).

To account for this effect, we could first suppose that a repressor effect on Tbx6 at the *Meso2* enhancer is relieved. Overexpressing Tbx6 would thus lead to a titration of this repressor and an activation of *Meso2*. We tested this hypothesis by overexpressing the C-terminal part of Tbx6 that does not contain the T-box domain; this should allow us to partially test the titration hypothesis as this construct has no DNA binding activity. However, no ectopic activation of the reporter was observed when overexpressing the C-terminal part of Tbx6 arguing against this hypothesis (while we cannot exclude that the repressor binds to the T-box domain).

We then briefly examined the mechanism that could mediate Tbx6 activation and we postulated the existence of post-translational modifications of Tbx6 able to rapidly modulate its activity. We first turned to phosphorylations, and found that phosphorylations of the mouse Tbx6 were predicted to occur on Y137 and Y151 based on a large-scale screen performed on C2C12 (Cell Signal Technologies 2008 – Phosphosite Plus database). While such screens can give a large number of false-positive candidates, the phosphorylation site at the site Y137 (mouse) was interesting for several reasons: first, it was conserved among the homologues of Tbx6 in mouse, chicken (Y182), and zebrafish (Figure 30A) and among all mouse T-box proteins (Miller et al., 2008); second, mutations at this site are associated with the Ulnarmammary syndrome for *Tbx3* and with congenital heart defects for *Tbx5* (Packham and Brook, 2003); last, mutating the tyrosine by a non-phosphorylable amino acid leads to a severe reduction of the transcriptional activity of T-Bet and Tbx3 (Miller et al., 2008, Lu et al., 2011). Therefore we tested the role of this residue by overexpressing a form of Tbx6 where the tyrosine is substituted by an alanine (not phosphorylable), and found that this mutant form was not able to activate the endogenous *cMeso2* as evidenced by *in situ* hybridization (Figure 30B). Furthermore, we tested the role of two other conserved amino acids (R264, R268) (Figure 30B), for which mutations reduced the ability of T-Bet to recruit the histone

A

```
Mouse       FPACRVSVTGLDPEARYLFLLDVVPVDGARYRWQGQHWEPSGKAEPRLPDRVYIHPDSPA 180
Zebrafish   FPQLRVKLSGLNPSLRYILLLDIVPVDSSRYRFQDNSWQVVGGAEARLPDRVFIHPDSPA 151
Chicken     FPQCKIKVSGLIPYAKYLMLVDFVPVDNFRYKWNKDQWEVAGKAEPQLPCRTYVHPDSPA 116


Mouse       TGAHWMRQPVSFHRVKLTNSTLDPHGHLILHSMHKYQPRIHLVRATQLCSQHWG-GVASF 239
Zebrafish   TGEHWQNRTISFHRAKLTNNTLDAQGYIILHSLHRYQPRVHVIEARDVL--MWGRTQHSF 209
Chicken     PGSHWMKEPVSFQKLKLTNNTLDQHGHIILHSMHRYKPRFHIVQADDLFSVRWS-IFQVF 175
```

B

| Tbx6 Y182A | Tbx6 R264A, R268A |

Figure 30 - Mechanism of *Meso2* activation

A. Alignment of Tbx6 homologues in mouse, zebrafish, and chicken. In red are indicated the residues identified by Miller and colleagues as necessary for the recruitment of chromatin modifying complexes involved for T-box transcriptional activation (Y182, K264/R268)

B. *In situ* hybridization for the endogenous *Meso2* after overexpression of constructs harboring the Y182A or R264A+R268A mutations

demethylase Jmjd3. Interestingly Miller and colleagues showed that the overexpression of Tbx6 in EL4 cells led to the activation of T-Bet targets, but this was blocked by knocking-down Jmjd3 suggesting that Tbx6 activity could follow a similar mechanism (Miller et al., 2010). In our hands, we similarly found that overexpressing this mutant construct does not induce the activation of *Meso2* (Figure 30B). We note that we did not check the stability of these fusion proteins, and cannot exclude a degradation induced by these mutations. Together, this suggests, however, that the mechanism of *Meso2* activation could be identical to the T-bet induction and involves the recruitment of chromatin modifying complexes (such as Jmjd3). Further studying the underlying mechanism and its regulation by the PSM regulators was, however, difficult to achieve technically and out of the scope of this thesis.

1.4 Identification of downstream targets of ERK

Previous work has linked the Fgf/ERK pathway to the control of *Mesp2* activation (Delfini et al., 2005, Niwa et al., 2011). Therefore we aimed to identify the targets of ERK in chicken embryos in order to find transcriptional regulators that could mediate its effect on *Mesp2*. For that purpose, we performed mass spectrometry of PSM tissues from embryos treated with the MEK1/2 inhibitor PD0325901. MEK are downstream effectors of the Fgf receptor that can phosphorylate the protein ERK (phosphorylated ERK - pERK). In turn, this activates the kinase activity of ERK, which ultimately leads to the regulation of a wide range of targets, notably transcription factors (Dorey and Amaya, 2010).

As the inhibition of the Fgf/ERK pathway rapidly leads to the activation of *Mesp2* (Niwa et al., 2011), we first determined the kinetics of ERK inhibition to identify the earliest time point of signaling blockade. We treated chicken embryos with PD0325901 (10μM) and examined the phosphorylation of ERK by immunostaining after 2/3/4/5 hours. We observed that after 2 hours, there was a strong diminution of the pERK signal, which was barely detectable after 4 hours (Figure 31A). We further confirmed by western blot that after 4 hours, phosphorylation of ERK was strongly suppressed compared to the vehicle control (Figure 31B). Therefore we chose to compare the proteomes of DMSO and PD0325901 treated embryos at this time point to detect direct effects. We dissected ~100 PSM of chicken embryos per condition and submitted the samples to the Thermo Fisher Center for Multiplexed Proteomics at the Harvard Medical School. Protein extracts were digested and then purified to enrich for phosphoproteins (Figure 31C). Quantification of the protein amount revealed a lower level than expected by preliminary experiment (~40μg), so that we could not perform triplicates as initially designed. The mass spectrometry results were analyzed and 76 quantified phosphopeptides were identified (Figure 32). However, only 3 phosphopeptides were downregulated (> 2-fold change) in the PD0325901 sample compared to the DMSO control, and no

A

| DMSO | PD03 |

B

| DMSO | PD03 | DMSO | PD03 |

C

1. Sample preparation

Culture of chicken embryos w/ and w/o PD03 for 4h

↓

Dissection of PSM ~100/conditon

↓

Lysis

2. Sample analysis

Precipitation MeOH/chloroform

↓

Digestion Trypsin/LysC

↓

Labeling (Tandem Mass Tag)

↓

Fractionation withTiO$_2$ beads

↓

LC-MS3 (Orbitrap)
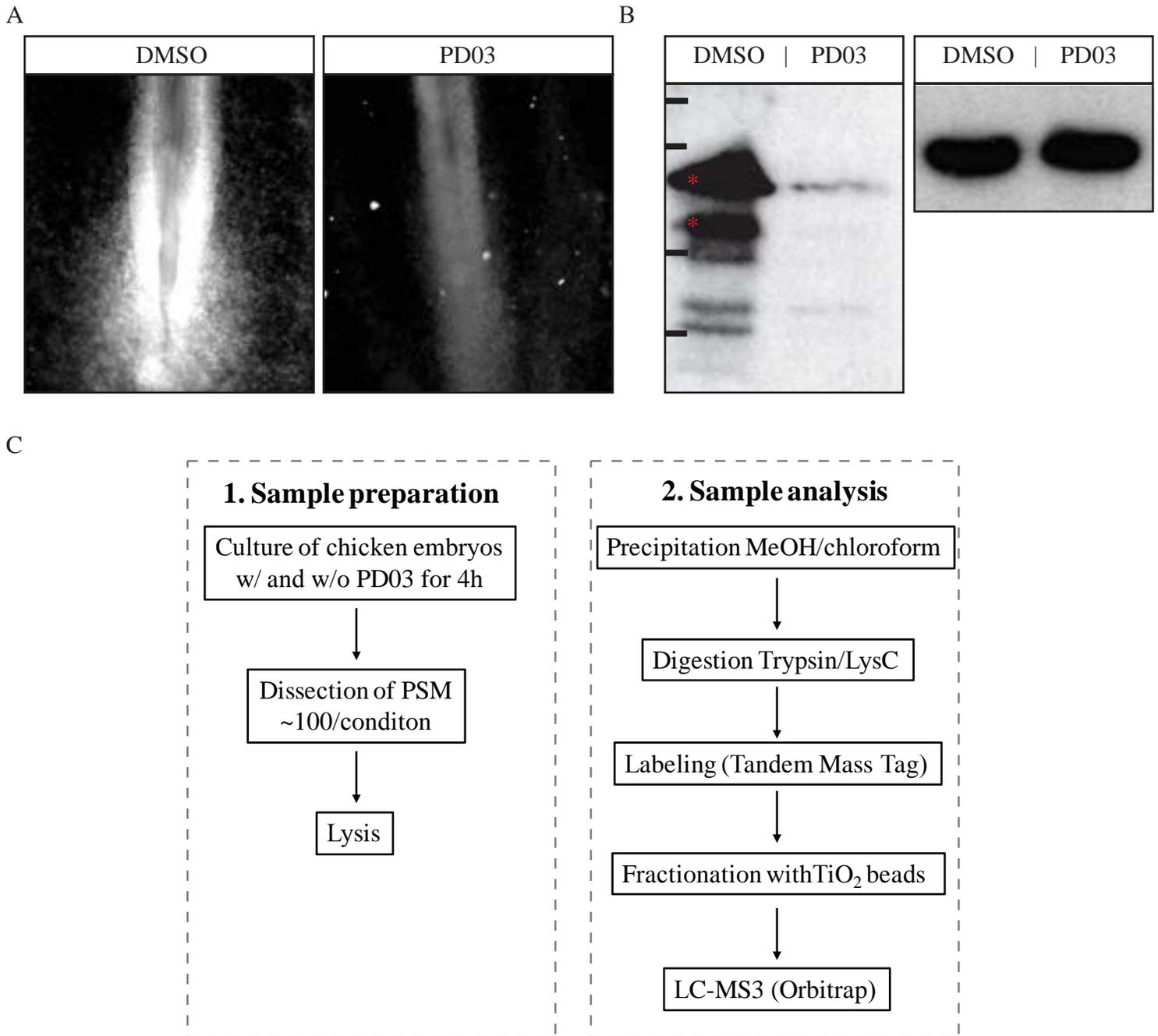
Figure 31 - Identification of pERK downstream targets in the chicken PSM

A. Immunostaining for pERK after 4h of treatment with the MEK1/2 inhibitor PD0325901 (10μM) or the vehicle control (DMSO)

B. (*Left*) Western blot for pERK after 4h of treatment with the MEK1/2 inhibitor PD0325901 (10μM) or the vehicle control (DMSO) (8 PSM/condition). Red asterisks indicate the position of pERK based on the antibody manufacturer's indications. (Molecular weight scale: 72/55/36/28kDa). (*Right*) Loading control (β-actin).

C. Experimental protocol for the detection of pERK targets. Both bound fractions to the TiO$_2$ beads (enriched for phosphopeptides) and unbound fractions (depleted for phosphopeptides) were analyzed by Orbitrap.

A
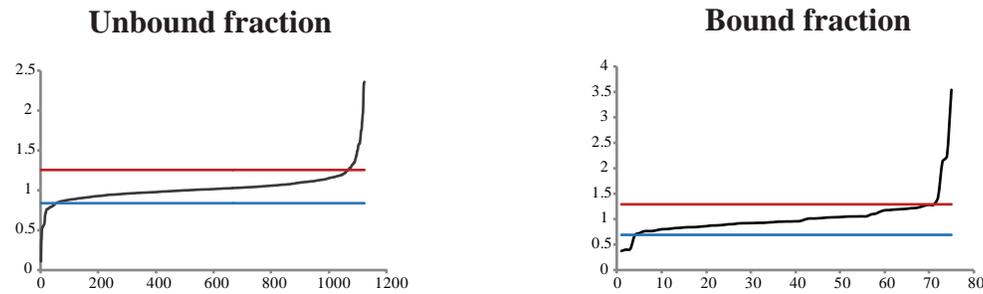
Unbound fraction **Bound fraction**

B

Upregulated by PD03

Unbound

	Protein Name	Ratio PD03/DMSO
F1NH09	disheveled-associated activator of morphogenesis 1	2.36
P01014	Ovalbumin-related protein Y	2.35
E1BRK6	KxDL motif containing 1	2.34
Q8JIG5	Alpha-1-acid glycoprotein	2.25
P29332	G2/mitotic-specific cyclin-B2	2.08
E1BXF4	Reticulocalbin 1	1.97
F1NIW6	TraB domain-containing protein	1.95
P09642	Tubulin alpha-3 chain	1.89
P02659	Apovitellenin-1	1.86
E1BYN5	E1BYN5	1.79
P01012	Ovalbumin	1.76
F1NK75	tropomyosin 4	1.74
H9L074	tropomyosin 3	1.74
P00698	Lysozyme C	1.69
O42273	Protein TENP	1.65
Q5ZIK9	Coatomer subunit epsilon	1.62
E1BXG0	Peptidyl-prolyl cis-trans isomerase	1.58
P02845	Vitellogenin-2	1.58
H9L1I6	Uncharacterized protein	1.58
F1NMQ3	PEST Proteolytic Signal Containing Nuclear Protein	1.58
P79781	Ubiquitin-40S ribosomal protein S27...	1.57
E1BYU8	nucleoporin 98kDa	1.56
E1BXK5	RNA binding motif protein 5	1.54
P19121	Serum albumin	1.51
F1NT45	FHA domain-interacting nucleolar phosphoprotein	1.50
E1BQJ3	NudC domain containing 1	1.49
P24032	Myosin regulatory light chain 2, sm...	1.47
F1NW95	H Dehydrogenase (Ubiquinone) 1 Alpha Subcomple	1.44
Q5F375	Serine/threonine-protein kinase 24	1.44
E1BQC2	Ovotransferrin	1.42
R4GLH7	Enoyl CoA Hydratase 1, Peroxisomal	1.40
F1NW02	Alpha-amylase	1.40
F1NGH1	Phosphatidylinositol Transfer Protein	1.38
O93532	Keratin, type II cytoskeletal cochl...	1.36
F1NB10	G Protein Pathway Suppressor 1	1.35
Q90WU3	ATP-dependent RNA helicase DDX1	1.35
F1NCM5	Prostaglandin Reductase 1	1.34
E1C7M7	Catenin alpha-1	1.34
F1NDA0	Glycylpeptide N-tetradecanoyltransf...	1.33
P80585	Tubulin-specific chaperone A	1.33
F1NZS9	Thymopoietin	1.32
E1C279	NAD(P) Dependent Steroid Dehydrogenase-Like	1.32
H9KZP2	KERATIN 8	1.32
F1NJK8	PRMT8	1.31
F1P362	Spalt-Like Transcription Factor 3	1.31
F1P5I8	(Acyl-CoA Binding Domain Containing 3)	1.30
E1BRQ5	Coiled-Coil Domain Containing 25	1.29
F1P1V2	poly(U)-binding-splicing factor PUF60-like	1.29
Q5ZKR8	DNA helicase	1.28
Q8UUW7	KH domain-containing, RNA-binding, ...	1.28
Q5ZKK1	Microtubule-associated protein RP/E...	1.28
F1NV02	Apolipoprotein B	1.28
Q5ZM76	far upstream element (FUSE) binding protein 3	1.27
E1BUJ1	RNA Binding Motif Protein 17	1.27
E1C928	Thioredoxin Reductase 3	1.27
F1NF53	Alpha-amylase	1.25

Bound

	Protein Name	Ratio PD03/DMSO
MYH9	Myosin-9	3.54
R4GJG8	NELF-E	2.24
HS90A	Heat shock protein HSP 90-alpha	2.13
F1NC33	Heat shock cognate protein HSP 90-beta	1.43

Downregulated by PD03

Unbound

	Protein Name	Ratio PD03/DMSO
E1C810	Ribosomal protein L37	0.10
F1NH93	Ribosomal protein S20	0.35
P08070	Tubulin alpha-2 chain	0.38
F1NJ97	Isocitrate dehydrogenase [NAD] subu...	0.50
E1BTE0	single-stranded DNA-binding protein, mitochondrial	0.52
P08250	Apolipoprotein A-I	0.53
F1NHD3	60S ribosomal protein L7-like 1	0.53
F1NCE1	eukaryotic translation initiation factor 3, subunit D	0.54
F1NLH8	DnaJ (Hsp40) homolog, subfamily A, member 4	0.55
Q5ZHW8	40S ribosomal protein S14	0.55
F1NTT1	histidyl-tRNA synthetase, cytoplasmic	0.56
F1NBD1	asparaginyl-tRNA synthetase, cytoplasmic	0.57
F1NKU2	maternal embryonic leucine zipper kinase	0.58
Q9PT88	RNA polymerase common subunit RPB6	0.61
F1NU18	polyribonucleotide nucleotidyltransferase 1	0.68
E1C2U4	minichromosome maintenance complex component 4	0.69
P50890	40S ribosomal protein SA	0.71
F1P212	thioredoxin-related transmembrane protein 3	0.72
F1P0T4	heterogeneous nuclear ribonucleoprotein L-like	0.74
F1NX56	O-linked N-acetylglucosamine (GlcNAc) transferase	0.75
P09645	Tubulin alpha-8 chain	0.76
R4GFK7	Uncharacterized protein	0.76
F1NIX0	60S ribosomal protein L8	0.76
F7BGT1	ix (nucleoside diphosphate linked moiety X)-type mo	0.76
Q5ZJJ8	Ubiquitin-like domain-containing CT...	0.76
R4GJ91	up-regulated during skeletal muscle growth protein 5	0.76
Q8UWG7	60S ribosomal protein L6	0.77
Q5ZJ02	DBIRD complex subunit ZNF326	0.77
Q5ZJ21	Uncharacterized protein	0.77
R4GMG2	Ribosome biogenesis protein BOP1	0.78
E1C2F7	SMARCA2	0.78
F1N8N2	RNA-binding protein 6	0.78
F1P0G0	ubiquitin-conjugating enzyme E2 G1	0.79
F1NAC6	ubiquinol-cytochrome c reductase core protein I	0.79
F1NJW0	A kinase (PRKA) anchor protein 12	0.79
E1C5I9	SRSF protein kinase 1	0.79
P02272	Histone H2A.V	0.79
F1NQG5	Ribosomal protein L15	0.79
P27731	Transthyretin	0.79
P23007	Citrate synthase, mitochondrial	0.80
Q5F3J5	Proteasome activator complex subuni...	0.80
Q5ZJ56	60S ribosomal protein L7	0.80
P35062	Histone H2A-III	0.80
E1BT53	urin, cytoskeletal calmodulin and titin-interacting Rho	0.80
F1NSS7	ribosome biogenesis protein BRX1 homolog	0.81
E1C297	microsomal glutathione S-transferase 3	0.81
H9L1A3	Uncharacterized protein	0.81
Q5ZL26	Phosphoribosyl pyrophosphate syntha...	0.82
E1C8V9	small nuclear ribonucleoprotein polypeptide G	0.82
Q9W7I5	Histone-binding protein RBBP4	0.83
Q9IAY5	Protein syndesmos	0.83
F1N9U8	electron-transfer-flavoprotein, alpha polypeptide	0.83
P0C1H3	Histone H2B 1/2/3/4/6	0.83
P08023	Actin, aortic smooth muscle	0.83
Q5ZMR4	splicing factor, arginine/serine-rich 13A	0.84
Q5F4A3	Acidic leucine-rich nuclear phospho.	0.84

Bound

	Protein Name	Ratio PD03/DMSO
TOP2B	TOP2B topoisomerase (DNA) II beta	0.37
F1NDA0	Glycylpeptide N-tetradecanoyltransferase	0.40
O93481	HP1-gamma	0.41
H9L3J8	UBAP2L	0.68

Figure 32 - Putative targets of the ERK pathway in chicken PSM

A. Graph showing the fold-changes upon PD03 treatment for the proteins of the unbound fraction (n=1122) and bound fraction (n=76). Blue and red bars delimitate the top 5% proteins upregulated and downregulated.

B. Tables indicating the proteins downregulated or upregulated upon PD03 treatment (top 5% in each condition) with the ratio of normalized spectral counts between the control and PD03 treatments.

classical targets of ERK such as the ETS transcription factors, were identified in this screen. Those proteins were: DNA topoisomerase 2-beta; Glycylpeptide N-tetradecanoyltransferase; Heterochromatin Protein 1 gamma (HP1γ). The latter was a potential candidate, as i) it is a transcriptional repressor, ii) HP1γ was shown to be regulated by phosphorylation (Lomberk et al., 2006, Shimada et al., 2009), iii) it could be part to a repressor complex containing the T-box protein Mga and able to bind to T-box elements (Ogawa et al., 2002). However, the poor quality of the mass spectrometry data (absence of canonical Fgf/ERK targets, low number of candidates) led us to not pursue this hypothesis.

1.5 Existence of a bistable transition

To explain the sharp activation of *Mesp2*, a bistable state was postulated in the anterior PSM. Bistability refers to the existence of two possible stable states for one system parameter. In the context of the PSM, this would involve the existence of an undetermined state (Mesp2-negative) and a determined state (Mesp2-positive) for the same range of Fgf signal. In the posterior PSM, only the former is stable, while both become stable as Fgf signaling decreases and cells are passed by the determination front. In this bistability window, the segmentation clock would trigger the transition to the determined state (Cooke and Zeeman, 1976, Goldbeter et al., 2007) (Figure 33A).

To test this hypothesis, we aimed to probe hysteresis, one of the main features of bistability. A system exhibits hysteresis when its state depends on its history. In the context of the PSM, undetermined cells experiencing a decrease of Fgf ("forward path") remain undetermined in the bistability window, while determined cells artificially replaced in this bistability window ("reverse path"- e.g. by increasing Fgf) stay in the determined state: for one condition, cells can be in two distinct states depending on their history (Figure 33A).

In order to follow the cell state, we first developed a fluorescent reporter for *Msgn1* (also known as *Mespo*). The rationale was to combine both *Msgn1* and *Meso2* reporters. Along the "forward path" of determination, cells would become *Msgn1+/Meso2-*, then *Msgn1-/Meso2+*. After graft of the determined cells in the posterior PSM ("reverse path"), cells should revert to the *Msgn1+/Meso2-* state. Such transition could be detected by combining a stable *Meso2* reporter and a destabilized *Msgn1* reporter: only cells positive for both reporters (secondary activation of the *Msgn1* reporter and persistence of the *Meso2* reporter) would have been determined, and then brought back to the posterior PSM state. To build the *Msgn1* reporter, we follow a similar strategy as for the *Meso2* reporter: a 5kb genomic region upstream of the start codon was placed in front of the coding sequence for Venus. This reporter was specifically expressed in the paraxial mesoderm; however, we detected expression of the reporter in the tailbud contrary to the endogenous gene (Figure 33B) (Gomez et al., 2008). As for the *Meso2* reporter, the Venus fluorescence persists in the anterior somite due to the stability of the protein, but *in situ* hybridization for the *Venus* transcript showed
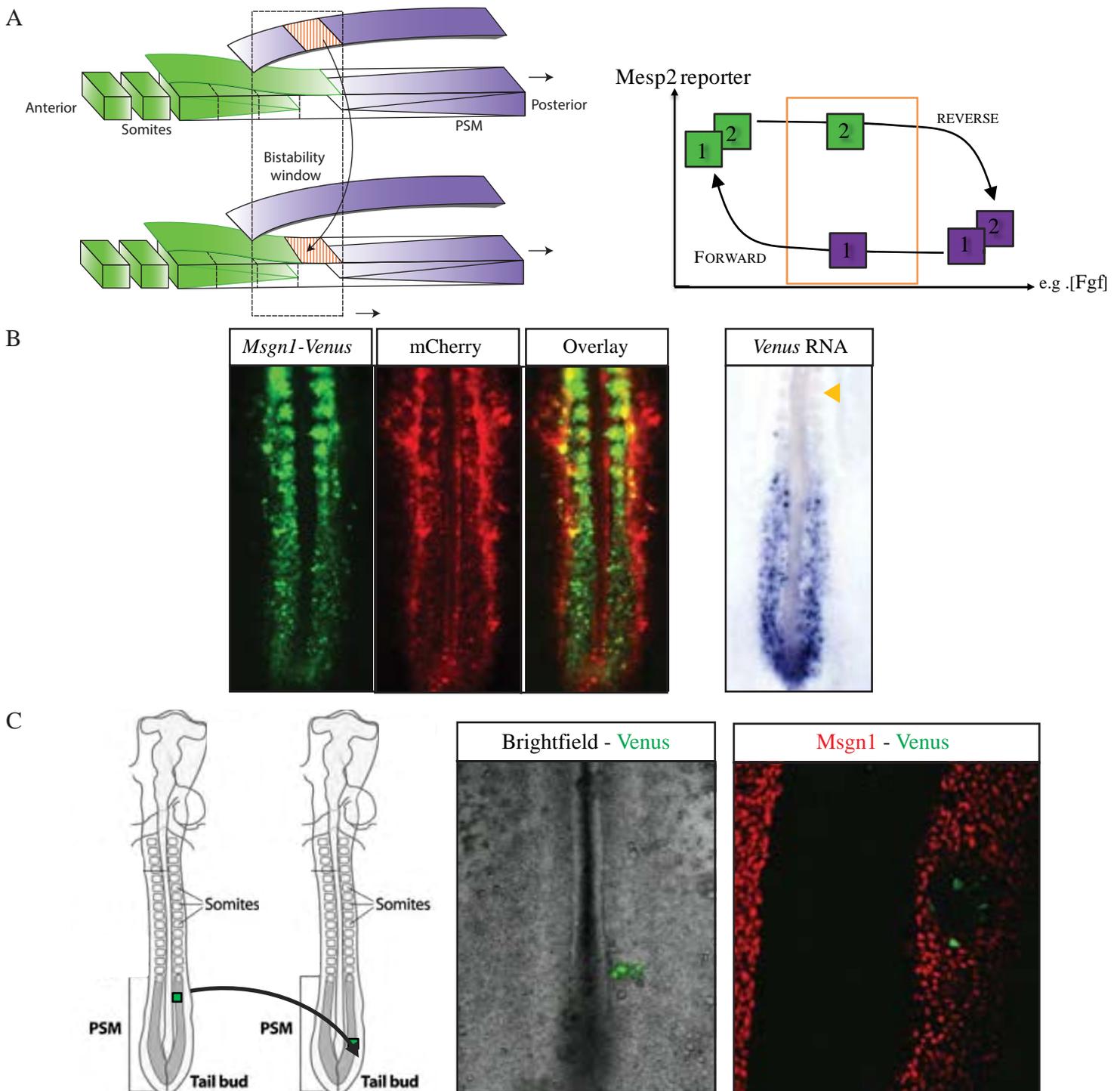
Figure 33 - Hysteresis in PSM determination

A. (*Left*) Scheme representing the proposed bistable transition between the undetermined state (purple) and the determined state (green). (*Right*) Experimental design to test hysteresis in PSM determination: in the bistability window (orange box), cells could either be in a Mesp2-positive or Mesp2-negative state

B. *Msgn1-Venus* reporter (*Left*) Fluorescence pattern of the *Msgn1* reporter along with a constitutevely expressed mCherry as electroporation control. (*Right*) *In situ* hybridization for *Venus* of an embryo electroporated with the *Msgn1*-reporter (the arrow marks the limit of the Venus fluorescence)

C (*Left*) Experimental design to probe the reversibility of PSM determination. (*Right*) Pictures of the graft and immunostaining for Msgn1 and Venus

106

that the reporter activation is confined to the PSM (Figure 33B). We then tried to destabilize the reporter by using the PEST domains as well as the endogenous 3'-UTR. However, we were not able to generate a construct able to follow the extinction and re-activation of the reporter, which led us to not further pursue this approach. To bypass the problem of fluorescent protein folding and degradation, we tried to use the *Spinach* RNA aptamers (Paige et al., 2011) (the fluorophore becomes fluorescent when bound to the RNA) under the control of the *Msgn1* reporter; however, no signal was detected compared to the control. As an alternative method to the fluorescent reporters, we performed simple grafts of cells from the anterior PSM in the posterior PSM (Figure 33C); the donor embryo was electroporated with a plasmid constitutively expressing Venus (either constitutively with a CAGGS promoter or with the *Meso2* reporter) to follow the graft cells. For all grafts (8/8), cells were not dedifferentiated after 8h, as evidenced by the absence of Msgn1 immunostaining and by the formation of epithelial structures, reminiscent of the somites. While we cannot exclude that the grafted region was "too far" in the differentiation path or that the conditions were not strong enough to bring it back to the undetermined PSM state, this experiment would argue against a reversibility of the PSM determination, making difficult to actually probe the existence of hysteresis.

2. Tools to study the formation of the Fgf8 gradient

In this section, we briefly present our efforts to quantify the Fgf8 gradients in chicken embryo. We first tried to quantify the gradient of RNA (Figure 34A). We used the quantitative method of *in situ* hybridization developed by Cheung and colleagues, where the digoxygenin-labeled probe is directly recognized by a fluorescent anti-digoxygenin antibody (Cheung et al., 2014). However, this method was poorly sensitive in our hands as only the tailbud showed a weak signal. We tried to adapt a single-molecule method developed by the group of T.Gregor (personal communication). In this technique, small fluorescent probes "coat" the transcript allowing the detection of single transcript. To adapt this method, we first performed RACE experiments to sequence the 5'-UTR and 3'-UTR of *Fgf8b* with the idea of maximizing the sequence length, and thus the number of fluorescent probes and we were able to clone the 3'-UTR. However, following the protocol communicated by T.Gregor, we were not able to detect any signal compared to a control embryo (no probe). It is likely that the lower number of fluorescent probes (19 probes) prevent the detection of single molecules (even if Raj and colleagues reported the detection of single spots with only 12 probes (Raj et al., 2008)). Alternatively the group of A.Raj reported that tissue section can "*have a host of problems*" and can generate a higher background, so it is likely that wholemount hybridization are more challenging. We note that we are able to detect the gradients of both RNA and protein Fgf8 using amplification by the horseradish peroxidase (Figures 34B-35); however, such method is not amenable to

A.
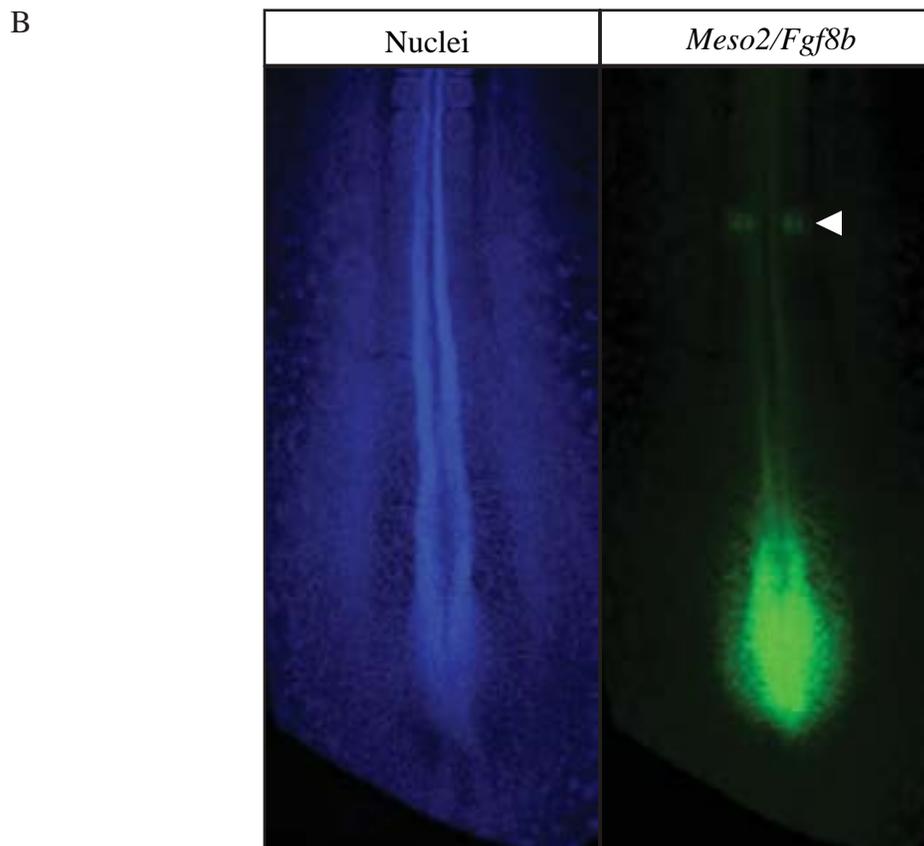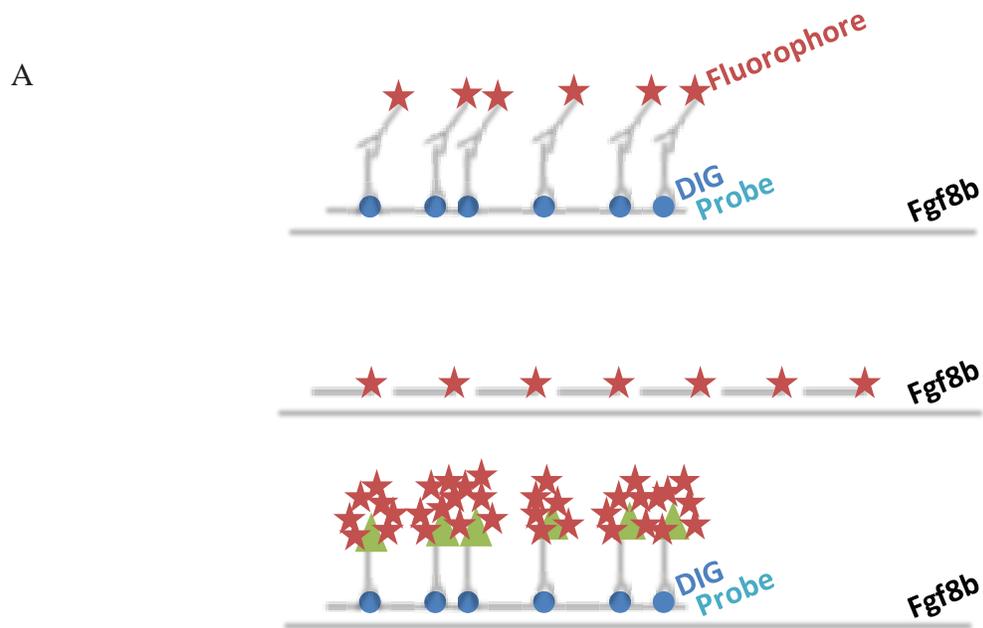
Figure 34 - RNA gradient of *Fgf8b*

A. Strategies to detect the gradient of *Fgf8* mRNA. (*Top*) Cheung and colleagues method: an *in situ* hybridization probe is detected by a primary antibody anti-digoxigenin (DIG). (*Middle*) Single-molecule detection using multiple fluorescent probes. (*Bottom*) Classical Tyramide Signal Amplification (TSA) method

B. (*Left*) Nuclei staining of day2 chicken embryo. (*Right*) Fluorescent *in situ* hybridization (TSA) for *Meso2* (anterior stripe - white arrow) and *Fgf8b* (posterior gradient).
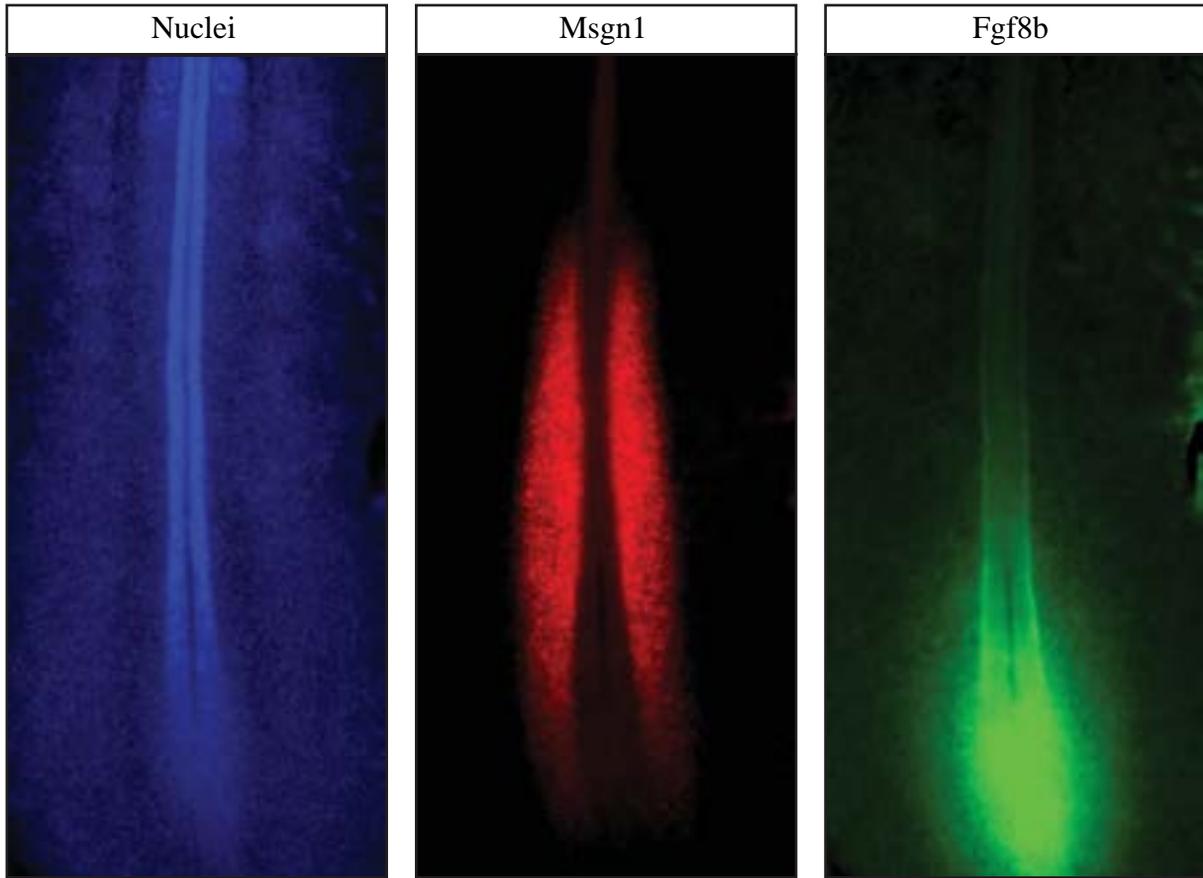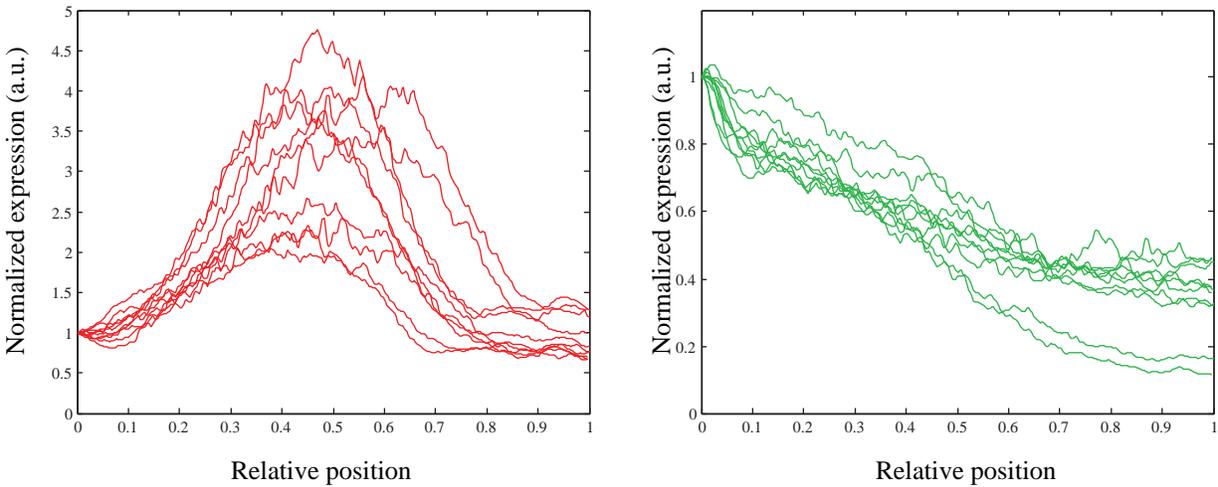
Figure 35 - Protein gradient of Fgf8b

A. Pictures of a day 2 embryo (*Left*) Nuclei staining. (*Middle*) Immunostaining for Msgn1 (*Right*) Immunostaining for Fgf8b

B. Graphs showing the profiles of Msgn1 (*left*) and Fgf8b (*right*) proteins along the presomitic mesoderm (0 corresponds to the posterior beginning of the PSM; 1 corresponds to its anterior boundary)

quantification as it is classically considered as non-linear. Furthermore, we experienced some variability between embryos for the detection of the RNA detection.

Last, we present the construction of a fluorescent fusion between FGF8B and Venus to study the diffusion of the ligand (Figure 36A). The aim was to study the diffusive properties of FGF8B by FRAP and variant techniques. Notably, the asymmetric induction of Fgf/ERK signaling by a Fgf-soaked bead (Delfini et al., 2005) suggested a possible biased transport of the ligand. We followed the strategy of Yu and colleagues (Yu et al., 2009) with a construct [FGF8B signal peptide]::[Fluorescent protein]::[FGF8B] under the control of a CAGGS driver. As fluorescent proteins, we tried Venus and the photoconvertible proteins, mEOS2 and Dendra2. These constructs were weakly visible probably due to a short half-life (in the case of mEOS2, no signal was detectable), and we focused on the Venus fusion that displays a higher signal-to-noise ratio (Figure 36A). In some embryos, we noticed a reticular organization of Fgf8-Venus reminiscent of the HSPG meshwork. Its overexpression recapitulated the phenotype of Fgf8 gain-of-function (blockade of somite formation, long PSM – Figure 36B). Therefore, to avoid artifacts due to a saturation of the system, we tried to express the fluorescent fusion under the control of a weaker promoter. Notably, we used a driver comprising a 3.1 kb genomic region homologue to the *CR2* enhancer identified in mouse by Beerman and colleagues as sufficient for the expression of *Fgf8b* in the tailbud (Beermann et al., 2006). Using this enhancer along with the HSV-TK promoted did lead to expression of a stable Venus in the tailbud at weak level. However, the Venus-Fgf8b fusion could not be detected using this construct.

Because of the difficulties in quantifying the gradient, and because another work showed that the scaling of the phase-gradient of the segmentation clock (for which no reporter was available in chicken) was central to the scaling of somitogenesis, we chose to not further pursue this project.
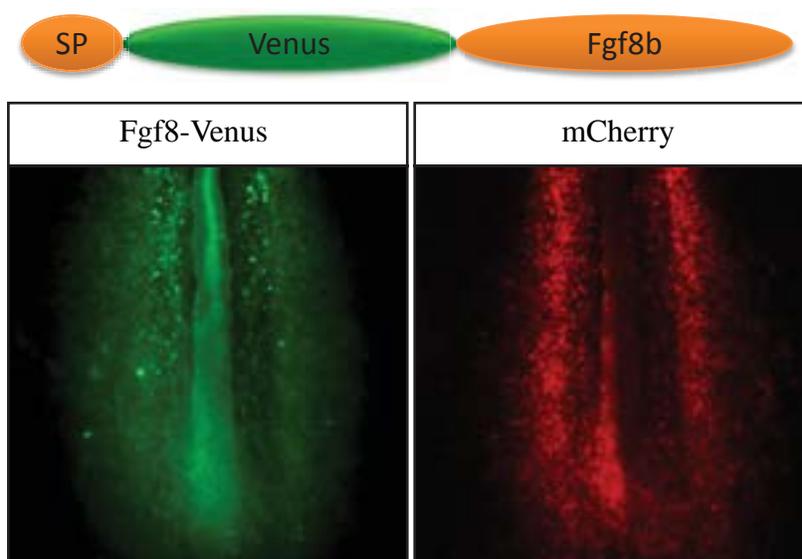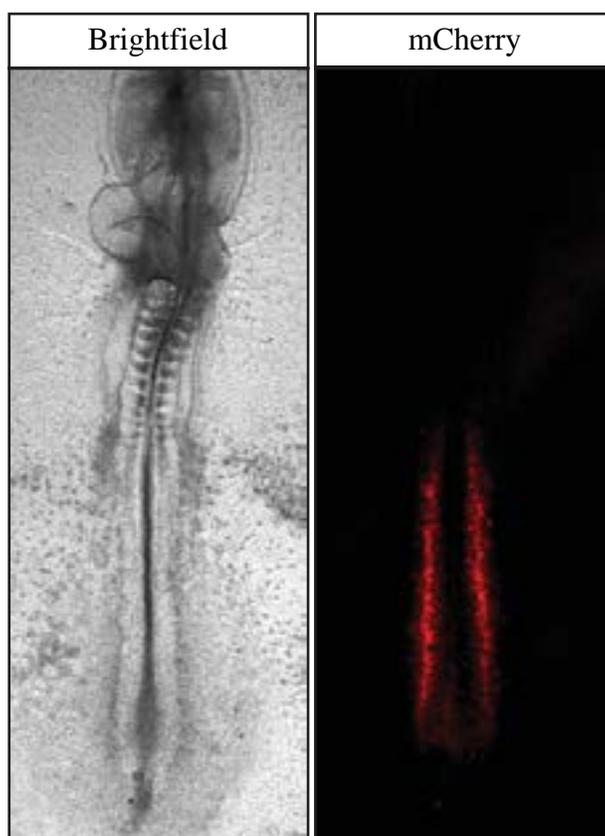
Figure 36- Fusion Fgf8b-Venus

A. (*Top*) Construct desgin: signal peptide of Fgf8b (SP) in N-terminal, Venus and Fgf8b. (*Bottom*) Pictures showing the fluorescence of Fgf8-Venus and an electroporation control (intracellular mCherry) in a day2 embryo

B. Picture of a day2 embryo electroporated with Fgf8-Venus and an electroporation control (mCherry) displaying an elongating PSM and absence of somite

Discussion

In this part, we addressed two questions: the molecular basis of the determination front downstream of Fgf signaling, and its spatial regulation. We showed that overexpression of Tbx6 was sufficient to activate *Mesp2* in the posterior PSM, but we were unable to identify downstream targets of Fgf/ERK or to quantify the gradient with high precision.

Repression of Mesp2

While we identified an effect of Tbx6 expression, it is not clear how relevant this regulation is. Indeed, transient electroporation using the CAGGS promoter leads to very high dose of transgene expression, which could not be a physiological situation. In mice embryos, Wehn and Chapman showed that ectopic expression of Tbx6 in the somites led to various defects in axial skeleton, but they did not address the effect in more posterior PSM due to their experimental design (Wehn and Chapman, 2010). Besides the question of the physiological relevance, a simple mechanism based solely on Tbx6 regulation appears unlikely, since this factor activates several other targets in the posterior PSM. A better understanding of the chromatin regulation at the *Mesp2* enhancer and the role of Tbx6 in this process could answer those questions. We showed that mutating sites necessary for the transcriptional activity of T-box proteins abolished the effect of Tbx6 overexpression. Interestingly, similar observations were made with Tbx3 in the differentiation of mouse embryonic stem cells (mESC) into primitive endoderm (PE) (Lu et al., 2011). Tbx3 is expressed in mESC, but its overexpression leads to the PE lineage. This is mainly due to the activation of the *Gata6*, a "bivalent gene", whose promoter is marked by both activating and repressing chromatin marks (H3K4me3 and H3K27me3) with a poised polymerase II (Mikkelsen et al., 2007, Williams et al., 2015). The activation of *Gata6* upon Tbx3 overexpression was also abolished by a mutation of the Y149 residue (identical to the Y182 in chicken Tbx6), and was associated with the recruitment of H3K27 demethylase complex. Therefore, we could suppose that overexpression of Tbx6 similarly relieves the repressive regulation at the poised *Mesp2* promoter. It would be worthwhile to characterize the chromatin marks and to determine whether there is transcriptional pausing at this locus. Such mode of regulation would confer interesting properties in the context of somitogenesis, as it was shown that poised transcription leads to better synchronicity in the response of a group of cells (Gaertner and Zeitlinger, 2014). Interestingly, in our phosphoproteomics data, we found that inhibition of Fgf/ERK led to an increase of NELF-E phosphorylation (also known as RD), a component of NELF that blocks transcription elongation. It was shown that phosphorylation of NELF-E by P-TEFb releases NELF from a paused promoter and promotes transcription elongation (Fujinaga et al., 2004). While we must remain circumspect to the quality of our proteomics data, this

finding could imply that blocking Fgf/ERK signaling indirectly leads to a transcriptional activation of poised genes, and potentially, *Mesp2*.

Fgf gradient in the PSM

In order to understand the coupling between elongation and segmentation, we tried to quantify the distribution of the Fgf8 gradient and to identify mechanisms regulating its spatial range. While we were unable to develop methods robust enough for quantitative analysis, it would still be interesting to study the formation of this gradient in more qualitative manner. Many questions remain open, such as the factors regulating FGF8 diffusion. Notably, it is known that heparan sulfate can alter the activity and/or diffusion of Fgf ligands (Duchesne et al., 2012). In the PSM, *hs6st*, an enzyme catalyzing the sulfation of heparan sulfate is expressed in a gradient in the mouse and chicken PSM (*hs6st2*) (Chal et al., 2015) and its inhibition in zebrafish leads to severe segmentation defects (Bink et al., 2003). Similarly, other Fgf ligands are expressed in distinct patterns in the PSM, such as *Fgf10* and *Fgf18* (Ohuchi et al., 2000, Karabagli et al., 2002), and while their knockdown in mice did not reveal any obvious axial segmentation phenotype (Itoh and Ornitz, 2008), more subtle effects could influence the formation and interpretation of the Fgf gradient in the PSM.

Last, it remains to be determined whether the scaling of somitogenesis is due to a scaling of the gradient of Fgf8. The latter could control the phase gradient described by Lauschke, Tsiairis and colleagues (Lauschke et al., 2013). Such interplay between patterning and morphogenesis is reminiscent to the development of the wing disc, where the gradient of Dpp scales with the disc size (Wartlick et al., 2011). In this regard, it will be important to establish a model combining the effect of Fgf on the clock dynamics and the elongation of the axis.

CHAPTER II

Emergence of oscillations and their molecular control

In this chapter, we present the main work of this thesis about the emergence of oscillations in an *ex vivo* system of mouse PSM. First, to study the segmentation clock, we established a system to monitor oscillations and perturb the signaling pathways. This addresses two potential caveats of previous work: the lack of dynamic information and the problem of secondary effects such as problem of PSM specification in Fgf/Wnt mutants. Then, using this *ex vivo* system, we aimed to understand the role of Fgf signaling on the PSM determination, and more specifically, how this pathway interacts with the segmentation clock. This question was relevant after the work of Niwa and colleagues (Niwa et al., 2007, Niwa et al., 2011) showing a crosstalk between the Fgf, Hes and Notch oscillators in the mouse PSM, but also after the work of Lauschke, Tsiairis and colleagues suggesting "*a tight interdependence between segmentation oscillator and differentiation front definition*" (Lauschke et al., 2013). During the course of this work, we had to better understand the underlying mechanism of oscillations and waves in our *ex vivo* system. Therefore, to provide a better framework to the effect of Fgf signaling, we examined how oscillations are created by examining the different levels of organization (single cell, local, global). This has led us to propose a model of excitable system underlying the oscillations of *Lunatic fringe* in our experimental setup. Last, we tried to better understand the factors regulating the transition to the oscillatory regime.

1. Explant system to study the segmentation clock

In order to have a better visualization and quantification of the processes involved, we used a two-dimensional assay, where we cultured PSM tissues on a glass dish coated with fibronectin. Initially we used the medium composition developed in our group to differentiate mouse embryonic stem cells into PSM-like cells. This medium consists in DMEM (high glucose) with 15% FBS, non-essential amino-acids, L-Glutamine, β-mercaptoethanol, penicillin-streptomycin (a classical base medium routinely used for the culture of undifferentiated mouse embryonic stem cells), in presence of the GSK3β inhibitor CHIR99021 (CHIR) and the BMP inhibitor LDN193189 (LDN). We first dissected the tailbud region as described by Lauschke, Tsiairis and colleagues. But, we noticed in our hands some inefficient and variable spreading, which led us to add the ROCK inhibitor Y-27632 (that facilitates the spreading of the explant) and to dissect the region corresponding to the tailbud mesenchyme at E9.5 (Figure 37A). For that purpose, we used a solution of Accutase (commercial solution containing a mixture of enzymes degrading the extracellular matrix) to microdissect this region. To better ensure a stable pH, we also included the buffer HEPES and cultured the cells at 7.5% CO_2. In these conditions, we still observed a differentiation of the explants as evidenced by the arrest of *LuVeLu* oscillations. This led us to tune two other pathways: activating the Fgf pathway by adding the ligand mFgf4 and its co-activator heparin, and repressing the retinoic acid pathway by use
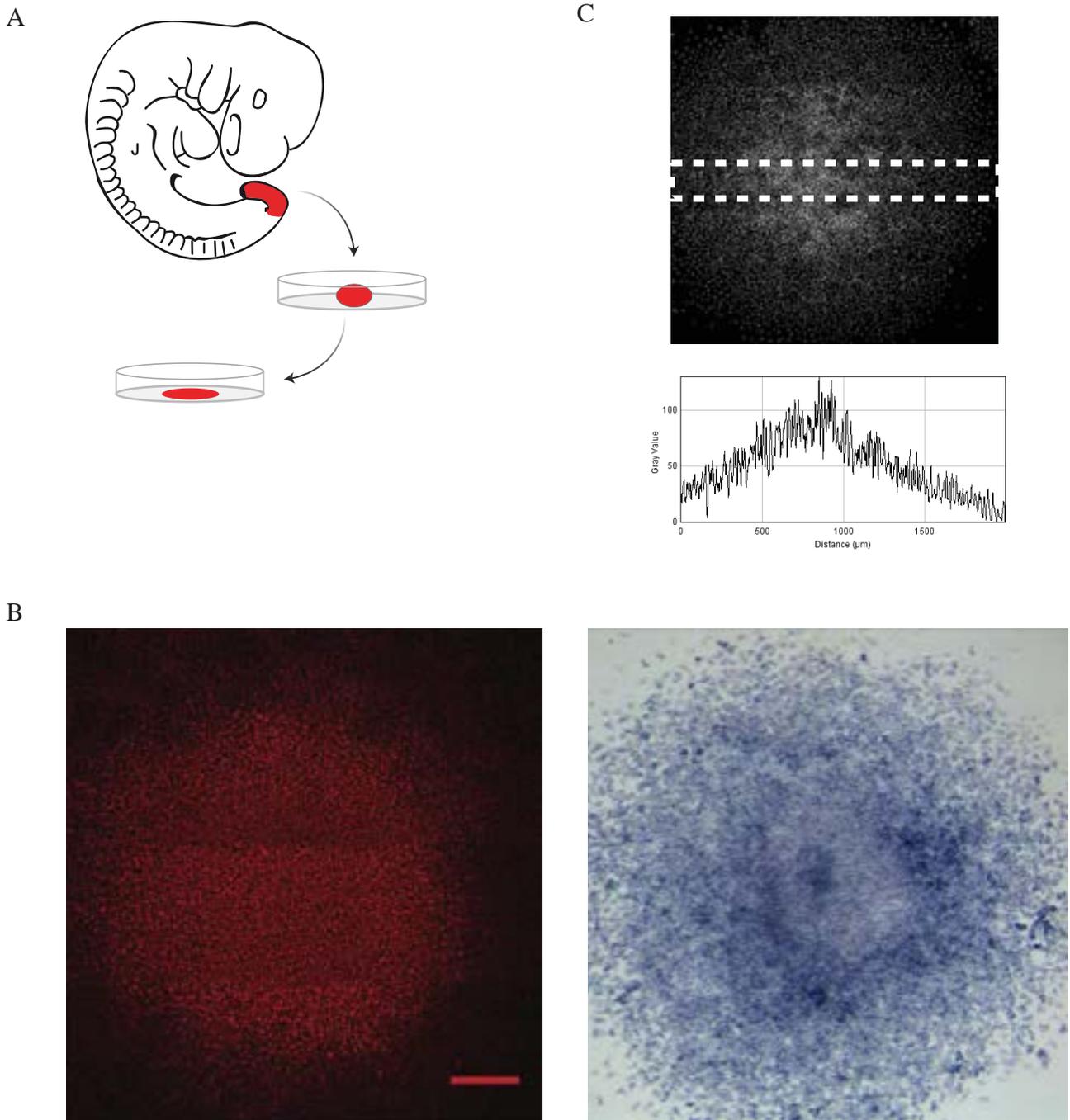
Figure 37 - Dissection and culture of mouse tailbud mesenchyme

A. Scheme of the dissection: the tailbud mesenchyme was dissected and plated on a fibronectin-coated dish

B. (*Left*) Immunostaining for the PSM marker, Tbx6 after 20-24h of culture (scale bar: 200µm). (*Right*) *In situ* hybridization for the mesodermal marker *T*.

C. Nuclei staining of an explant after 20-24h of culture (*top*) and intensity of the signal along the dashed region showing the gradient of cell density (*bottom*)

of the pan-RAR inverse agonist BMS-493. We chose the ligand Fgf4 as its recombinant form has a higher activity than Fgf8b according to the manufacturer (R&D Systems; ~18-fold based on the proliferative effect on 3T3 cells) and both ligands are genetically redundant in the mouse mesoderm (Naiche et al., 2011). Heparin is required for the binding of Fgf ligands to their receptor, and adding this factor was shown to increase their activity and stability (Chen et al., 2012a). These conditions are the standard conditions we used in this work.

We observed that the tailbud mesenchyme expands to form a quasi-monolayer disk of about 1mm radius, positive for the posterior PSM markers Tbx6 and *T* (Figure 37B-C). Oscillations of the *LuVeLu* reporter were stably observed for 48 hours before a dampening of the reporter intensity (Figure 38A-C). Contrary to what was observed by Lauschke, Tsiairis and colleagues, this differentiation was mostly disorganized and started at the center of the explants (as evidenced by *in situ* hybridization for *Mesp2* or *Raldh2*). We suppose that the high cell density and/or the long incubation time induce some "drift" in the system.

Concerning the pattern of the oscillations, we first observed a spatially homogenous oscillation, and latter traveling waves in the form of target patterns. Those early steps showed some variability probably due to the heterogeneity during the dissection. Preliminary experiments where the explants expansion is blocked by micropattern of fibronectin suggested that waves are formed when the diameter of the explant is superior to 250µm. We noted that the center of the target pattern is not necessarily positioned at the center of the explant. The period of the oscillations remained stable over the culture, and after the initial phase of spreading, was not detectably different between the center and the periphery of the explant (Figure 38D). Therefore, there is a phase-gradient without apparent gradient of frequency as in the PSM.

To better characterize the system, we removed the region from which originate the oscillations either with a two-photons laser or mechanically, and observed that oscillations in the remaining tissues continued to occur (Figure 39A). This argues against the existence of a different population of pacemaker cells at the origin of the target pattern. Dissociation of several explants and reaggregation by spinning (as initially developed in (Tsiairis and Aulehla, 2016)) led to the reformation of oscillations and target patterns, suggesting a homogeneous population of oscillators (Figure 39B). Furthermore, waves were still observed after cutting the explants, indicating that it is not a trigger wave but rather a kinematic wave. This stable oscillatory pattern was also observed after dissecting the posterior PSM (without the tailbud mesenchyme), implying that this behavior is not restricted to a special population of the PSM but rather to the culture conditions. We next present a more detailed analysis of the medium composition.
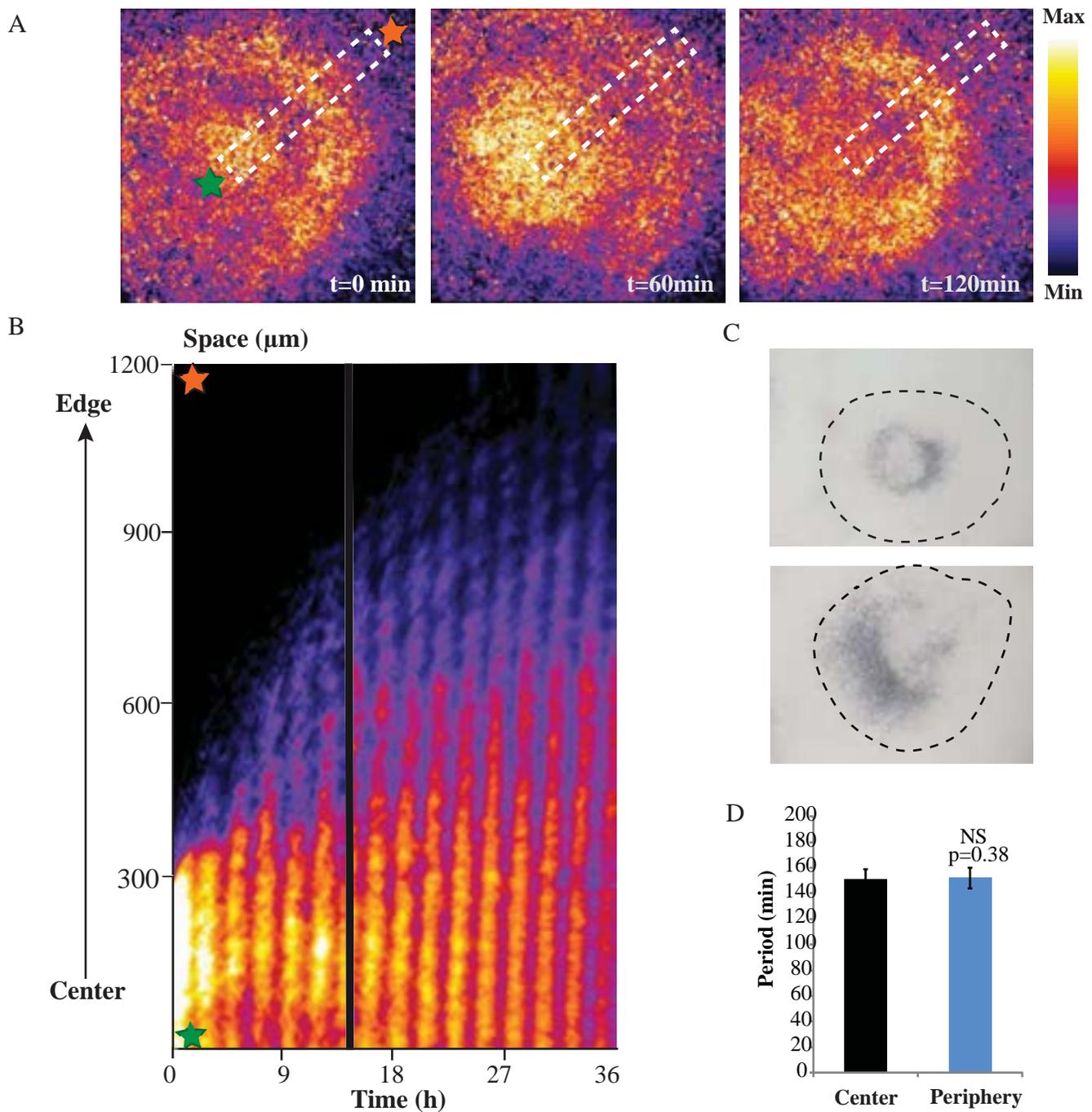
Figure 38 - *LuVeLu* oscillations in the explant system

A. Snapshots of an explant showing the fluorescence signal of the *LuVeLu* reporter over a period of 120 minutes. Stars and dotted rectangle indicate the region selected for the kymograph shown in the figure **B**.

B. Kymograph showing the fluorescence profile along the dotted rectangle in Fig.1B (note that the discontinuity is due to a medium change).

C. *In situ* hybridization for *Hes7* (intronic) for two different explants showing the oscillation and traveling waves of this gene(dotted lines mark the periphery of the explants)

D. Period of the *LuVeLu* oscillations at the center and periphery of explants (4 explants - n=33 - T-test p=0.38).

A
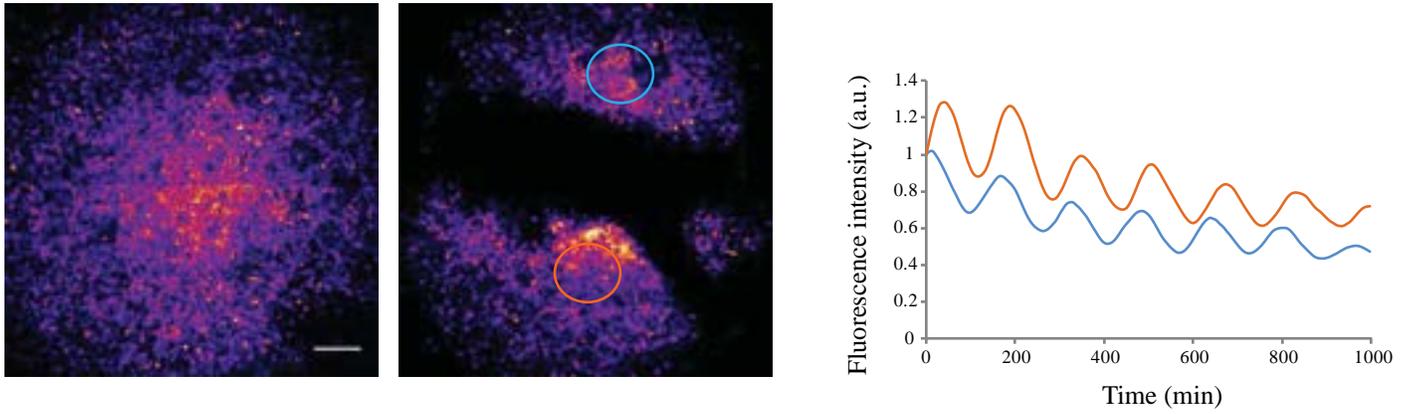
B
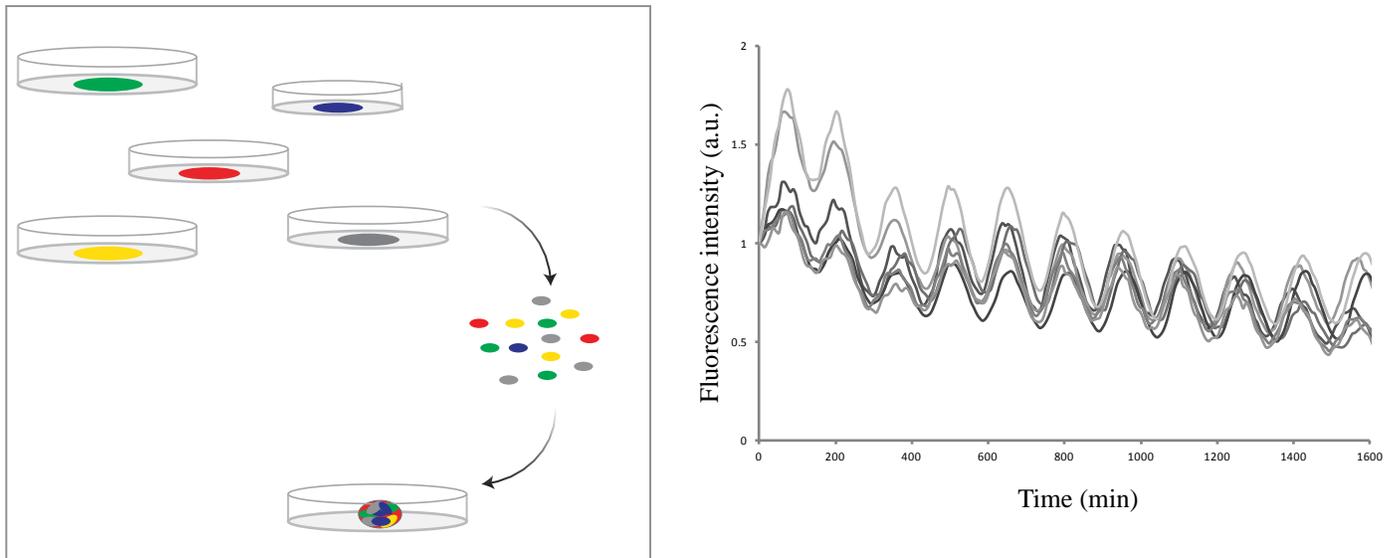
Figure 39 - Persistence of oscillations after removal of the center and reaggreagation

A. (*Left*) Removal of the center of an explant (scale bar: 200 μm). (*Right*) Fluorescence intensity of the *LuVeLu* reporter in the two regions indicated by blue and orange circles over time

B. Oscillations of the *LuVeLu* reporter after reassociation of cells from multiple explants. (*Left*) Scheme of the experimental design. (*Right*) The movie starts 2 hours after the reassociation of explants. Each line corresponds to the fluorescence intensity of the *LuVeLu* reporter for a newly assembled aggregate over time.

2. Culture conditions

We used the following medium as a "base medium" to study the role of the different factors: DMEM, 15%FBS, non-essential amino acids, L-Glutamine, penicillin-streptomycin, HEPES, β-mercaptoethanol, ROCK inhibitor (Figure 40A-B).

This base medium alone induced the differentiation of the explant after one day in a manner reminiscent to the *ex vivo* system of Lauschke, Tsiairis and colleagues, *i.e.* a progressive arrest of the oscillations starting from the periphery of the explant. We observed that differentiation of the explant is associated with an increase in the reporter intensity, followed by a complete disappearance of the fluorescence. Similarly, adding the Wnt activator CHIR, the BMP inhibitor LDN or the retinoic acid inhibitor BMS-493 led to a centripetal differentiation (we note that for some explants in basal medium (1/3) or LDN alone (1/3), several "foci" could be observed).

Surprisingly, when only Fgf4 (with heparin) was added to the medium, the intensity of the reporter was lower and no oscillation of the *LuVeLu* reporter was observed (no oscillation: 4/5; oscillation with lower amplitude: 1/5). Similar behavior was obtained when both Fgf4 and CHIR were added to the medium. We examined the expression of some key markers in the Fgf4/CHIR condition, and observed several changes compared to the control, notably a downregulation of *Notch1* and *Dll1*, and an upregulation of *Cyp26a1* (Figure 40C). The former could explain the absence of oscillations, as Notch signaling was shown to be required for *Lfng* oscillations *in vivo*. The latter observation suggests that in presence of CHIR and Fgf4 alone, explants could be in a state closer to the tailbud. As we will discuss later, this is consistent with other findings showing that blocking the BMP pathway leads to an exit of the tailbud state. Accordingly, adding the BMP inhibitor LDN to Fgf4 or Fgf4/CHIR triggered the oscillatory and wave patterns observed in normal conditions. When explants were cultured with Fgf4 and LDN, differentiation still occurred after 30 hours, while it was not observed after 40 hours in the presence of CHIR. Addition of the retinoic acid inhibitor in presence of Fgf4/CHIR also enabled the apparition of oscillations, but with lower amplitude than in the control and with a progressive dampening. As we will discuss later, this could also be explained by an exit from the tailbud state. Further addition of the retinoic acid inhibitor in the Fgf4/CHIR/LDN medium did not have a major effect on the culture; we noticed a "sporadic" differentiation of cells without BMS-493, probably due to the residual presence of retinoic acid in the serum. To summarize, we could distinguish three situations (Figure 40B): i) *type I*: oscillations with differentiation when Fgf and Wnt signaling are not sustained; ii) *type II*: absence of oscillations or dampened oscillations when Fgf4 is added to the medium in the absence of BMP inhibition; iii) *type III*: sustained oscillations when both Fgf and Wnt signaling are activated and the BMP pathway is inhibited.

A

Base medium

Time (47h)

+ LDN

Time (26h)

+ CHIR/Fgf/LDN

Time (40h)

+ Fgf4

Time (47h)

+ CHIR/Fgf4

Time (26h)

+ Fgf/LDN

Time (40h)

+ CHIR

Time (47h)

+ CHIR/Fgf4/BMS

Time (26h)

+ BMS493

Time (47h)

Space (from center to periphery)
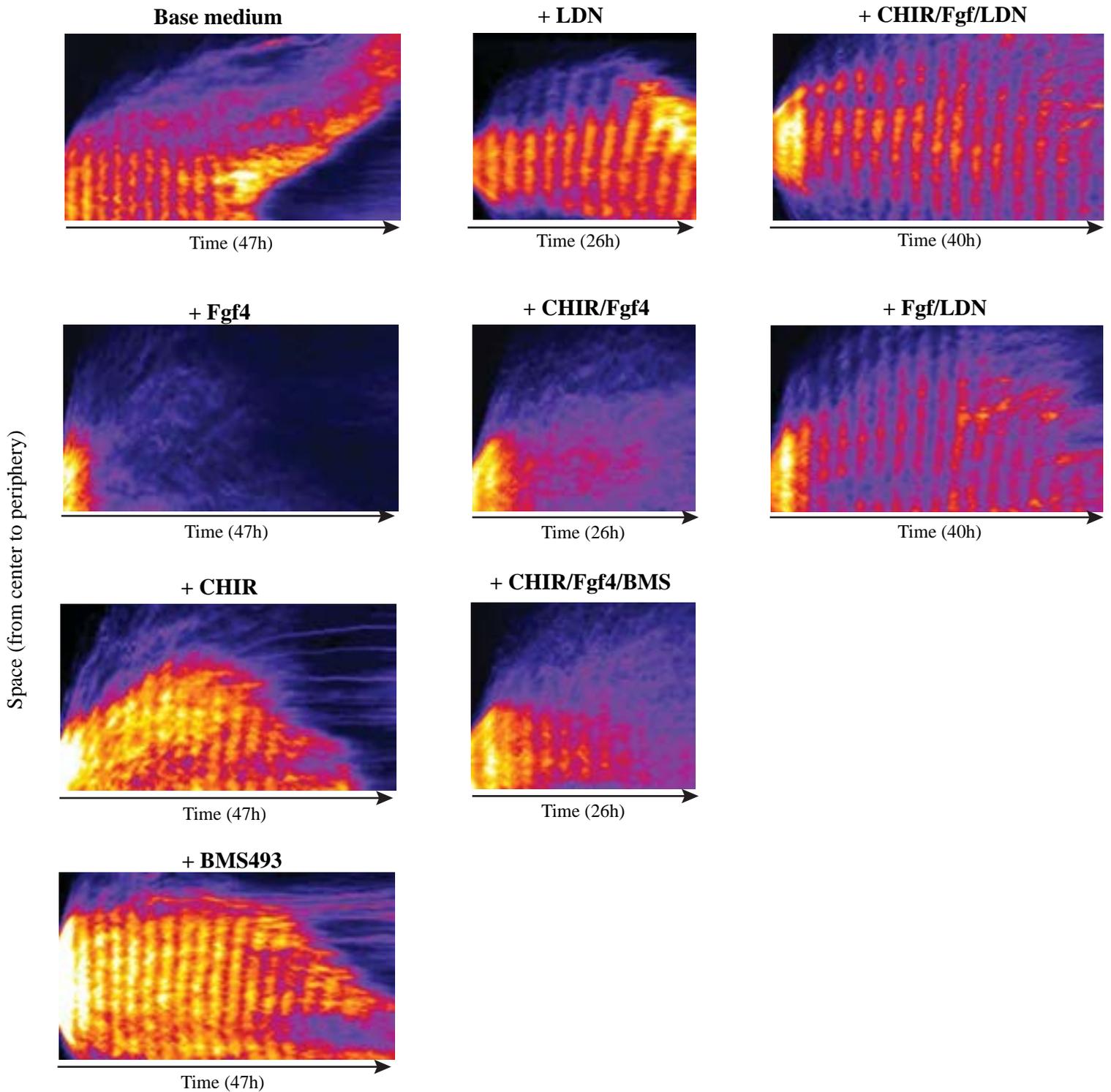
Figure 40 - Culture conditions for sustained oscillations

A. Kymographs of explants cultured in different conditions showing the fluorescent intensity for the *LuVeLu* reporter - Basal medium (3/3), LDN (3/3), CHIR/Fgf/LDN (1/1), Fgf4 (4/5), CHIR/Fgf4 (5/5), Fgf4/LDN (2/2), CHIR(3/3), CHIR/Fgf4/BMS (2/3), BMS (3/3). The region of interest corresponds to the axis from the center of oscillations to the periphery of the explant.

B

Type I - Oscillations / Differentiation
Base medium / CHIR/ BMS / LDN / Fgf4+LDN

Type III - Stable oscillations
CHIR+Fgf4+LDN / CHIR+Fgf4+LDN+BMS

Type II - No oscillation / Dampened oscillation
Fgf4 / CHIR+Fgf4 / CHIR+Fgf4+BMS

C

25.35 (± 0.8)

Msgn1 Tbx6 T Cyp26A1 Wnt3a Hes7 Sp5 Spry2 Dll1 Notch1 Lfng Bactin

D

Anterior PSM
Cessation of oscillations

↓Wnt ↓Fgf (↑RA)

Posterior PSM
Oscillations

↓BMP ↓Fgf (↓RA)

Tailbud
No oscillation/ dampened
oscillations

Figure 40 - Culture conditions for sustained oscillations *(continued)*

B. Three situations observed when testing the influence of different factors. A representative profile of the fluorescence intensity of the *LuVeLu* reporter is shown for the base medium (type I), Fgf4 (type II - *top left*) and CHIR/Fgf4/BMS (type II- *top right*), control (type III - *bottom*) conditions.

C. Gene expression levels in explants cultured for one day in control conditions (red) or in CHIR+Fgf4 (green). The fold-changes of 4 pooled explants are represented.

D. Model for the different cellular states in the PSM and their control by signaling pathways
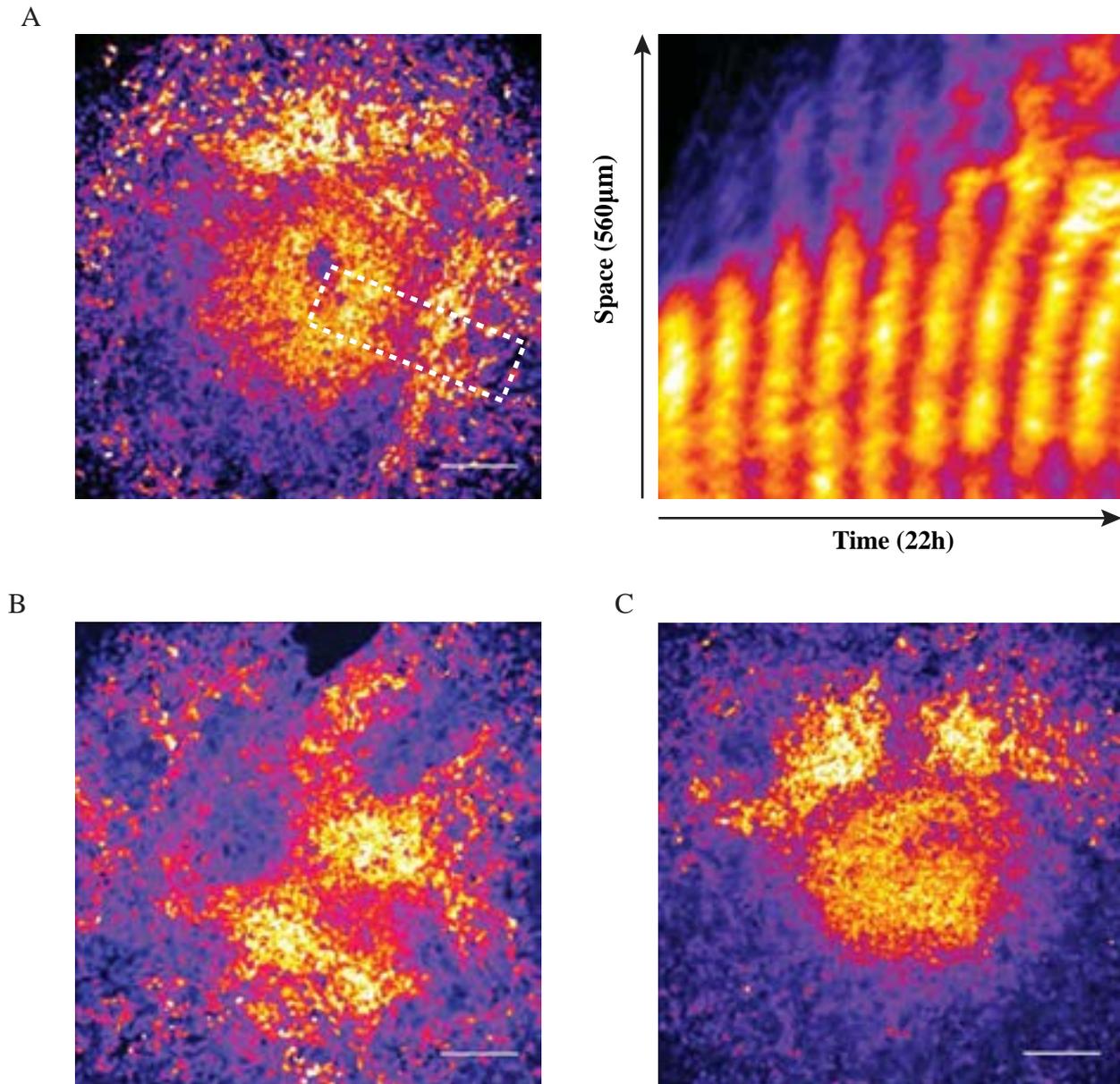
Figure 41 - Patterns of oscillations arrest

A. (*Left*) Snapshot of an explant cultured with low dose of Fgf4 (1 ng/mL) exhibiting a centripetal arrest of oscillations (scale bar: 200 μm). (*Right*) Kymograph for the region delimited by the dotted rectangle

B. Snapshot of an explant cultured with low dose of Fgf4 (1 ng/mL) showing the formation of different foci from where waves travel and stop (scale bar: 200 μm)

C. Snapshot of an explant cultured with low dose of Fgf4 (7 ng/mL) showing the bifurcation of the wave (top of the explant) when the oscillations arrests (scale bar: 200 μm)

As Fgf and Wnt signaling have been shown to act in a dose-dependent manner, we titrated either the level of Fgf4 or the level of CHIR (all other factors remaining unchanged). Reducing the concentration of Fgf4 below 7ng/mL led to the centripetal differentiation after 21 hours (Figure 41A), while even a 10-fold reduction of CHIR to 0.1µM was permissive for oscillations and did not induce the differentiation of the explant at the periphery (as evidenced by the lack of changes in reporter intensity described above). Interestingly, we observed the formation of several foci as the oscillations arrested and the explant differentiated in low Fgf4 conditions (1ng/mL: 2/4; 0.15ng/mL: 1/4) (Figure 41B). Furthermore, we noticed cases of bifurcation of the waves (Fgf4 1ng/mL: 3/4) as the arrest of oscillations was not centripetal and circular, but became split into two domains (Figure 41C). Those two observations are reminiscent from the findings of Tsiairis and Aulehla, and suggest a reaction-diffusion mechanism. However, we should remain cautious given the low number of observations and the variability between explants likely due to the differences in geometry and spreading.

Together this suggests that Fgf signaling maintains both the tailbud non-oscillatory state and the posterior oscillatory state. Inhibition of BMP signaling appears to mediate the transition between those two states. Wnt signaling further contributes to stalling the explant in the oscillatory state (as evidenced by Fgf4/LDN vs. Fg4f/LDN/CHIR) (Figure 40D). However, the differentiation of the explant seems to be mainly controlled by the reduction of Fgf signaling as suggested by the strong sensitivity to a reduction of Fgf4 dose.

3. Distribution of Fgf signaling

We next wanted to understand what controls the position of the oscillation foci and the direction of the wave. As previously mentioned, we could not detect any frequency gradient within the explant. This would argue against a requirement of the clock slow-down in order to create a phase gradient as proposed in the model of J.Lewis and variants.

After one day of culture, we examined the pattern of the mesodermal markers, Tbx6 (protein) and *T* (mRNA), and observed that they were expressed in the entire explants (Figure 37B). This contrasts with the explant systems of Aulehla and colleagues (both the original explant and reaggregation system), where there is a centripetal differentiation. Furthermore, we could not detect any gradient of phosphorylated ERK or *Sprouty2* expression when normalized by the cell density (Figure 42). These observations indicate that there is no gradient of Fgf signaling, and more generally, no gradient of differentiation within the explants.
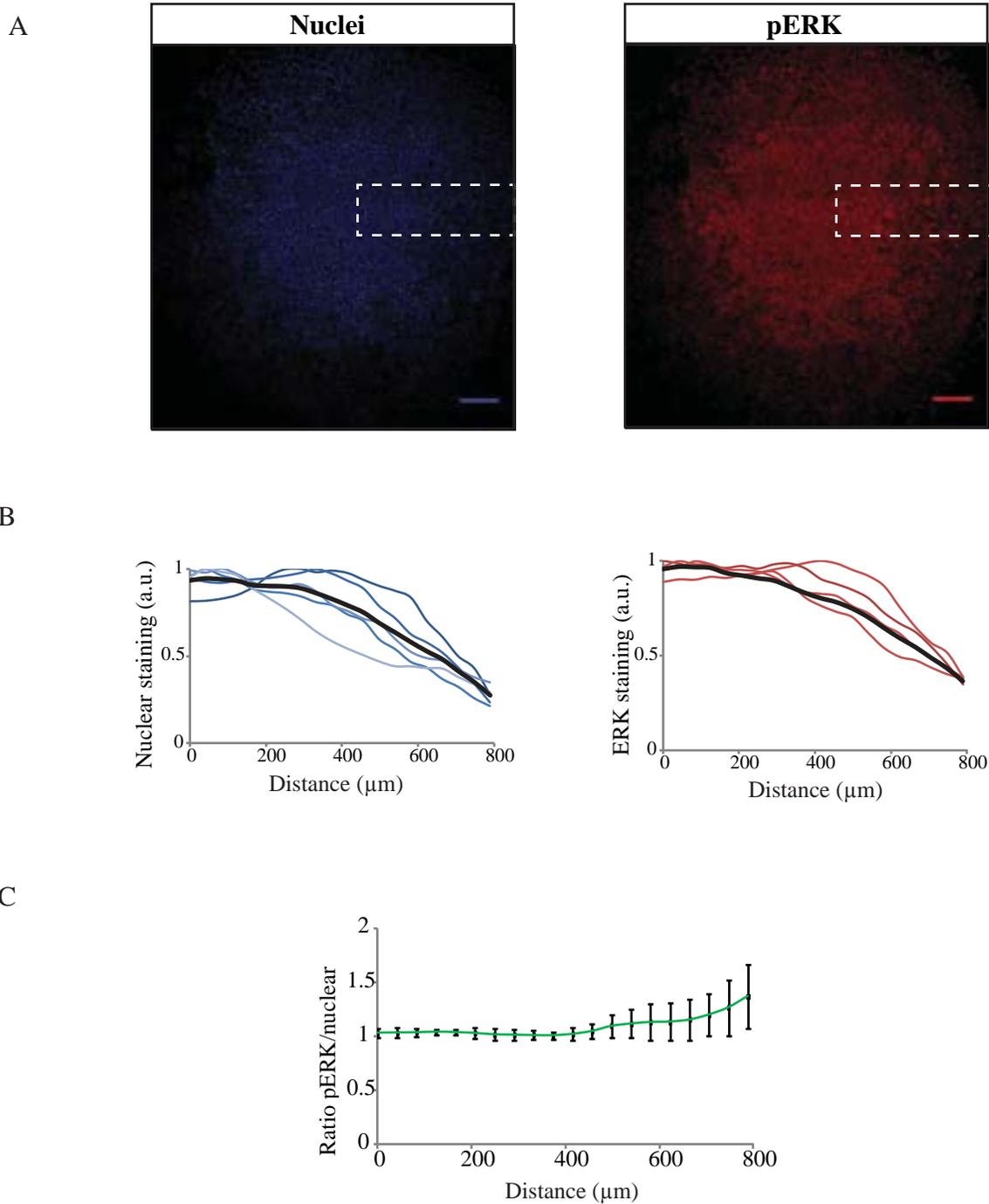
Figure 42 - Distribution of Fgf signaling in explants

A. Explants after one day of culture - (*Left*) Nuclei staining. (*Right*) Phosphorylated ERK immunostaining (scale bar: 200µm).

B. Quantification of the signal intensity for the nuclei staining (*left*) and pERK (*right*) over the dotted rectangle of figure 42A. Each line corresponds to one explant.

C. Ratio between the pERK signal and the nuclei staining signal over the dotted rectangle of figure 42A.

D

Nuclei	*Spry2*
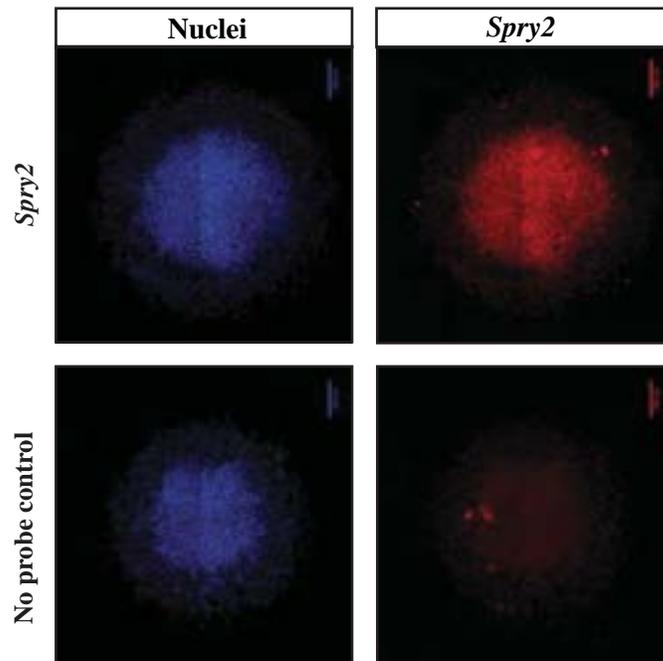
E
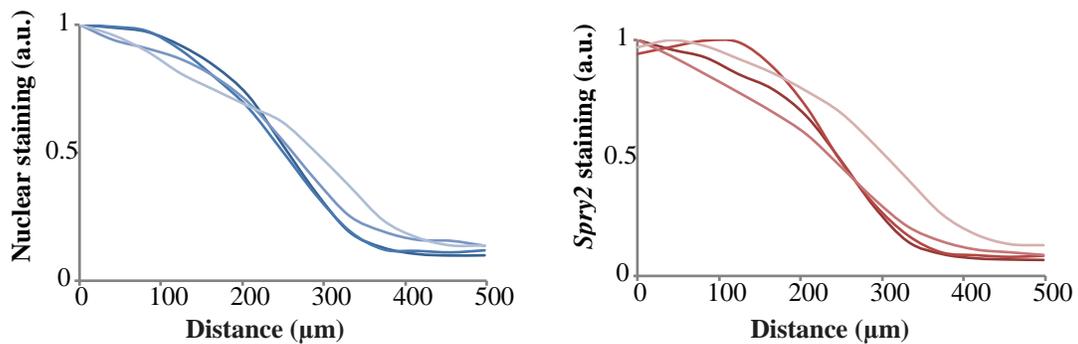
F
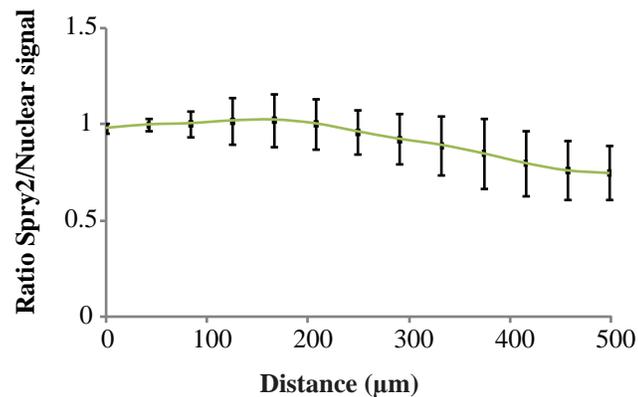
Figure 42 - Distribution of Fgf signaling in explants *(continued)*

D. Explants after one day of culture - (*Left*) Nuclei staining. (*Right*) Fluorescent *in situ* hybridization for the Fgf target *Sprouty2* (scale bar: 200μm).

E. Quantification of the signal intensity for the nuclei staining (*left*) and *Sprouty2* (*right*) from the center to the periphery of the explant

F. Ratio between the *Sprouty2* signal and the nuclei staining signal from the center to the periphery of the explant

Together, while it is difficult to ascertain the absence of frequency or signaling gradients, our findings argue for a self-organization of the oscillations and traveling waves in our system. To better understand how such behavior emerges, we next examined the different levels of organization of explant cells.

4. Dynamics at the cellular level

After dissection of the tailbud mesenchyme, we dissociated the cells and cultured them in the same condition as the explants. We then manually tracked a subset of cells and measured their fluorescence intensity (Figure 43). We were not able to detect any oscillatory pattern (n=5/5), but rather observed two features: i) an increase of the reporter before the cell division, and ii) sporadic pulses of *LuVeLu* reporter. This indicates that the dynamics at the single-cell level is aperiodic in these conditions. To bypass the global changes in intensity notably due to the cell cycle, we subtracted the intensity over a putative oscillation period (150 minutes – see methods) (Delaune et al., 2012), but we were still not able to detect clear oscillations. Accordingly, fast Fourier analysis of this subtracted series did not give a clear peak, but rather several peaks of similar amplitude. While we were not unable to observe oscillations of single cells in our conditions, we could not investigate other oscillators, notably the Wnt oscillator, which could still oscillate at the single-cell level. Furthermore, we cannot fully exclude that the reporter is not sensitive enough to detect low-amplitude oscillations or that other processes (e.g. cell division) mask the oscillations. However, as we will show later, experiments using micropatterns as well as gene expression data provide confirmatory evidence for the loss of oscillations in single cells.

To ensure that dissociated cells were in a correct state, we examined the expression of Tbx6 by immunostaining. We observed that ~70% of cells were positive for this marker after overnight culture (101/147) (Figures 44A-B). Furthermore, after culturing cells at low-density overnight, we reformed explants by detaching the cells and reaggregating them. This led to the reapparition of oscillations (4/4). However, we noticed a delay (~10h) before the detection of collective oscillations compared to a control (explants dissociated and instantly reaggregated for which the recovery is observed after ~2h – 3/3) (Figure 44C). This experiment suggests that dissociated cells are still able to oscillate when re-cultured at a higher cell density.

To further examine the role of cell density on the onset of oscillations, we plated cells on micropattern of fibronectin. We cultured several explants overnight, dissociated and mixed explants cells, and then plated them on $80\mu m^2$ circles of fibronectin. When cells were confluent, we observed
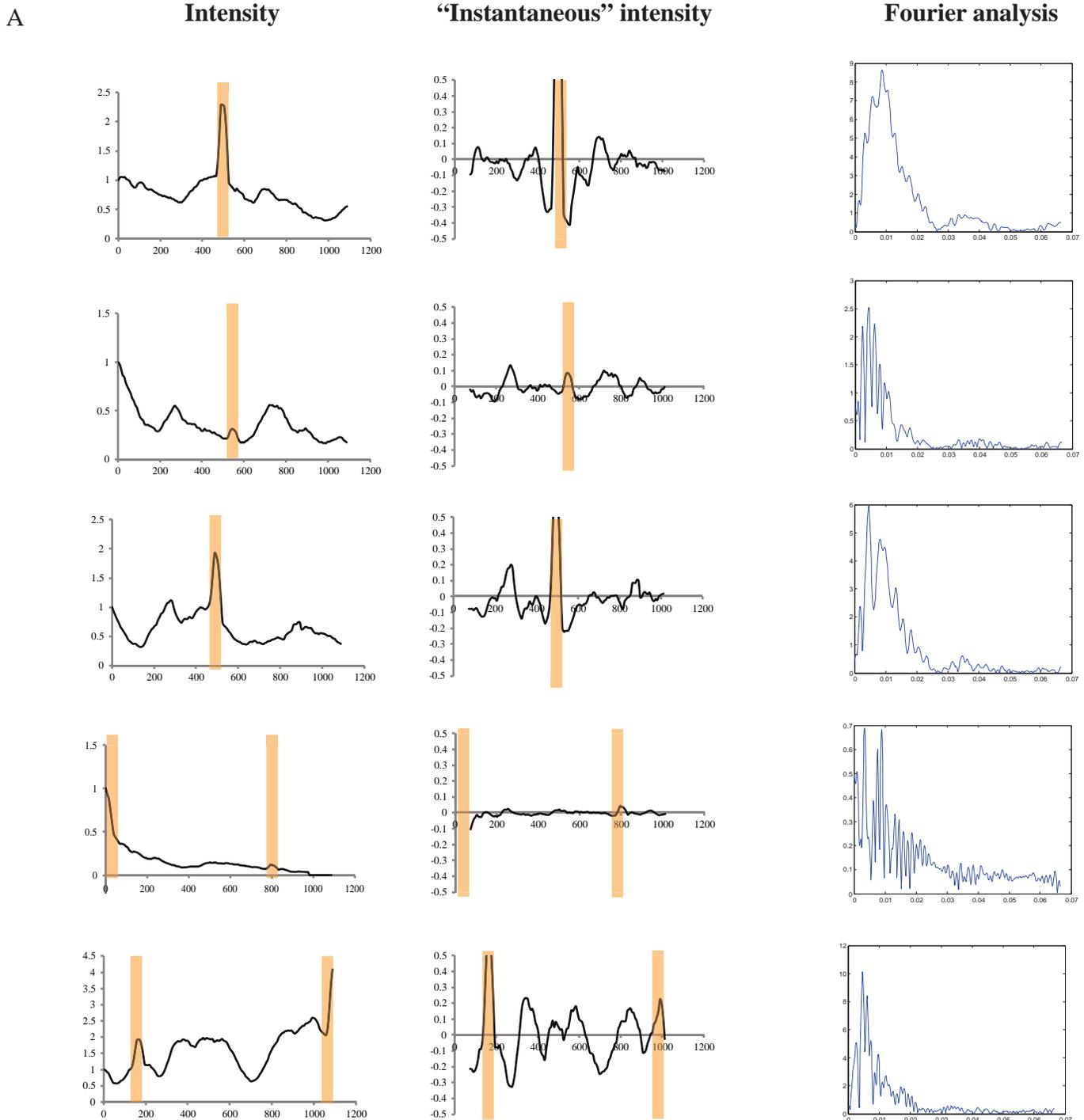
Figure 43 - Dynamics of the *LuVeLu* reporter in dissociated cells

(*Left)* Mean fluorescence intensity of the *LuVeLu* reporter for dissociated cells on fibronectin over time; orange windows indicate cell divisions; x-axis indicates the time in minutes; y-axis indicates the intensity in arbitrary units. (*Middle*) Mean fluorescence intensity of the *LuVeLu* reporter after subtraction of a moving average over 150 minutes; x-axis indicates the time in minutes; y-axis indicates the intensity in arbitrary units. (*Right*) Fast Fourier transform of the mean fluorescence of the *LuVeLu* reporter after subtraction of a moving average' x-axis indicates the frequency (min^{-1}), y-axis indicates the Fourier transform amplitude.
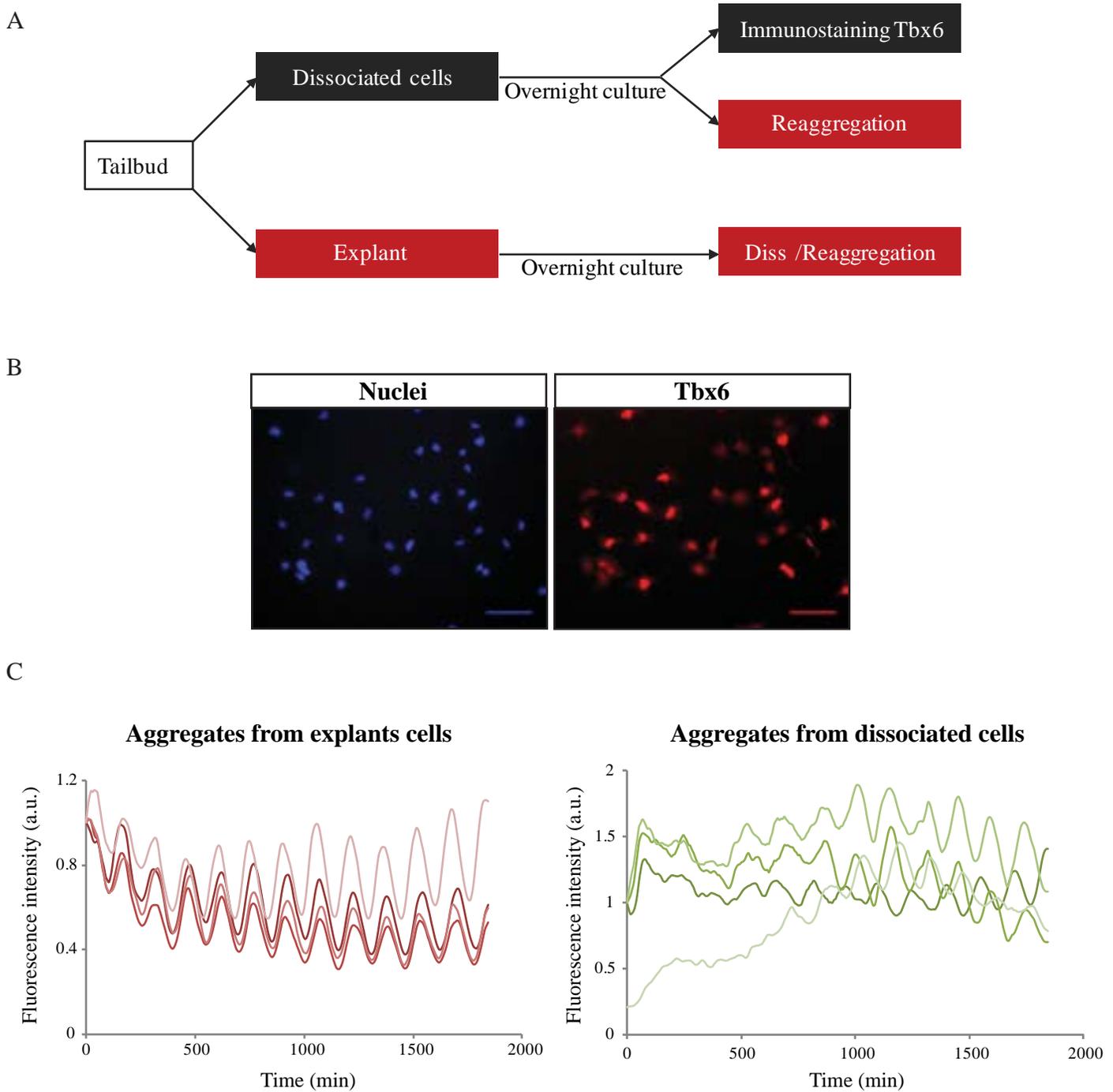
Figure 44 - Maintenance of oscillatory competency in dissociated cells

A. Experimental scheme to probe the maintenance of oscillatory competency

B. Dissociated cells (scale bar: 100 μm) - (*Left*) Nuclei staining. (*Right*) Immunostaining for Tbx6

C. Fluorescent intensity of the *LuVeLu* reporter over time for aggregates from explants cells (*left* - n=3) or dissociated explant cells (*right* - n=4). Each line corresponds to one aggregate.
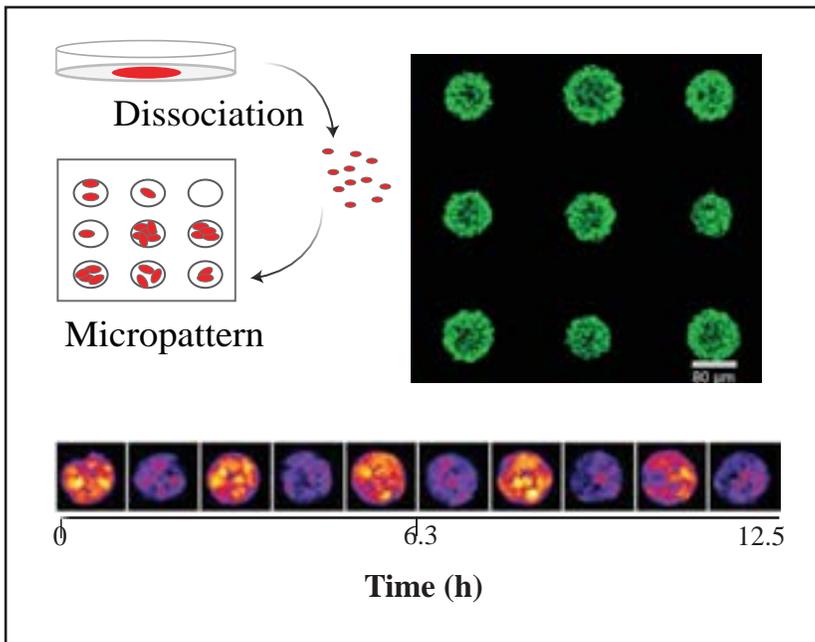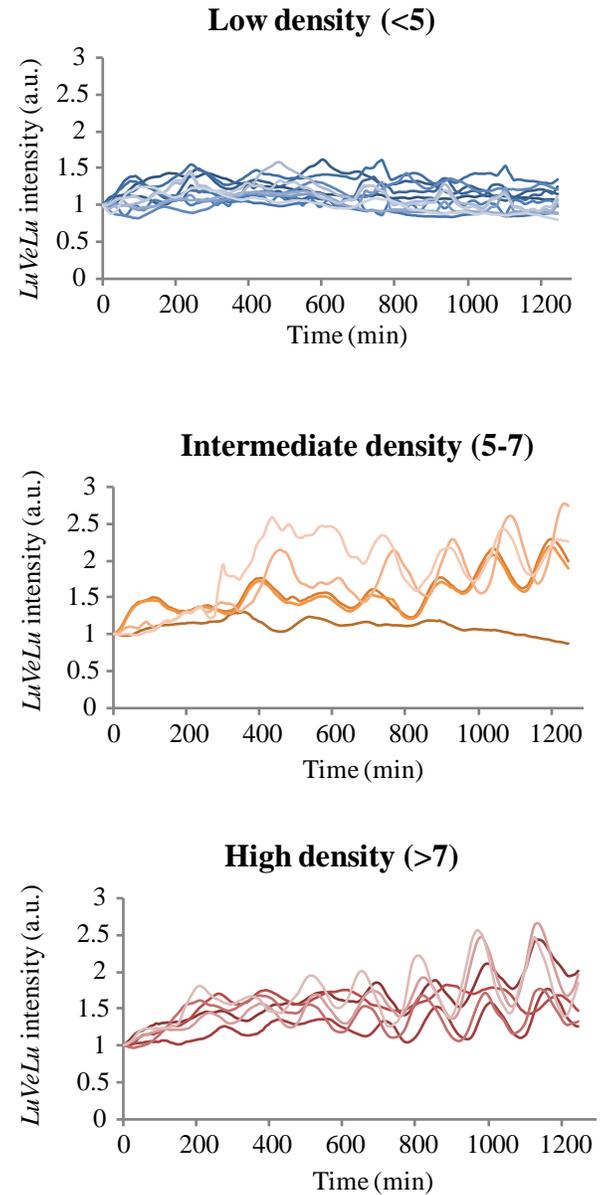
Figure 45 - Effect of cell density on collective oscillations

A. (*Top left*) Scheme illustrating the experimental protocol. (*Top Right)* Immunostaining of confluent cells on micropattern for Tbx6 (green - scale bar: 80μm). (*Bottom*) Snapshots showing expression of the fluorescent reporter at 75 minutes intervals in a micropattern

B. Graphs showing the fluorescence intensity of the *LuVeLu* reporter over time for several micropatterns with different initial cell density. Each line corresponds to one entire micropattern.

homogenous oscillations (Figure 45A). Furthermore, we observed that when cells where seeded at a low-density (<5 cells), no individual or collective oscillation was discernible, while at higher density, synchronous oscillations appeared (Figure 45B). This experiment indicates the existence of a signaling threshold dependent on the cell density. More generally, existence of a threshold controlling the onset of oscillations is indicative of an excitable system. Below this threshold, cells are quiescent and do not oscillate; noise in signaling or gene expression occasionally leads to cross this threshold and trigger the apparition of pulses of *LuVeLu* reporter. When cultured at high density, cells reach the oscillatory state and display traveling (kinematic) waves. Therefore, we propose that excitability underlies the *Lunatic fringe* oscillator and enables to better interpret our experimental observations, as well as other observations in the literature (see discussion). We note that the theoretical work was done in collaboration with L.Mahadevan, who first emitted the hypothesis of excitable system, and I.Regev.

5. Existence of a refractory period

As mentioned in the introduction, a feature of excitable systems is the existence of a refractory period. That is, after crossing the excitability threshold, the system cannot be excited again but do a large excursion in its phase plane before coming back to its initial state. To probe the existence of such refractory period, we cultured two explants next to each other so that they became in contact when they spred (Figures 46A-B). We observed two situations: in some cases one explant "took over" and its wave traveled into the neighbor explant (n=4/10); conversely, waves could annihilate each other and not cross in the other explant (n=6/10) (in-phase or out-of-phase) (Figures 46C-E). In the context of an excitable system, the former could be interpreted as an explant oscillating slightly faster than the other. Such hypothesis has been proposed to explain the formation of a single target pattern in the Belousov-Zhabotinsky reaction (Kuramoto, 2012). The situation of wave annihilation suggests the existence of a refractory period, as there is no further propagation of the wave on head-on collisions.

6. Role of the Notch pathway

We then asked how excitability could be controlled at the molecular level. The Notch pathway was a natural candidate, as it could mediate the density-effect observed earlier and as it is required for the oscillations of *Lunatic fringe in vivo* (e.g. *RBPJ-κ* and *Dll1* mutant – (Barrantes et al., 1999,
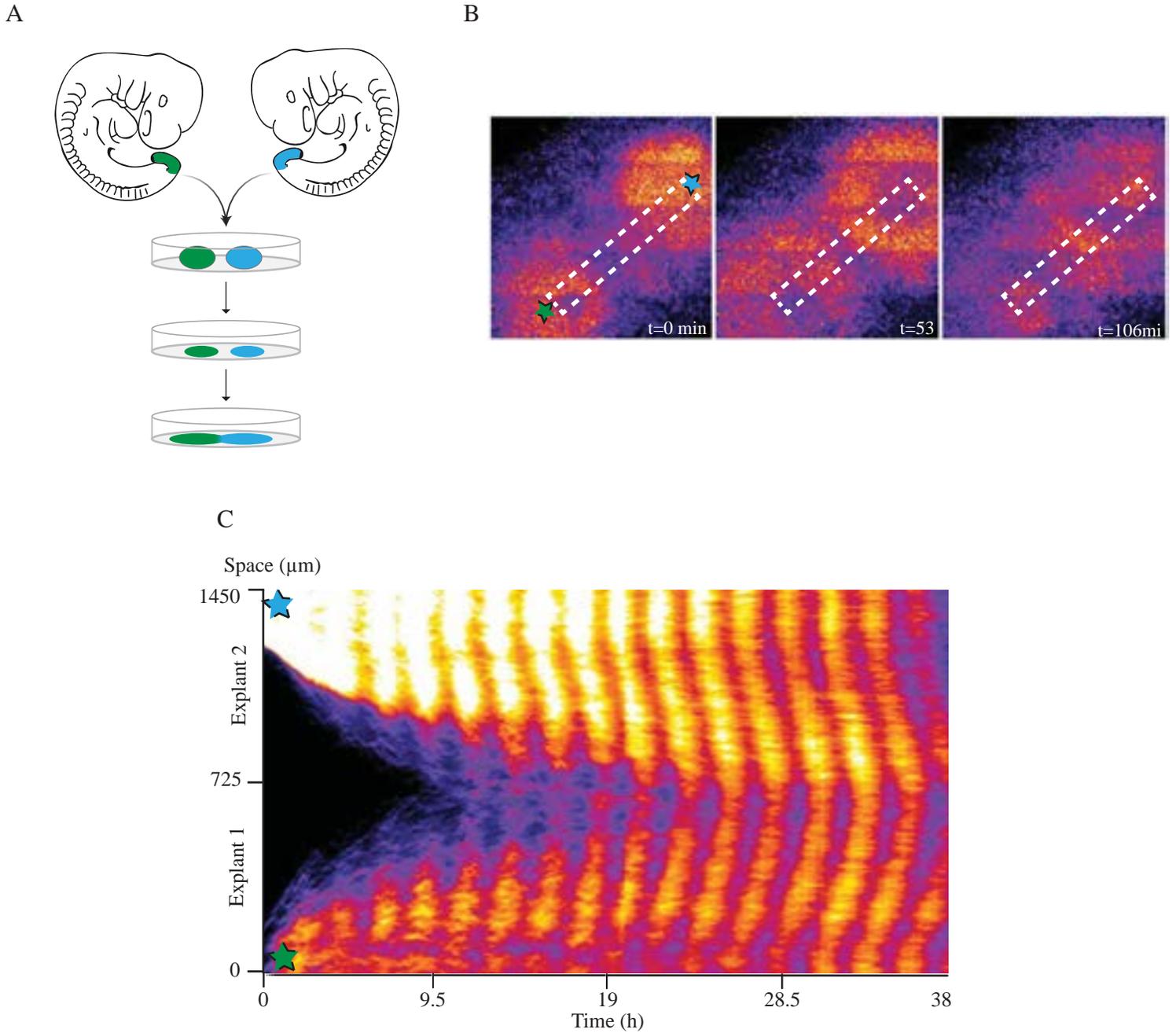
Figure 46 - Wave annihilation

A. Scheme of the experimental design to probe wave annihilation

B. Snapshots of two colliding explants showing the fluorescence intensity of the *LuVeLu* reporter

C. Kymograph for the region indicated by the dotted rectangle and stars in Fig B showing the annhilation of the waves (the discontinuity is due to a medium change)

D

Space (900 µm)
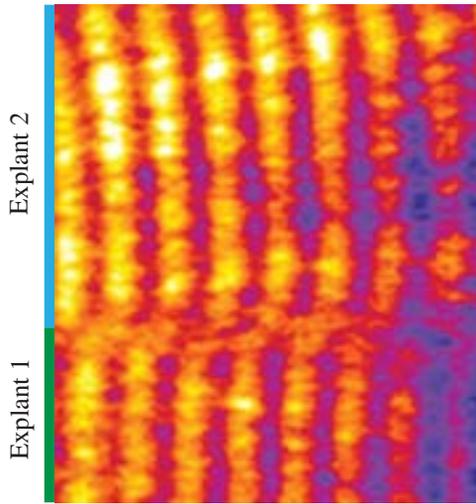
Explant 2

Explant 1

Time (19h)

E

Space (1050 µm)
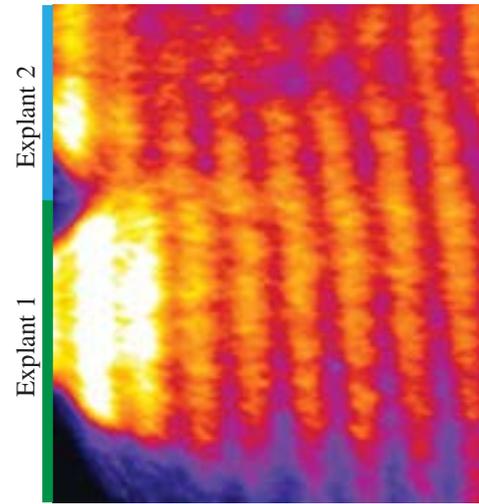
Explant 2

Explant 1

Time (19h)

Figure 46 - Wave annihilation (*continued*)

D. Kymograph for two other colliding explants showing an annhilation of the waves in a out-of-phase situation

E. Kymograph for two other colliding explants showing the top explant "taking over" the bottom explant

Ferjentsik et al., 2009)). To test the role of this pathway, we cultured explants overnight to reach a steady state, and then added an inhibitor of the γ-secretase (DAPT or LY-411575). We observed a dampening of oscillations and a loss of collective oscillations (Figure 47A). The intensity of the reporter decreased leading to a uniform expression of the reporter (we noticed transient spikes of the reporter corresponding to cell divisions). Furthermore, treatment with DAPT blocks the resynchronization and collective oscillations of cells on micropatterns (Figure 47B). We further confirmed that treating explants with DAPT abolished the expression and wave pattern of *Hes7* by *in situ* hybridization (Figure 47C). Consistently, a short treatment of explants with DAPT (6h) led to a strong decrease of *Hes7*, *Lfng*, and *Notch1* mRNA levels, further suggesting that Notch signaling directly acts on the segmentation clock and not only its synchronization in our system (Figure 47D) (in the Lewis model, DAPT should only have a modest effect ~20% on the level of cyclic genes expression - (Ozbudak and Lewis, 2008)). Because of the high cell density, we were not able to track individual cells without labeling techniques. This is a caveat of this experiment that we are now addressing; however, the absence of salt-and-pepper pattern and the reduction in reporter intensity strongly suggests that there is a loss of oscillations at the single-cell level.

In our framework of excitable system, Notch signaling would provide a signal that leads the cells to cross the excitability threshold and to oscillate. In zebrafish, it was rather proposed that blocking the Notch pathway induces a progressive desynchronization of single-cell oscillators. According to this model, Notch mainly affects the coupling strength between oscillators, while we propose that Notch is required for the emergence of oscillations. Those two hypotheses have different predictions concerning the recovery after DAPT treatment: if Notch signaling is only required for the synchronization of oscillators, we should observe a progressive apparition of collective oscillations, while if it is necessary for the oscillations, we would expect a sudden recovery as all cells cross the excitability threshold at the same time. Such transition would be similar to the model of dynamic quorum sensing described in *Dictyostelium discoideum* populations (Sgro et al., 2015). To test between these two predictions, we cultured explants overnight, dissociated them in single cells and cultured them on fibronectin micropattern in presence of DAPT. After 6 hours, we washed out the inhibitor and observed the immediate recovery of oscillations as expected for an excitable medium (Figure 47E). Observing an instantaneous synchronization would require to postulate a very strong coupling strength between oscillators in the case of a Kuramoto transition (first hypothesis).

If Notch signaling controls the switch between excitable to oscillatory dynamics, we should then rescue the loss of oscillations in single-cells by increasing Notch signaling. To test this hypothesis, we cultured dissociated cells on plate coated with Dll1 ligand. However, in these conditions, we were not able to observe single cell oscillations; as we will discuss later, this experimental condition had
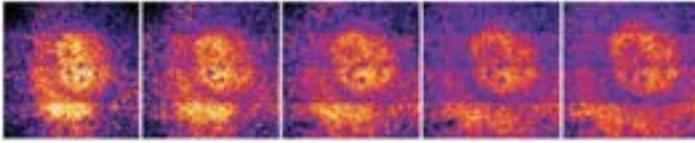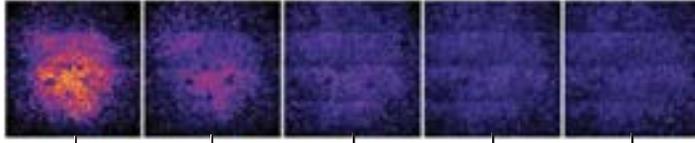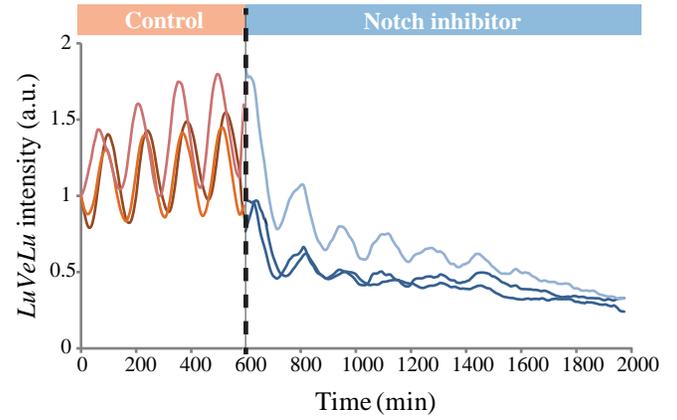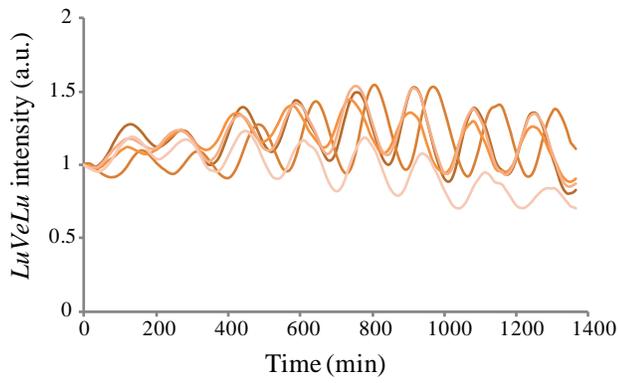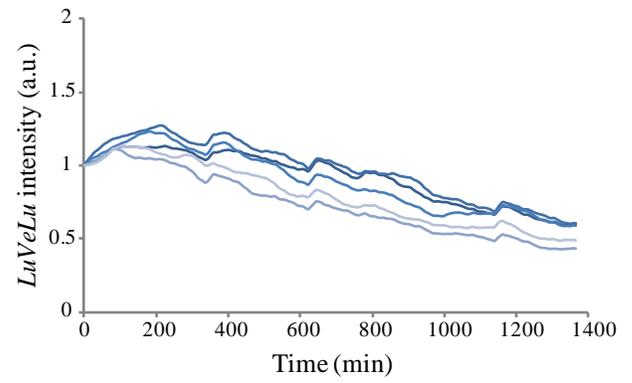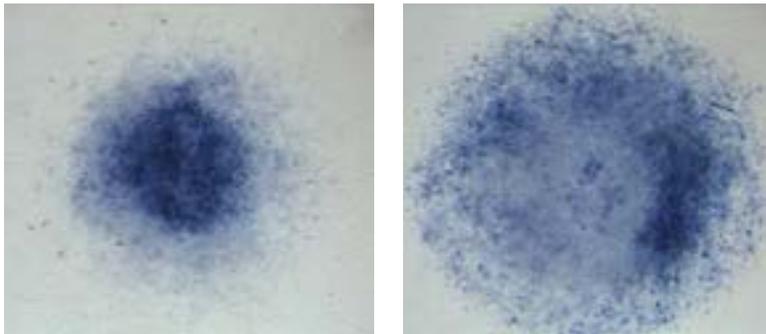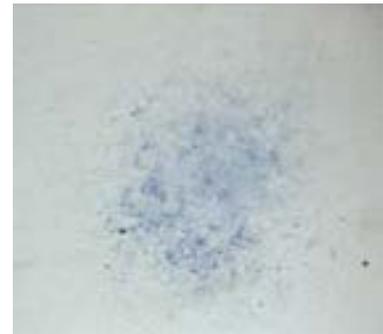
Figure 47 - Inhibition of the Notch pathway in explants

A. (*Left*) Series of snapshots of explants treated with DMSO or LY-411575 (100nM) showing the fluorescence intensity of the *LuVeLu* reporter. (*Right*) Graph showing the fluorescence intensity of the reporter before and after the addition of the Notch inhibitor over time - Each line corresponds to one explant.

B. Graphs showing the fluorescence intensity of the *LuVeLu* reporter for explant cells on micropattern. Addition of DAPT (20μM) after seeding of the cells blocks the formation of collective oscillations. Each line corresponds to one entire micropattern.

C. Pictures of *in situ* hybridization for *Hes7* (intronic) in explants treated overnight with DMSO or DAPT (20μM)

D

E
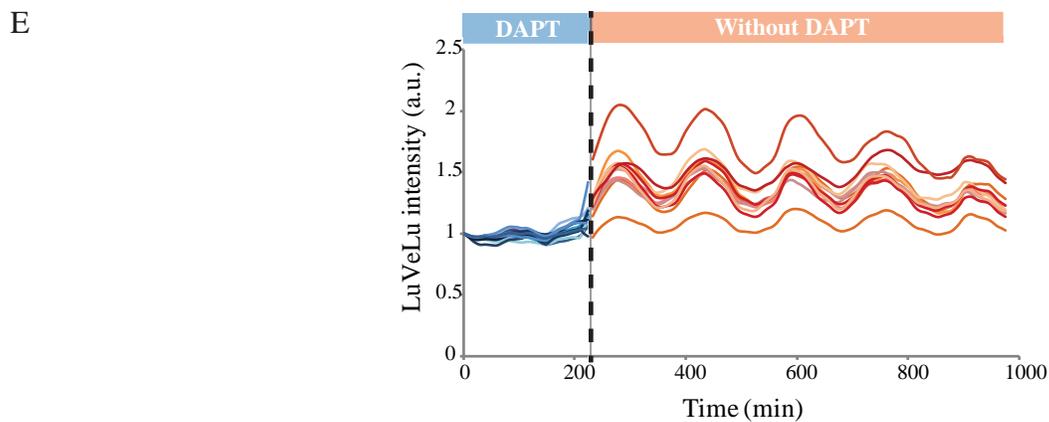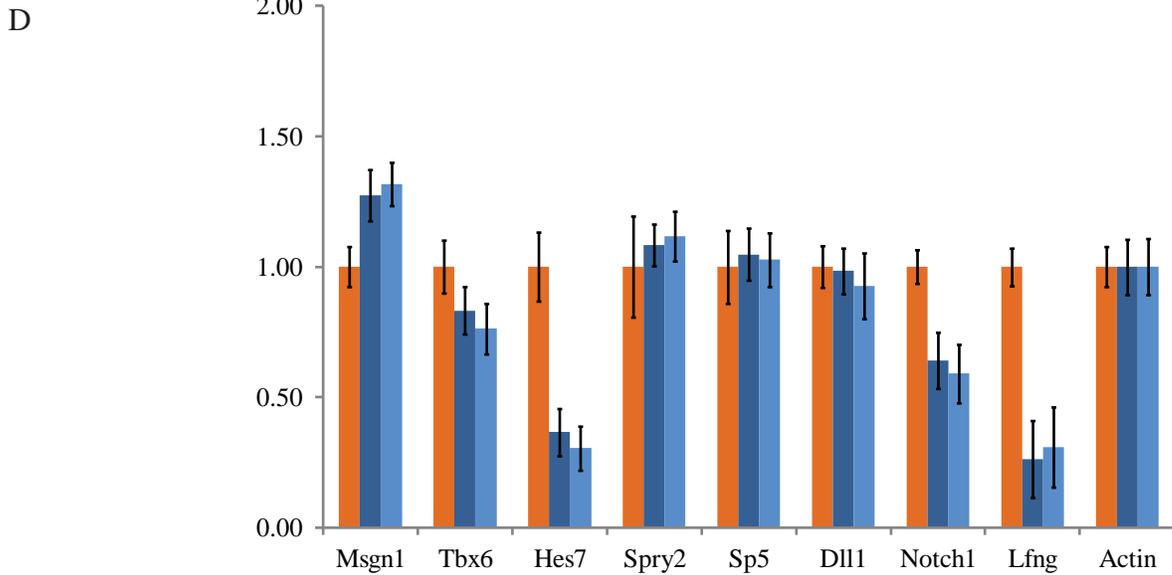
Figure 47 - Inhibition of the Notch pathway in explants *(continued)*

D. Graph showing the fold-change in gene expression for explants cultured for one day, and then treated for 6 hours with DMSO (orange) or DAPT (blue - biological replicates). One sample represents 3 explants pooled.

E. Graphs showing the fluorescence intensity of the *LuVeLu* reporter for explant cells on micropattern. The DAPT was washed out after 6 hours. Each line corresponds to one entire micropattern.

some artifactual effects due to changes in cell adhesion. As an alternative, we used a mouse line developed by Murtaugh and colleagues, where the Notch intracellular domain (NICD) is overexpressed after excision of *LoxP-STOP-LoxP* cassette by the Cre recombinase (Murtaugh et al., 2003, Feller et al., 2008). We used a cell-permeant form of Cre (fusion TAT-Cre), which we could simply add to the medium to induce recombination (Figure 48A). As the NICD construct is followed by an IRES-GFP, we could also directly detect the cells where recombination occurred (appropriate choice of filters allowed discriminating between the GFP and Venus signals) (Figure 48B-C). In these conditions, we detected GFP expression as soon as 6 hours after dissection and culture in presence of TAT-Cre (we noted that varying the dose of TAT-Cre could tune the mosaicism). However, we could not detect single-cell oscillations in GFP-positive cells, nor any effect of NICD overexpression on the *LuVeLu* oscillations in explants. The latter observation was surprising given that Feller and colleagues reported a quenching of *Lfng* oscillations in the *T-Cre;NICD*[+/Lox-STOP-Lox] embryos (Feller et al., 2008), and forced us to remain circumspect about this experiment.

While loss-of-function and recovery experiments are consistent with our excitable hypothesis, we were thus not able to recapitulate oscillations at the single-cell level upon restoration of Notch signaling. The discrepancy with Feller et al. could point to a technical problem that prevented to activate Notch signaling at a level high enough to cross the threshold. Notably for both excitable and oscillatory systems, overexpression of Notch should lead to a desynchronization and a loss of collective oscillations (Ozbudak and Lewis, 2008, Sgro et al., 2015). If Notch signaling was only required for the coupling, oscillators in the explant would become desynchronized upon NICD overexpression and only the *LuVeLu* expression level should be affected in dissociated cells according to the simulations from Ozbudak and Lewis (Ozbudak and Lewis, 2008). A better system to activate Notch signaling would thus enable to further study this hypothesis.

7. Role of mechanical factors and the Yap pathway

To further activate Notch signaling, we tried to remove the fibronectin coating as we reckoned that it could compete with the Dll1 coating. Surprisingly, we observed that dissociated cells on glass (with BSA instead of Dll1) displayed oscillations of the *LuVeLu* reporter. This indicated that mechanical factors could control the transition from excitable to oscillatory. To better understand this effect, we examined the expression of marker genes by qPCR between explant, dissociated cells on fibronectin and dissociated cells on glass (Figure 49A). For dissociated cells on fibronectin compared to the explants, we observed a downregulation in PSM markers (*Tbx6*, *Msgn1*), Wnt signaling (*Sp5*), Fgf signaling (*Sprouty2*), Notch signaling (*Dll1, Notch1, Lfng, Hes7*) and an upregulation of the Yap
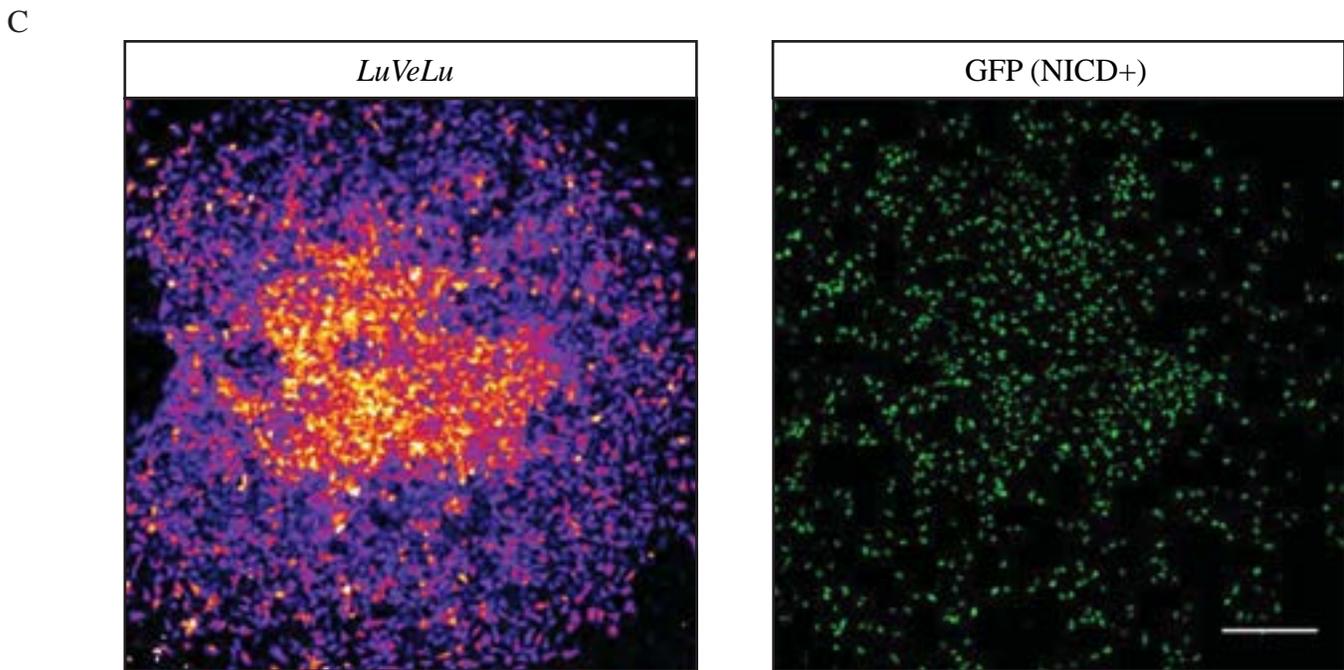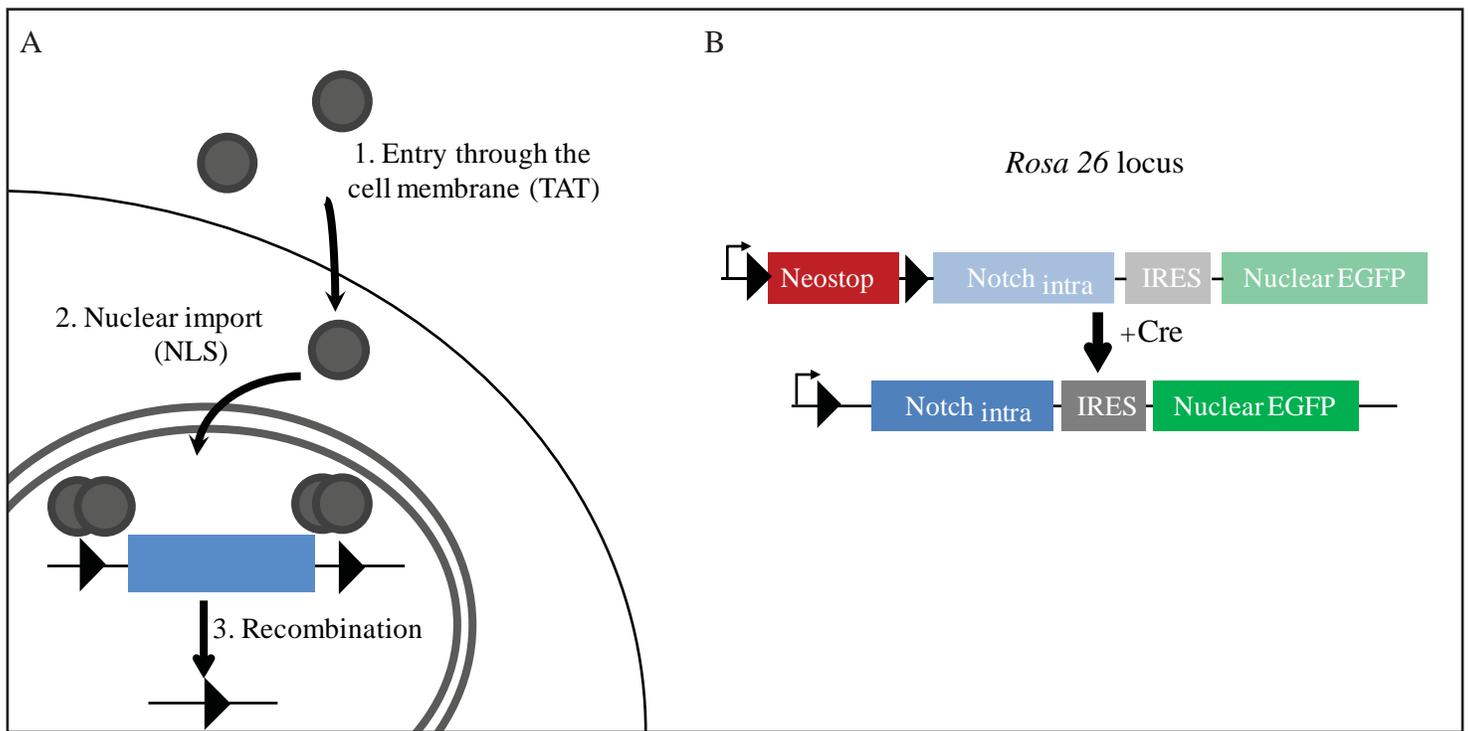
Figure 48 - Genetic activation of the Notch pathway

A. Scheme showing the mechanism of recombination mediated by the TAT-Cre

B. Scheme showing the genetic construct used to overexpress the Notch intracellular domain and to label the cells

C. (*Left*) Snapshot of an explant showing the fluorescence intensity of th *LuVeLu* reporter. (*Right*) Snapshot of the same explant showing cells positive for GFP (where recombination occured). The explant was cultured for 4 hours in presence of TAT-Cre (6μM) right after its dissection and the snapshot was taken at 15 hours post-dissection. (scale bar: 200μm)

target *ANKRD1*. By contrast, culturing the cells on glass partially rescued this phenotype and led to a strong downregulation of *ANKRD1*. We thus supposed that the Yap pathway could act on the *LuVeLu* oscillator. We note that our medium already contains a ROCK inhibitor, Y-27632, which should also repress the Yap pathway (Dupont et al., 2011); in our hands, it was necessary to add this compound for the viability and motility of dissociated cells.

Briefly, the Yap pathway is a conserved signaling pathway among animals that regulates cell proliferation and survival, and controls organ growth (Dupont, 2015). It is mainly controlled by the nucleo-cytoplasmic localization of Yap (or Taz): when Yap translocates to the nucleus, it interacts with the transcription factors TEAD1/2 to regulate gene expression (Figure 49C). Yap proteins can also have non-canonical functions, notably by interacting with other signaling pathways like Wnt or BMP (Hansen et al., 2015). Different input signals control the activation of the Yap pathway, such as the Hippo kinase cascade, metabolism or growth factors. Importantly mechanical cues of the cell environment can modulate Yap signaling: high cytoskeletal contractibility (because of a stiff matrix or stretching due to neighbors, matrix organization or a high adhesion surface) activates the pathway, while it is inactived in situations of low mechanical tension (soft matrix, low adhesion surface, cell crowding) (Dupont et al., 2011, Zhao et al., 2012, Dupont, 2015) (Figure 49D). In our case, plating cells on fibronectin or glass could modulate the adhesive surface and thus the activation of the Yap pathway.

To test this hypothesis, we first looked at the nucleo-cytoplasmic localization of Yap. By immunostaining, we observed that Yap was mostly localized in the nucleus on fibronectin (76%, 128/169), but both in the nucleus and cytoplasm on glass (75%, 97/129) (Figure 49B). This suggested that culturing cells on glass dampened the Yap pathway, consistently with the downregulation of *ANKRD1*. To further demonstrate a role of Yap, we used two drugs known to repress the Yap pathway: verteporfin and latrunculin A. The former prevents the interaction of Yap with the transcription factors TEAD in the nucleus, while the latter indirectly inhibits the Yap pathway by preventing actin polymerization and thus reducing cytoskeletal contractibility. In our hands, verteporfin was toxic. Conversely, treatment of dissociated cells on fibronectin with latrunculin A led to a decrease of the Yap targets, *ANKRD1*, *CTGF* and *Cyr61* compared to cells on fibronectin with DMSO (Figure 50A). The nucleo-cytoplasmic localization of Yap was more difficult to assess given the round, compact morphology of the cells, but we observed a difference compared to untreated cells, as Yap could be either in the cytoplasm or both in the nucleus and cytoplasm (Figure 50B). Therefore, treating with latrunculin A inhibited the Yap pathway in our system. Furthermore, under these conditions, dissociated cells exhibited clear oscillations of the *LuVeLu* reporter (n=5/5) (Figure 51A). This effect was independent of Notch signaling as treatment
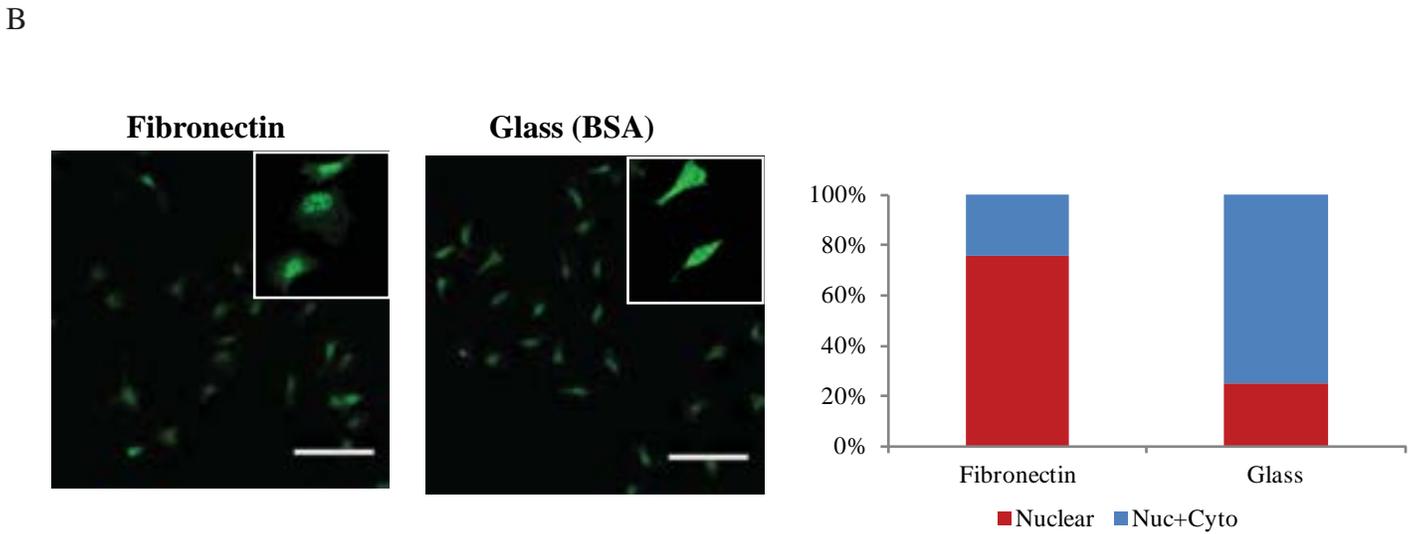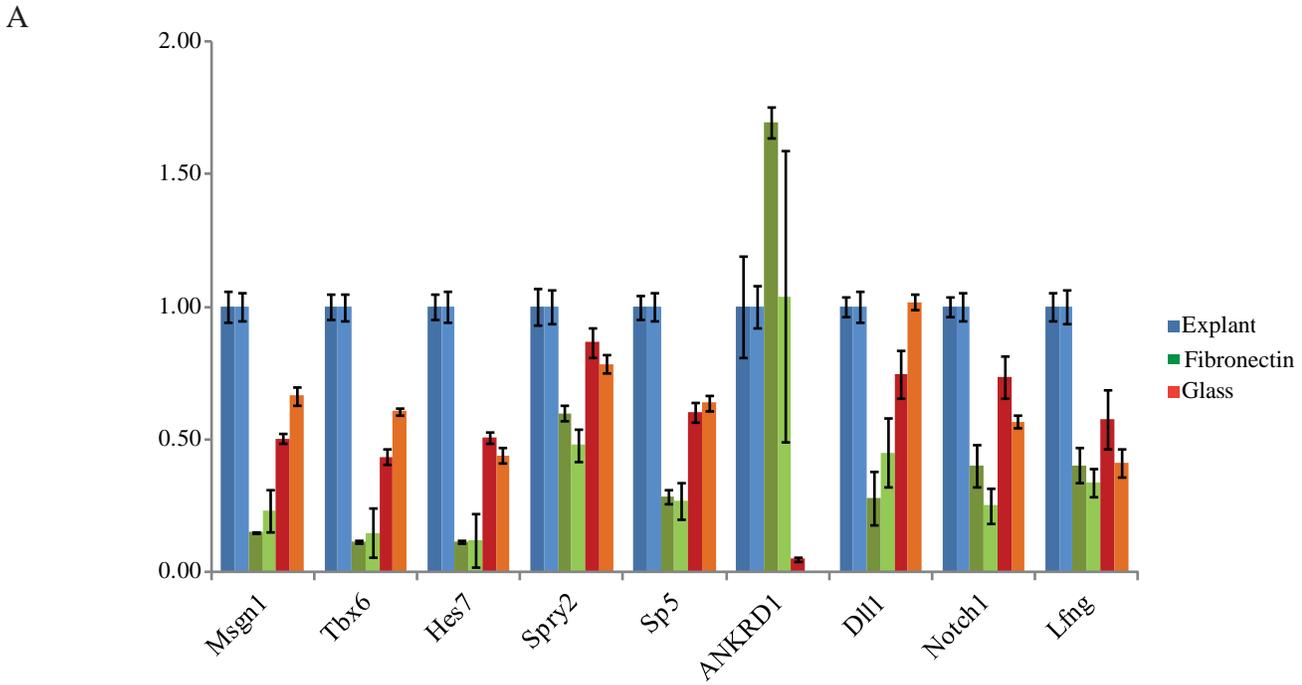
Figure 49 - Effect of the substrate on dissociated cells

A. Graph showing the fold-change in gene expression between explants, dissociated explant cells cultured on fibronectin or glass (BSA control)

B. (*Left*) Immunostaining for Yap of dissociated cells cultured on fibronectin or glass. The excerpt show examples of cells where Yap was scored as nuclear or as both nuclear and cytoplasmic. (Scale bar: 100μm). (*Right*) Graph showing the proportion of cells for which Yap is nuclear or both nuclear and cytoplasmic (Nuc+Cyto)

C
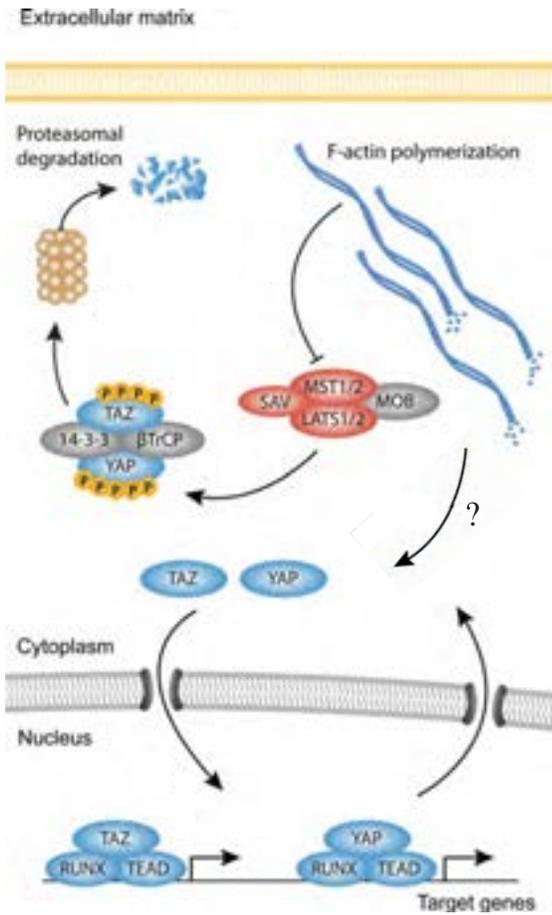
D
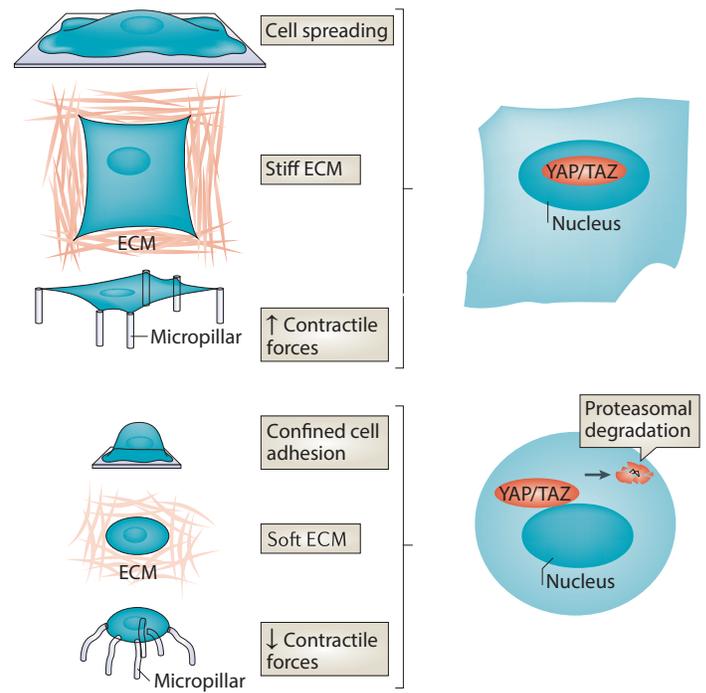
Figure 49 - Effect of the substrate on dissociated cells (*continued*)

C. Yap pathway - Phosphorylation of Yap by the Mst/Lats complex leads to degradation. Upon inhibition of F-actin polymerization, this complex is inactive and Yap migrates to the nucleus where it activates several target genes in concert with TEAD factors. The Yap pathway can also be activated by other inputs, such as Wnt or GPCR.

D. Effect of mechanical conditions on Yap activation - Yap is activated in situations of high intracellular resisting forces (e.g. high adhesive surface, stiff matrix) and inactivated in situations of lower contractility (e.g. sotf matrix, cell crowding).

Modified from Piersma et al. (2015), Halder et al. (2012)
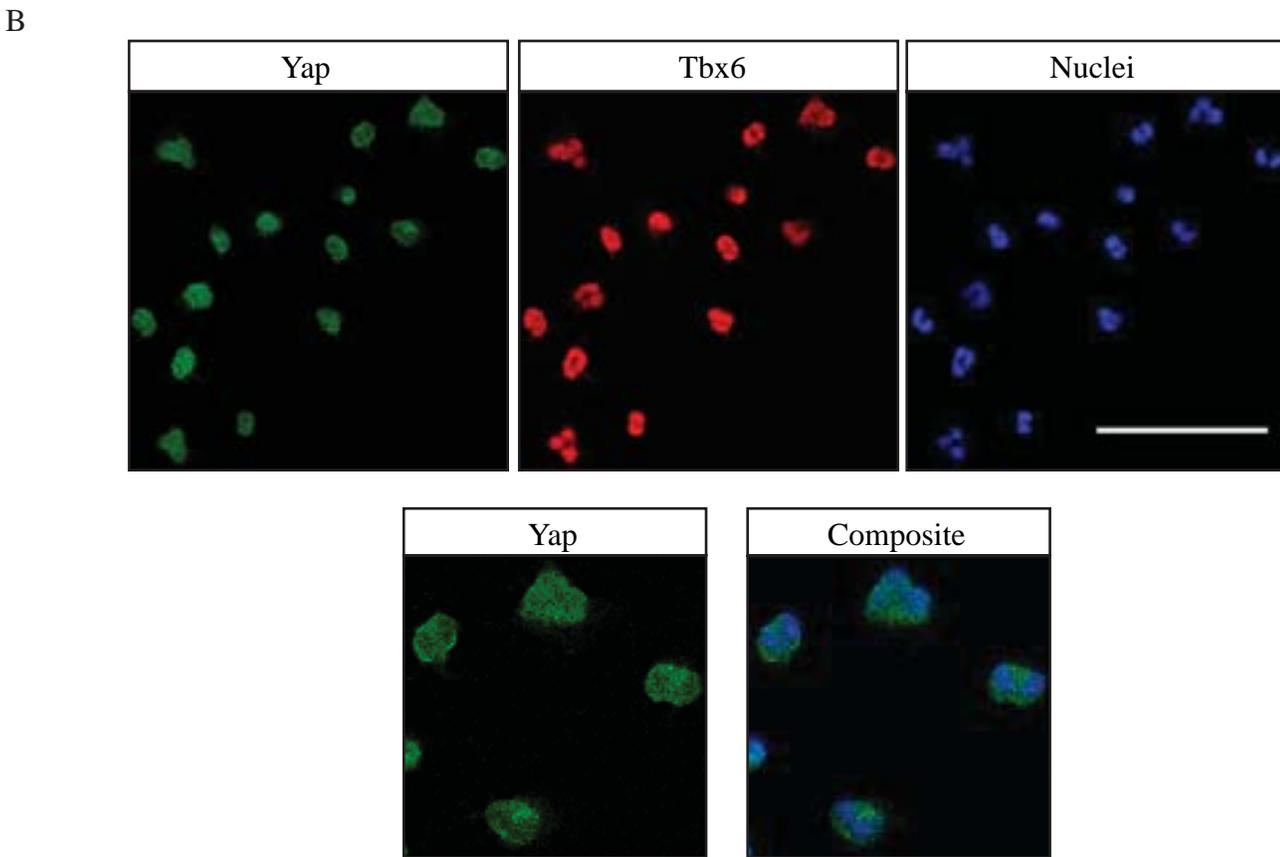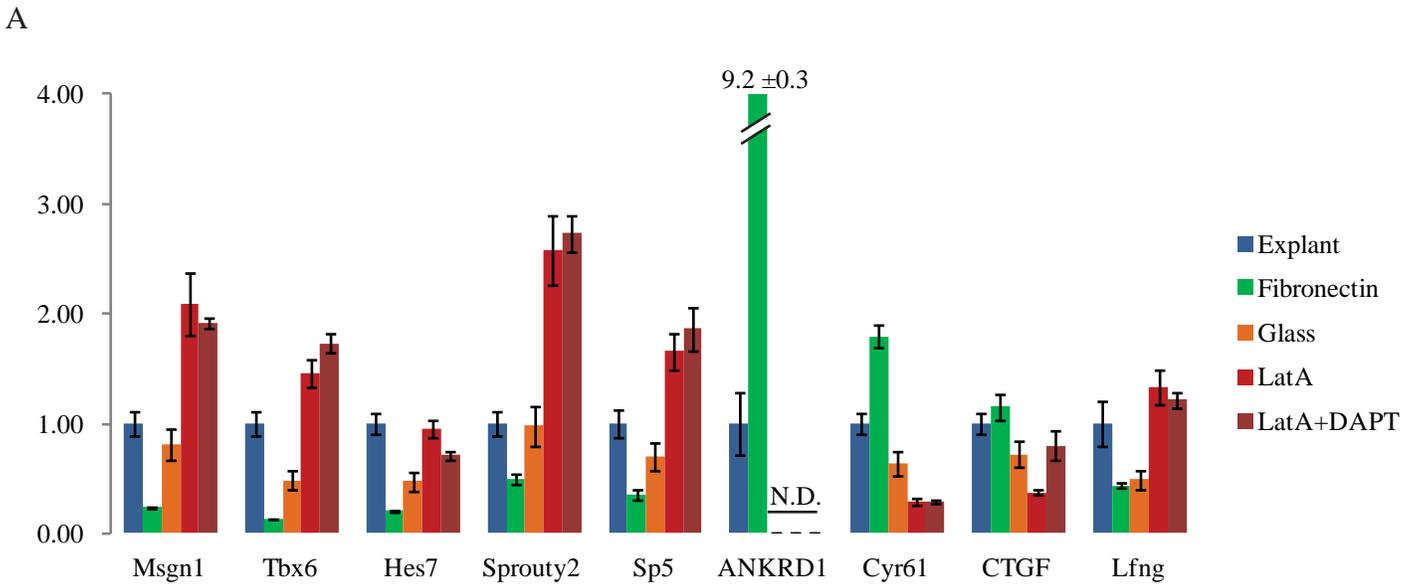
Figure 50 - Effect of latrunculin A treatment on dissociated cells

A. Graph showing the fold-change in gene expression between explants, dissociated explant cells cultured on fibronectin with DMSO, latrunculin A (0.5μM) or latrunculin A with DAPT (20μM), and dissociated explant cells cultured on glass. N.D: not detected.

B. (*Top*) Immunostaining for Yap, Tbx6 and nuclei staining of dissociated cells cultured on fibronectin with latrunculin A. (Scale bar: 100μm). (*Bottom*) Excerpt showing the relative localization of Yap and nuclei.
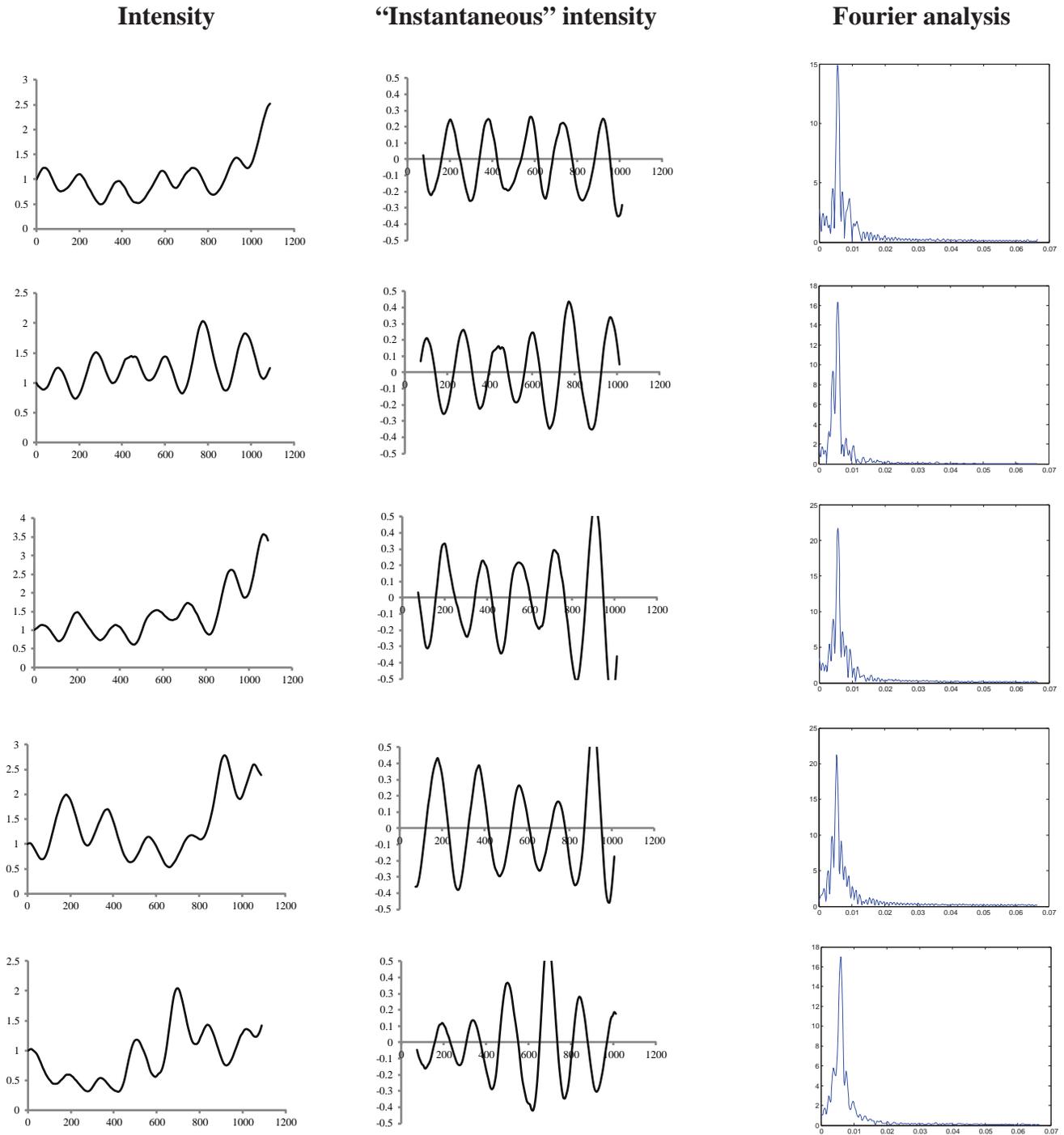
Figure 51 - Dynamics of the *LuVeLu* reporter after latrunculin A treatment

A. (*Left*) Mean fluorescence intensity of the *LuVeLu* reporter for dissociated cells on fibronectin treated with latrunculin A (0.5µM) over time; x-axis indicates the time in minutes; y-axis indicates the intensity in arbitrary units. (*Middle*) Mean fluorescence intensity of the *LuVeLu* reporter after subtraction of a moving average over 150 minutes; x-axis indicates the time in minutes; y-axis indicates the intensity in arbitrary units. (*Right*) Fast Fourier transform of the mean fluorescence of the *LuVeLu* reporter after subtraction of a moving average' x-axis indicates the frequency (min^{-1}), y-axis indicates the Fourier transform amplitude.

B
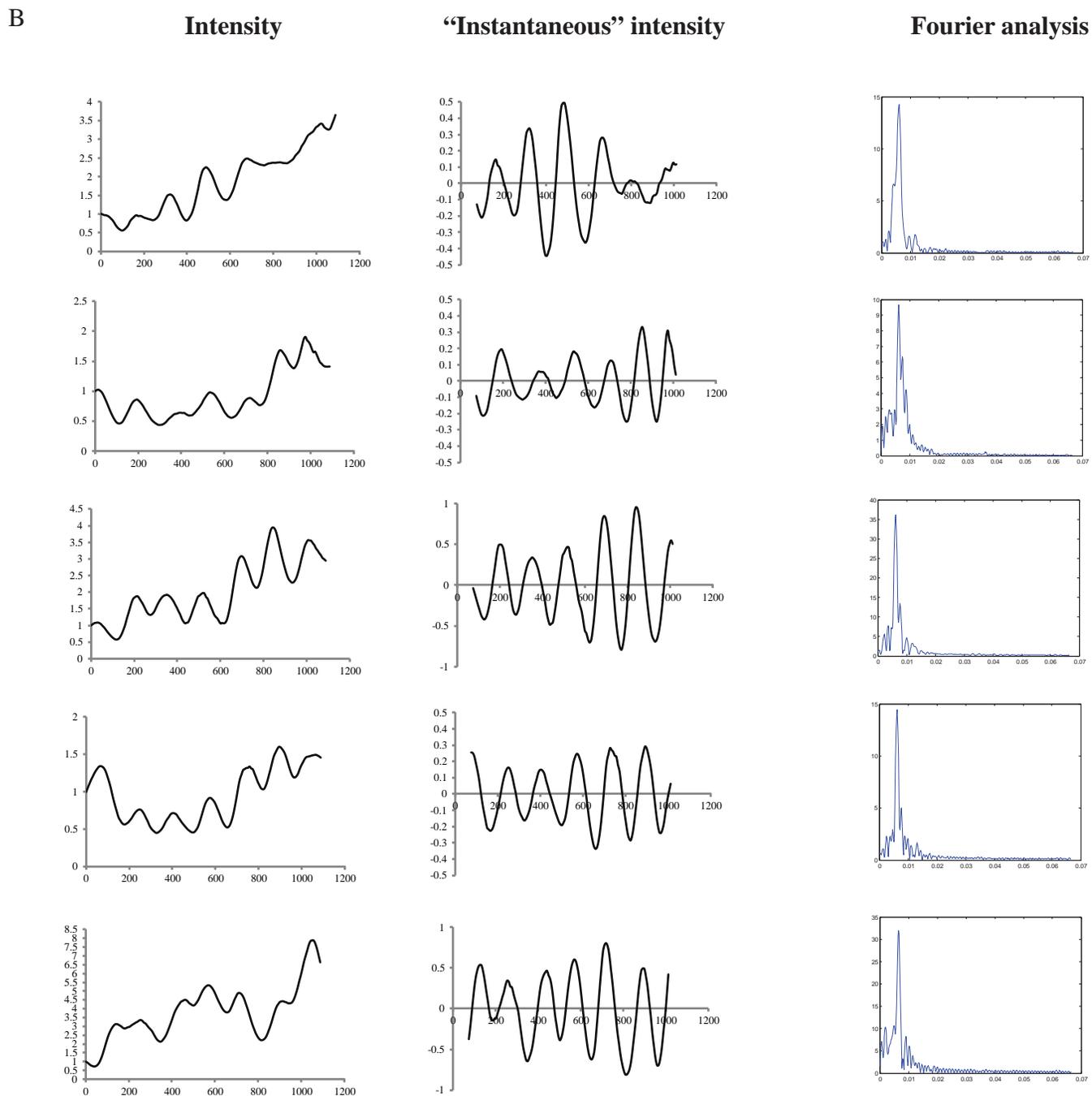
Figure 51 - Dynamics of the *LuVeLu* reporter after latrunculin A treatment *(continued)*

B. (*Left*) Mean fluorescence intensity of the *LuVeLu* reporter for dissociated cells on fibronectin treated with latrunculin A (0.5μM) and DAPT (20μM)) over time; x-axis indicates the time in minutes; y-axis indicates the intensity in arbitrary units. (*Middle*) Mean fluorescence intensity of the *LuVeLu* reporter after subtraction of a moving average over 150 minutes; x-axis indicates the time in minutes; y-axis indicates the intensity in arbitrary units - note that for two graphs, we changed the y-scale. (*Right*) Fast Fourier transform of the mean fluorescence of the *LuVeLu* reporter after subtraction of a moving average' x-axis indicates the frequency (min^{-1}), y-axis indicates the Fourier transform amplitude.

with DAPT did not abolish the oscillations observed upon latrunculin A treatment (n=5/5 cells) (Figure 51B). This control was especially important as sister cells remained attached together after cell division, making possible that the effect observed was the consequence of cell-cell contacts. The period in latrunculin A and latrunculin A/DAPT was similar to the period of explants (168±9 minutes). PSM markers were similarly expressed for latrunculin A-treated cells with or without DAPT, notably *Hes7* and *Lfng* (Figure 50A). While we cannot fully exclude that the changes in cell morphology compared to the control situation made the detection of oscillations easier to detect, such changes in gene expression support a real effect of the drug. Furthermore, Fourier analysis of the *LuVeLu* fluorescence intensity (mean fluorescence after subtraction of a moving average to remove the effects of long-term intensity fluctuations) revealed single and isolated peaks distinct from the spectrum obtained for cells without latrunculin A (Figures 51A-B). Together this suggests that the Yap pathway controls the transition from the excitable to the oscillatory state. According to this hypothesis, treating explants with latrunculin A should rescue the loss of oscillations after blockade of Notch signaling. Indeed, we observed that explant cells oscillated in a desynchronized way with DAPT in presence of latrunculin A (Figures 51C-D). This could explain the discrepancy with previous findings by Tsiairis and Aulehla (see discussion)

As treatment with latrunculin A could act on other pathways, we tried to confirm the role of Yap signaling by direct genetic manipulation of the pathway. For this purpose, we used lentivirus that could readily infect explants. To show that inhibition of Yap was required for oscillations at the single-cell level, we infected dissociated cells with a construct expressing a shRNA against *Yap1* (Rosenbluh et al., 2012), but we did not detect any reduction of the protein level after two days compared to the shRNA-scramble. We are now trying to overactivate the Yap pathway by use of a constitutively active Yap (Yap-5SA: non-phosphorylable form of Yap that cannot translocate to the nucleus); this should lead to a loss of the oscillations triggered by latrunculin A.

8. Role of Fgf signaling in the PSM determination

We next addressed the question of the determination of the PSM. Indeed, as explants can be stably cultured in an oscillatory, undetermined state, we could control the timing of differentiation by adding different factors.

We first examined the role of Fgf signaling, as reducing its dose led to an arrest of the oscillations. Therefore, we cultured explants overnight to reach a steady state, and we added the MEK1/2 inhibitor PD0325901 that blocks Fgf/ERK signaling. Treatment with this inhibitor led to a

C

Space (~900µm)

| Control | Latrunculin A |
| DAPT | DAPT + Latrunculin A |

Time (22h)
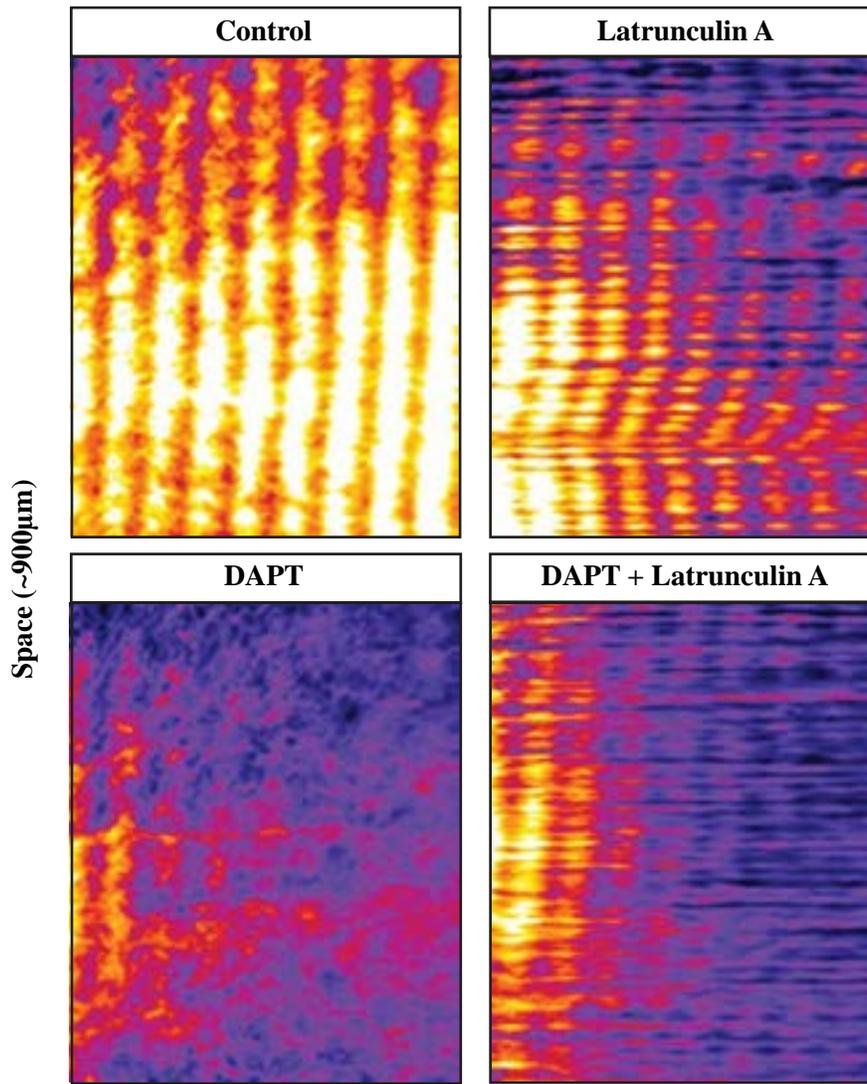
D
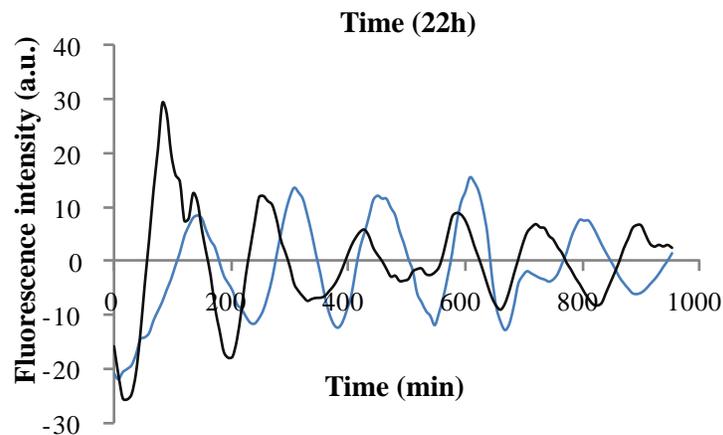
Figure 51 - Dynamics of the *LuVeLu* reporter after latrunculin A treatment *(continued)*

C. Kymographs of explants treated with a combination of DAPT (20µM) and latrunculin A (0.5µM). The "pointil-list" aspect of explants treated with latrucunlin A is due to the changes in cell morphology and motility.

D. Graph showing the fluorescence intensity of the *LuVeLu* reporter over time for two close cells treated with DAPT and latrunculin A.

progressive arrest of the oscillations (~4 cycles) (Figure 52). We observed a progressive increase in intensity of the *LuVeLu* reporter (~ 2.5 fold) and an increase in the period of oscillations (~ 1.3 fold) (Figures 52B-C). However, this was not an irreversible process: we treated explants with the MEK inhibitor, and washed out the dug after 2h30 or 7h30. In these conditions, we observed a recovery of the oscillations suggesting that explants were not irreversibly committed after short Fgf/ERK inhibition (Figure 53).

Inhibiting Fgf/ERK led to the determination of the explants as evidenced by the loss of Tbx6 (Figure 54A). We validated by *in* situ hybridization that MEK inhibition induced the loss of the posterior marker *Msgn1* (Figure 54B). We obtained similar results with the Fgf receptor inhibitor PD173074. The determination of the explant tended to be centripetal as in the previous experiments where Fgf4 concentration was reduced; however, this occurred in a more abrupt and disorganized way. In some cases, we observed "islands" of cells, where Tbx6 persisted for a longer time (Figure 54A). Therefore, inhibiting Fgf/ERK led to a progressive determination of the explants. To further validate that it mirrored the determination occurring in the PSM, we performed microarray analysis for explants treated with and without PD0325901: we cultured the explants (in triplicates) for 17h to reach a steady state, and then we added the inhibitor; we monitored the arrest of oscillations by live imaging and lysed the explants after 14.5h. We compared the expression profile to the microarrays series of M.Oginuma, where single PSM were dissected and divided along the antero-posterior axis to follow the sequence of PSM maturation (Figure 54C) (Chal et al., 2015). We used two methods to replace our explant samples along this series: clustering using the Euclidean distance and principal component analysis. The former revealed that the non-treated samples were more similar to the posterior PSM (non-tailbud) and the PD0325901-treated clustered with the anterior PSM (level of Mesp2 expression) (Figure 54D). Principal component analysis separated the samples between *ex vivo* and *in vivo* samples and between posterior and anterior samples; while it clearly showed an anterior shift upon MEK inhibition, we observed that both samples were positioned in a more anterior position than in the clustering analysis (middle PSM and somite levels) (Figure 54E). In a more biased manner, the expression of known marker genes indicated that the untreated samples were more similar to the posterior, non-tailbud, PSM (similar expression levels for *T*, *Tbx6*, but no expression of *Cyp26a1*, *Fgf4*) and the treated samples, to the anterior PSM (expressing *Ripply2*, *Raldh2*) (Figure 54F) (annotation was performed by O.Tassy using Manteia (Tassy and Pourquié, 2013)).

We further quantified the effect of Fgf/ERK on the oscillations by titrating the amount of inhibitor using micropatterns to limit the variability due to explants geometry or size (Figure 55). With this setting, the number of oscillations observed before their arrest decreased as the dose of inhibitor

A. Snapshots of an explant cultured after inhibition of the Fgf/ERK inhibitor PD03 showing the fluorescence intensity for the *LuVeLu* reporter. Note that the reporter persists in a subset of cells (also positive for Tbx6) but becomes ultimately off.
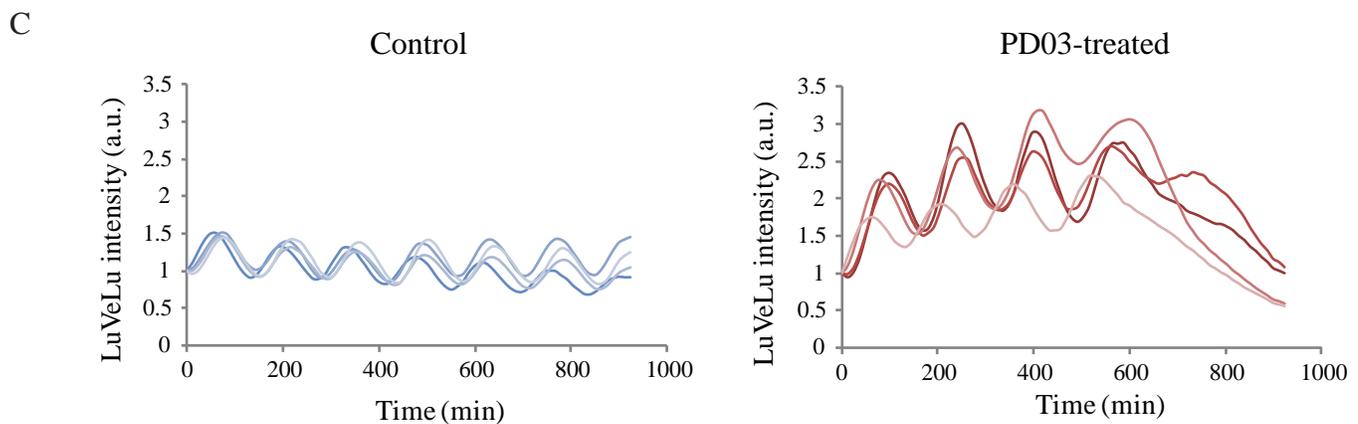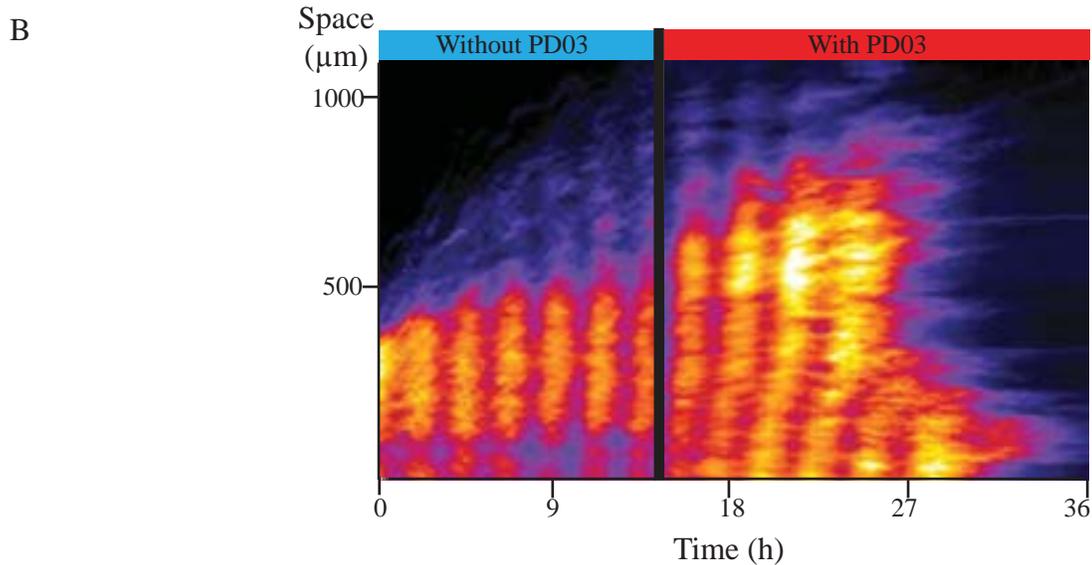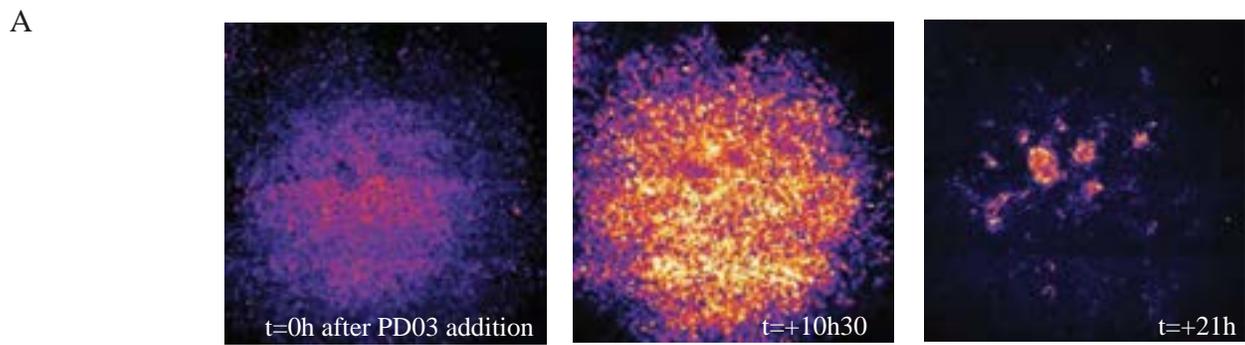
Figure 52 - Effect of Fgf/ERK inhibition on explants

A. Snapshots of an explant cultured after inhibition of the Fgf/ERK inhibitor PD03 showing the fluorescence intensity for the *LuVeLu* reporter. Note that the reporter persists in a subset of cells (also positive for Tbx6) but becomes ultimately off.

B. Kymograph of an explant (from the center to the periphery) cultured overnight and then treated with the Fgf/ERK inhibitor PD03.

C. Graphs showing the evolution of the fluorescence intensity of the *LuVeLu* reporter at the center of explants during the treatment with the Fgf/ERK inhibitor or vehicle control. Each line corresponds to one explant.
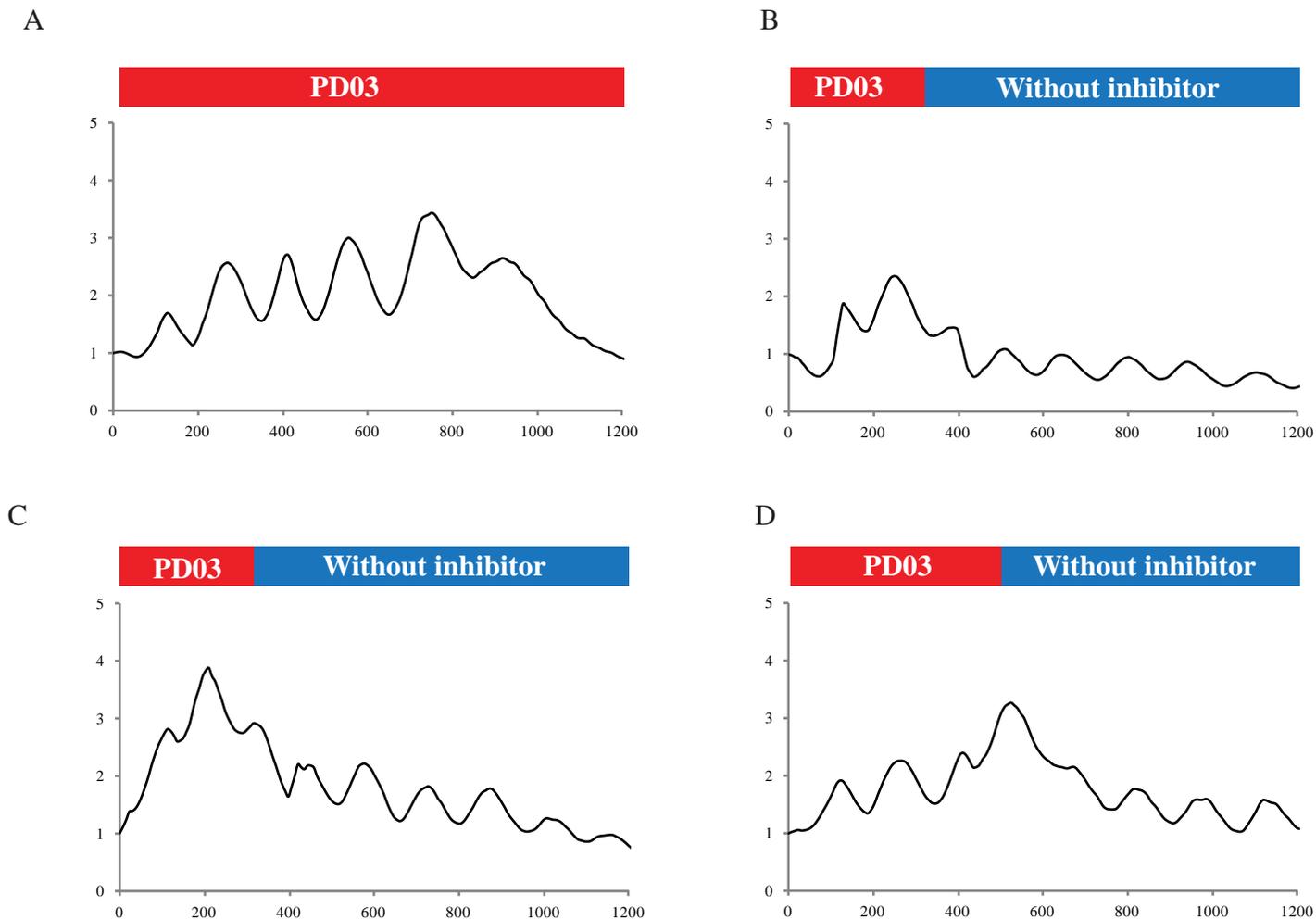
Figure 53 - Reversibility of Fgf/ERK inhibition

After overnight culture without drug, explants were cultured in presence of the Fgf/ERK inhibitor PD03. Each graph represents the fluorescence intensity of the *LuVeLu* reporter for one explant over time.

A. Continuous treatment with PD03 (2μM) (4/4)

B. Treatment with PD03 (2μM) for 2h30, then removal of the drug (4/4)

C. Treatment with PD03 (10μM) for 2h30, then removal of the drug (4/4)

D. Treatment with PD03 (2μM) for 7h30, then removal of the drug (3/3)

149
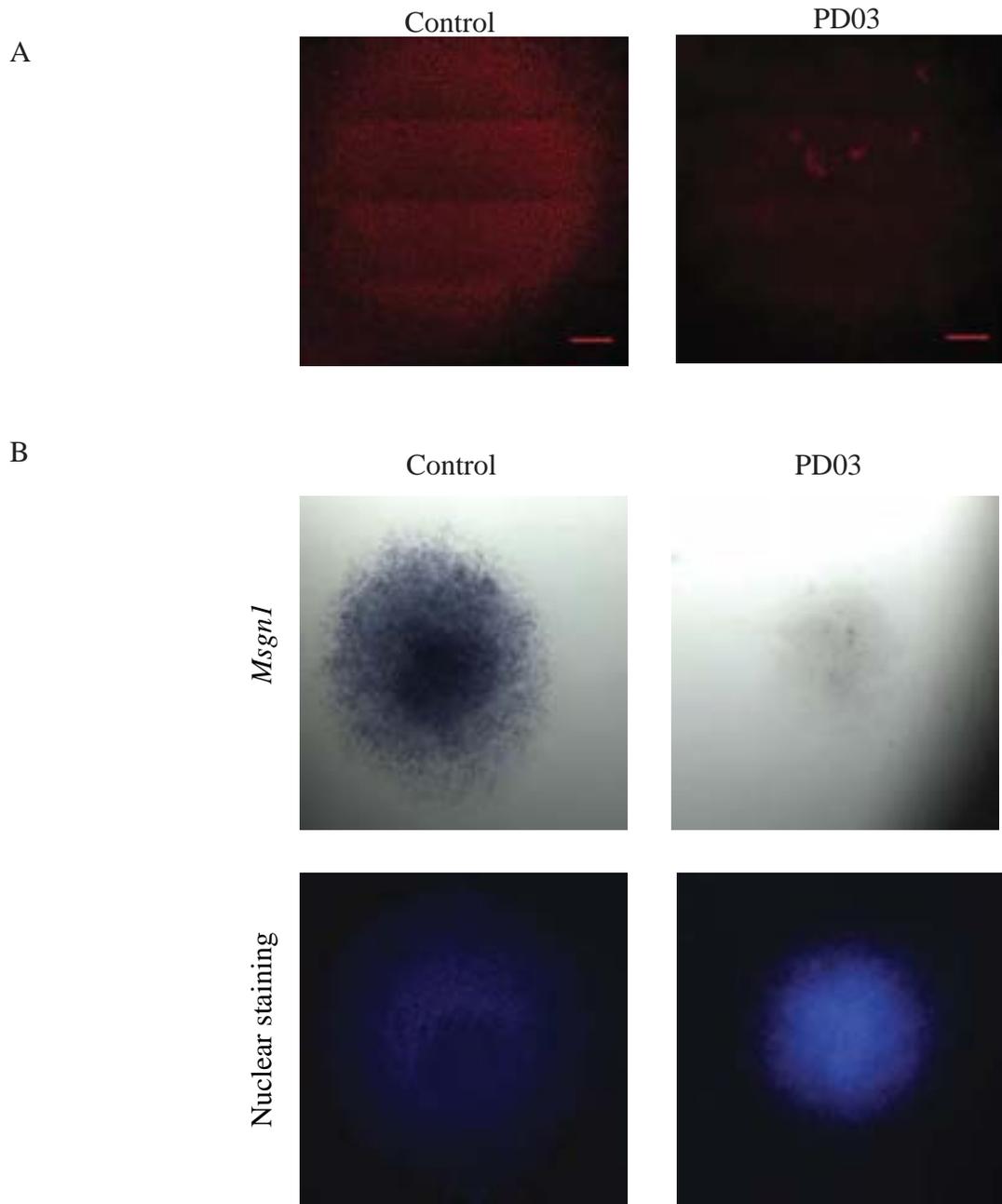
Figure 54 - PSM determination upon Fgf/ERK inhibition

A. Immunostaining for Tbx6 in an explant treated with the Fgf/Erk inhibitor PD03 (1µM,15h) or with the vehicle control (control explants positive for Tbx6: n=5/5; treated explants negative for Tbx6: n=5/5)

B. (*Top*) *In situ* hybridization for *Msgn1* for explants treated with vehicle control (left –explants positive for *Msgn1*: n=4/4) or the Fgf/ERK inhibitor PD03 (2µM, 15h) (right –explants negative for *Msgn1*: n=2/2) (*Bottom*) Nuclear staining for the corresponding explants.
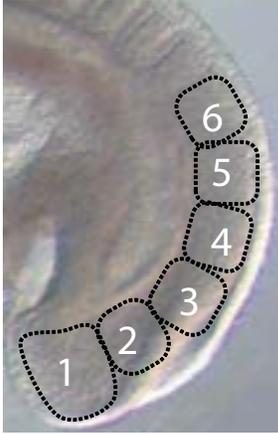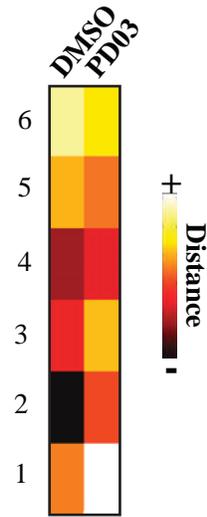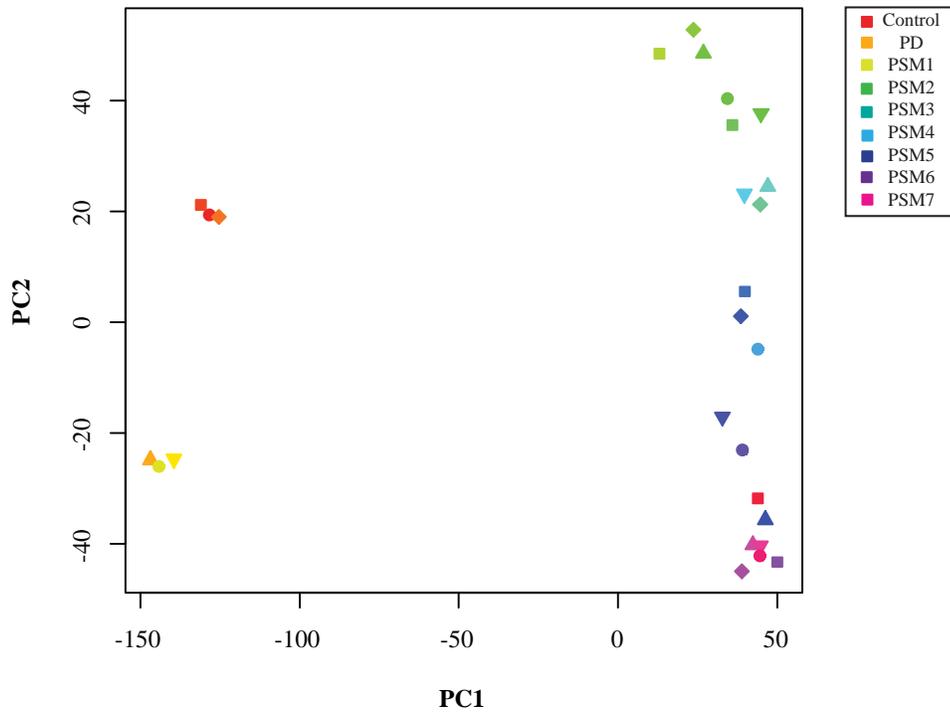
Figure 54 - PSM determination upon Fgf/ERK inhibition (*continued*)

C. Photography of a E9.5 mouse tail showing the different regions dissected for microarray analysis. *Modified from Chal et al. (2015)*

D. Heat-map showing the distance between the DMSO and PD03 samples and the *in vivo* PSM series

E. Principal component analysis for the explants and *in vivo* PSM series

F **Posterior PSM markers**

Gene	Control	PD	PSM1	PSM2	PSM3	PSM4	PSM5	PSM6
Cyp26a1	44.9	20.0	3275.0	195.3	55.6	54.6	123.6	33.2
Brachyury, T	2729.5	437.2	5193.0	2820.9	1508.1	779.0	460.2	136.2
Fgf17	19.3	6.3	359.8	111.1	23.7	8.1	13.9	4.7
Wnt5a	2300.7	1649.6	1806.9	1158.5	814.6	778.3	748.5	265.9
Rspo3	1711.8	1228.1	4232.4	3053.4	1865.1	1129.0	610.5	169.0
Evx1	218.5	53.5	1059.2	329.4	115.3	53.5	59.0	27.6
Fgf4	6.4	6.7	314.9	44.3	14.7	7.5	8.2	6.4
Dkk1	71.7	241.4	528.3	304.1	59.2	14.3	22.2	16.9
Tbx6	1045.1	129.4	808.0	1215.4	934.7	761.0	339.6	80.4
Mixl1	46.1	22.3	468.4	89.0	51.6	32.8	25.6	25.7
Fgf15	23.8	34.1	612.0	355.5	238.7	119.8	62.8	38.6
Wnt3a	92.1	40.9	544.7	156.8	71.2	52.9	59.7	49.3

Anterior PSM markers

Gene	Control	PD	PSM1	PSM2	PSM3	PSM4	PSM5	PSM6
Ripply2	4.5	180.0	6.1	5.2	7.1	220.8	945.1	627.1
Meox1	31.4	137.7	42.4	63.4	464.1	1809.6	2452.5	3078.8
Fgf18	14.3	61.4	25.0	17.8	76.0	653.5	1564.5	1212.9
Aldh1a2	94.4	786.1	23.1	50.8	234.7	828.1	1402.8	1617.9
Cer1	7.3	31.9	9.2	7.6	8.6	15.0	297.8	532.1
Dmrt2	18.6	581.4	4.8	4.8	6.5	15.2	101.1	340.5
Uncx	4.7	6.5	5.7	5.8	7.5	21.2	102.0	388.7
Foxc2	12.4	459.7	95.1	668.1	1189.2	2209.1	3139.8	2963.1
Meox2	6.1	18.6	6.1	6.4	6.7	14.1	286.0	290.9
Ephrin B2	121.7	1543.7	86.2	71.0	148.0	578.2	1263.6	1618.7
Tcf15	397.7	479.2	173.8	286.9	599.6	1380.7	1842.1	2848.5
Pcdh8	263.5	848.9	174.6	862.2	1240.5	1572.4	2832.7	1824.9
Cdx2	113.1	62.2	913.9	234.9	109.6	45.1	62.3	40.4
Pcdh8	504.7	1416.8	584.9	2877.0	3637.4	4527.2	6772.4	4782.7
Tbx18	6.1	9.2	9.4	7.2	8.8	30.8	125.9	191.5
Nr2f2	8.9	10.1	30.5	85.7	176.9	411.0	474.8	416.5
Follistatin	197.8	331.0	20.7	73.6	206.3	339.6	245.9	248.8
Meis1	49.2	160.8	67.0	283.3	420.4	632.5	794.6	819.3
Meis2	44.5	57.2	292.5	1279.4	1888.8	2321.3	1876.0	1473.4
Notch1	1142.2	938.0	1236.3	2541.3	3058.9	4143.8	6394.7	6839.9
Mesp2	20.5	71.8	24.2	22.8	36.0	337.4	223.3	66.5
Dll1	1628.4	850.1	1336.1	1077.0	1212.6	2217.5	1271.0	294.0
Pax3	78.1	145.5	294.5	195.0	172.5	350.6	967.1	1285.8

Figure 54 - PSM determination upon Fgf/ERK inhibition (*continued*)

F. Tables showing the normalized expression levels (RMA) for genes differentially expressed in the PSM. Control refers to the average of three explants treated with vehicle control; PD refers to the average of three explants treated with the Fgf/ERK inhibitor PD03; PSM1-6 refers to the *in vivo* PSM series in (Chal et al., 2015)
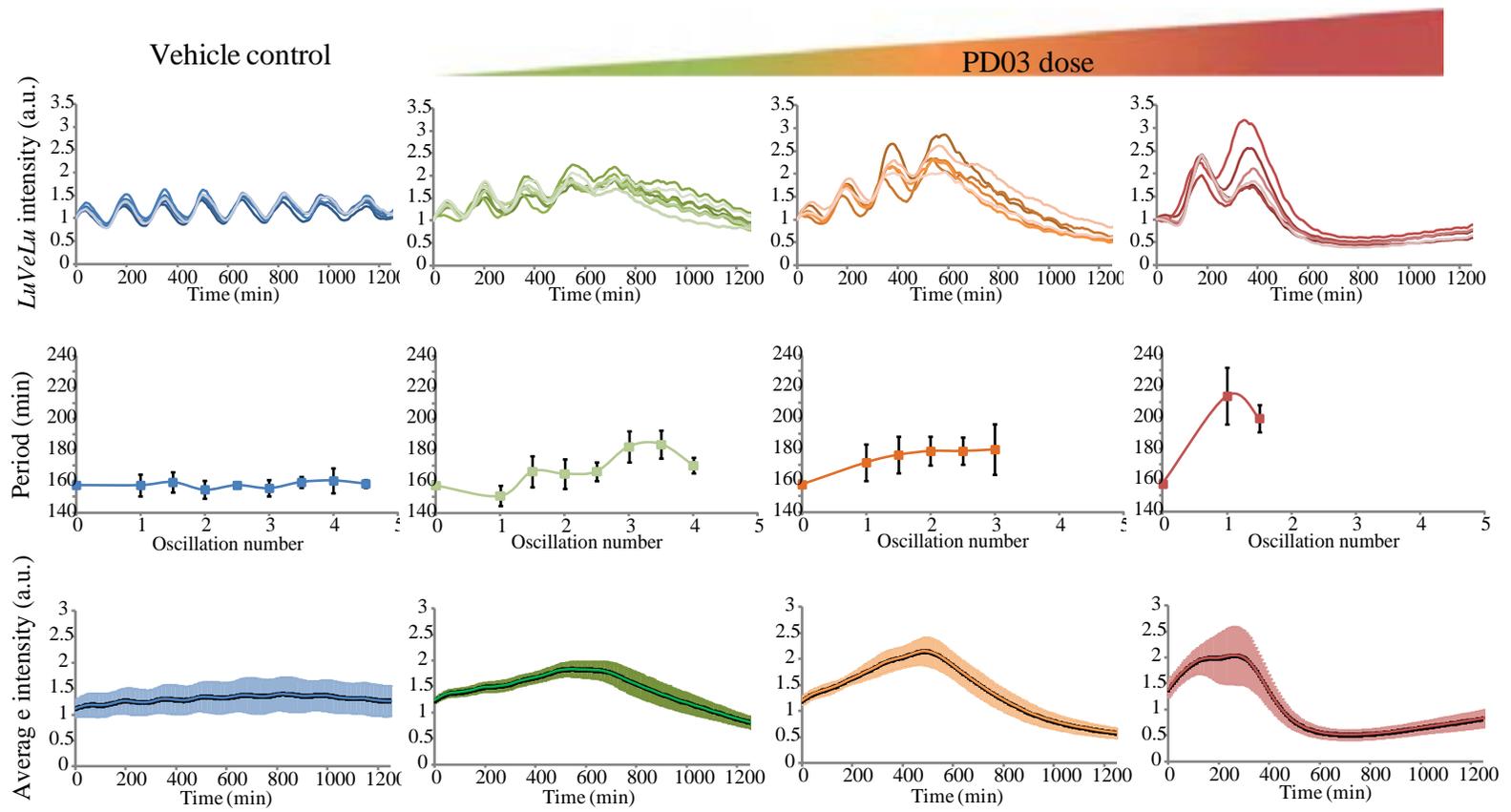
Figure 55 - Dose-dependent effect of Fgf/ERK inhibition on the *LuVeLu* dynamics

(*Top*) Fluorescent intensity profile for cells on a micropattern treated with different doses of the Fgf/Erk inhibitor or vehicle control (blue), 0.4μM (green), 0.65μM (orange), 10μm (red); each line represents one micropattern. (*Middle*) Instantaneous period for the different conditions (±SD). (*Bottom*) Average reporter intensity (±SD- over a window of 3h).

increases: for instance, treatment with a low-dose of inhibitor (0.4μM) led to an arrest of oscillations after 5 cycles, while increasing the dose to 0.65μM or 1μM led to an arrest after 4 cycles and 3 cycles respectively. This dose-dependent effect argues against the existence of a single threshold that would control the PSM differentiation as posited in the classical clock-and-wavefront model. Together, this rather indicates that Fgf signaling provides positional information by controlling the dynamics of the Notch oscillator.

To better understand how this could be explained in the context of an excitable system, we performed preliminary simulations using the FitzHugh-Nagumo model, a classical activator-inhibitor model, initially devised to capture the excitability of neural cells (Figures 56A-B). It is a non-Turing reaction-diffusion system, where only the activator propagates and recapitulates the main features of an excitable system (existence of an excitability threshold, refractory period, different time scales between activation and repression). Such model also recapitulates the transition from an excitable to oscillatory regime as the stimulus increases through a Hopf bifurcation (in the neural context, the stimulus corresponds to the external current applied). Increasing the amplitude of the stimulus could lead to a further disappearance of the limit cycle, a phenomenon known as "excitation block". We simulated the behavior of a two-dimensional micropattern of cells using the FitzHugh-Nagumo formalism. We supposed that the strength of Fgf inhibition correlates with the rate of increase in the external stimulus, meaning that there is a higher basal production of the activator. *In vivo,* this could relate to the increase in Notch signaling in the anterior PSM, as evidenced by the increase in NICD, *Notch1* and Notch targets (e.g. *Hes5*) expression (Huppert et al., 2005, Bone et al., 2014). We observed that, in this situation, we were able to reproduce the dose-dependent effect observed with the Fgf/ERK inhibitor in micropatterns (Figure 56C). This could explain how oscillations stop at a finite period, contrary to previous models that suggest an infinite period in the anterior PSM. However, in the absence of molecular details (identification of the activator/repressor couple, link between Fgf and excitability), it is difficult to further develop this model, as the findings could be specific to the model used and not general to all excitable systems.

9. Role of Wnt signaling in the PSM determination

We next examined the role of the Wnt pathway in the control of the PSM determination. We used three different inhibitors (in absence of CHIR): the extracellular inhibitor Dkk1, the compound IWR-1 that prevents the degradation of the Wnt inhibitor Axin2, and ICRT14 that blocks the interaction of TCF and β-catenin. All compounds led to a delayed arrest of oscillations and determination of the explants (after ~ 6 cycles) (Figure 57A). However, they displayed different behaviors: in the case of

A

$$\delta u/\delta t = 1/t_u \cdot u(a-u)(1-u) - v + I + J\nabla^2 u$$
$$\delta v/\delta t = 1/t_v \cdot (u - g.v)$$

u : concentration of the activator U
v : concentration of the inhibitor V
t_u : time scale of expression changes in U
a : excitability threshold
I : external stimulus
J: coupling strength between oscillators
t_v : time scale of expression changes in V
g: degradation rate of the repressor

B

$\delta v/\delta t=0$
$\delta u/\delta t=0$

Excitable

Oscillatory

C

Activator level

Period

Mean intensity

- Stimulus variable +
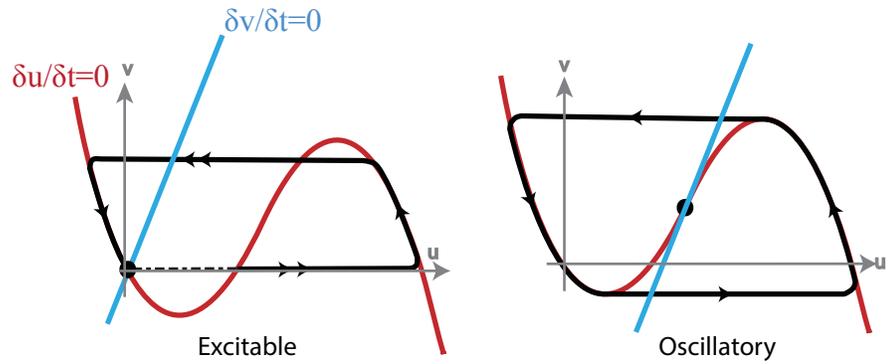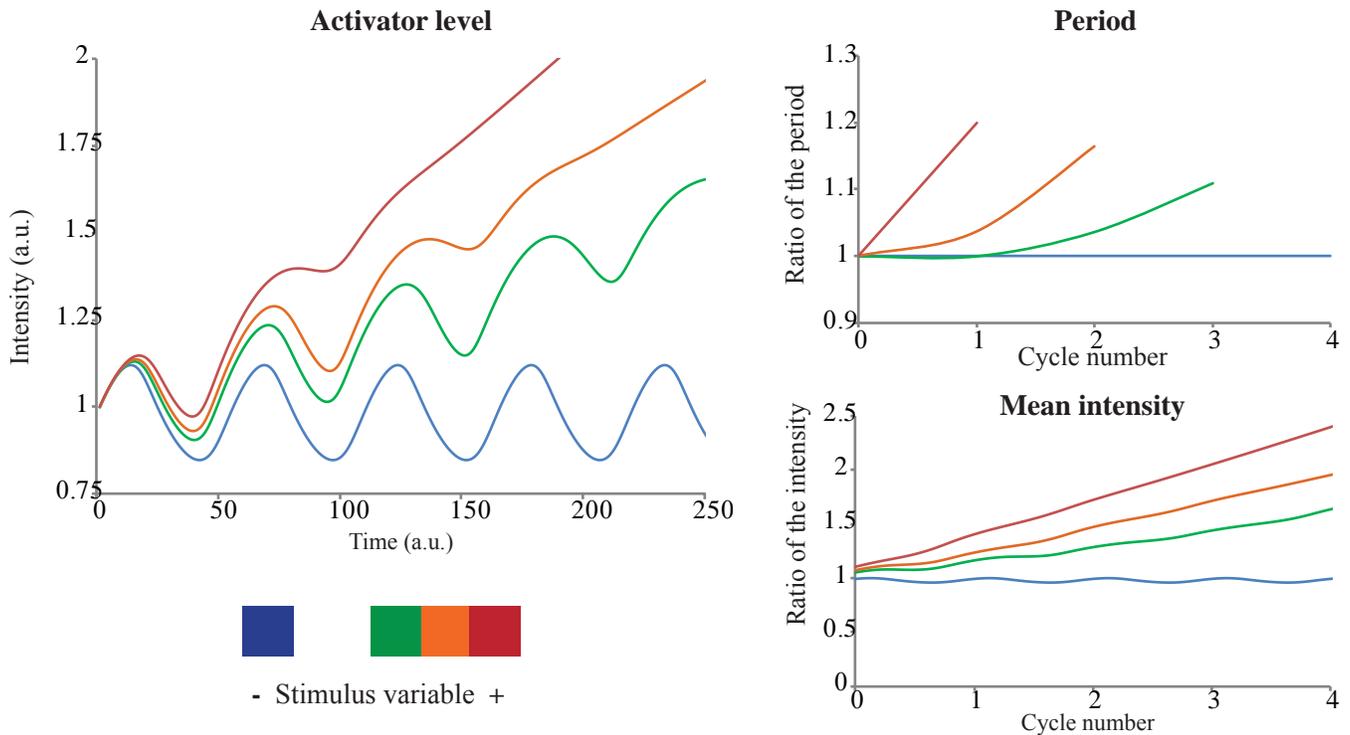
Figure 56 - Modeling the effect of Fgf/ERK inhibition

A. FitzHugh-Nagumo model: differential equations describing the evolution of activator-inhibitor couple.

B. (*Left*) Phase portrait of the activator-inhibitor couple in the excitable state. The red line represents the nullcline for the activator, and the blue line represents the nullcline for the repressor. Their intersection marks a fixed point (black dot) that is stable in this regime, but the system can undergo burst (trajectory ►►). (*Right)* Phase portrait of the activator-inhibitor couple in the oscillatory state. The fixed point is unstable and the system continuously oscillate.

C. Simulations using the FitzHugh-Nagumo model for different levels of stimulus (I). (*Left*) Activator level over time. (*Top right*) Ratio of the period to the initial period for each oscillation cycle. (*Bottom right*) Ratio of the mean intensity (intensity averaged over a period) to the initial intensity for each oscillation cycle.

155

Dkk1, there was no increase in intensity or period of the oscillations, while treatment with ICRT14 and IWR-1 led to a centrifugal arrest of oscillations with increase of intensity as previously observed for the MEK inhibitor (but the reporter persisted for a longer time after the arrest of oscillations). These differences could arise from a variation in the inhibition strength or from different responses of the pathway depending on the component targeted. Thus, we must remain circumspect about these findings, and future work should address the inhibition of Wnt signaling.

We also examined the interaction between the Fgf and Wnt pathways. To probe for such effect, we used the micropattern setting and inhibited Fgf signaling with the MEK inhibitor in presence of various doses of the Wnt activator, CHIR. We observed that the dose of Wnt signaling changed the number of cycles before the oscillations arrest (2 cycles for a low dose, 3 cycles for a normal dose, and 4 cycles for a high dose) (Figure 57B). This shows an interaction between the Fgf and Wnt pathways as previously reported *in vivo* by Aulehla and colleagues (Aulehla et al., 2008), and further suggests that Wnt signaling modulates the point of oscillations arrest after Fgf/ERK inhibition. We must note that the inhibitor CHIR could also act on other signaling networks than the canonical Wnt pathway, e.g. GSK3β is known to interact with NICD and modulate its activity (Foltz et al., 2002).
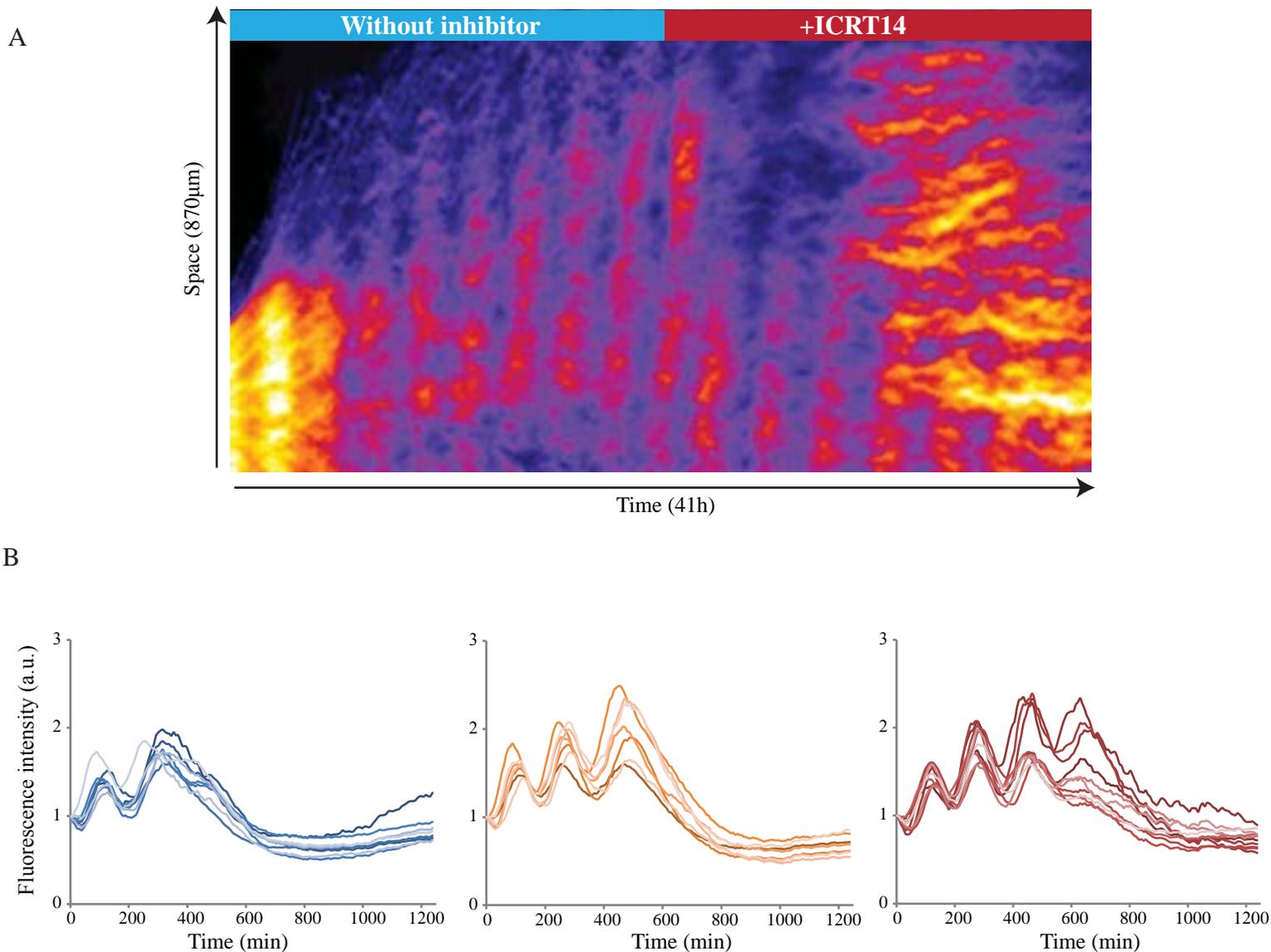
Figure 57 - Effect of Wnt signaling

A. Kymograph showing the fluorescence intensity for one explant first cultured in normal conditions, and then in presence of ICRT14 (10μM - 3/3).

B. Graphs showing the fluorescence intensity of the *LuVeLu* reporter for explant cells on micropatterns. Cells were treated with the Fgf/ERK inhibitor PD03 (2μM) in the presence of different doses of Chir: 1μM (*left*), 3μM (*middle*), and 6μM (*right*). Each line represents one micropattern.

Discussion

Mechanism of oscillations

Ex vivo model

Here we present an explant model to study the mechanisms underlying the oscillations and their arrest. We found that stalling the explant into an oscillatory state mainly necessitates the combination of three actions: activation of the Fgf pathway, inhibition of the BMP pathway, and activation of the Wnt pathway. In absence of Fgf and Wnt signaling, centripetal differentiation was observed. Surprisingly, we found that high levels of Fgf/Wnt alone were not permissive for oscillations, and that BMP inhibition was required to observe the cycling of the *LuVeLu* reporter. As we observed an upregulation of *Cyp26a1* without LDN, we supposed that the explant is in a more naïve state similar to the tailbud. Several findings from the literature suggest that BMP signaling promotes a tailbud state: i) Beck and colleagues showed that the pathway is active in the *Xenopus* tailbud as evidenced by Smad1/5/8 staining and injection of BMP4 can cause ectopic tail with somites (Beck et al., 2001); ii) Row and Kimelman observed a similar pattern of Smad1/5/8 in zebrafish and showed that overactivation of the pathway led to an expansion of the tailbud and the *T*-positive region, indicative of an accumulation of progenitors (Row and Kimelman, 2009); iii) O'Neill and Thorpe similarly showed that cells of the *chordin/spadetail* zebrafish mutant that accumulate in the tailbud could migrate and differentiate upon dorsomorphin treatment (a molecule similar to the LDN we used) (O'Neill and Thorpe, 2013); iv) work from Sharma and colleagues indicates that BMP4 maintains the mouse PSM in an undifferentiated state (Sharma, 2015). We also found that inhibiting the retinoic acid pathway could induce oscillations of smaller amplitude in presence of Fgf4/CHIR. This is consistent with recent findings by Cunningham and colleagues, who showed that *Raldh2* mutant mice displayed a reduction of *Sox2* in the caudal lateral epiblast (where axial stem cells reside) and an increase of *Tbx6*. This observation would indicate that in the absence of retinoic acid, tailbud cells acquire a more mature state corresponding to the posterior PSM (Cunningham et al., 2015).

Excitability of the Lunatic fringe oscillations

By analyzing the different levels of organization of the segmentation clock, we suggest that excitability underlies the oscillations of *Lunatic fringe* in our system. This mainly stems from two observations: i) a density-dependence and Notch-dependence for oscillations suggesting the existence of a signaling threshold; ii) the ability to switch from an aperiodic state to an oscillatory

state upon latrunculin A treatment, suggesting a transition from an excitable state to an oscillatory regime. This framework enables us to capture the different dynamics we observed, such as the quiescent state upon Notch inhibition, the wave annihilation, and the burst dynamics in dissociated cells.

Excitable systems classically present a refractory period, during which they cannot be excited. While wave annihilation is indicative of such state, it does not firmly prove its existence. This would require triggering a signal (e.g. Notch) right after a pulse and observing the absence of response from the system. Interestingly, Bone and colleagues showed that Notch1 and Dll1 are oscillating in the mouse PSM (Bone et al., 2014). This could provide a molecular basis to the refractory period, as after the activation of Notch signaling, Notch1 is endocytosed, making the cell unable to respond to a subsequent stimulation. Besides, excitable systems are generally characterized by a rapid activation (usually non-linear) and a slow inhibition. In the context of Notch signaling, the activation is likely rapid as it only requires post-translational modifications (cleavage of Notch1, nuclear translocation), while the repression likely involves the genetic expression of negative regulators such as Lfng or Nrarp. However, in certain conditions (latrunculin A treatment or explant of Tsiairis and Aulehla), *LuVeLu* oscillations are observed without Notch signaling. This indicates that the molecular control of *Lunatic fringe* oscillations is more complex than previously thought and that the *LuVeLu* reporter is not only a readout of the Notch oscillator. It rather points to the sempiternal question of the clock pacemaker in mouse somitogenesis. Those Notch-independent oscillations could be driven by oscillations of Hes7 in a cell-autonomous manner. However, this leaves open the question of the pacemaker for the Wnt oscillator and the coordination between the Hes7/Fgf/Notch module and the Wnt module. Alternatively, a common pacemaker mechanism could control both oscillators. Besides its fundamental aspect, identifying the pacemaker has practical consequences: without knowledge of the pacemaker mechanism, it is difficult to formally prove the excitability of *Lfng* oscillations. Indeed, a clear demonstration of excitability would require generating single pulses and probing the refractory period with controlled stimulations from the pacemaker. Even if we interpret the pulses of *Lfng* in explants dissociated cells as transient excitation of the system, we cannot exclude that this expression pattern is caused by other mechanisms (e.g. cell cycle, variation in gene expression) and not by spike triggered after superthreshold stimulation. In other words, while we observed a transition from a non-oscillatory state to an oscillatory state, this could be described by other kinds of bifurcation.

It is important to note that this framework of excitability is a more general model that includes previous models of oscillators in the PSM. The oscillatory regime is only a situation of excitability, where the system is constantly above its excitability threshold. However, we would argue that this

framework better encompasses different observations made on the segmentation clock (Figure 59A). Notably, it could explain the phenotypes of Notch inhibition in various contexts, especially how this pathway could be involved in both the emergence and synchronization of oscillations. In zebrafish, it was proposed that Notch mutants display a salt-and-pepper pattern of cyclic genes, indicating a desynchronization of individual oscillators. However, a close examination to the Her1 reporter in those mutants reveal a behavior closer to the burst we observed in dissociated cells than uncoupled oscillators (Delaune et al., 2012). Accordingly, it is hard to reconcile this observation with the regular, precise oscillations observed in single-cells by Webb and colleagues (Webb et al., 2016). That is, Notch signaling is classically seen as a coupler counteracting the noise of individual oscillators, we should then expect that individual cells display the same level of noise than in Notch mutants, and similar irregularities in their oscillations. We thus propose that the reduction of Notch signaling in zebrafish embryos brings the cells below the excitability threshold, which can be occasionally crossed because of noise or other signals. In other words, what was considered as noisy oscillations could correspond to the pulsatile behavior of an excitable system close to criticality. In mouse, there is also a discrepancy between the different phenotypes observed after a blockade of the Notch pathway: *RBPJ-κ-/-* and *Dll1-/-* mutants or γ-secretase treated embryos completely lose the oscillations of *Lfng* (Ferjentsik et al., 2009), while dampened oscillations are observed in our explant system and stable, desynchronized oscillations in the *ex vivo* culture of Tsiairis and Aulehla (Tsiairis and Aulehla, 2016). We propose that this is mainly due to the culture conditions, especially the mechanical cues experienced by PSM cells. Indeed, we showed that latrunculin A rescued the loss of oscillations in dissociated cells and in DAPT-treated explants. We could thus simply explain the phenotypes observed as follows: in the Notch mutant embryos, the PSM cells become quiescent and lose the oscillations of *Lfng*, while in the system of Tsiairis and Aulehla, mechanical signals bring the cells to the oscillatory regime so that they remain above the excitability threshold in absence of Notch. This could further explain the difference in zebrafish between the dissociated cells of Webb and colleagues and the Notch mutants, as the former are in the oscillatory state and the later in an excitable state. Interestingly, the authors noticed a correlation between the cellular morphology and the oscillations of single cells: "*other substrates we tested caused cells to flatten on the glass and the loss of oscillating fluorescent signal over the course of the recording*"(Webb et al., 2014). As increasing the adhesion surface leads to an activation of the Yap pathway (Dupont et al., 2011), those cells would become quiescent in our model. More generally, the modulation of the segmentation clock by mechanical conditions prompts us to be careful when using *ex vivo* approaches. Indeed, we must wonder whether *ex vivo* systems are in physiological situations, where studied factors do have a regulatory role *in vivo* and not only in the dish. For instance, we could imagine that the mechanical conditions in the embryo are always permissive for oscillations, and thus our system would reveal a regulation that does not exist *in vivo*. Last, we could provide another interpretation to the findings of

Webb and colleagues. They observed the succession of trains of oscillations and quiescence, and interpreted it as cells being close to a Hopf bifurcation (Webb et al., 2016). We would propose that this bifurcation corresponds to the transition between the quiescent and oscillatory states of an excitable system, as a variable slowly fluctuates and occasionally crosses the excitability threshold.

Excitability and synchronization

While such excitable framework enables us to describe various observations, what could it predict concerning the synchronization of oscillators? The central property of an excitable system is the existence of a threshold, above which oscillations are produced. This could have important consequences for the initiation of the segmentation clock during development. Indeed, excitability allows for a sudden jump from the quiescent to the oscillatory state, and therefore can directly synchronize individual oscillators. Such synchronization is especially effective when intercellular signals (e.g. Notch signaling) regulate the excitability of cells as the emergence of individual oscillations is concomitant with the apparition of collective oscillations. This behavior is similar to the "dynamic quorum sensing" described in glycolytic oscillations in yeast or cAMP oscillations in *D.discoideum* (De Monte et al., 2007, Mehta and Gregor, 2010, Sgro et al., 2015). We showed that Notch signaling could mediate this sudden transition from quiescent to oscillatory, as evidenced by the experiment of DAPT washout or by the quasi-immediate resynchronization after dissociation/reaggreagation. In the case of a Kuramoto transition, the initiation of oscillations would require that individual oscillators locally synchronize before displaying collective oscillations or that there is a tight synchrony in the acquisition of the oscillatory state (Kamino et al., 2011).

An excitable framework could also account for the various observations made in zebrafish about oscillator synchronization. Notably, Lewis and colleagues used an elegant system of heat shock in zebrafish to generate pulses of Delta-c (Soza-Ried et al., 2014). While the *bea* mutant (mutant for *Delta-c*) does not display a homogenous pattern of *Her1* levels, they showed that only two pulses of Delta-c were necessary to obtain the classical (synchronized) pattern of *Her1* waves. This observation is very similar to our experiment of DAPT washout. We should note that Riedel-Kruse and colleagues showed that a similar treatment in zebrafish requires ~10 oscillations before the recovery of normal somitogenesis and interpreted it as the progressive resynchronization of oscillators as in a Kuramoto transition (Riedel-Kruse et al., 2007). However, there are two limitations to this hypothesis: i) the authors used a qualitative phenotype (somite boundaries) that is difficult to quantify and to relate to the actual oscillations; ii) they did not examine the pattern of cyclic genes during this recovery phase. Such long delay before the restoration of collective oscillations is also inconsistent with the observations of Soza-Ried and colleagues. Besides the question of the timing of synchronization, an excitable model could bring new properties related to the effect of noise. While

noise is assumedly detrimental to the behavior of a self-sustained oscillator, excitable systems show complex responses to noise (Lindner et al., 2004). Notably they can display coherence resonance, where noise can induce regular oscillations in an excitable system, or stochastic resonance, where subthreshold signals are amplified because of the noise.

Excitability and waves

Having considered how an excitable framework could explain different features of single-cell oscillations and synchronization, we moved to the formation of traveling waves. We proposed that our explant system creates target patterns without detecting a specific pacemaker population or a frequency gradient. It is yet unclear what determines the position of the oscillations center. We frequently observed these foci in region of high cell density, but not necessarily at the center of the explant. It is possible that their position is controlled by the initial spreading of the explants, by the boundaries or by local heterogeneities. While we propose that excitability underlies the *LuVeLu* oscillator in our system, it is still uncertain whether the explants can be considered as an excitable medium. Indeed, there is no strict propagation of an excitation, since activation of the Notch pathway in one cell should not transmit any signal to its neighbor (in a very speculative manner, we could imagine that the induction of *Notch1* by Notch signaling enables a propagation with delay by relieving the cis-inhibition of Dll1 in its neighbors). Furthermore, removing the center of oscillations or cutting the explants do not block the formation or propagation of waves, suggesting that the system is in the oscillatory (self-sustained) regime at high cell density and in presence of Notch signaling. Those experiments are more consistent with a kinematic wave than a trigger wave. Nevertheless, we cannot exclude that the heterogeneities in our explants cause the creation of target patterns while being in the excitable regime. Indeed theoretical studies indicate that heterogeneity can produce stable target patterns both in excitable and oscillatory medium (Stich, 2003, Stich and Mikhailov, 2006, Stich et al., 2009). We should note that we did not observe spirals, a common wave pattern of excitable media (but also possible in oscillatory medium), except in very rare occasions, when we removed part of the explant. Alternatively, other mechanisms can generate self-organized target patterns such as birhythmicity in the oscillatory regime or three-component reaction-diffusion in the excitable regime (Stich, 2003). In the latter, adding a third diffusing substance in the activator-repressor couple can stabilize the target pattern providing that it diffuses faster than the activator (Stich et al., 2009). Three-components reaction-diffusion can generate new properties for patterning (Meinhardt, 2004) and could be of interest in the context of the PSM where different oscillators interact each other with distinct "diffusion" (e.g. pERK vs. *Hes7*/NICD (Niwa et al., 2011) or *Axin2* vs. *Lfng* (Lauschke, 2013)). The generation of self-organized target patterns is especially interesting

in the light of the findings of Tsiairis and Aulehla, where mixing cells of different PSM create target patterns with a specific wavelength, indicative of a reaction-diffusion mechanism.

Such self-organization would explain why we observe traveling waves without measurable gradient of frequency. It is a classical feature of excitable media and dissipative self-oscillatory media, while conservative self-oscillatory media tend to globally synchronize (except if initial conditions are periodic) (Shiogai and Kuramoto, 2003, Carpio, 2005). This is different from previous models, where such frequency-gradient is necessary for the emergence of stable traveling waves (Oates et al., 2012). Nevertheless, this case could be specific to our artificial system, as a frequency-gradient is sufficient to generate traveling waves and could control their formation *in vivo.*

Role of the Yap pathway

We showed that treatment with latrunculin A, an inhibitor of actin polymerization, appears to control the transition from an excitable to an oscillatory state, as oscillations are readily observed in single cells and in DAPT-treated explants. This is also associated with important changes in gene expression indicative of a mechanotransduction. It is likely due to an inhibition of the Yap pathway. However, we could not exclude that other pathways are regulated by mechanical cues. For instance, the Wnt pathway has been shown to be activated by mechanical stresses during development (Fernandez-Sanchez et al., 2015); notably, Brunet and colleagues elegantly showed that it was induced at the marginal zone of zebrafish embryo and promoted the expression of *Brachyury* during gastrulation (Brunet et al., 2013). We observed a strong decrease of Wnt signaling upon dissociation of the cells that is rescued by treatment with latrunculin A. However, treatment with higher dose of the Wnt activator did not lead to detectable oscillations in dissociated cells and no major difference in the mechanoinducible phosphorylation of β-catenin Y654 was observed on glass compared to fibronectin-coated substrate (data not shown).

How Yap signaling regulates this oscillatory transition remains to be studied. The Yap pathway could regulate the excitability by directly controlling the expression of PSM genes, notably of factors such as *Msgn1* and *Tbx6*. Indeed, those transcription factors are necessary for the oscillations of several cyclic genes in mice embryos and are activated by treatment with latrunculin A in dissociated cells. Alternatively, the Yap pathway could interact with other signaling pathways. Several groups have put in evidence an interaction between the Yap and Wnt pathways, as Yap is part of the β-catenin degradation complex (Azzolin et al., 2014) and could activate different Wnt targets such as *Dkk1* (Park et al., 2015). However, we did not observe a correlation between the nuclear localization of Yap and an increase of Wnt signaling contrary to previous reports (Varelas et al., 2010, Azzolin et al., 2014).

Which factor would regulate the Yap pathway in the embryo? Previous work showed that it could be activated by a variety of input signals (Dupont, 2015). Among them, the Hippo pathway has been well described in Drosophila, where it negatively regulates Yap through Lats1/2 kinases and controls the organ size (Zhao et al., 2010). Wnt and G-protein coupled receptors signaling can also modulate Yap activity (Dupont, 2015). Several studies have demonstrated that Yap acts as a mechanotransducer and is regulated by mechanical cues, such as the matrix stiffness or cell spreading. It has been proposed that fibronectin adhesion and the integrin signaling ("outside-in") could regulate the Yap pathway. Accordingly, integrin signaling can activate Yap through a FAK/Src/PI3K cascade (Kim and Gumbiner, 2015, Elbediwy et al., 2016) and ILK (integrin-linked kinase) can activate Yap activity by inhibiting of Hippo kinases (Serrano et al., 2013). However, culturing cells on a poly-lysine substrate (where integrin are not engaged) can also activate Yap suggesting that mechanical cues could be transduced by different mechanisms or that several mechanotransduction pathway converge to a common signaling node (Dupont, 2015). As we observed oscillations in the presence of fibronectin with latrunculin A, the involvement of integrin signaling seems unlikely. Even if we cannot exclude that we blocked the pathway downstream of the integrins, this seems unlikely as integrin signaling induces Wnt signaling in the chicken PSM (as discussed below), while dissociated cells without latrunculin A had lower levels of the Wnt targets *Msgn1* and *Sp5*. Furthermore, preliminary experiment where we cultured dissociated explant cells in presence of RGDS, a peptide blocking the interaction between fibronectin and integrin, did not lead to oscillations (up to 1mM - data not shown).

The Yap pathway is important for the early development of Vertebrates. In mice, homozygous mutants for *Yap1* display strong defects starting at E8.5 and die because of vascular defects (Morin-Kensicki et al., 2006). These embryos still form anterior somites, but show a shortened antero-posterior axis apparently due to a defect in convergent-extension. Similarly, double mutants for *Tead1*/2 die around E9.5 and display a lateral displacement of the paraxial mesoderm consistent with the widened morphology of *Yap1* mutants (Sawada et al., 2008). Mutants for the gene *Taz* (homologous of Yap) are viable and only display minor skeletal defects (shorter stature likely due to defects in ossification) (Hossain et al., 2007). Interestingly, Yap signaling is also involved in the axis elongation of *Xenopus* and zebrafish, as both inhibition and overactivation of the pathway cause a shortened axis (Gee et al., 2011). In preliminary studies, we electroporated chicken embryos with a constitutively active form of Yap (Yap-5SA), and observed a shortened axis as cells tend to stay in the primitive streak. Future studies will need to bypass the effect of Yap signaling on gastrulation to address its role in segmentation. We must note that two other studies have identified a role of mechanotransduction on somitogenesis, but did not seem to involve Yap signaling. In chicken, Rallis and colleagues showed that β1-integrin signaling induces the Wnt pathway and regulates the

expression of Notch targets (Rallis et al., 2010). While this phenotype appears to be essentially localized to the anterior PSM, the authors noticed that *β1-integrin* is expressed in the primitive streak at the level of the chordo-neural hinge, and that its knockdown reduces the expression of *Fgf8* and *T*. Interestingly, this would suggest that integrin signaling and/or adhesion is required for the maintenance of axial stem cells. In another study, Giros and colleagues generated mice mutants lacking the RGD motif of fibronectin necessary for its interaction with integrins. The embryos died at ~E10 and showed defects in axis elongation, decreased *Fgf8* expression and perturbed expression of *Lfng* (left-right asymmetric pattern and irregular expression of *Lfng*) (Girós et al., 2011). It is not clear how those mechanisms relate to the effect we observed with latrunculin A. Therefore, to assess the functional relevance of this finding, we examined the nucleo-cytoplasmic localization of Yap at stage E9.5. Yap was largely cytoplasmic along the PSM and in somites (Figure 58). On some transversal sections, we observed Yap both in the nuclei and cytoplasm of cells in the tailbud mesenchyme (mostly ventral). It would be interesting to examine this further at stages where the primitive streak is readily observable. Indeed, we could hypothesize that ingression of cells in the primitive streak changes the mechanical environment of PSM cells and leads to the inactivation of the Yap pathway. As we showed that such inhibition is associated with an oscillatory state, the Yap pathway could possibly couple the onset of oscillations with gastrulation. Given the complex regulation of this signaling, other pathways present in the primitive streak/tailbud could also control its activity, such as BMP, Wnt (Hansen et al., 2015), integrin signaling (Rallis et al., 2010), glycolysis (Ozbudak et al., 2010, Enzo et al., 2015)(M.Oginuma, personal communication) or the mevalonate pathway (Olivera-Martinez et al., 2014, Sorrentino et al., 2014).

Role of Fgf signaling and models of PSM determination

Different models of determination

We showed that inhibiting Fgf signaling led to a determination of the explants and recapitulated the *in vivo* situation, where both the oscillations period and the overall intensity of cyclic gene increase (Shih et al., 2015). Importantly, we showed that there was not a binary but rather a gradual dose-dependent effect; this contradicts a simple version of the clock-and-wavefront model, where the wavefront acts as a single threshold independently of the segmentation clock. It rather points to a dynamic control of the determination front by Fgf signaling. This result also indicates a direct regulation of the oscillatory dynamics by this pathway, consistently with the interdependence between the clock and the wavefront postulated by Aulehla and colleagues (Lauschke et al., 2013).

A
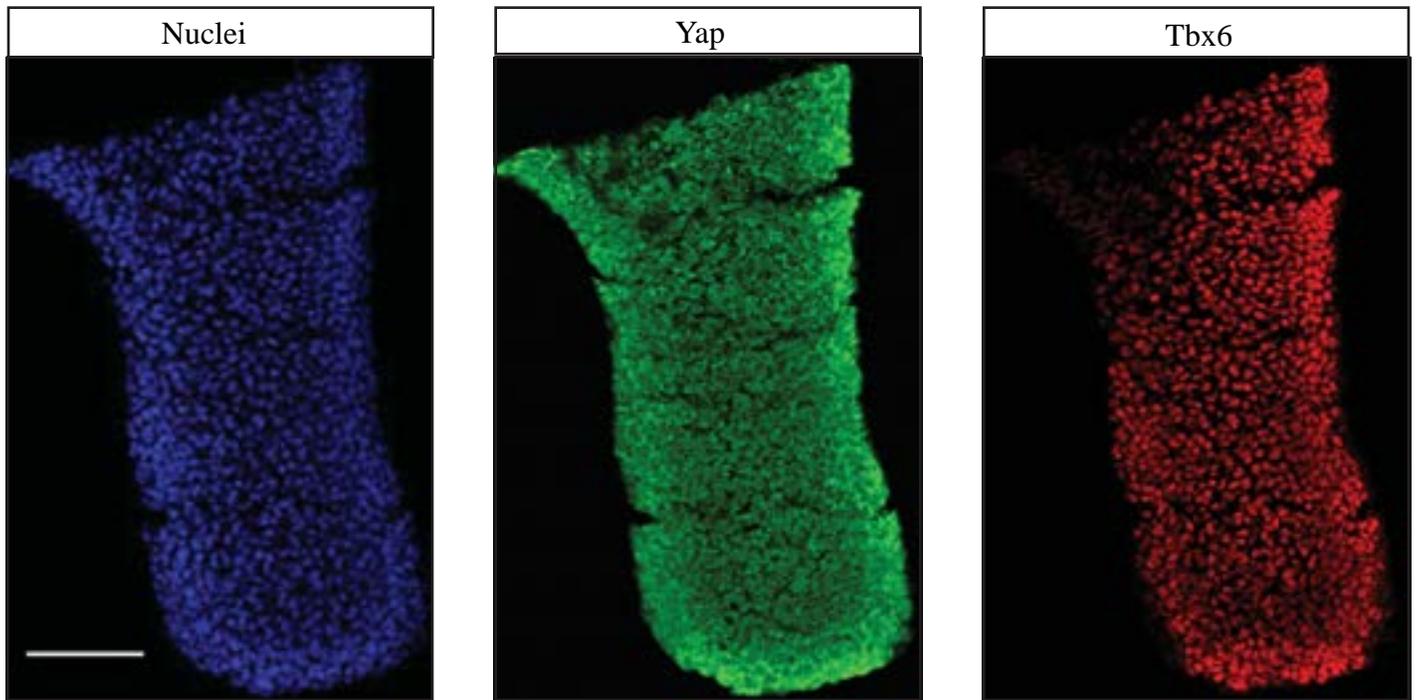
Figure 58 - Yap signaling *in vivo*

A. (*Left*) Nuclei staining of a longitudinal section of E9.5 mouse tail. (*Middle*) Immunostaining for Yap. (*Right*) Immunostaining for Tbx6. (Scale bar: 100μm)

B
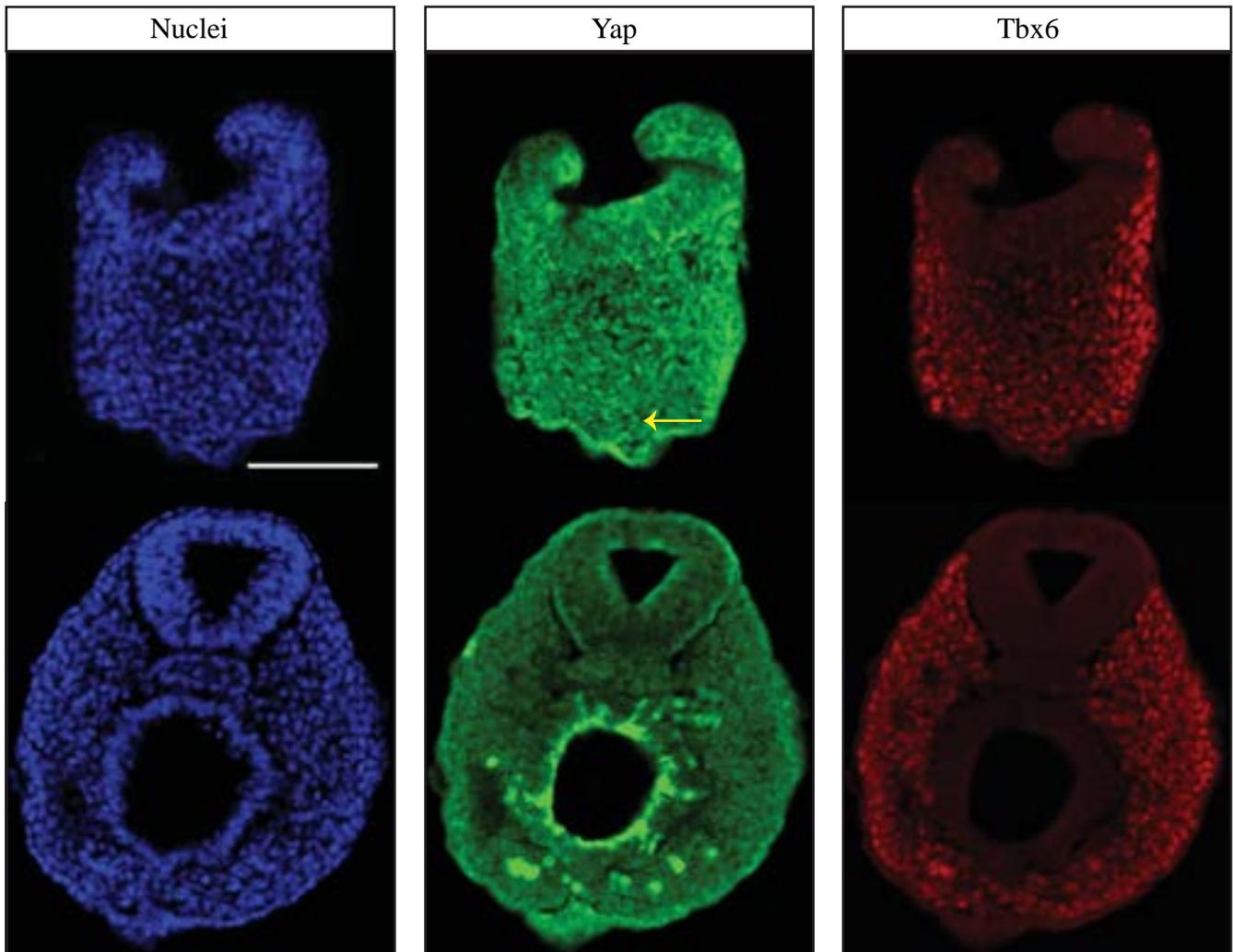
Figure 58 - Yap signaling *in vivo (continued)*

B. (*Left*) Nuclei staining of transversal sections of E9.5 mouse tail. (*Middle*) Immunostaining for Yap. (*Right*) Immunostaining for Tbx6. (Scale bar: 100μm). Note the localization of Yap in both the nucleus and cytoplasm of posterior cells (arrow)

Which model would thus better describe the observations we made? We could imagine three mechanisms (Figure 59B):

i)   A timer version of the clock-and-wavefront (hourglass): this model would conserve the essence of the initial clock-and-wavefront model – a periodic inductive signal (the clock) and a moving front of competency (the determination front) – with an additional dynamic regulation of the wavefront. This would take into account that Fgf signaling does not act as a single threshold. The regression rate of this determination front would rather depend on the strength of Fgf inhibition and be similar to a developmental timer (in other words, the timer runs slower at high dose of Fgf signaling). This could occur by slow changes (activation/degradation) of a factor dose. Such timer mechanism has been proposed to account for the determination of oligodendrocyte precursors cells (OPC) in rodents (Raff, 2007): when placed in culture, OPC stopped dividing and differentiated at about the same time (~ 8 days). It was shown that this timing correlated with the slow accumulation of several proteins (p27, p18, p57), while another inducer signal (thyroid hormone) triggered the differentiation. Similarly, the activation of the midblastula transition, a classical example of developmental timer where the maternal transcriptome is degraded and the zygotic genome becomes activated, appears to be regulated by the progressive dilution of maternal factors and the amount of DNA (Lee et al., 2013).

ii)   A ratchet model: this model would be based on a determination signal that is built up at each oscillator cycle; when cells reach a threshold, they become determined. A version of this model was notably proposed by Schnell and Maini in the context of somitogenesis ("clock-and-induction") (Schnell and Maini, 2000). In our system, at each oscillator cycle, the segmentation clock would produce a factor that accumulates over time, and Fgf signaling could regulate its accumulation rate. While the previous hypothesis supposes the coexistence of a clock and a determination timer, a ratchet model would only need an oscillator that provides its own timing. Ratchet models have been previously proposed to account for the progressive cell differentiation in other contexts (Figure 59B). Levine and Elowitz showed that such strategy could explain the deferred differentiation of *B.subtilis* (Levine et al., 2012). Upon nutrient limitation, those bacteria proliferate before differentiating into spores. They showed that this behavior was based on a pulsed positive feedback: the master regulator Spo0A induces the expression of kinases that in turn promotes Spo0A activity. After nutrient deprivation, *B.subtilis* experience pulses of phosphorylated Spo0A until it reaches a plateau that triggers sporulation. Providing that the positive feedback occurs in a polyphasic manner (that is, the two activation steps successively occur at different phases of the cycle), Levine and Elowitz showed that this mechanism enables timing, which is more robust to noise and cell divisions than a dilution mechanism or a mechanism based on an instantaneous pulsed positive feedback (Levine and Elowitz,
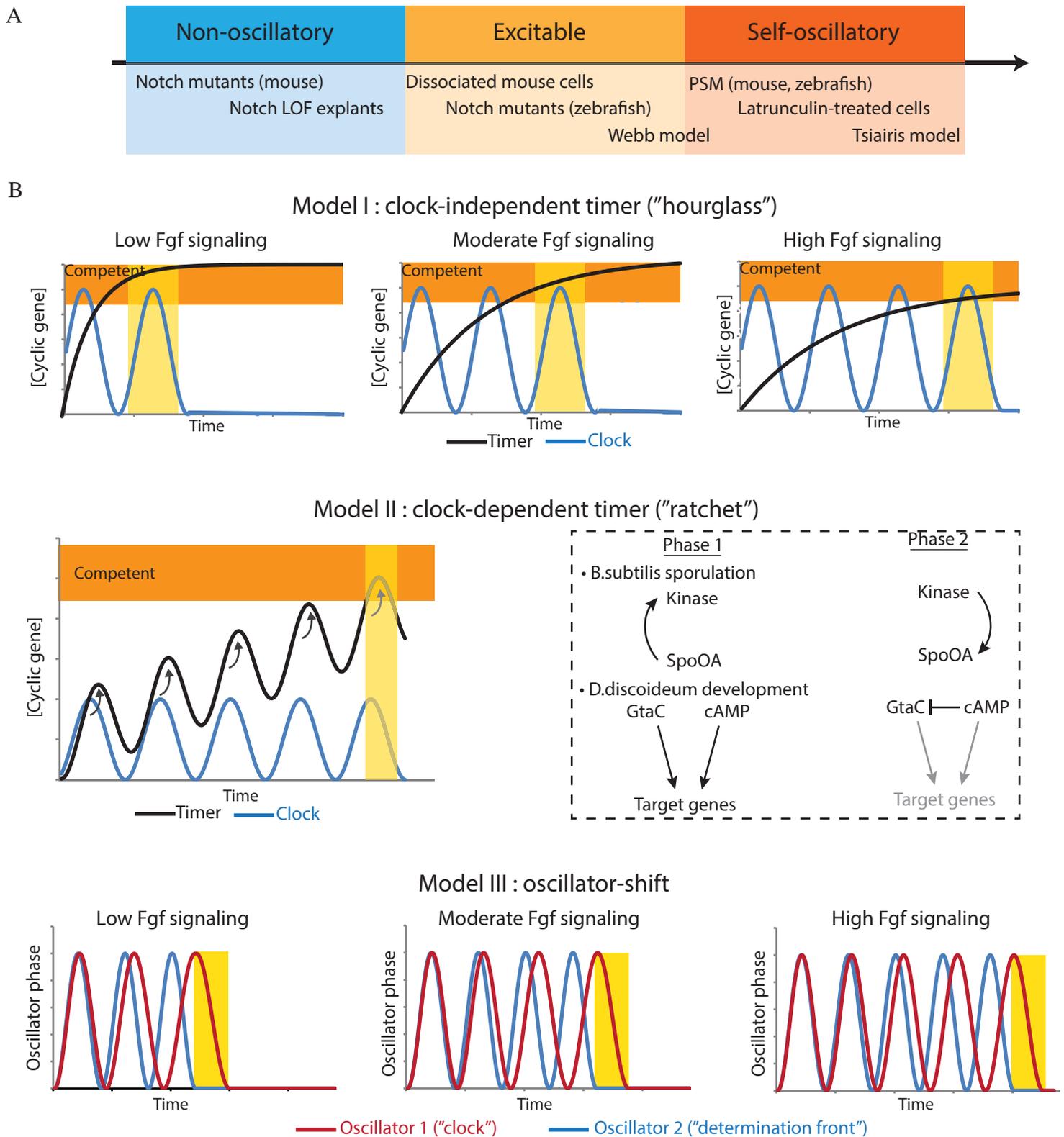
Figure 59 - Roles of Fgf and Notch signaling in the PSM

A. Interpretation of different observations with the framework of excitability (LOF: loss-of-function)

B. Models of PSM determination by Fgf signaling (see text for details) - the yellow region marks the determination
Excerpt:polyphasic oscillators with timing property in *B.subtilis* and *D.discoideum*

2014). This behavior also predicts the succession of pulses with higher intensity as we observed in our system. A similar ratchet mechanism has been proposed to regulate *Dictyostelium discoideum* morphogenesis after starvation (Cai et al., 2014). Here, oscillations of cAMP control the expression of developmental genes through the coordinated activation by cAMP signaling and by the transcription factor GtaC; after a delay, the transcription is no longer active as cAMP signaling induces the nuclear exit of GtaC (type 1 incoherent feedforward loop). Such polyphasic regulation enables the accumulation of proteins that can be modulated by the strength of cAMP signaling (e.g. cAMP concentration) or by the number of cycles at a finite concentration of cAMP.

iii)   A phase-shift model: according to this model, determination occurs when two oscillators shift between each other. This idea was put forward by Kageyama and colleagues as the shift between the pERK and Notch oscillators was thought to define the region where *Mesp2* is activated (Niwa et al., 2011); it was further developed by Aulehla and colleagues, who identified a shift between *Axin2* and *LuVeLu* oscillations in their explant system, predictive of the segment size. In our model, we observed that the strength of Fgf inhibition correlates with the rate of increase in period of the *LuVeLu* reporter. Providing that another oscillator (e.g. Fgf or Wnt) cycles at a constant period, this would create a phase-shift and the time required to achieve a particular phase-shift could be modulated by the strength of Fgf inhibition. It is reminiscent of the situation of "rippled wavefront" described by Kageyama and colleagues (Niwa et al., 2011). Therefore, the timing of determination would rely on the reorganization of the gene regulatory network. Such mechanism has been recently described by Balaskas and colleagues, who suggested that it underlies the patterning of the mouse neural tube, as Shh signaling rearranges several feedback loops during development so that the final output depends on the duration and overall level of morphogen (Balaskas et al., 2012). This was later interpreted as a consequence of the criticality of the system (*i.e.* its proximity to a bifurcation), in the sense that when the undetermined state becomes unstable, the system is still attracted to it (trajectories point to this "ghost attractor") slowing the transition to the new determined state (Tufcea and François, 2015).

Testing the models

To summarize, there are three main hypotheses: a clock-independent timer (hourglass), a clock-dependent timer (ratchet), and a phase-shift process. In all cases, Fgf signaling essentially acts on the time to reach a threshold or phase-shift. What would be the role of Wnt signaling? In the mechanisms based on thresholds, we could suppose that Wnt signaling positions this threshold. This would be consistent with the anterior shift of Mesp2 in the non-degradable β-catenin mutant and its partial rescue by loss of Fgf signaling (Aulehla et al., 2008). In the same line, we observed that

modulating Wnt signaling can change the number of cycles before the arrest of oscillations induced by inhibition of the Fgf/ERK pathway. In the oscillator shift model, Wnt could act in an opposite manner of Fgf inhibition and slows down the shift.

The mutant overexpressing the Notch intracellular domain (NICD) can distinguish between the first two models, supposing that the Notch oscillator acts as the determination ratchet. Feller and colleagues reported that *Mesp2* was expressed as a single band in this mutant (Feller et al., 2008). This would contradict the hypothesis of a "clock-dependent timer" as the timer should immediately cross the determination threshold when the Notch pathway is constitutively activated and activated Notch. However, three points could still support the clock-dependent timer. First, the ratchet mechanism might be ramped up by oscillations of Notch signaling and not simply by its overactivation. Accordingly, gene expression can be regulated at the level of the signal dynamics (Levine et al., 2013, Sonnen and Aulehla, 2014), and as mentioned in the introduction, different targets are induced by oscillatory and steady stimulations of the NF-κB pathway. Similarly, activation of the Wnt pathway by a non-degradable β-catenin does not lead to a steady expression of its cyclic targets, but rather an increase in their amplitude (Dunty et al., 2008, Aulehla et al., 2008). Second, the response to NICD overexpression is complex and not linear: even if some Notch targets like *Hes5* are upregulated, other targets like *Lfng* are downregulated (Feller et al., 2008). The ratchet could thus be stalled rather than freely running. Such situation was observed for the development of social amoebae described above: frequent cAMP stimulations block the ratchet mechanism because of the incoherent feedforward loop and impede the accumulation of the differentiation signal (Cai et al., 2014). Third, even if Notch signaling is necessary for the induction of *Mesp2*, we cannot exclude that the ratchet mechanism is controlled by another signaling. As seen for the *Lfng* oscillations, the pacemaker mechanism could be independent of the Notch signaling. The ratchet could be based on Tbx6, as we showed that overexpression of Tbx6 in chicken leads to the instantaneous activation of *Mesp2*. Therefore, a clock-dependent timer is still a plausible scenario, but not a parsimonious one.

We now examine the phase-shift model. The mutant overexpressing NICD is also informative in this regard. The authors proposed that the dynamic expression of *Mesp2* was lost as they only observed one band of transcripts by *in situ* hybridization in the mutants in contrast to the mixture of one band or two bands in the wild-type. *Mesp2* would thus be expressed as a single band moving steadily toward the posterior end. While this remains to be firmly proven by live imaging, this observation would argue against a phase-shift model involving the Wnt oscillator. Indeed, Feller and colleagues showed that the Wnt oscillator was still operating in the NICD mutant, as evidenced by the cyclic expression of *Axin2*, while the Notch oscillator was frozen. This Notch "phase" appears permissive for the activation of *Mesp2*, since the gene is readily expressed. Considering this and the fact that the

Wnt oscillator is still cycling, we should then expect that the system is periodically in the specific phase-shift between Notch and Wnt that should lead to the periodic activation of Mesp2. The steady expression of *Mesp2* argues against such situation. Similar observations have been reported for the *Hes7* mutant, where *Axin2* oscillations are observed (Hirata et al., 2004) and *Mesp2* is steadily moving as evidenced by live imaging (Niwa et al., 2011). By contrast, a phase-shift between the Notch and Fgf oscillators is still a possible scenario, as oscillations for the Fgf targets were not observed in the NICD mutant (Feller et al., 2008), and seemingly not in the *Hes7* mutant (even if Dale and colleagues reported the persistence of some cyclic Fgf targets (Ferjentsik et al., 2009)). Niwa and colleagues proposed that such shift between NICD and phosphorylated ERK could control the activation of *Mesp2* in mouse. Preliminary results in our explant system would argue against such view, since pERK is rapidly dampened (after 3h of PD03 treatment) while several oscillations are still observed. Similarly in zebrafish, the pERK boundary is more posterior than the *Mesp2* stripe (Akiyama et al., 2014), and in chicken, we observed a gradient of pERK without clear boundary (data not shown and (Delfini et al., 2005)). However, several targets of the pathway display a boundary in the anterior PSM of mouse (e.g. *Snail1* (Dale et al., 2006, Ferjentsik et al., 2009)) or chicken (e.g. *Mkp3* – Geisha database), suggesting that the phase of downstream targets of pERK could still provide a positional information.

Several observations could argue in favor of a "maturation" timer in the PSM. First, careful observation of the microarrays series performed by M.Oginuma reveals that the anterior markers *Foxc2*, *Paraxis*, *Meox1* are gradually expressed, more posteriorly than *Mesp2* in mouse and chicken (Figure 60A) (Chal et al., 2015). Second, preliminary data in explants treated with the Fgf/ERK inhibitor indicate an induction of *Foxc2* as soon as 7h30 after the addition of the drug (Figure 60B). However, such progressive maturation is also compatible with a phase-shift model, as there must be a mechanism inducing the sliding between oscillators. Such changes could also be independent from the segmentation as we discussed in the introduction. While precise monitoring and perturbations of the system would be required to distinguish between these two hypotheses, we would favor a phase-shift model for the following reasons:

- As noted by others (Kondo, 2014, Stern and Piatkowska, 2015), any mechanism using a single threshold would likely not be robust to small variations in gene expression or in the cell antero-posterior position. It is thus unlikely that a mechanism could operate over such a long distance (PSM length: ~ 0.5-1mm), especially given the extensive cellular movements in the PSM.
- Several reports point to an interaction between the segmentation clock and the determination front, such as the explant system of Aulehla and colleagues or the saltatory regression of pERK in zebrafish. Such feedback from the clock on the determination front seems difficult to conceive for a
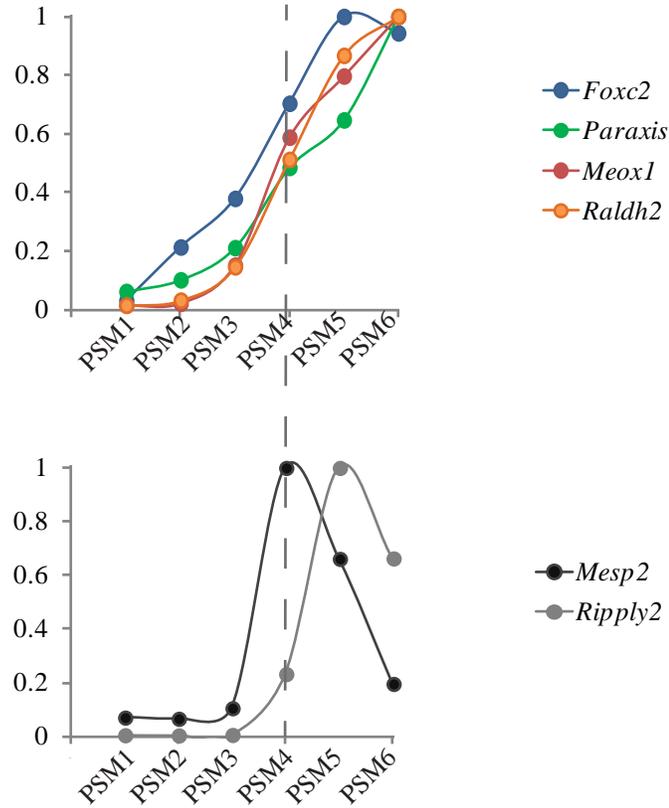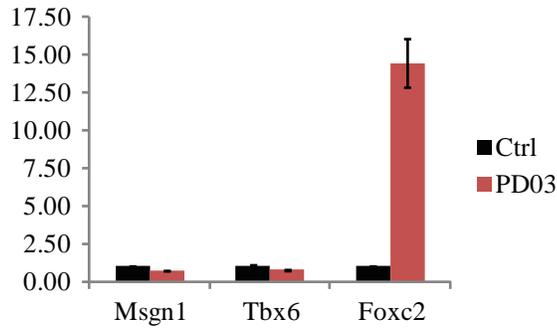
Figure 60 - Distribution of anterior PSM markers

A. (*Top*) Expression level (RMA) of anterior PSM markers in the microarrays series along the mouse PSM (PSM1: most posterior; PSM6: most anterior). (*Bottom*) Expression level (RMA) of the determination front (*Mesp2*) in the microarrays series along the mouse PSM.

B. Graph showing the fold-changes in explants for PSM markers after 7.5h of treatment with the Fgf/ERK inhibitor PD03 (1µM).

timer mechanism, while it would be a natural consequence of the interaction between oscillators for a phase-shift mechanism.

- Experiments from the Aulehla group indicate that blocking the tail growth result in smaller somites; interestingly, they found that removing the tailbud rescues this phenotype (personal communication). Such communication between the tailbud and the anterior PSM cannot be explained by a timer mechanism, while it could be readily explained by the existence of traveling waves of the Fgf and Notch oscillators.

- Tsiairis and Aulehla elegantly showed that the PSM determination display signs of self-organization using an *ex vivo* system. This feature is difficult to explain considering an intracellular timer (as it is a cell-autonomous mechanism), while it is natural for coupled oscillators in a spatial setting.

Summary

Together this argues for a phase-shift model (more generally a mechanism based on a Notch oscillator and a dynamic Fgf wavefront). However, it is not strictly incompatible with a clock-dependent timer and it remains to be determined whether the intensity, and not only the phase, of the oscillator encodes information. While gradual processes such as timer or signaling gradients are also involved in this process, we would argue that oscillators are more reliable to convey positional information by sharpening the cellular response. It is consistent with the findings that pulsatile or oscillatory circuits are more robust to noise in order to gate cellular decisions (Schultz et al., 2013, Levine and Elowitz, 2014, Pfeuty and Kaneko, 2014). Besides, if coupled, oscillations can synchronize the cellular responses and periodically gate the competence of a group of cells. Last, traveling waves seem a more effective way to transmit positional information over a long distance. Such idea has been proposed to explain the communication within the *Xenopus* egg, where trigger waves coordinate mitosis (Chang and Ferrell Jr, 2013). In the case of the PSM, this communication could additionally coordinate elongation and somitogenesis, and enable properties such as scaling. Such oscillator-shift mechanism would thus be consistent with the view of the segmentation clock as a "developmental ruler" and not as a process measuring time.

CHAPTER III

Role of the translation rate on the segmentation clock

In the previous chapter, we have seen that inhibiting Fgf signaling causes an increase of the overall fluorescent intensity of the *LuVeLu* reporter. This led us to suppose that the PSM determination could be associated with an increase in the global expression rate. Therefore we examined the role of the translation rate on the segmentation clock.

1. Effect of the translation inhibitor cycloheximide

We first used the translation inhibitor, cycloheximide, which interferes with the translation elongation. We cultured explants in presence of the inhibitor (80μM), and observed a rapid decrease in the *LuVeLu* reporter intensity (~ 66% reduction of the signal) (Figure 61A). Surprisingly, this treatment leads to a ~1.2 fold increase in the oscillations period. Increasing the dose of cycloheximide leads to a further increase in the period (up to ~1.4 fold for 480nM – Figure 61B).

Preliminary results suggest that treating explants with cycloheximide does not induce large changes in the Fgf, Wnt, or Notch signaling as evidenced by the expression of their downstream targets Figure 61C). However, the translation rate seems to interact with the effect of Fgf/ERK inhibition, as treatment with 80nM of cycloheximide delays the arrest of oscillations induced by PD03 (1μM): cells on micropattern undergo 3 oscillations before their arrest (6/7), while we observed 4 oscillations with cycloheximide (7/7). Further work should confirm and study this interaction.

2. Regulation of the translation

We then aimed to connect the cellular signaling to the control of translation (Figure 62A). Protein synthesis can be regulated at different levels, and we only present preliminary results examining the main candidates. Among them, the mTOR pathway integrates different signals (Laplante and Sabatini, 2012), such as the energy status of the cell or the growth factors signaling (notably ERK – (Ma et al., 2005)), to tune the translation rate. This is achieved by the phosphorylation of eIF4E-binding protein 1 (4E-BP1) and p70 ribosomal S6 kinase 1(S6K1); the former is necessary for cap-dependent translation, while the later controls several targets and ultimately leads to an increase of protein synthesis. However, use of the mTORC1 inhibitor, Ku-0063794 (up to 1 μM), did not lengthen the period of the *LuVeLu* oscillations (while we did not check the actual inhibition of the pathway, we used a concentration shown to strongly ablate S6K and 4E-BP1phosphorylations in cultured cells (García-Martínez et al., 2009)).
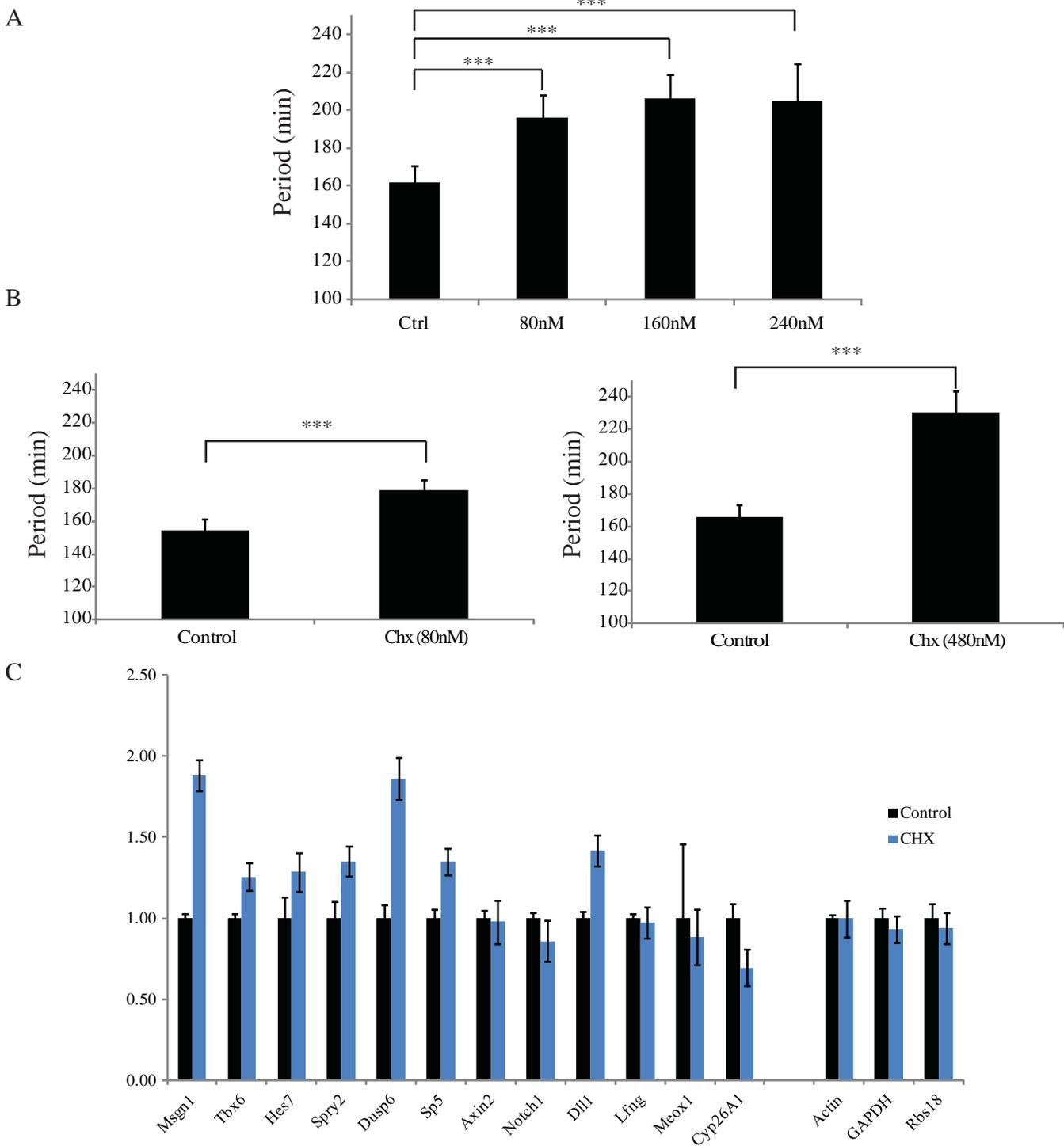
Figure 61 - Effect of cycloheximide treatment on *LuVeLu* oscillations

A. Graph showing the period of the *LuVeLu* reporter in explants with different concentrations of cycloheximide (n=3 explants for control; n=2 for cycloheximide-treated explants)

B. Graph showing the period of the *LuVeLu* reporter with the micropatterns setting using two concentrations of cycloheximide (Chx) (n=7 micropatterns)

C. Graph showing the fold-changes in gene expession after a 5h treatment with cycloheximide (CHX - 240nM). Each condition represents a pool of three explants.

We next turned to the role of eIF2α phosphorylation (Ron and Harding, 2007). Briefly, eIF2α indirectly controls the activity of the small GTPase eIF2, which binds to the initiator methionine-tRNA. The phosphorylated form of eIF2α inhibits eIF5, the GEF (Guanine Exchange Factor) activating eIF2, and thus represses translation initiation. Multiple signals control the phosphorylation of eIF2α through four kinases (PERK, Gcn2, HRI, PKR), such as amino acid deprivation or cellular stress. To test the effect of this pathway, we use the small molecule Sal003 that blocks the dephosphorylation of eIF2α, and should therefore repress translation. We found that treatment of explants with this drug (10 μM) leads to an overall decrease in the reporter intensity (~ 50%) and to an increase of the *LuVeLu* oscillations period of about 1.13-fold (155±6 min vs. 176±9min) (Figure 62B). We performed the converse experiment by treating the explants with the PERK inhibitor ISRIB (20 and 200nM), but we did not manage to detect an effect on the period. We did not check the phosphorylation status of eIF2α, and we cannot exclude that other kinases of eIF2α are involved in this process. While this suggests that translation can be tuned through the eIF2α pathway, further work needs to validate the relevance of such regulation.

3. Visualization of protein synthesis

We next addressed the question of the spatial regulation of protein synthesis. Notably, as mentioned above, we wanted to examine the correlation between translation rate and PSM determination. For this purpose, we used the SunSET method, where cells are treated with the antibiotic puromycin for a short period, and then nascent proteins are detected by immunostaining with an anti-puromycin antibody (Schmidt et al., 2009). It was previously shown that the incorporation of puromycin into polypeptides correlates with the translation rate, and thus this method enables to visualize protein synthesis. The SunSET method worked on explants and chicken embryos (day2) as evidenced by the lack of staining after cycloheximide treatment (Figure 62C). We did not observe obvious patterns of translation rate. However, we noticed several technical problems: the puromycin mostly stained the outer embryonic tissues suggesting a poor diffusion through the epithelium, and the staining was higher at the periphery of the explants (which might be linked to the density-dependent uptake of puromycin (Cass, 1972)). The use of the SunSET method thus requires further improvement to visualize the pattern of protein synthesis in the PSM and other *ex vivo* systems.
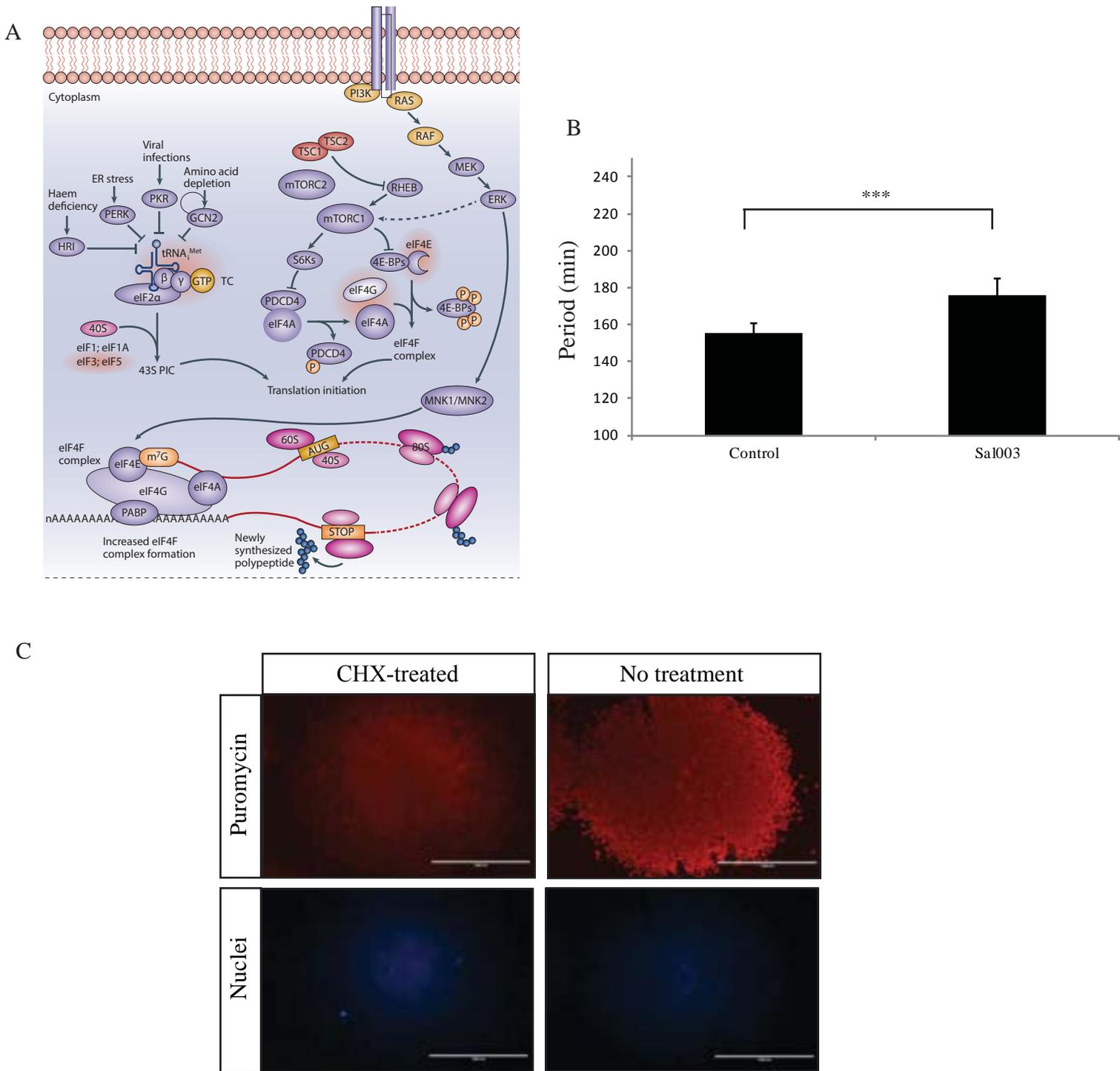
Figure 62 - Regulation of protein synthesis rate

A. Scheme showing the main regulatory pathways affecting the protein synthesis rate (eIF2α, mTOR, eIF4)
Modified from Bhat et al. (2015)

B. Period of *LuVeLu* oscillations in explants treated with Sal003 (10µM - n=3 explants) or vehicle control (n=2)

C. Immunostaining for puromycin-incorporated peptides. Translation initiation was blocked with cycloheximide as a control.

4. Role of other processes of gene expression

We briefly mentioned ongoing efforts to examine the role of other processes of gene expression on the clock period. The role of transcription has been difficult to examine due to the toxicity of the RNA-PolII inhibitor, α-amanitin, and further work is needed in that regard. We examined the role of protein degradation on the *LuVeLu* oscillations by treating explants with the proteasome inhibitor, MG-132. It was previously shown that this drug abolished oscillations of *Hes1* in mouse embryos at a concentration of 100 µM (Hirata et al., 2002). In our system, at high doses (>0.3µM), we observed an important cell death, while at lower dose (0.1µM) we did not observe any effect. Interestingly, for an intermediate concentration (0.2µM), we observed a strong increase (~ 4-fold) in the *LuVeLu* reporter intensity (that contains a PEST sequence targeting the fluorescent proteins to the proteasome), but oscillations were still observed with a similar period (n=3/4) (Figure 63). This is particularly intriguing as most of the oscillator models are strongly sensitive to changes in the degradation rate. Notably, Hirata and colleagues showed that a decrease of 33% in the degradation rate of Hes7 protein should abolish its oscillations in the model of autoinhibition with delay of J.Lewis (Hirata et al., 2004). By contrast, using their mathematical model, we were not able to reproduce the strong effect of translation inhibition seen in our model (as first reported in (Lewis, 2003)): reducing the protein synthesis rate by 10-fold only leads to a 5% decrease in the period (considering all other parameters unchanged). These results would therefore argue against a single pacemaker oscillating with an autoinhibitory loop with delay, and suggest a different architecture of the segmentation clock. We must note, however, that the presence of the PEST domain in the *LuVeLu* reporter forces us to remain cautious about these findings.
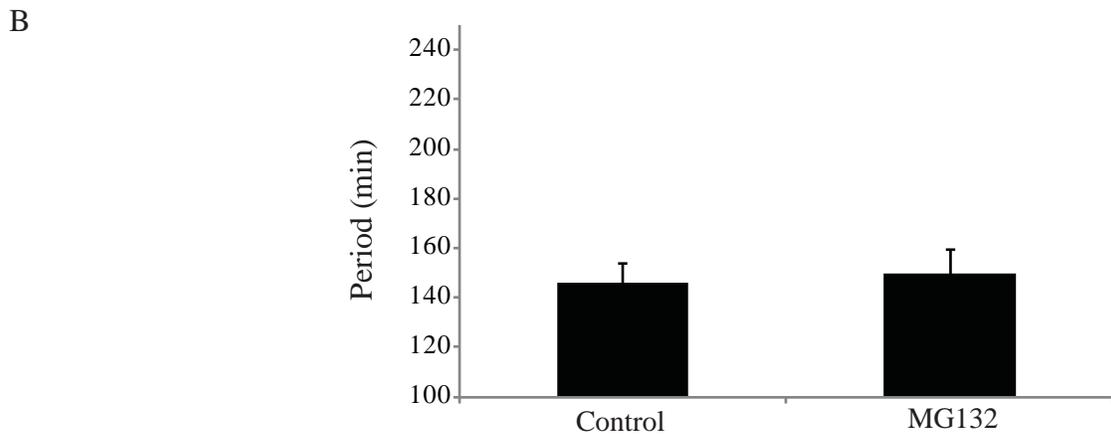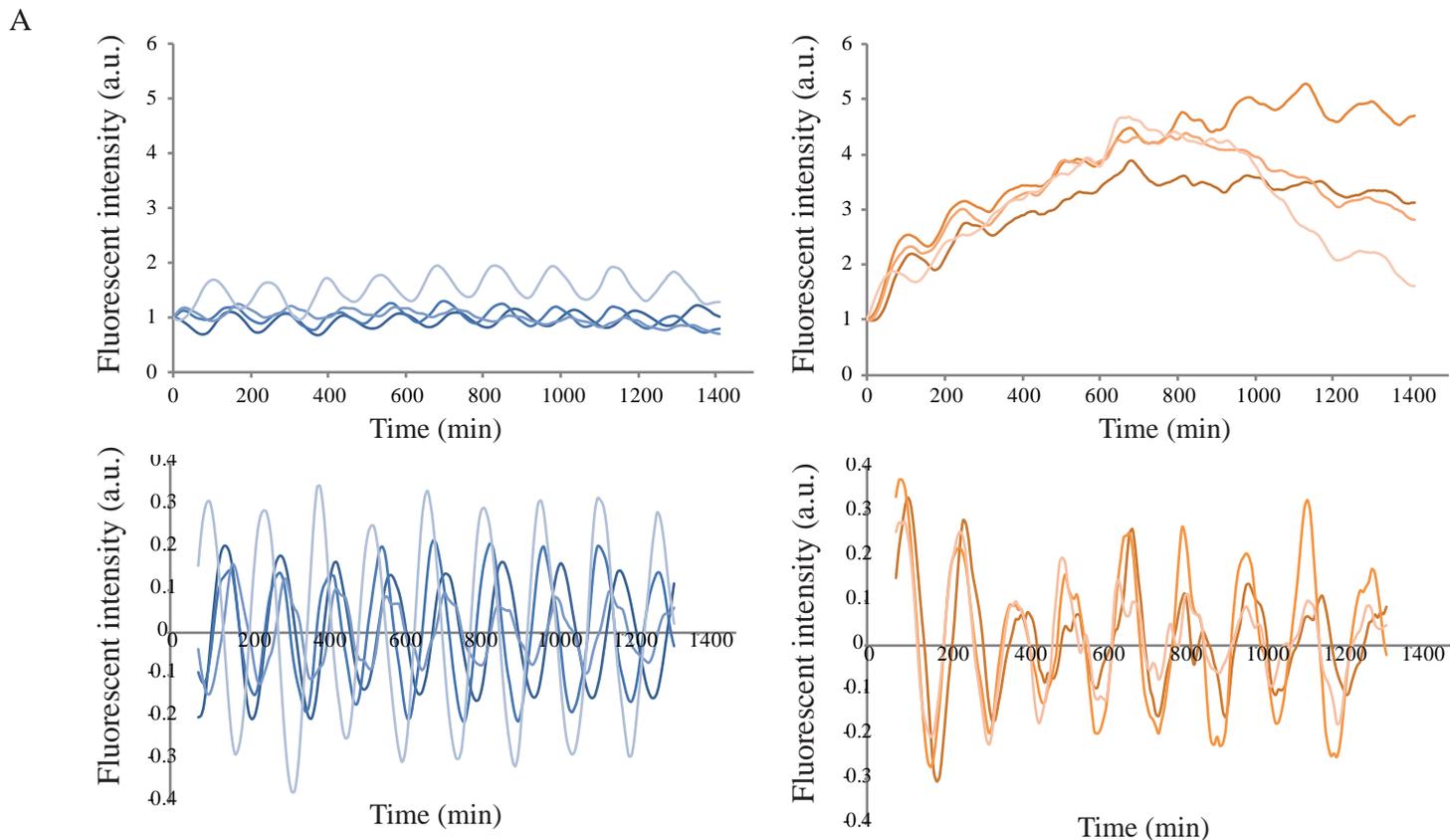
Figure 63 - Effect of MG132 treatment on *LuVeLu* oscillations

A. (*Top*) Fluorescent intensity profile of explants treated with MG132 (*right*) or vehicle control (*left*). Each line corresponds to one explant.
(*Bottom*) "Instantaneous intensity" profile (subtraction of a moving average to compensate for changes in intensity) of explants treated with MG132 (*right*) or vehicle control (*left*). Each line corresponds to one explant.

B. Graph showing the period for the explants of figure **A**

Discussion

In this chapter, we showed that reducing the translation rate led to an increase in the period of *LuVeLu* oscillations in our system. While these findings need to be properly confirmed *in vivo*, it raises several intriguing questions.

Is the translation rate regulated?

Previously, it was shown that changing the temperature could modulate the period of somitogenesis in zebrafish and the period of *LuVeLu* oscillations in mouse explants (Schröter et al., 2008, Lauschke et al., 2013). However, it is unlikely that those changes have a functional impact, especially in endotherm animals with an internal development. One could similarly argue that the changes observed upon diminution of translation do not reflect any functional regulation, but rather a lack of compensation of the segmentation "clock". Nevertheless, a growing body of evidence supports a regulation of translation during development. Work of the Barna group and others has demonstrated that use of specialized ribosomes provides another layer of regulation during embryogenesis. Interestingly, several mutants for ribosomal proteins display axial defects, such as axial transformation or kinked tails (Shi and Barna, 2015). In *Drosophila*, mutants for ribosomal proteins, such as the *Minute* mutant, have impaired Notch signaling (Schultz, 1929, Mourikis et al., 2010); however, we were not able to monitor a strong change in Notch signaling after cycloheximide treatment. While this addresses a specific regulation of the transcriptome translation, other studies point toward a global role of the translation rate on development (Buszczak et al., 2014). Klein and Melton showed that overexpression of eIF4E in ectodermal *Xenopus* explants induces a mesodermal differentiation associated with an overall increase in translation (Klein and Melton, 1994). Furthermore, Signer and colleagues demonstrated that hematopoietic progenitors have a lower translation rate than other hematopoietic cells, and that a precise level of protein synthesis was required to maintain their functionality (Signer et al., 2014). Interestingly, translational quiescence seems to be a common theme of stem cells, as it has been shown that satellite cells maintain a low protein synthesis rate (through phosphorylation of eIF2α) (Zismanov et al., 2016) and that differentiation of *Drosophila* germline stem cells is associated with a global increase in translation (Sanchez et al., 2015). Last, as mentioned in the introduction, there is a periodic synthesis of ribosomes and specific phases of translation during the circadian rhythm, which could provide another layer of regulation to the circadian clock. Examining the "cyclic proteome" by methods such as ribosome profiling would likely provide insights into the post-transcriptional regulation at work in the PSM. Together, this demonstrates the regulatory potential of changes in translation during development, and supports its study in somitogenesis.

How is the translation rate regulated?

Translation can be regulated by many pathways (e.g. mTOR, eIF2α, eIF4E). To our knowledge, no viable mutant display segmentation defect. Concerning the mTOR signaling, mTOR mutants have implantation defects (Gangloff et al., 2004, Murakami et al., 2004), but loss-of-function and gain-of-function mutants (*Rheb* and *Tsc1* mutants respectively) have a normal segmentation (Kwiatkowski et al., 2002, Goorden et al., 2011). Concerning the eIF2α pathway, mutants for *PERK* (Zhang et al., 2002a), *GCN2* (in normal feeding diet (Zhang et al., 2002b)), *HRI* (Han et al., 2001), and *PKR* (Abraham et al., 1999) are viable. Last, concerning the eIF4E pathway, *Mnk1*/2 double knockout mutants also display a normal development (Ueda et al., 2004). However, we should note that those pathways are generally activated by cellular stresses, so it is possible that standard laboratory conditions hide a role in somitogenesis. Accordingly, the severity of segmentation defects in mouse heterozygous mutants of the Notch pathway is potentiated by hypoxia (Sparrow et al., 2007).

For these pathways, the changes in protein synthesis are often caused by an alteration of metabolism. It is especially interesting in the light of recent studies highlighting a link between the patterning of the PSM and its metabolism. It was notably shown that the PSM maturation is associated with a transcriptional switch from anaerobic glycolysis to respiration (Ozbudak et al., 2010)(M.Oginuma, personal communication). Hypoxia also induces defects in somitogenesis (Sparrow et al., 2007, Bajard and Oates, 2012). Therefore, it will be interesting to study whether those metabolic changes induce downstream changes in the translational rate and in the segmentation clock period. Inversely, the protein synthesis rate could be upstream of different processes during Vertebrate development. In a very speculative way, we could imagine that the control of the clock period by the protein synthesis rate ensures a coupling between axis elongation and somitogenesis, as a decrease in temperature or nutrients would dampen both the clock period and the cellular processes responsible for the elongation (e.g. cell motility, cell proliferation) through translation.

It would also be interesting to compare the translation rates of different Vertebrate species and to correlate it with the segmentation clock period. Indeed, a fundamental question of the field is to understand the differences in period among species. A role in the delay induced by RNA export and splicing has been proposed (Hoyle and Ish-Horowicz, 2013). However, we could speculate that variations in protein synthesis (and more generally in metabolism) are involved. Besides protein synthesis, it has become more evident that metabolism can regulate gene expression through metabolites; for instance, acetyl-CoA influences histone acetylations and metabolites such as α-ketoglutarate or SAM modulate histone methylations (Lu and Thompson, 2012). It would thus be fascinating to study how the different modes of development and environments influence translation and metabolism across species.

CHAPTER IV

Reconstituting the segmentation clock *in vitro*

In this part, we present our efforts to reconstitute the segmentation clock in mouse embryonic stem cells (mESC) differentiated in a PSM-like state.

The purpose of this project was two-fold: first, to build a controllable material available in large quantity and second, to understand the conditions necessary to the birth of oscillations in the PSM ("*what I cannot build, I cannot understand*"). Indeed, as previously mentioned, several protocols have been established to differentiate mESC into paraxial mesoderm. Using this method would enable us to follow the events that lead to the initiation of the segmentation clock, and how they are controlled during the PSM determination. Especially, we aimed to take advantage of the control of cell differentiation in different lineages. As discussed in the introduction, an important question is to understand which parameters are permissive for oscillations (transcription rate, translation rate, degradation rate, various time delays, etc,) and how they are regulated so that some genes are specifically cycling in the PSM. Using an *in vitro* system to compare different cell types would thus allow us to address this link between the PSM fate and the oscillatory state. Furthermore, generating an *in vitro* model of the segmentation clock would enable to perform biochemistry experiments, which usually require large amount of materials. Such system would also be amenable to controlled perturbations, where mouse embryo culture is more challenging, such as microfluidics chamber.

1. Derivation and characterization of a *LuVeLu* mESC line

To study the segmentation clock *in vitro*, we used the *LuVeLu* reporter. E3.5 blastula (BL6 background) were isolated by S.D. Vincent, and then cultured in 2i+LIF conditions on feeders. 15 out of 16 blastulae gave rise to colonies, and 7 out of 15 were positive for the *LuVeLu* reporter. We also checked that the transgene was not silenced in the transgenic father.

We first used a "one-step" protocol developed in our group by Chal and colleagues (Figure 64A). In this protocol, cells previously cultured with LIF on feeders are directly differentiated into PSM-like cells by adding the GSK3β agonist, CHIR99021, the BMP receptor ALK2/3 inhibitor, LDN-193189, and DMSO in presence of serum. It was shown that this protocol induced the expression of PSM markers, such as *Msgn1* or *Tbx6*, after 3 days of culture in this medium. We validated this approach for two *LuVeLu* cell lines: the PSM markers (*Hes7*, *Tbx6*) were strongly upregulated after 3 days of culture; the transcripts for the endogenous *Lfng* and *LuVeLu* were also upregulated (3-fold and 7-fold-change respectively) (Figure 64B). We then examined the dynamics of the *LuVeLu* reporter from day3 to day4 using live microscopy. In this setting, we did not observe oscillations of the reporter but rather a behavior reminiscent from the dissociated explant cells with a basal level of
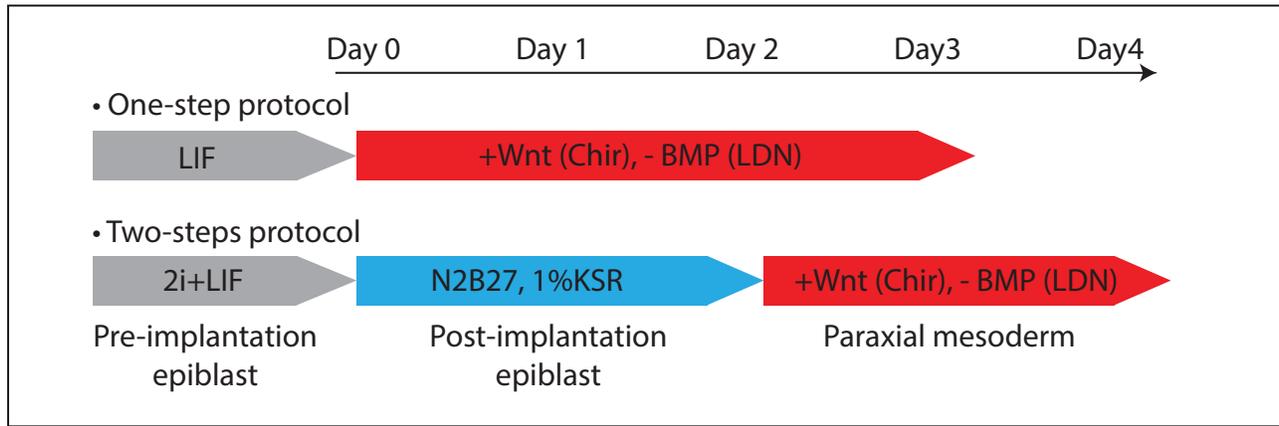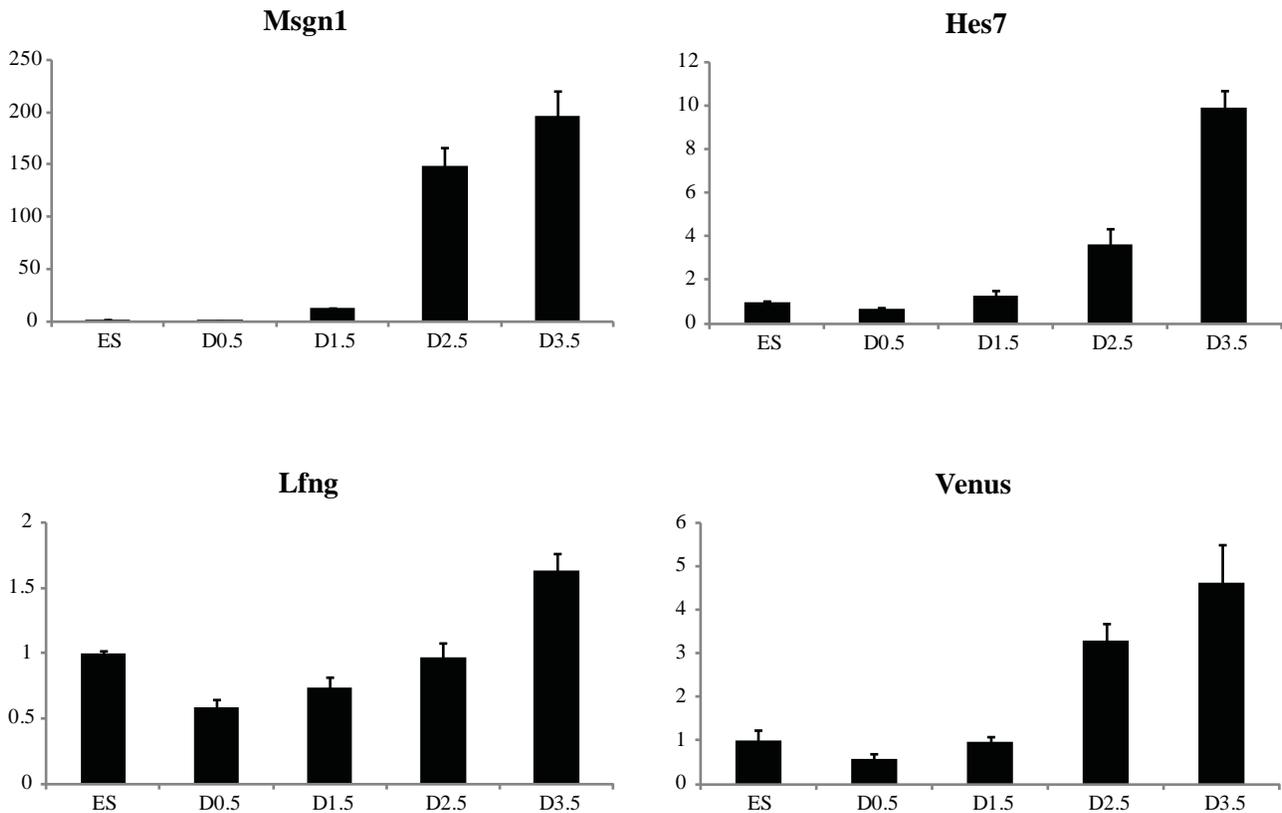
Figure 64 - Differentiation in a PSM-like state of *LuVeLu* mESC

A. Differentiation protocols to the paraxial mesoderm state

B. Graphs showing the changes in expression of *Msgn1, Hes7, Lfng* and *Venus* during the one-step differentiation of *LuVeLu* mESC. The fold-change compared to the mESC state (ES) is represented.

fluorescence. We also noticed that the reporter intensity often increased before a cell division. In few cells, we observed bursts of *LuVeLu* but without clear periodicity. As we did not see any difference between the two cell lines, we arbitrarily selected one.

We then adopted an improved version of the protocol ("two-steps protocol") (Figure 64A), where mESC are cultured in 2i+LIF conditions, then switched to a serum-free medium with 1% KSR (Knock-OUT Serum Replacement that contains amino acids, transferin, insulin, albumin, ions and antioxydants) for two days, and finally incubated in CHIR/LDN medium (as before) (Chal et al., 2015). Using this protocol, however, we did not observe by live microscopy any difference with the one-step protocol.

2. Creation of a *LuVeLu/Msgn1-mCherry* cell line

As mentioned in the previous sections, *LuVeLu* oscillations appear sensitive to the cell density. This would be consistent with *in vivo* observations reporting that Notch signaling requires cell-cell contacts and is necessary for the maintenance of the oscillations. We therefore decided to develop a reporter to select only the cells differentiated in the PSM state and to culture them at high density. We took advantage of a method based on a transcriptional reporter for *Msgn1* (Wittler et al., 2007, Chal et al., 2015) (Figure 65A). Using this reporter, Chal and colleagues were able to obtain ~50% *Msgn1-Venus* positive cells at day 4. We made several modifications compared to the original reporter: i) we replaced the Venus by mCherry to make the reporter compatible with the *LuVeLu*; ii) we introduced two NLS (nuclear localization sequence of the SV40 large antigen) to facilitate the tracking of single cells; iii) we introduced a PEST sequence (half-life of ~4h) to avoid the persistence of the fluorescent proteins and better identify the cells in the PSM state. Cells were transfected and selected for the integration of the reporter. We then amplified single clones that we screened for mCherry expression at day4. We note that we did not remove the selection cassette and did not determine the copy number of transgenes. We validated the reporter by performing an immunostaining for Tbx6 showing an overlap between mCherry and Tbx6 (Figure 65B). We further validated this cell line by sorting cells by flow cytometry and analyzing the expression of PSM markers between mCherry-positive and mCherry-negative cells (Figure 65B). The positive population displayed an enrichment of the PSM markers, *Tbx6* and *Msgn1*, and a depletion of the neural marker *Sox2*. Consistently with the findings of Chal and colleagues, we observed the activation of the reporter after 4 days of differentiation using the two-steps protocol and obtained induction levels around 50%. At day4, we noticed by confocal microscopy that there was a
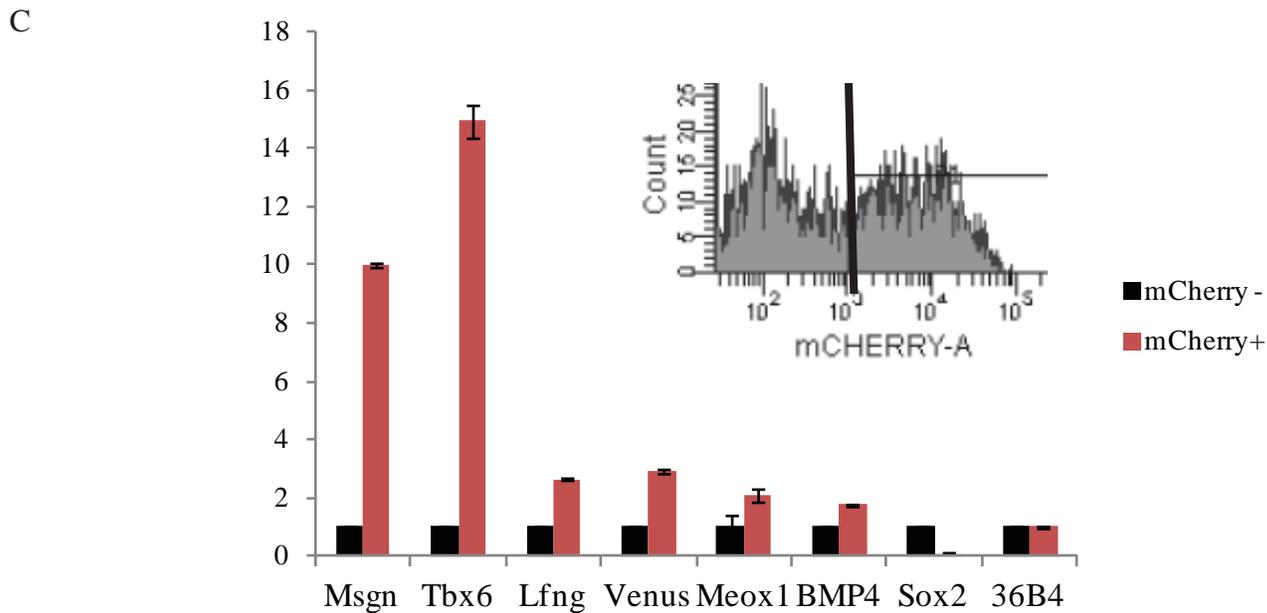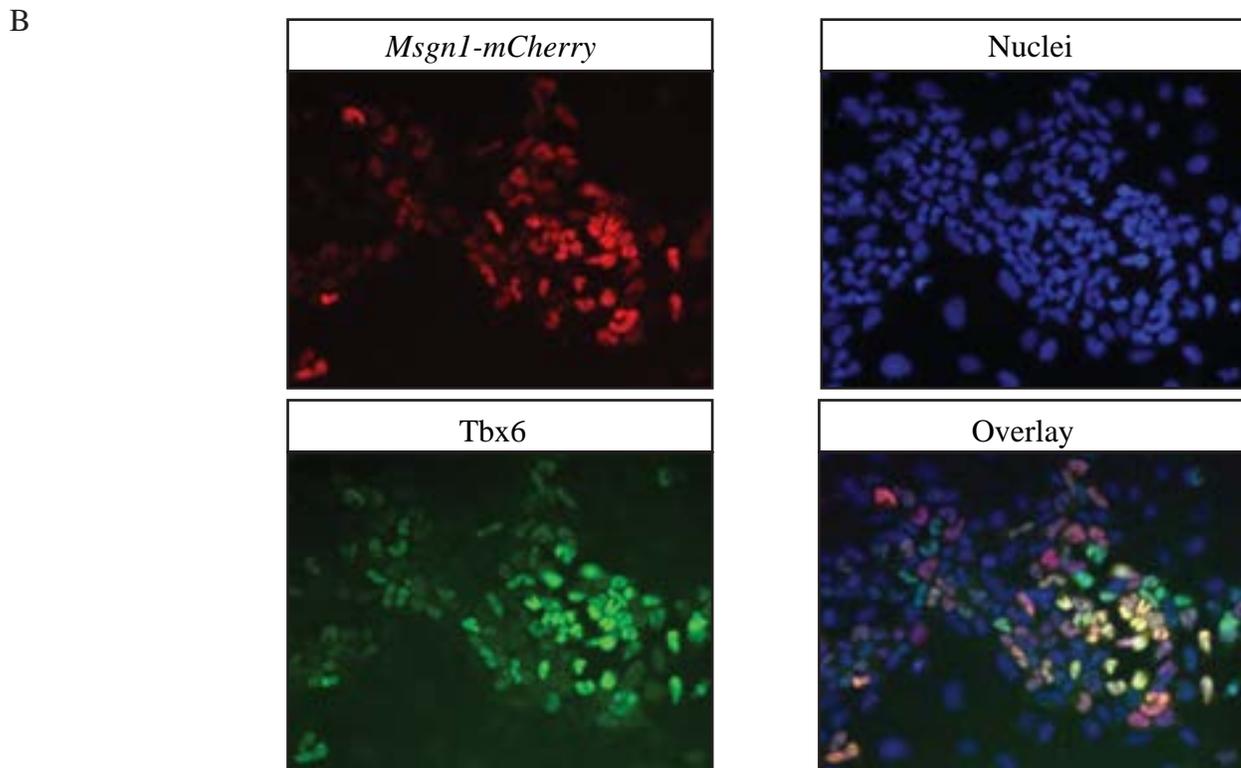
Figure 65 - Construction of a *Msgn1* reporter

A. Design of the construct used

B. Pictures of cells with the *Msgn1* reporter after 4 days of differentiation (two-steps protocol). Immunostaining for Tbx6 (green), fluorescence of the mCherry reporter (red), nuclei (blue).

C. Graph showing the differences in gene expression between *Msgn1-mCherry* negative and *Msgn1-mCherry*-positive populations. Fold-changes compared to the negative population are represented. The excerpt shows the fluorescence profile by flow cytometry and the gating for cell sorting.
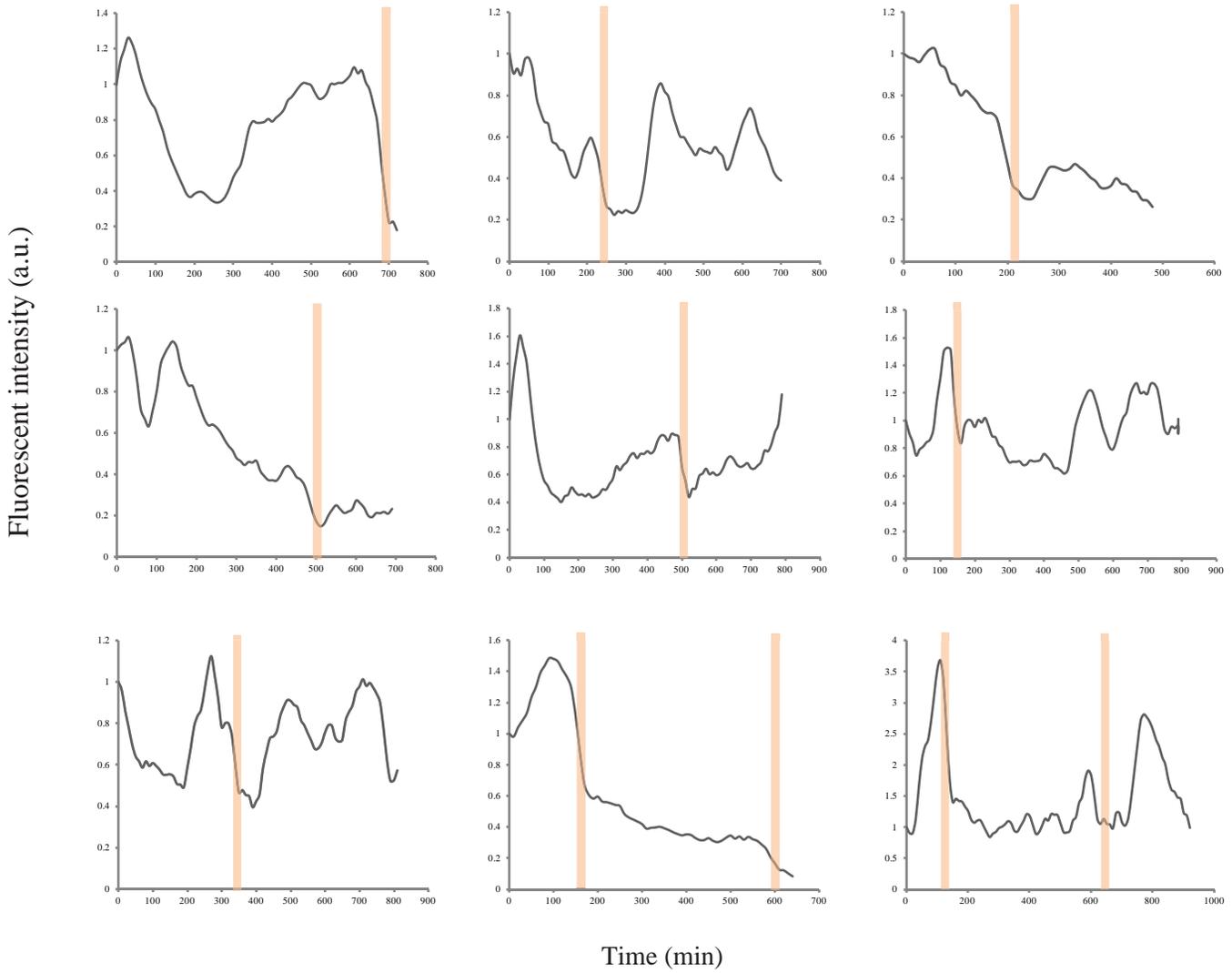
Figure 66 - Dynamics of the *LuVeLu* reporter in PSM-like cells

Fluorescent profiles of the *LuVeLu* reporter in PSM-like cells (day4 - after sorting with the *Msgn1-mCherry* reporter). Each graph shows the dynamics of one cell. Orange windows indicate cell divisions.

Experiment	Rationale	Protocol
Inducing Notch signaling	Notch signaling is required for somitogenesis and coculture of C2C12 cells with Dll1-expressing cells can induce Hes1 oscillations in vitro	Culture on Dll1-coated plate (5ng/µL) at day 4
Inducing Fgf signaling	Fgf signaling kicks off the segmentation clock in zebrafish and is required for Lfng oscillations in mice	Culture with mFgf4 (50ng/mL) at day 4
Inhibiting BMP signaling	Previous results of J.Chal and colleagues suggested that the strength of BMP inhibition correlated with the expression level of Hes7 (upregulation with the more potent LDN193189 compared to Noggin)	Use of DMH1 (5 µM) a dorsomorphin derivative that is supposedly more selective and potent than the LDN193189 (Cross 2011 ACS) from day 2
Using serum-free conditions	Better controlling the composition of the medium	Culture in N2B27, 10%KSR, Chir3µM, LDN 100nM, Fgf4 25ng/mL, Heparin 1 µg/mL, BMS493 1 µM
Using the explant medium	Using conditions that are permissive for LuVeLu oscillations with explant tissues	Culture with explant medium at day 4
Coculture with explant cells	Inducing oscillations if intercellular interactions (e.g. Notch) or paracrine signal are needed	Dissociation of explants and coculture with Msgn1-mCherry+ cells on micropattern or in aggregates formed by spinning
Reducing the glucose concentration	Preliminary results in our group from A.Aulehla suggested that high concentrations of glucose led to a dampening of oscillations	Differentiation with 1g/L glucose instead of 4.5g/L (one-step protocol)
Serum shock	A serum treatment (culture of cells at 0.2% FBS for one day, then increase to 5%) induces oscillations of Hes1 in cultured cells	Short serum shock by culturing cells at 0.5% or 50% serum for 2h15, and then back at 15% (one-step protocol)

Figure 67 - Conditions tested

A

B
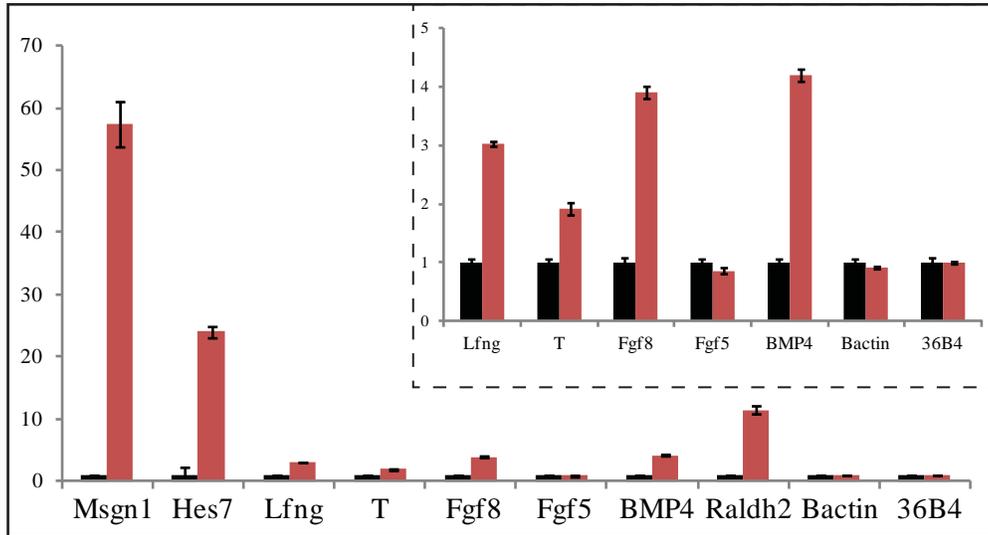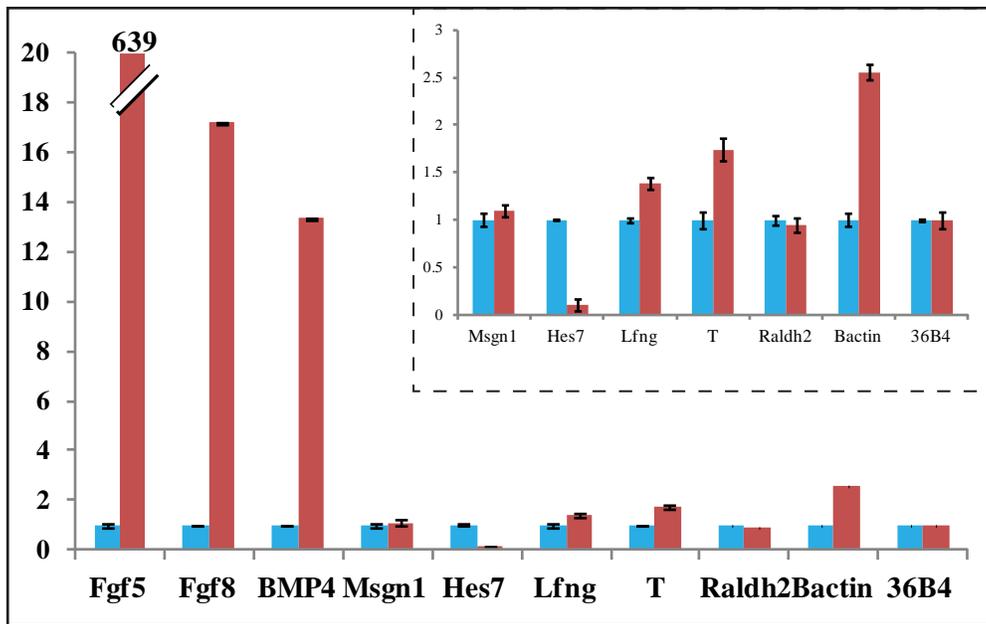
Figure 68 - Comparaison of gene expression profile

A.Graph showing the differences in gene expression between *Msgn1-mCherry* negative (black) and *Msgn1-mCherry*-positive (red) populations. Fold-changes compared to the negative population are represented.

B. Graph showing the differences in gene expression between the same *Msgn1-mCherry* positive (red) and explant cells (blue). Fold-changes compared to the explant are represented.

C
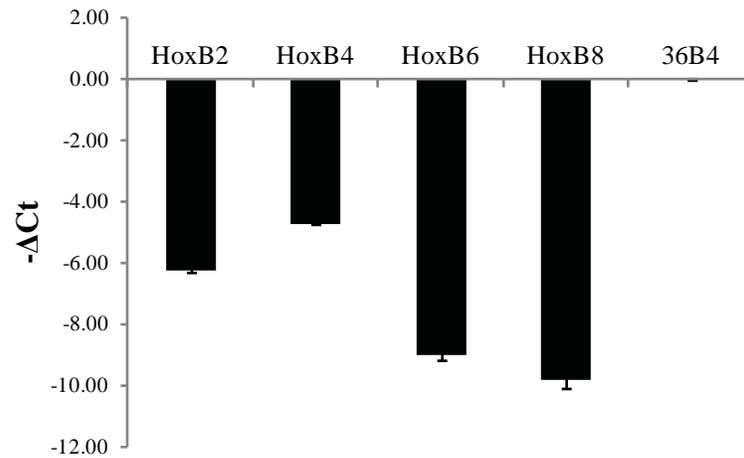
Figure 68 - Comparaison of gene expression profile (*continued*)

C.Graph showing the expression of *HoxB* genes in differentiated mESC (day 4 - *Msgn1-mCherry* positive cells).
 -ΔCt are represented (the highest value corresponds to the most expressed gene compared to the housekeeping gene 36B4).

population positive for *LuVeLu* and negative for the *Msgn1-mCherry* reporter. As we could not sort the *LuVeLu* cells with the flow cytometer available, we could not further study these populations.

3. Conditions for the apparition of oscillations

We then examined the dynamics of the reporter after sorting of the cells at high density. We tracked 135 cells, out of which 40% (54/135) were positive for the *LuVeLu* reporter and only 6 display a burst pattern (on-off-on-off). As reported above, we mainly observed transient pulses and a progressive downregulation of the reporter (Figure 66). To further increase the density between cells, we followed a suggestion by C.Tsiairis: we span the cells to generate aggregates and let them spread after. However, we did not observe individual or collective oscillations, probably due to the salt-and-pepper pattern of *LuVeLu* reporter. We also differentiated cells on PDMS to generate embryoid bodies that we plated at day4; the rationale was to promote cell-cell interactions for a longer period, but we did not see major differences with the previous experiments. Last we tried the "gastruloid" method reported by the group of A.Martinez-Arias, where cells are cultured in three-dimensions and received a 24h-pulse of CHIR resulting in the polarization and elongation of the aggregate (van den Brink et al., 2014). Unfortunately, using the exact same conditions, we were not able by three times to observe the elongation of the embryoid bodies.

We then tried to optimize the culture conditions to observe oscillations. In that regard, we tried the conditions described in Figure 67. All these conditions led to a negative outcome as judged by the absence of single-cell oscillations.

To bypass the problem of cell contacts, we tried to culture cells on glass or with latrunculin A, as this allowed to make dissociated explant cells oscillate. Preliminary results suggest that such treatment does not induce oscillations with the one-step protocol, but it remains to be studied in more details.

To better understand why differentiated cells were not able to oscillate, we looked at the expression of key genes of the PSM state. Even if *Msgn1-mCherry* positive cells showed an enrichment of PSM markers compared to undifferentiated mESC or mCherry-negative cells, they expressed *Hes7* at a lower level than explants or embryo tail (about 10-fold) (Figure 68). We next wanted to discriminate between two hypotheses: i) the entire population displays lower levels of PSM markers or ii) the mCherry-positive population is heterogeneous, and an "elite" subpopulation exists that we need to identify and purify. To test those ideas, we performed single-cell analysis of mCherry-positive cells using the Fluidigm system (we note that the set-up for PSM analysis was done by S.D.Vincent and

that the experimental procedure was performed by C.Fugier). However, technical problems of the Fluidigm system precluded us to finalize this experiment. Last, we looked at the *Hox* genes to approximate the axial identity of those cells. At day4 of differentiation, we analyzed the expression of *Hoxb2*, *Hoxb4*, *Hoxb6*, and *Hoxb8*. We observed that *Hoxb2* and *Hoxb4* were relatively more expressed than *Hoxb6* and *Hoxb8* at day 4 suggesting an anterior identity (Figure 68C).

We then sought to use an alternative method of purifying the cells to culture them at high density. Since not all the *Msgn1-mCherry* positive cells were expressing the *LuVeLu* reporter, we supposed that using a cyclic gene could enrich for cells that have specifically "unlocked" the segmentation clock program. Furthermore, we substituted the transgenic approach by a knock-in strategy in order to better monitor the PSM state and to reduce the risks of artifacts. We thus generated a reporter in the *LuVeLu* mESC line, where a stable fluorescent protein (3xNLS-mKate2) was inserted at the C-terminal end of the protein Hes7 and cleaved using a P2A tag (Figure 69). We turned to the CRISPR-Cas9 system to enhance the occurrence of homologous recombination, and to reduce the risks of off-target effects, we used the nickase version developed by F.Zhang group, where two cleavages are necessary (Ran et al., 2013). We then validated the insertion of the construct by PCR, and further screened for single insertion by estimating the copy number by qPCR. However, after removal of the selection cassette, we were not able to see any signal by confocal microscopy.

4. Generation of alternative cyclic and cell fate reporters

Cyclic reporters

We then wanted to generate another cyclic reporter to exclude the possibility that these problems came from the *LuVeLu* reporter. Notably, since *Lunatic fringe* was considered as a Notch target, we opted for Hes7 that could theoretically cycle in a cell-autonomous manner. Following the same logic, we tried to create three knock-in reporters for the cyclic gene *Hes7*.

First, we tried to generate a knock-in line with the classical method (without CRISPR). To avoid potential dominant negative effects of a fusion, we inserted the reporter at the start codon of *Hes7*, similarly to the constructs developed by the Kageyama lab (Takashima et al., 2011) (Figure 69). We also tried to improve the fluorescent construct compared to the *LuVeLu*: i) we added a translational enhancer (part of the 5'-UTR of VEGF); ii) we added NLS; iii) we used a human-codon optimized version of the superfolder GFP that we dimerized to improve the signal; iv) to avoid the accumulation of a basal fluorescence as observed for the *LuVeLu*, we added a CL1 degradation
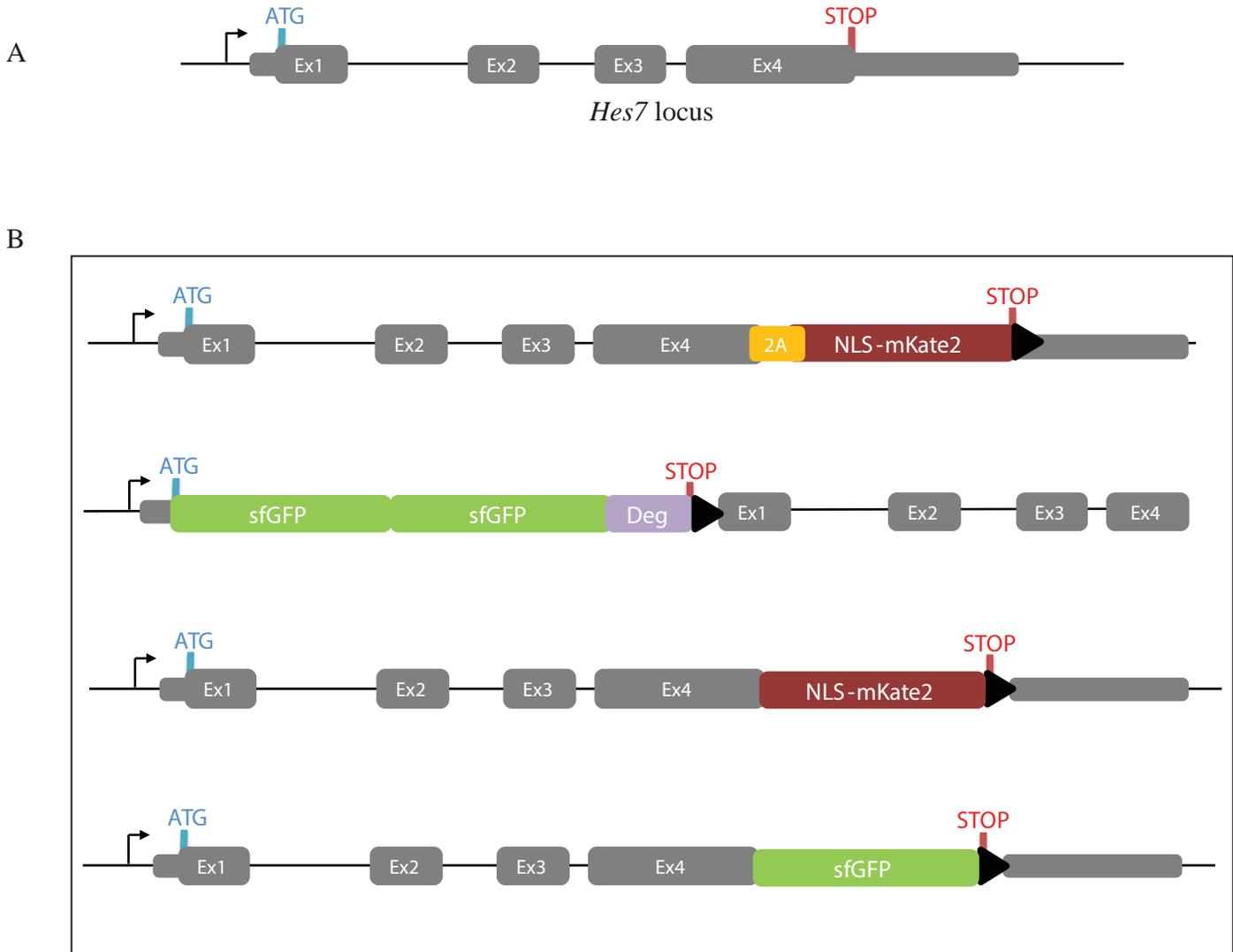
Figure 69 - Construction of Hes7 fluorescent reporters

A. Genomic locus of the mouse *Hes7* gene

B. Different constructs used (*from top to bottom*): a stable red reporter, a cyclic reporter with a destabilized protein, two cyclic reporters as protein fusions (see text for details)

domain to the PEST domain. We tested that this construct was indeed fluorescent by electroporation in the PSM of chicken embryos. However, we did not have any positive mESC clone (over ~200 clones tested).

We then tried to generate a Hes7 knock-in line with a C-terminal fusion of the fluorescent protein mKate2 (Figure 69). We followed the same strategy as reported by Delaune and colleagues, who noticed that only a C-terminal fusion of Her1 was working in zebrafish (Delaune et al., 2012). We did this experiment in the *T-GFP* line of G.Keller lab (Fehling et al., 2003) in order to purify PSM-like cells at an earlier stage and to avoid selecting cells that have passed the oscillation window; another advantage of this cell line is to harbor a validated knock-in reporter compared to the *Msgn1* transgene. We used the CRISPR-Cas9 (nickase) system as presented earlier, and we were able to identify positive clones. However, we were not able to observe any fluorescent signal by confocal microscopy, despite similar levels of expression between the fusion and the wild-type alleles.

Last, we designed a C-terminal fusion with the superfolder GFP, and the knock-in was performed by the Mouse Clinical Institute as part of the European program Phenomin (Figure 69). However, as for the previous cases, we did not detect any signal by confocal microscopy despite a similar expression level with the wild-type allele.

Reporters for the anterior PSM markers

We wanted to better control the transition from the posterior PSM state to the determined, anterior PSM. As we observed that cells extinguished the *Msgn1-mCherry* reporter, we supposed that maintaining them in the posterior state for a longer time would enable us to better manipulate and observe oscillations. For that purpose, we differentiated cells with the two-steps protocol, then sorted *Msgn1-mCherry* positive cells at day4, and cultured them in the explant medium (see above). As this medium contains activators of the Fgf and Wnt pathways and repressor of the RA pathway, it should supposedly delay the transition to the anterior PSM state. However, we still observed a decrease of the *Msgn1-mCherry* reporter intensity and its complete extinction at day6 (Figure 70).

To study this process and to negatively select determined cells, we tried to generate reporters for anterior PSM markers in collaboration with a master student, I.Amblard. We chose to build red transgene reporters for *Foxc1* and *Meox1* into the *Msgn1-Venus* cell line developed by J.Chal. This should enable us to better screen for conditions that prevent the determination of PSM-like cells by monitoring both the posterior and anterior states. As this stage, we were not able to find the correct regulatory sequences to drive the expression of the reporters.
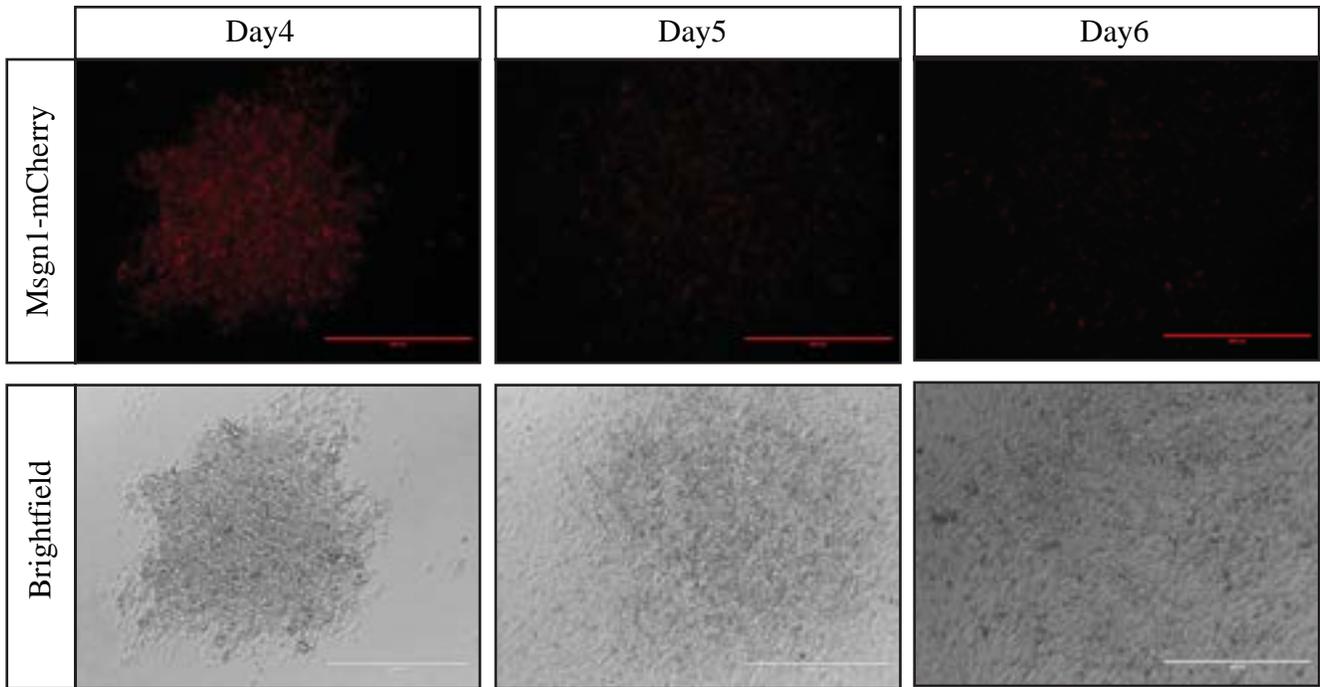
Figure 70 - Maintenance of PSM-like cells

Pictures of PSM-like cells (day 4 - *Msgn1-mCherry* positive, span and plated on fibronectin plate) cultured in explant medium.

(*Top*) Fluorescence for the *Msgn1-mCherry* reporter. (*Bottom*) Brightfield (scale bar: 400µm)

5. Control of signaling gradients by microfluidics

In parallel to the work on mESC cells, we wanted to develop a system where we could generate and control gradients of small molecules or ligands. The initial idea was to rebuild the signaling gradients of the PSM *in vitro* and to combine this device with PSM-like cells. Specifically, we wanted to test the hypothesis that the gradient of Fgf controls the phase gradient of *LuVeLu* described by Lauschke and colleagues.

For that purpose, we chose to use the "Christmas-tree" device developed by Dertinger and colleagues (Fig71) (Dertinger et al., 2001). Briefly, three input channels with different concentrations of a substance are progressively mixed by diffusion through a series of PDMS channels. In collaboration with C.Paoletti and the group of G.Charvin, we constructed such "Christmas-tree" device with dimensions adapted to the PSM size and our confocal microscope setting. To validate this device, we first used a fluorescent dextran (conjugated with tetramethylrhodamine isothiocyanate) with a molecular weight of 4'400 $g.mol^{-1}$ (as an intermediate between the weights of ligands and small molecules– $482g.mol^{-1}$ for the MEK inhibitor PD0325901, and 22'000 $g.mol^{-1}$ for Fgf4 monomer). By using either gravity or a pump, we were able to successfully generate a gradient of dextran along the chamber. We then tried to adapt this device to cultured cells. To make the device compatible with aggregates and embryonic tissues, we aimed to inject the tissues not by bonding the glass to the PDMS, but by clamping the PDMS to tissues already cultured on glass. We experienced several difficulties to achieve reproducible gradients or functioning devices (*i.e.* without leak or bubble). Because of the lack of resource and expertise, we did not pursue this work and we decided to focus on other projects.

A
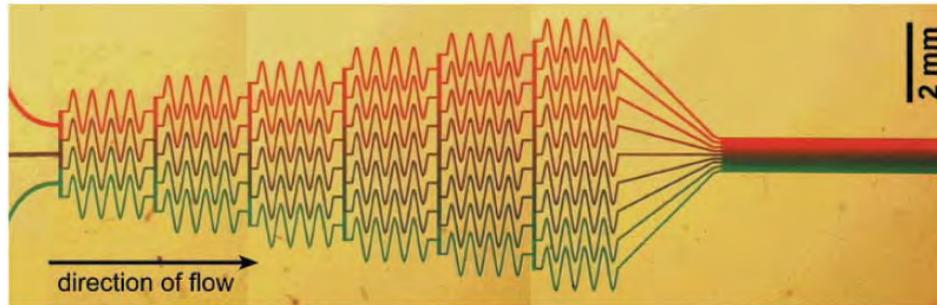
B
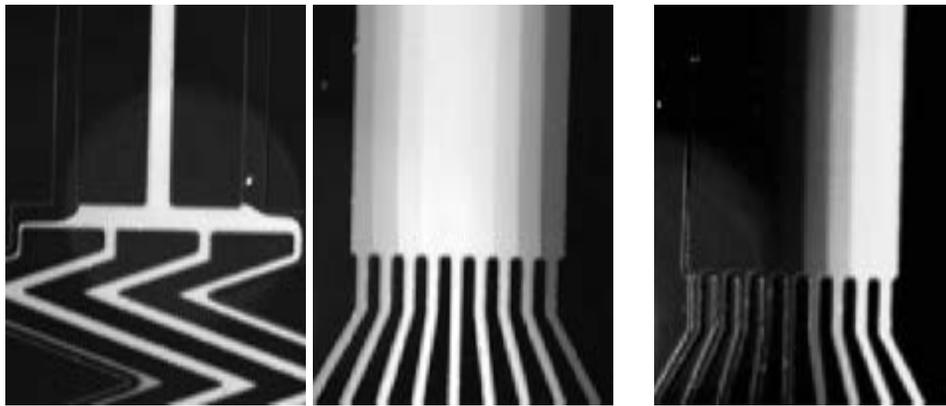
Figure 71 - Microfluidics device to generate gradients

A. Design of the "Christmas-tree" to generate gradients
Modified from Dertinger et al. (2001)

B. Pictures of the input channel with a fluorescent dye (*left*) and of the culture chamber in two different configurations (*middle:* dye in the central input, *right:* dye at the right input*)*

Discussion

The aim of this project was to develop an *in vitro* system recapitulating the signaling dynamics of the PSM, notably its oscillations and its gradients. At this stage of the project, we were not able to detect oscillations with the *LuVeLu* cell line. We can propose three hypotheses to account for these observations:

- Detection problem: the system is not adapted to detect oscillations of cyclic genes;
- Cell identity: the differentiation protocol partially recapitulates the determination into the PSM state and does not activate the segmentation clock program;
- Culture conditions: the cells are competent for oscillations but a special setting is required (factors, cell arrangement, etc.).

We examine each hypothesis and propose future directions.

Hypothesis 1: The Detection Problem

We derived a mouse embryonic stem cells line with the *LuVeLu* reporter developed by A.Aulehla. While this reporter has some issues regarding its low signal and its basal fluorescent level, it is in our opinion the best cyclic reporter up-to-date. While oscillations are more difficult to detect compared to "simpler" phenotypes (e.g. expression of a marker), the fact that oscillations are readily observable with the dissociated explant cells (with latrunculin) suggests that our system is able to detect oscillations. Nevertheless, in our system, we could imagine that the segmentation clock is operating, but that several factors prevent us to observe it: the short time window (a cell experiences ~3/4 oscillations *in vivo* (Aulehla et al., 2008)), the noise due to the lack of synchronization, the changes in period inherent to the PSM differentiation or the effect of cell division. We tried to extend this time window to better study the cell behavior, but we were unable to poise the cells in a PSM state. Furthermore, to ensure that the problem was not specific to this reporter, we tried to generate reporters for Hes7. The lack of success can come from the low expression of *Hes7* in those cells or from technical issues. While we think that the hypothesis of a detection problem is unlikely, development of high-throughput methods with automatic tracking and quantitative analysis of the *LuVeLu* reporter would provide better conditions to detect oscillations. Notably, micropatterns (as presented earlier) enabled us to better track single-cells, and could be used to standardize the analysis.

Hypothesis 2: The Cell Identity Crisis

Working with embryonic stem cells leads to the problem of recapitulating embryo cell states in the dish. While the protocols available to generate paraxial mesoderm clearly recapitulate part of the PSM program, they might only partially reprogram mESCs into PSM cells. Of note, we observed lower levels of *Hes7* in the differentiated mESCs than in the cultured explants. As we discussed in the introduction, the acquisition of the oscillatory state requires a precise balance of cellular parameters (time delay, RNA and protein degradation, etc.) to allow oscillations. It is yet to be determined how wide this parameter space is. Furthermore, we have no idea about the degree of canalization of the differentiation of embryonic stem cells, that is, their ability to robustly adopt specific fates during development. This idea was developed by C.Waddington, who visualized differentiation as cells moving downwards along bifurcating valleys and stopping in depression of the landscape. Canalization originates from the deep valleys containing the movement of the ball and large basins attracting it. This concept was later adapted in terms of dynamical systems theory: a depression corresponds to a local equilibrium solution of the equations describing the gene regulatory network (also referred as "attractors"), the valleys represent the system trajectories and the branch points correspond to bifurcations (Enver et al., 2009, Jaeger and Monk, 2014). This conceptual framework not only helps us to capture the dynamics of cell differentiation, but also has important consequences to optimize the differentiation protocols. Accordingly, cells could adopt a limited subset of cell fates and only "roll down" along the Waddington landscape; in this case, expression of a master regulator of the PSM state would be sufficient to predict the entire PSM program and the problem lies in the culture conditions (hypothesis 3). Alternatively, cells could adopt a multitude of states and partially activate the PSM program; in this case, only the combination of different markers could signal the correct cell fate and the problem lies in the differentiation conditions. Published work would support the latter hypothesis; for instance, many protocols of differentiation of human embryonic stem cells into pancreatic β-cells generated cells that did not recapitulate all the features of β-cells (e.g. response to glucose, markers expression) and displayed mixed cell states (e.g. secretion of both glucagon and insulin) (Pagliuca et al., 2014). Work in our lab also suggested that in the absence of BMP inhibition, a hybrid state of lateral and paraxial mesoderm was obtained with expression of both *Msgn1* and *BMP4* (even if we cannot exclude that this is due to the labeling of a common progenitor and to the stability of the reporter). Theoretical work on reprogramming from Mehta and colleagues further indicates that partially-reprogrammed states can arise when the bias toward a particular cell fate is weak in a high-dimensional landscape (in other words, there are many small attraction basins connected by superficial valleys) (Lang et al., 2014). Of note, they showed that those "spurious attractors" are the combination of different cell fates. PSM-like cells could thus be a result of a combination of different mesodermal states. The fact that PSM-like cells with our protocol cannot reside in the *Msgn1-mCherry* positive state in high Fgf, high Wnt conditions but differentiate further suggests that the PSM-like state is a poor attractor *in vitro*.

Last, in the introduction, we discussed about the separation of different "programs" in the PSM, such as the PSM maturation (e.g. epithelialization and differentiation in the somite derivates) and the segmentation. A paramount case of this compartmentalization lies in the "somites without clock" of Stern and colleagues (Dias et al., 2014). We could thus hypothesize that PSM-like cells partially activate some of the paraxial mesoderm programs but not the program controlling the segmentation clock. This could explain why not all *Msgn1-mCherry* cells express the *LuVeLu* reporter. Therefore, we envisage two ways to improve the current differentiation protocol: better targeting the cell state competent for oscillations (identifying the "right basin") and stabilizing the path toward this state ("making deeper the valleys and depression").

Concerning the cell state, a first step would be to better understand the combination of cell fates present in PSM-like cells (if any), and to compare this state to *in vivo* states. Because the cell state appears high-dimensional, it will be important to combine multiple markers and to analyze the fate at the single-cell level. In other words, cell fates cannot be described by a handful of markers or cellular features, as the latter cannot discriminate between different cell states. Recent experimental (single-cell transcriptomic, CyTOF, etc.) and theoretical (mathematical description of the Waddington landscape, clustering methods, etc.) progresses have enabled to analyze and formalize the cell state dynamics using high-dimensional methods (Lang et al., 2014, Marr et al., 2016, Semrau and van Oudenaarden, 2015). This approach could be combined with dynamic, "low-dimensional" methods to better understand and guide the differentiation. Use of live reporters performing Boolean logic computation is an attractive tool for that purpose: several groups have used orthogonal TALEN or ZFN to build "AND" or "NAND" gates reporters (Lohmueller et al., 2012). We could imagine transposing these tools to distinguish between the partially programmed states and fully programmed states (e.g. building a reporter for the "PSM AND NOT lateral mesoderm" or "PSM AND NOT differentiated PSM"). However, it might be challenging to perform single-cell analysis if the desired state requires some collective state (e.g. high density, Notch signaling, etc.) as observed for the dissociated explant cells. Using conditions where those explants cells can individually oscillate would bypass this problem (e.g. latrunculin). Our work with explant cells also suggests that mechanical factors could have a significant impact on the cell state; therefore, non-canonical factors such as metabolic or mechanical conditions should be studied to better specify the PSM state. Besides, another avenue of research concerns the axial identity of the PSM-like cells. Indeed, preliminary results indicate that those cells mostly express anterior *Hox* genes, but it is not clear in the embryo how the most anterior somites are specified. As mentioned in the introduction, the patterning of the most anterior somites might be differently controlled. Mutants with PSM defects (*T, Wnt3a, Msgn1, Tbx6*) still form the most anterior paraxial tissues, suggesting that the gene regulatory network might be different. Similarly, the segmentation clock could evolve along the axial level, as

mutants overexpressing NICD still form anterior somites. Producing a more posterior tissue would require to generate the bipotent axial progenitor state. This population appears to be amplified at the tail stages (Tzouanacou et al., 2009), where they reside for a long-time in the tailbud and give rise to the more posterior tissues (Cambray and Wilson, 2007). Working with this population would also synchronize the cells in their differentiation path and provide a material closer to the explants, for which we have established appropriate culture conditions.

Concerning the differentiation path, obtaining more posterior axial progenitors will likely require a modulation of the BMP and Wnt signaling. Several groups have shown that adjusting the timing of Wnt signaling can alter the axial identity of stem cells during differentiation (Gouti et al., 2014, Lippmann et al., 2015). Besides, BMP signaling seems necessary to the maintenance of a tailbud state (as discussed above). Therefore, in the current protocol, early inhibition of BMP signaling could advance the transition to the PSM state and block the induction of the progenitor state. Alternatively, it was proposed that the acquisition of the neuromesodermal progenitor state depends on a special niche in the tailbud (Cambray and Wilson, 2007, Wymeersch et al., 2016). This would justify the use of organoids and other tridimensional cultures to recreate such environment. Another question related to the differentiation path is to avoid partially reprogrammed states. As discussed above, the PSM-like cells could be a combination of cell fates. Use of epiblast stem cells or human embryonic stem cells could improve the differentiation protocol by shortening the path to the PSM and reduce the likelihood of partially-reprogrammed states along the way. Tuning the dynamics of added factors could also guide the differentiation toward the PSM state. Indeed, most of the published protocols are based on the simple addition of factors. However, cells in the embryo are exposed to signals varying in space and time. Several studies have shown that the dynamics of a morphogen could encode information; for instance, Sorre, Warmflash and colleagues demonstrated that the speed of change to TGFβ can regulate its downstream signaling (Sorre et al., 2014). Other works point toward a tight control of the timing of differentiation, either because of a specific competency window (Jackson et al., 2010) or because of a "temporal race" between differentiation programs. Such competition between programs has been proposed in *B.subtilis* (Kuchina et al., 2011) and mouse embryonic stem cells (Turner et al., 2014b). More generally, biases in the differentiation trajectories could explain why some cellular types (e.g. neurons, cardiomyocytes) have been easily obtained in the field, while other cellular types are more difficult to target.

Together, this argues for a precise study of the attractors and differentiation trajectories and for a systemic sensitivity analysis of differentiation factors. It would likely require an experimental set-up able to screen a large number of conditions and to better explore the parameter space. Interesting progresses have been made in that regard, such as microfluidics device for high-throughput analysis

(Frank and Tay, 2013, Titmarsh et al., 2013) or automated culture of stem cells (Paull et al., 2015, Maury et al., 2015). Other advances have been reported to better interpret these observations using a theoretical framework, such as identification of "master regulators" (D'Alessio et al., 2015, Rackham et al., 2016) or evaluation of the reprogrammed state (Cahan et al., 2014, Morris et al., 2014, Uosaki et al., 2015). Importantly, these methods could detect partial reprogramming after directed differentiation or forced conversion, even if those cells displayed classical phenotypes of the desired state (Cahan et al., 2014). For instance, cardiomyocyte-like cells were able to contract with calcium oscillations and intracellular action potential, but a closer analysis revealed that they only established a small part of the cardiomyocyte gene regulatory network (Cahan et al., 2014). This forces us to remain cautious when evaluating a differentiation protocol and to prefer genome-wide comparison to *in vivo* tissues. For all these reasons, the so-called "network approach" or "stem cell engineering" will likely improve the existing protocols and better predict the parameters to control than the current "trial-and-error" approach.

Hypothesis 3: The Right Environment

An alternative (and not fully exclusive) hypothesis is that the generation of *LuVeLu* oscillations requires a special environment or special intercellular interactions. The former seems unlikely since we used the same experimental conditions for which explant cells display robust oscillations. The latter is, however, more likely, since dissociated explant cells did not show apparent oscillations of the *LuVeLu* reporter. Based on the expression of some PSM genes, we noticed that PSM-like cells have lower *Hes7* levels as dissociated explant cells. Few cells also display spikes of *LuVeLu* similar to the dissociated explant cells. Therefore, it is possible that PSM-like cells are stuck in an excitable state. We showed that an oscillatory state can be achieved either by increasing the cell density or by modifying the mechanical conditions (e.g. glass substrate or latrunculin). Since not all *Msgn1-mCherry* positive cells express *LuVeLu*, this could explain why even high density of cells activating the reporter cannot induce oscillations. In other words, the actual density of excitable (*i.e.* competent) cells is lower than the density of total *Msgn1-mCherry* positive cells. Identifying and adapting the conditions, for which dissociated explant cells autonomously oscillate, is therefore crucial to identify oscillations and optimize the differentiation protocol. Moreover, the behavior of other oscillators in PSM-like cells could be examined. Indeed, the different oscillators (e.g. Wnt, Fgf, metabolic, cell cycle) might be desynchronized and this lack of locking between oscillators could generate the aperiodic pattern we observed.

Limits of the stem cell approach

The initial rationale of using PSM-like cells was i) to better understand the establishment of the oscillatory state and ii) to provide a tool, notably for biochemical studies. We should, however, address the limits of this project. Concerning the understanding of the oscillatory state, one might argue that *ex vivo* systems offer now a better alternative since they are less prone to artifacts and better reflect the embryonic state. The progress in mouse embryo imaging and culture also enables to better observe the early embryonic stages *in vivo* when the segmentation clock first appears. Furthermore, it was shown that, even if cell states act as attractors, there is no unique trajectory leading to the final state. This was elegantly shown by examining the differentiation of neutrophils using two different protocols (Huang et al., 2005). In other words, it is not clear that the path taken by embryonic stem cells reflects the *in vivo* differentiation, especially considering the artificial culture conditions. Indeed, there is a growing recognition that mechanical and metabolic conditions are not only permissive factors, but can directly act on cell differentiation. We must thus remain circumspect in our conclusions and extrapolations to the embryo. Concerning the use of differentiated stem cells as a tool, major technological advances have been made to study biological processes, even at the single-cell level, such as RNA-seq, ChIP-seq, or proteomic. The need of a tool available in large quantity should likely diminish in the future, especially considering the major advantages of single-cell techniques. Moreover, one-step generation of mutants with CRISPR by direct injection in the zygote also eases the genetic manipulation of mouse embryo (Wang et al., 2013). Nevertheless, the use of differentiated stem cells has still much potential in the field of human biology, since embryonic systems are obviously unavailable. Stem cells have also a tremendous potential in translational research for regenerative medicine and for pharmacology studies. Notably, using a model of PSM cells *in vitro* could be beneficial in the study of scoliosis and in the identification of environmental factors favoring such malformations.

CONCLUSION

The points discussed in this thesis indicate several questions to address:

i)   What is the molecular mechanism underlying the activation of *Mesp2*? Mechanistic studies often provide a descriptive view of developmental processes, but rarely address their relevance in terms of patterning. However, in the case of Mesp2, understanding its regulatory mechanism will have important consequences to identify the molecular basis of the determination front and the final effector of the segmentation clock, but also to study how they are spatially controlled. This will clarify the role of each signaling and enable a better interpretation of experiments that mostly identify correlations with signaling pathways.

ii)   Another question follows: how is the segment determination spatially controlled? Especially, which mechanism provides positional information and how are the signaling gradients interpreted? Recent studies have challenged the classical clock-and-wavefront model, and proposed alternative parameterization of somitogenesis. Accordingly, somite size could be determined by the phase-gradient of the Notch oscillator or by the length-scale of a mechanical self-organization. If the Fgf/Wnt gradients do not position the determination front by a simple threshold, it will be important to understand how they are interpreted in the PSM and how the dynamics of this determination front is controlled (e.g. oscillator shift or a more general rearrangement of the gene regulatory network). Moreover, other works indicate a feedback of the segmentation clock on the "determination front" (as suggested by the interactions between the Hes oscillator and pERK pattern). This effect is worth studying to decipher whether there is a *bona fide* determination front that can be independently tuned or only a self-regulatory clock. More generally, the importance of self-organization *in vivo* remains to be clarified. Self-organization generally refers to a process by which only local interactions generate order at a higher level ("emergence"). However, the embryo already presents strong heterogeneities and polarities that preimpose an order. For instance, the maturation of the PSM is already ordered through the axis elongation and the gradients of Fgf/Wnt, so even if a gradient of maturation can emerge from a homogenous population *ex vivo*, it is not clear how this mechanism operates *in vivo*. Similarly, the fact that local mechanical interactions are sufficient to form somites does not preclude the existence of an upstream mechanism controlling the somite size in the embryo. In other words, self-organizing mechanisms can have an intrinsic length scale, but the relevant spatial information could still come from a more global, pre-ordered, system in the embryo. A last question related to the spatial organization of the PSM comes from the recent findings of Tsiairis and Aulehla, who identified a self-organization of PSM cells determination even in absence of collective Notch oscillations. The underlying mechanism has yet to be identified: by which process the cells communicate with each other to self-organize? A natural candidate is the Wnt oscillator, as it has self-organizing properties in other developmental systems and can operate independently of the Notch/Hes7/Fgf oscillators. Together, these findings have challenged the classical view of segmentation and prompt us to examine in more details the spatial control of somitogenesis.

iii)   What is the central pacemaker of somitogenesis? This long-standing question of the field is even more perplexing after the discovery of several independent oscillators and of a more complex regulation of the Notch oscillator (e.g. *Lfng* oscillations). The precise role of Notch signaling in this process remains to be elucidated, especially considering the different dynamics observed between models and species. Similarly, the function of the Wnt oscillator is poorly understood, as well as its architecture and its synchronization. Last, as mentioned in the introduction, other regulatory layers could work in addition to the transcriptional loops, such as metabolism or biomechanical and post-transcriptional processes, but their importance remains to be studied. Examining this molecular control would require the establishment of systems, where defined perturbations are applied and the response could be dynamically monitored and quantified. In contrast to the strong perturbations caused by genetic mutations, this should give us a finer understanding of the segmentation clock.

iv)   How to explain the interspecies differences in body axis organization? We have discussed the relationship between the axial elongation and the existence of a clock mechanism. How this coupling occurs (passive vs. active) and how it can be tuned during evolution to produce patterns with different number, size or identity of segments remain to be answered. For instance, the differences in clock periods are poorly understood, and tentative to modify it (e.g. introns mutants) often failed to generate viable animals. This is even more puzzling considering that only a minor change in the oscillation period (~9%) disrupts the segmentation clock in these embryos, while large variations have been adopted during evolution (e.g. ~4.5-fold between zebrafish and mouse). Similarly, changes in somitogenesis rate can occur along the axial position (up to 4-fold in marsupials (Keyte and Smith, 2012)). As the genetic network appears relatively inflexible, the observed plasticity could originate from upstream regulations in metabolism, but how evolution can act on this process and how it can be uncoupled from other heterochronies (notably the *Hox* patterning) remain elusive. Therefore, a future challenge will be to comprehensively predict and engineer embryos with different axial patterning.

MATERIAL AND METHODS

Chapter I

Chicken embryos culture – Embryos manipulations were performed as in (Benazeraf et al., 2010). Briefly embryos were incubated in a humidified incubator 38°C. For electroporations, embryos were incubated for 23-24h and prepared for Early Chick (EC) cultures on a paper ring. For electroporation, a DNA solution (~5.0 μg/μl) with Fast Green was microinjected in the space between the vitelline membrane and the epiblast surrounding the anterior primitive streak level which contains the precursors of the paraxial mesoderm. *In vitro* electroporations were carried out with five successive square pulses of 8V for 50ms, keeping about 4mm distance between anode and cathode using Petri dish type electrodes (CUY701P2, Nepa Gene, Japan) and a CUY21 electroporator (Nepa Gene, Japan). Embryos were cultured on a plate consisting of Bacto-Agar (BD Biosciences) and albumen in presence of glucose (0.15%), sodium chloride (61.5mM) and penicillin-streptomycin (10U/mL). Movies were performed as described in (Benazeraf et al., 2010). For chemical treatment, 100μL of PBS with drug or vehicle control were dispensed below and above the embryo.

Chicken *in situ* hybridization – Wholemount *in situ* hybridization was performed as in (Henrique et al., 1995). For fluorescent *in situ* hybridization, we used the anti-digoxygenin POD antibody (Roche – 1:1000); after washes, we rinsed three times in PBT (0.1% Tween-20), once with the amplification buffer of the TSA Plus Fluorescein kit (Perkin Elmer) without fluorophore, and then we incubated in fresh amplification buffer with fluorophore (1:100) for 15 minutes at room temperature. Embryos were then washed three times with PBT. For double fluorescent *in situ* hybridization, the Venus probe was synthesized using Fluorescein-12-dUTP; after the first revelation of the Meso2-digoxigenin probe, embryos were incubated in PBT, 3% H_2O_2 to inactivate the HRP ; the same procedure was performed using the anti-fluroescein antibody coupled to HRP and the TSA Plus Cy3 kit (Perkin Elmer). Probes used were: Meso2 (Buchberger et al., 2002) and exonic Fgf8b (Dubrulle and Pourquié, 2004). For single-molecules Fgf8, chicken embryos were similarly processed until the hybridization step. Hybridization was performed in 2x SSC, 35% formamide, 0.1% Tween-20, 0.1g/mL dextran sulfate, 0.1mg/mL Salmon sperm ssDNA, 2mM Ribonucleoside Vanadyl Complex, 20 μg/mL RNAse-free BSA. RACE experiment to determined the 3'-UTR of Fgf8b was performed using the ExactSTART Eukaryotic mRNA 5'- & 3'-RACE Kit according to the manufacturer's instructions. Customed probes for Fgf8b were obtained from Stellaris with Quassar 570 dye:

atgaacacgtagctgaagag; caggcagaggacgaacaagt; ggactgaacagttacctggg; cctcacatgctgtgtaaaat; ctgagctgatctgtcaccag; ttgtccaagatctgcacgtg; ggccatcgcattgattttct; gagcttggcgtgcacatccc; caaaggtgtcggtctcgacg; cctttgatgcgcacgcggct; gttactcttgccgatcagtt; tcgtacttggcgttctgcag; cttcatgaagtgcacctcgc; gtagttgaggaactcgaagc; ttttgctcctgcggttgaag;

caccctggcgctggagtttc; aatgtctctacgtcagtcca; ccccgttgggtttttttttt; agcatgtagttctcgtatcc.

Probes were incubated overnight at 30°C, then embryos were rinsed and washed twice in 2X SSC, 35% formamide, 0.1% Tween-20; last embryos were washed three times in PBT and mounted in FluoromountG.

Meso2 and Msgn1 reporter – 3 kb genomic region upstream of Meso2 starting codon (using the following primers: cacccactgcgggtgtaaaggtttc and ggcagccctggctttatgtg) and 5 kb genomic region upstream of Msgn1 starting codon (using the following primers: caccgtatcagtgcaatggcaggaag and agcaccacaagtgctaagatgg) were amplified using the Accuprime Pfx DNA polymerase (Life Technologies) according to the manufacturer's instructions. After purification, this region was cloned into the pENTR/D-TOPO vector (Life Technologies) using TOPO cloning according to the manufacturer's instructions. The region was then cloned into the pGL4.10-RFA-Venus vector, a plasmid made by N.Denans where an enhancer region can be inserted upstream of the Venus coding frame.

Constructs – Fgf8-Venus fusion, Tbx6 ORF, destabilized were cloned using the Accuprime Pfx DNA polymerase (Life Technologies) according to the manufacturer's instructions using the PCR assembly method and standard restriction-ligation techniques.

Chicken immunohistochemistry– Chicken embryos were fixed in PBS, 4% PFA at 4°C for approximatively 2h30-3h (depending on the dissection order). Embryos were dissected in PBS and washed 2x10 minutes with PBT (Tween-20, 0.1%). Endogenous peroxidases were inactivated by incubating the embryos in cold PBT, 1% H_2O_2 at 4°C with gentle agitation. Embryos were rinced once and washed 3x10 minutes in PBT at RT. Embryos were incubated in blocking solution (PBS, 5% FBS, 1% BSA, 0.1% Tween-20, 0.05% TritonX-100) for 5 minutes at RT, then blocked 2x30 minutes at 4°C (or 2x5 minutes at RT). Blocking solution was change and primary antibody (N-19, Santa Cruz) was added at 1:100 for 2 days at 4°C. Embryos were washed 3x10 minutes, 6x30 minutes in PBTT (0.1% Tween-20, 0.05% TritonX-100) at RT with gentle agitation. Embryos were incubated blocked in the previous blocking solution for 1 hour at 4°C (or 15 min at RT). Blocking solution was changed and secondary antibody (Donkey anti-Goat, HRP-coupled, Santa-Cruz) was added at 1:500 at 4°C overnight. Embryos were washed 3x10 minutes, 6x30 minutes in PBTT at RT with gentle agitation. PBTT was removed as much as possible and embryos were incubated for 5 minutes in diluent buffer of TSA kit (Perkin Elmer). Diluent buffer with Tyramide-fluorescein (1:100) was incubated in the dark at RT for 30 minutes. Embryos were then rinced and washed 3x10min in PBTT at RT. DAPI (Invitrogen) was added in PBTT at 1:1000 for 20 minutes at RT, then washed 2x10 minutes in PBTT. Embryos were mounted in Fluoromount G. For double immunohistochemistry with Msgn1, rabbit polyclonal antibody from J.Chal was added at 1:400. For

single immunohistochemistry with Msgn1 alone, embryos were fixed overnight, washed were done using PBT. For immunohistochemistry of phosphorylated ERK, we followed a protocol from J.Rossant lab, where embryos are fixed in PFA, 6%, dehydrated in EtOH after fixation; we used the mouse monoclonal antibody MAPK-YT (Sigma – 1:250).

Phosphoproteomics – Chicken embryos were incubated for 2 days (~stage HH10), and prepared on filter. They were then reincubated for at 38°C in presence of PD0325901 (10μM) or DMSO for 4-4.5 hours. Embryos were then dissected in cold PBS using pancreatin using tungsten needles. We dissected both PSM, rinsed into cold lysis buffer (from M.Washburn (Stowers Institute): 20mM HEPES pH7.4, 10% glycerol, 0.35M NaCl, 1.5mM $MgCl_2$, 0.2mM EDTA, 0.1%TritonX-100) with proteases and phosphatases inhibitors (Roche), then PSM were transferred into fresh lysis buffer and snap frozen in liquid nitrogen. Samples were then processed by the Thermo Center for Multiplexed Proteomics: proteins were precipitated using methanol/chloroform, digested using LysC and trypsin, and labeled with TMT reagent (channels 127-128). Protein amount were quantified using the micro-BCA assay (Pierce): DMSO sample:44μg; PD03 sample:38μg). Labeled peptides were combined, desalted, resuspended in binding buffer and incubated with Titanium dioxide coated beads. Beads were washed several times, and phosphopeptides were eluted and desalted. Eluates and unbound fractions were analyzed on an Orbitrap Fusion mass spectrometer: peptides were separated using a gradient of 0 to 25% acetonitrile in 0.125% formic acid over 255 minutes. Peptides were detected (MS1) and quantified (MS3) in the Orbitrap. Peptides were sequenced (MS2) in the ion trap. MS2 spectra were searched using the SEQUEST algorithm against a Uniprot composite database derived from the chicken proteome containing its reversed complement and known contaminants. Phosphopeptide spectral matches were filtered to a 1% false discovery rate (FDR) using the target-decoy strategy combined with linear discriminant analysis. The proteins were filtered to a <1% FDR Proteins were quantified only from peptides with a summed SN threshold of >=100 and MS2 isolation specificity of 0.5.

Standard procedures were followed for the western blot. Briefly, protein lysates were denatured in Laemmli buffer and heated at 100°C for 10 minutes. The samples were then loaded on a 12.5% acrylamide gel, transferred on a nitrocellulose membrane, blocked in PBT/5% milk and incubated with the following primary antibodies: dpERK (Cell Signaling, #4370 - 1:2000) and β-Actin (Abcam, AC15 - 1:5000). After washes, membranes were incubated with the following secondary antibodies: Goat anti-Mouse (Jackson, #115-035-062 - 1:20 000) and Donkey anti-Rabbit (GE healthcare Amersham, NA934VS – 1:15 000), washed and revealed with the Immobilon kit (EMD Millipore) according to the manufacturer's indications.

Chapters II & III

Explant cultures – All animal experiments were performed according to the institutions guidelines. *LuVeLu* male mice were crossed with wild-type CD1 female mice. Several genetic backgrounds were used without any noticeable effect on our experiments: 100% BL6 *LuVeLu* +/- males, 50%BL6;50%CD1 *LuVeLu* +/- males; 50%BL6;50%DBA/2 *LuVeLu* +/- males; 50%BL6;25%DBA/2;25%CD1 *LuVeLu* +/+ males (for most of the experiments). Embryos were collected at E9.5: the uterus was dissected and single embryos were isolated in PBS. Embryo tails were then dissected out in DMEM with penicillin-streptomycin. Tails were then rinsed twice with PBS to remove blood traces, rinsed once in Accutase (Life Technologies) and incubated in fresh Accutase at 37°C. After 5min30, embryos were gently swirled, and after 6min30 were rocked back-and-forth (this step supposedly helps to detach the ectoderm). After 7min30, embryos were taken out of the incubator and examined; at this step, the ectoderm should appear detached from the tailbud mesenchyme (this is a key landmark for the following dissection: a poor detachment impedes the correct isolation of the tailbud mesenchyme, while an excessive dissociation produces "loose" tissues). If the dissociation was insufficient, embryos were rocked back-and-forth and further incubated in Accutase at room temperature. Embryos were then rinsed once in DMEM, and incubated in dissection medium (DMEM 4.5g/L Glucose, 15% FCS ESC-tested, 2mM L-Glutamine, 100U Penicillin, 100 µg/ml Streptomycin, 1x non-essential amino acis, HEPES 10mM). The tailbud mesenchyme was then isolated from the surrounding tissues and transferred into a Petri dish. Tailbuds were then rinsed once in explant medium (dissection medium with 0.1mM of β-mercaptoethanol, CHIR-99021 (Sigma/Tocris) 3µM, LDN-193189 (Sigma/Stemgent) 200nM, BMS-493 (Sigma) 2.5 µM, mFgf4 (R&D) 50ng/mL, heparin (Sigma) 1µg/mL and Y-27632 (P212121/Tocris) 10µM) and transferred into culture dishes. Up to five embryos were cultured in one well of a LabTek 8-well dish (450-500µL) and positioned to avoid contact. Dissection medium was filtered using a 0.22µM filter and kept in the dark at 4°C for up to two weeks (we did not notice any noticeable effects between FBS batches). All factors were aliquoted and kept at -80°C; hydrophobic compounds were kept in the dark at 4°C for up to two weeks, Fgf4 and Y-27632 were kept in the dark at 4°C for up to one week, and heparin was kept at in the dark at 4°C for up to one month.

Explants were cultured on LabTek dishes coated with human plasma fibronectin: a solution of 4µg/mL fibronectin in PBS was incubated for 2-3 hours at room temperature (250µL for a well of a LabTek 8-wells dish). The dish was rinsed twice with PBS and incubated for at least 1h in dissection medium without HEPES. For experiments using the micropatterns, explants were cultured on 96-wells plate (tissue-culture treated) that was similarly coated with fibronectin; one explant was cultured per well in 100µL.

For the experiment with NICD overexpression, a male homozygous for the transgene Gt(ROSA)26Sor[tm1(Notch1)Dam] was crossed with a female homozygous for the *LuVeLu* transgene.

Time-lapse imaging – Imaging was performed on a Zeiss LSM780 microscope using a 20X/0.8 objective at 37.2°C, 7.5% CO_2. Explants were excited using a 514-nM argon laser (the intensity was determined to obtain a good signal without saturation), and the signal was recorded with GaAsp detectors array. A single section (~19.6μm wide) with tiling (3x3) of a 512x512 pixels field (with 10% overlap) was acquired every 7.5 minutes (for most of the experiments) at 8-bits resolution.

Micropattern experiment – For micropattern experiments, ~35 explants were cultured overnight, rinsed with PBS and dissociated with 27μL of trypsin 0.05%-EDTA (18mM) at room temperature with gentle rocking. Trypsin was blocked using the explant medium (~75μL- medium from the overnight culture), explants were dissociated by pipetting up-and down twice and collected in 1.5mL Eppendorf tubes. Cells were then spinned with an Eppendord centrifuge 5430 (1810rpm/370rcf for 4min at room temperature). The supernatant was then aspired and cells were resuspended in 400μL of fresh explant medium by gently pipetting up-and-down the pellet. 100μL of cells suspension was dispensed on a Cytoo 4-wells chamber with a CYTOOchip Arena coated with fibronectin. The chamber was previously rinsed twice with PBS and incubated with dissection medium without HEPES for ~20 minutes. The chamber was let at room temperature for 10 minutes (without any movement to let the cells attach), then carefully transferred in a cell culture incubator at 37°C. After ~45 minutes, the medium was carefully aspired to remove floating cells and cells were rinsed once with 250μL of dissection medium. Cells were then cultured with fresh explant medium (250μL per well).

Explant manipulation – For dissociation-reaggregation experiment, we followed a similar procedure as for the micropattern experiment with the following modifications: cells were mixed and the equivalent of ~2 explants was spun in a single tube, the pellet was very gently detached and transferred in a dish.

For removal of explant regions, we either removed the region using a pipette tip or a two-photons laser two-photons laser (Ti:Sapphire laser – Chameleon-Ultra coherent at a wavelength of 800 nm).

Genotyping – Genotyping was performed by digesting tails in lysis buffer (500μL /tail – composition: NEB Taq PCR buffer, 0.2% Tween-20, 250ug/mL of proteinase K) at 55°C with shaking (300rpm, on thermomixor). The proteinase K was denatured by incubating at 95°C for 10 minutes. Tubes were spun down to remove hair and kept at 4°C. PCR was performed using the following primers: `gtaaacggccacaagttcagc` and `ttgtagttgtactccagcttgtgc`. To identify homozygous *LuVeLu* mice, tail samples were analyzed by Transnetyx and we evaluated the number of copies based on the qPCR amplification.

Microarrays- Six explants from littermate embryos were cultured for 17 hours, before addition of PD0325901 (2μM) and vehicle control (DMSO). Two explants for each condition were imaged to check the representativeness of the experiment. After 14.5 hours, explants were lysed using Trizol (ThermoFisher Scientific) and RNA was extracted according to the manufacturer's instructions. Purified RNA were analyzed by the Molecular Biology Core Facilities at the Dana-Farber Cancer Institute according to the protocol used in (Chal). Bbriefly, cRNA was amplified, fragmented and hybridized on Affymetrix GeneChip Mouse Genome 430 2.0. Preprocessing, including background correction, quantile normalization and summarization, was performed using the RMA method. To measure the distance between samples, we used the Euclidean method (Quackenbush, 2001) by comparing the transcripts expression in each triplicate to their average expression in embryonic tissues. To enrich for genes whose expression changes during PSM differentiation, we selected transcripts with a fold-change above two between the maximal and minimal values in the PSM1-6 series in (Chal et al., 2015). A heatmap was done using Matlab showing the average distance to each of the PSM pieces (PSM1-6). To perform the PCA analysis, we used the bioconductor package with RMA normalization on R.

Immunohistochemistry - Explants were rinsed with PBS and fixed in fresh PBS, 4% PFA, then rinsed, washed three times in PBT and blocked with 10%FBS. Explants were then incubated overnight at 4°C with the following antibodies in PBT, 5% FBS: anti-Tbx6 (gift from Yumiko Saga– 1:400), anti-phospho-p44/42 MAPK (Erk1/2)(Thr202/Tyr204) (D13.14.4E) (Cell Signaling Technology #4370 - 1:200), anti-Brachyury (R&D Systems - AF2085 –1:1000), anti-Yap (Santa Cruz 63.7 – 1:200). Explants were then rinsed twice and washed six times for ~15 minutes at room temperature in PBT. Explants were block with PBT, 10% and secondary antibodies coupled with Alexa fluorophores (Life technologies) were incubated overnight at 4°C in PBT or for 2 hours at room temperature, 5% FBS. Nuclear staining was performed with Hoechst33342 (1:4000) and explants were mounted in FluoromountG.

In situ **hybridization** – Explants were fixed in fresh PBS, 4% PFA, and then rinsed, washed twice in PBT for 5 minutes. Samples were dehydrated in a sequence of PBT/MeOH (1:3, 1:1, 3:1), rinsed twice and incubated for ~30-60 minutes with pure cold methanol. Samples were rehydrated with a sequence of PBT/MeOH and washed three times with PBT for 5min. Explants were treated with proteinase K (1μg/mL in PBT) for 5min, then rinsed with PBT and fixed with PBT, 4% formaldehyde, 0.2% gluraldehyte for 20 minutes at room temperature. Samples were then washed twice in PBT, once in PBT/hybridization solution and twice in hybridization solution. The hybridization solution composition is 50% formamide, 5xSSC pH4.5, 1% SDS, 50μg/mL yeast tRNA, 50μg/mL heparin. Fresh hybridization solution was added and samples were incubated at 70°C for at least 2h. After this prehybridization, fresh hybridization solution with 500ng/mL of

digoxigenin-labeled probes was heated at 70°C for ~10min and added to the samples for an overnight incubation at 70°C. Samples were rinsed twice and washed three times for 10-15 min with prewarmed Solution I (50% formamide, 5xSSC pH4.5, 1% SDS), and then rinsed once and washed three times for 10-15min with prewarmed Solution III (50% formamide, 2xSSC pH4.5, 0.11% Tween-20). Samples were cooled in Solution III at room temperature, rinsed twice and washed three times with TBT (TBS, 0.1% Tween-20). Explants were blocked twice using TBT, 20% GS, 2% Boehringer Mannheim blocking reagent. Antibody against digoxigenin coupled to alkaline-phosphatase coupled (Roche) was incubated overnight at 4°C in blocking solution. Samples were rinsed twice and washed six times with TBT. Then, explants were rinsed twice and washed three times with NTMT. Last, samples were rinsed once and incubated with BM Purple (Roche) at room temperature. For fluorescent *in situ* hybridization, an additional step with 3% H2O2 was performed after methanol dehydration. The anti-Digoxigenin-POD (poly), Fab fragments from Roche (11633716001) was used at 1:200 and the TSA Plus Cyanine 5 System kit was used with a dilution of 1:100 and an incubation time of 20 minutes. Pictures were taken on Leica M205FA (note that the tissue culture plate produced an inhomogeneous illumination and that the BM Purple staining reduced the intensity of the nuclear staining).

Probe preparation- *in vitro* transcription was performed on linearized plasmids or PCR products using the T3, T7 or Sp6 polymerases. DNA was then degraded using RQ1 DNase1 and RNA was precipitated using LiCl and ethanol. Probes were analyzed on agarose gel to confirm the purity and the size of the solution. The probes used were: intronic Hes7 (first intron), Msgn1 (coding sequence), Spry2 (Wahl et al., 2007).

Treatments – Explants were treated with PD0325901 (Sigma- concentration as described in the text), PD173074 (Sigma - 250nM), DAPT (Sigma - 20μM), LY-411575 (Sigma - 100 nM), cycloheximide (Sigma - concentration as described in the text), Sal003 (Sigma -10μM), ISCRIB (Sigma – 20/200nM), RGDS peptide (Cayman - 1mM), Dkk1 (R&D – 500ng/mL), ICRT14 (Sigma - 10 μM), IWR-1 (Sigma - 5μM) , MG-132 (Sigma – 0.2μM), KU-0063794 (Sigma - 1μM), latrunculin A (Tocris – 0.5μM), TAT-Cre (Excellgen -6 μM).

Image analysis - Kymographs were done in Fiji by drawing a rectangle from the starting center of the traveling waves to the edge of the explant perpendicular to the direction of the wave. The intensity along the long axis was measured and the image was smoothened (this filter replaces each pixel with the average of its 3×3 neighborhood).

Fluorescence intensity profiles were done by selecting a circular region of interest in FiJi and by measuring the total intensity over time for this region; *LuVeLu* intensity is given in arbitrary units (normalized by the initial value) and a smoothing function (average over three points) was applied.

For the quantification of nuclear staining and pERK intensity, a rectangular region of interest was drawn (as shown in Fig.1) and analyzed using Matlab: the region (830μm in length) was divided in 20 boxes along the center-periphery axis; the fluorescence intensity signal was measured within each box, and then normalized by the minimal value of the serie.

For single-cell tracking, we manually tracked cells that have no/few contacts with other cells. For cells on fibronectin, a contour was manually drawn using FiJi for each time point; for latrunculin A treated cells a circle of constant area was drawn for all time-points. We obtained the raw mean fluorescence of the *LuVeLu* reporter and subtracted the mean background fluorescence of a region near the cells; we then normalized all data by dividing to their first value. Fluorescence intensity shows the mean fluorescence smoothed by applying a moving average over five points (with equal weight). To obtain the "instantaneous" intensity, we subtracted the mean fluorescence averaged over 150 minutes ("moving average") to the mean fluorescence at each point as in (Delaune et al., 2012), and then applied a smoothing over five points. Fast fourier analysis was performed and plotted with Matlab using the fft function.

For the quantification of micropattern experiments, a region of interest encompassing the entire surface of one circle (80 μm diameter for Fig.2B, 225μm diameter otherwise) was drawn and the *LuVeLu* intensity was measured using the Time Series Analyzer V3 plugin on Fiji. The period in Fig.4E was measured by measuring the time between two peaks or two troughs. The average intensity was measured by averaging the intensity over 3 hours to avoid instantaneous variations dues to the oscillations.

Statistics - For the measurement of the period between the center and the periphery, four explants were used and the period was measured as the time between two troughs. This gave 33 measurements for each condition (center vs. periphery), a two-tailed (equal variance) t-test was performed using Excel. We performed similar procedure to analyze the effect of translation inhibitors on the period. The same test was used for the period with translation inhibitors.

SunSET method – Explants were treated with 10μg/mL of puromycin (Sigma) for 20min at 37°C. As control, cycloheximide (16μg/mL) was added 15 minutes before the puromycin incubation. Explants were then fixed and standard immunostaining was performed using the anti-puromycin antibody (clone 12D10– EMD Millipore at 1:8000).

qPCR – RNA were extracted using Trizol (Life Technologies) according to the manufacturer's instructions. RNA concentrations were measured using a Nanodrop. Reverse transcription was performed with the same amount of total RNA using the Superscript III kit (Life Technologies) according to the manufacturer's instructions (with a 1:1 mix of oligo-dT/random hexamers). Real time PCR was performed on a Biorad CFX384 using iTaq Universal SYBR Green Supermix

according to the manufacturer's instructions. For the real-time PCR, triplicates were performed and analyzed using the ΔΔCt method: i) Ct values were automatically retrieved from the CFX manager software (Biorad); ii) triplicates were averaged (if one sample was obviously different from the two others, it was excluded); iii) for each sample, the Ct for actin was subtracted (ΔCt); iv) for each sample, the ΔCt of the reference sample was subtracted (ΔΔCt); v) the fold change was determined as $2^{-\Delta\Delta Ct}$. Standard deviations s_i for the Ct values were calculated, then standard deviations s_i^* for the ΔCt values were calculated as follows: $s_i^* = \sqrt{\left(\sqrt{s_i^2 + s_{housekeeping}^2}\right)}$; the range for fold change was determined as $2^{-\Delta\Delta Ct \pm si^*}$.

Primers were validated by checking that the melting curve had a single defined peak and by validating the efficiency (between -3.6 and -3.2) of amplification using serial dilution.

Gene	Forward primer	Reverse primer
Msgn1	CGGCTTAGTCGAGCTGGATTA	CTCCGCTGGACAGACATCTTG
Tbx6	ATGTACCATCCACGAGAGTTGT	GGTAGCGGTAACCCTCTGTC
Hes7	CGGGAGCGAGCTGAGAATAG	CACGGCGAACTCCAGTATCT
Sprouty2	CATCAGGTCTTGGCAGTGTG	AGAGGATTCAAGGGAGAGGG
Actin	GTGACGTTGACATCCGTAAAGA	GCCGGACTCATCGTACTCC
Pea3	CAGGTACCGGACAGTGATGAG	GGTTCCTTCTTGATCCTGGTG
Sp5	GGCCTTCAAGCAGTAGCCA	GAGTGCTTGCCCAGGTCC
Foxc2	AACCCAACAGCAAACTTTCCC	GCGTAGCTCGATAGGGCAG
Ripply2	AAGATGACCGCATTATGTTCACG	TGACAAAGCCAATAGACTTGAGG
Dusp6	CTGGTGGAGAGTCGGTCCT	CGGCCTGGAACTTACTGAAG
Pea3 (intronic)	CAGACAAATCGCCATCAAGTC	GAGGCTCTGCTGCTGTTCTG
Dkk1 (intronic)	TCCTGACACATCGTCACTGGC	TCTCAAGTGCCCCAAGGCTC
Dkk1 (exonic)	CTCATCAATTCCAACGCGATCA	GCCCTCATAGAGAACTCCCG
Dll1	TCAGATAACCCTGACGGAGGC	AGGTAAGAGTTGCCGAGGTCC
Notch1	GCCGCAAGAGGCTTGAGAT	GGAGTCCTGGCATCGTTGG
Lfng	TGTTTGAGAACAAGCGGAAC	CAGGGTGTGTCTGGGTACAG
CTGF	AGGAGTGGGTGTGTGACGAG	ATGTGTCTTCCAGTCGGTAGG
Cyr61	GAAGAGGCTTCCTGTCTTTGG	GTCTGAACGATGCATTTCTGG
ANKRD1	ACGTCTGCGATGAGTATAAACG	CCAGCCTCCATTAACTTCTCC

Simulations – Simulations were performed on Matlab. We used the following FitzHugh-Nagumo equations:

$$\frac{\delta u}{\delta t} = \frac{1}{ta} u(a-u)(1-u) - v + I + J\nabla^2 u$$

$$\frac{\delta v}{\delta t} = \frac{1}{tb}(u - gv)$$

With ta=10, tb=0.6, J=0.1, g=0.4; initially both substances are absent. We simulated the behavior of a grid of cells using the Runge-Kutta method. To simulate the dose-dependency of Fgf/ERK inhibitor, we hypothesized that inhibiting Fgf increases the variable I over time such as:

$$I(t) = \exp(c.t)$$

We first let the system reached a steady state and then increase the intensity: we assumed that c is proportional to the strength of Fgf inhibition (c=0/0.0012/0.0017/0.0024). We measured the period as the time between two peaks and the average intensity as the average intensity over one period.

Section – E9.5 embryos were fixed in PFA 4%, then rinsed twice and washed three times with PBT. Embryos were transferred in 10/20/30% sucrose and incubated overnight in 30% sucrose. Embryos were then transferred in OCT and frozen. Sections were performed using a Leica cryostat CM3050S. Standard immunostaining was then performed.

Lentivirus production – Plasmids expressing shRNA-scramble and shRNA against Yap1 (pLKO.1 backbone) were obtained from Addgene (#1864 and #42540 - gifts from the groups of D.Sabatini and W.Hahn). Lentiviruses were produced in 293T cells: cells were seeded on plates coated with poly-ornithine. After one day, cells were transfected with the CaCl$_2$ method (using pLKO.1 plasmids, psPax2, and a plasmid coding for VSG-G). The medium was changed the next day and cells were incubated for another day. The supernatant was collected, filtered using a 0.45μm membrane, and kept at 4°C for up to two weeks. For the infection, explants were cultured in 96-wells plates in 80μL explant medium/ 20μL supernatant in presence of polybrene (8μg/mL). After 8h, the medium was removed and fresh explant medium was added.

Chapter IV

Derivation and culture of mESC – Blastocysts were collected from E3.5 embryos by flushing in M2 medium. Single blastocysts were transferred in a 96-well plate with inactivated embryonic feeders in ES medium (DMEM 4.5g/L Glucose, 15% FCS ESC-tested, 2mM L-Glutamine, 100U Penicillin, 100 µg/ml Streptomycin, 1x non-essential amino acis, 0.1mM β-mercaptoethanol) in presence of LIF (~1750U/mL) and "2i": PD0325901 (1µM) and CHIR99021 (3µM). mESC were cultured at 37°C in5%CO_2 in ES+LIF on feeders for the one-step protocol or ES+LIF+2i on feeders for the two-steps protocol. Cells were passed using trypsin-EDTA.

Msgn1-mCherry reporter – A cassette comprising the NLS sequence of the SV40 large antigen, the ORF of mCherry, the PEST d4 sequence (Clontech) and the bovine hormone growth hormone polyadenylation sequence was assembled by PCR and cloned into the a plasmid containing a 6.5kb enhancer sequence of Msgn1 (Wittler et al., 2007). The plasmid was linearized and transfected using Lipofectamine 2000 according to the manufacturer's instructions. Clones were selected using G418 (350µg/mL) and single colonies were picked.

One-step differentiation - Cells were differentiated for three days using ES base medium in presence of CHIR99021(1µM), DMSO 0.5% and LDN-193189 (0.1µM). Culture dishes were coated with fibronectin (2µg/mL for at least one hour in PBS) and cells were seeded at a density of 11'000 cells per cm^2.

Two-steps differentiation - Cells were differentiated for two days using N2B27, 1% KSR and two days in ES base medium in presence of CHIR99021(1µM), DMSO 0.5% and LDN-193189 (0.1µM). Culture dishes were coated with fibronectin (2µg/mL for at least one hour in PBS) and cells were seeded at a density of 11'000 cells per cm^2.

qPCR –Total RNA was extracted with Trizol (Life Technologies) according to the manufacturer's instructions. Reverse transcription was performed using the Quantitect reverse transcription kit (Qiagen) according to the manufacturer's instructions. Real-time quantitative PCR was performed using the Quantifast SYBR Green RT-PCR Kit (QIAGEN) in a LightCycler 480 II System (Roche). Analysis was performed using the ΔΔCt method as previously explained.

Immunohistochemistry – Cells were fixed with PBS, PFA 4% for 30 minutes, washed three times for 10 minutes with PBT (Tween 20, 0.1%), permeabilized for 10 minutes with PBT, 0.1% TritonX-100, blocked with PBT, 10% FBS. Antibody against Tbx6 (polyclonal antibody from Y.Saga - 1:400) was incubated overnight at 4°C. Cells were rinsed, and then washed three times with PBT. Secondary antibody coupled to Alexa 488 (1:500) was incubated overnight at 4°C. Cells were rinsed, and then washed three times with PBT.

FACS – Cells were dissociated, filtered and sorted using a FACS Aria (BD Biosciences) or S3 cell sorter (Bio-Rad) at room temperature.

Knock-in generation – To generate knock-in, we designed sgRNA using the Genome Engineering software from Feng Zhang's lab: `accttggccctgagcttttgggg` and `caaggtctccaaaacgcgggcgg`. We cloned two sgRNAs into the pX335 vector (F.Zhang lab – containing the nickase form of the Cas9) using BbsI. Those plasmids were transfected with the targeting vector (described below) at a molar ratio of 1:1:1 using Lipofectamine 2000 according to the manufacturer's instructions. mESCs were then selected using G418 (350µg/mL) and single colonies were picked. Cells were lysed in the following buffer: Roche Long Expand Buffer 2 (1X), Proteinase K200µg/mL, Tween20 0.1%, and incubated overnight at 55°C. Proteinase K was then inactivated by a 30 minutes incubationg at 85°C. Clones were first screened by performing a PCR with a primer specific to the recombination cassette and a primer targeting a sequence outside the short arm of the targeting vector using the Roche Long Expand polymerase according to the manufacturer's instructions. Positive clones were further screened for the number of copies by performing qPCR with primers amplifying the Neo^R cassette (Neo-fd1: `cttcccgcttcagtgacaac;` Neo-rv1: `cctgaatgaactgcaggacg;` Neo-fd2: `cgtcctgcagttcattcagg;` Neo-rv2: `ttgggtggagaggctattcg`) and the Msgn1 locus (qPCR primers). The selection cassette was then removed by transient transfection of the flippase; single clones were picked and tested for antibiotic resistance.

Targeting vector for the C-terminal fusion of mKate2 in the Hes7 locus: two homology arms (~4 kb each: 5' arm: [`gaattctaccactgaaccaccaatg…cgcccgcgttttggagaccttggccc`]; 3' arm: [`gcttttggggggctggggcggggattgggggtgg…tcagatcatgggtctcctgttctttgggagggg tc`] were cloned by the J.M. Garnier with a FseI site in-between. A cassette comprising a sequence for a flexible linker (GSGAAAAGGS), the ORF of mKate2 (kind gift of A.Oates) and a selection cassette FRT-PGK-Neo-FRT was inserted in the FseI site.

Targeting vector for the C-terminal insertion of mKate2: the same homology arms were used. A cassette comprising a sequence for a flexible linker (GGGSG), a sequence for the self-cleaving peptide P2A, and the ORF of mKate2 was inserted in the FseI site.

Knock-in for the C-terminal fusion of sfGFP in the Hes7 locus: the knock-in was performed by the Mouse Clinical Institute. We used the following design: a C-terminal fusion of a flexible linker (GSGAAAAGGS) followed by the ORF of the human codon optimized sfGFP (kind gift of Michael Knop lab) and a LoxP-Neo-LoxP cassette.

Microfabrication - Masks were designed using Autocad and printed by the company Selba. Molds for PDMS were prepared at the IPCMS of Cronenbourg with C.Paoletti: wafer were incubate at 200°C for at least 10 minutes and let cool. SU-8 was added, spinned and baked at 65°C, then 90°C (pre-exposure baking). The wafer was exposed to UV with the mask, and then baked 65°C, then 90°C (post-exposure baking). After development, the wafer was dried and hard-baked at 200°C.

To prepare PDMS chips, we put together PDMS and its catalyst (Sylgard 184 – Dow Corning) at a 10:1 ratio and thoroughly mixed. Air bubbles were removed with a vacuum. The PDMS was baked at 60°C overnight, at 80°C for 2h or at 90°C for 1h. The PDMS was made hydrophilic by a treatment with plasma cleaner and immediately sealed to a glass coverslip.

References

ABRAHAM, N., STOJDL, D. F., DUNCAN, P. I., MÉTHOT, N., ISHII, T., DUBÉ, M., VANDERHYDEN, B. C., ATKINS, H. L., GRAY, D. A. & MCBURNEY, M. W. 1999. Characterization of transgenic mice with targeted disruption of the catalytic domain of the double-stranded RNA-dependent protein kinase, PKR. *Journal of Biological Chemistry,* 274**,** 5953-5962.

ABU-ABED, S., DOLLE, P., METZGER, D., WOOD, C., MACLEAN, G., CHAMBON, P. & PETKOVICH, M. 2003. Developing with lethal RA levels: genetic ablation of Rarg can restore the viability of mice lacking Cyp26a1. *Development,* 130**,** 1449-59.

AHN, S. & JOYNER, A. L. 2004. Dynamic changes in the response of cells to positive hedgehog signaling during mouse limb patterning. *Cell,* 118**,** 505-16.

AKIYAMA, R., MASUDA, M., TSUGE, S., BESSHO, Y. & MATSUI, T. 2014. An anterior limit of FGF/Erk signal activity marks the earliest future somite boundary in zebrafish. *Development,* 141**,** 1104-9.

AL-MUTAIRI, M. S., CADALBERT, L. C., MCGACHY, H. A., SHWEASH, M., SCHROEDER, J., KURNIK, M., SLOSS, C. M., BRYANT, C. E., ALEXANDER, J. & PLEVIN, R. 2010. MAP kinase phosphatase-2 plays a critical role in response to infection by Leishmania mexicana. *PLoS Pathog,* 6**,** e1001192.

ALHO, J. S., LEINONEN, T. & MERILÄ, J. 2011. Inheritance of vertebral number in the three-spined stickleback (Gasterosteus aculeatus). *PLoS One,* 6**,** e19579.

ALLARD, J. & MOGILNER, A. 2013. Traveling waves in actin dynamics and cell motility. *Curr Opin Cell Biol,* 25**,** 107-15.

ALON, U. 2007. Network motifs: theory and experimental approaches. *Nat Rev Genet,* 8**,** 450-61.

ARCURI, P. & MURRAY, J. D. 1986. Pattern sensitivity to boundary and initial conditions in reaction-diffusion models. *J Math Biol,* 24**,** 141-65.

ARES, S., MORELLI, L. G., JORG, D. J., OATES, A. C. & JULICHER, F. 2012. Collective modes of coupled phase oscillators with delayed coupling. *Phys Rev Lett,* 108**,** 204101.

ARNOLD, S. J. & ROBERTSON, E. J. 2009. Making a commitment: cell lineage allocation and axis patterning in the early mouse embryo. *Nat Rev Mol Cell Biol,* 10**,** 91-103.

ASHALL, L., HORTON, C. A., NELSON, D. E., PASZEK, P., HARPER, C. V., SILLITOE, K., RYAN, S., SPILLER, D. G., UNITT, J. F. & BROOMHEAD, D. S. 2009. Pulsatile stimulation determines timing and specificity of NF-κB-dependent transcription. *Science,* 324**,** 242-246.

AULEHLA, A. & JOHNSON, R. L. 1999. Dynamic expression of lunatic fringe suggests a link between notch signaling and an autonomous cellular oscillator driving somite segmentation. *Dev Biol,* 207**,** 49-61.

AULEHLA, A. & POURQUIE, O. 2010. Signaling gradients during paraxial mesoderm development. *Cold Spring Harb Perspect Biol,* 2**,** a000869.

AULEHLA, A., WEHRLE, C., BRAND-SABERI, B., KEMLER, R., GOSSLER, A., KANZLER, B. & HERRMANN, B. G. 2003. Wnt3a plays a major role in the segmentation clock controlling somitogenesis. *Dev Cell,* 4**,** 395-406.

AULEHLA, A., WIEGRAEBE, W., BAUBET, V., WAHL, M. B., DENG, C., TAKETO, M., LEWANDOSKI, M. & POURQUIE, O. 2008. A beta-catenin gradient links the clock and wavefront systems in mouse embryo segmentation. *Nat Cell Biol,* 10**,** 186-93.

AY, A., KNIERER, S., SPERLEA, A., HOLLAND, J. & ÖZBUDAK, E. M. 2013. Short-lived Her proteins drive robust synchronized oscillations in the zebrafish segmentation clock. *Development,* 140**,** 3244-53.

AZZOLIN, L., PANCIERA, T., SOLIGO, S., ENZO, E., BICCIATO, S., DUPONT, S., BRESOLIN, S., FRASSON, C., BASSO, G. & GUZZARDO, V. 2014. YAP/TAZ incorporation in the β-catenin destruction complex orchestrates the Wnt response. *Cell,* 158**,** 157-170.

BAEK, J. H., HATAKEYAMA, J., SAKAMOTO, S., OHTSUKA, T. & KAGEYAMA, R. 2006. Persistent and high levels of Hes1 expression regulate boundary formation in the developing central nervous system. *Development,* 133**,** 2467-76.

BAJARD, L., MORELLI, L. G., ARES, S., PECREAUX, J., JULICHER, F. & OATES, A. C. 2014. Wnt-regulated dynamics of positional information in zebrafish somitogenesis. *Development,* 141**,** 1381-91.

BAJARD, L. & OATES, A. C. 2012. Breathe in and straighten your back: Hypoxia, Notch, and Scoliosis. *Cell,* 149**,** 255-256.

BALASKAS, N., RIBEIRO, A., PANOVSKA, J., DESSAUD, E., SASAI, N., PAGE, K. M., BRISCOE, J. & RIBES, V. 2012. Gene regulatory logic for reading the Sonic Hedgehog signaling gradient in the vertebrate neural tube. *Cell,* 148**,** 273-84.

BARRANTES, I. B., ELIA, A. J., WÜNSCH, K., HRABE DE ANGELIS, M. H., MAK, T. W., ROSSANT, J., CONLON, R. A., GOSSLER, A. & DE LA POMPA, J. L. 1999. Interaction between Notch signalling and Lunatic fringe during somite boundary formation in the mouse. *Curr Biol,* 9**,** 470-80.

BARRIOS, A., POOLE, R. J., DURBIN, L., BRENNAN, C., HOLDER, N. & WILSON, S. W. 2003. Eph/Ephrin signaling regulates the mesenchymal-to-epithelial transition of the paraxial mesoderm during somite morphogenesis. *Curr Biol,* 13**,** 1571-82.

BARSI, J. C., RAJENDRA, R., WU, J. I. & ARTZT, K. 2005. Mind bomb1 is a ubiquitin ligase essential for mouse embryonic development and Notch signaling. *Mechanisms of development,* 122**,** 1106-1117.

BEASTER-JONES, L., KALTENBACH, S. L., KOOP, D., YUAN, S., CHASTAIN, R. & HOLLAND, L. Z. 2008. Expression of somite segmentation genes in amphioxus: a clock without a wavefront? *Dev Genes Evol,* 218**,** 599-611.

BECK, C. W. 2015. Development of the vertebrate tailbud. *Wiley Interdiscip Rev Dev Biol,* 4**,** 33-44.

BECK, C. W., WHITMAN, M. & SLACK, J. M. 2001. The role of BMP signaling in outgrowth and patterning of the Xenopus tail bud. *Developmental biology,* 238**,** 303-314.

BEERMANN, F., KALOULIS, K., HOFMANN, D., MURISIER, F., BUCHER, P. & TRUMPP, A. 2006. Identification of evolutionarily conserved regulatory elements in the mouse Fgf8 locus. *Genesis,* 44**,** 1-6.

BELGACEM, M. R., ESCANDE, M. L., ESCRIVA, H. & BERTRAND, S. 2011. Amphioxus Tbx6/16 and Tbx20 embryonic expression patterns reveal ancestral functions in chordates. *Gene Expr Patterns,* 11**,** 239-43.

BENAZERAF, B., FRANCOIS, P., BAKER, R. E., DENANS, N., LITTLE, C. D. & POURQUIE, O. 2010. A random cell motility gradient downstream of FGF controls elongation of an amniote embryo. *Nature,* 466**,** 248-52.

BÉNAZÉRAF, B. & POURQUIÉ, O. 2013. Formation and segmentation of the vertebrate body axis. *Annu Rev Cell Dev Biol,* 29**,** 1-26.

BERTRAND, S., ALDEA, D., OULION, S., SUBIRANA, L., DE LERA, A. R., SOMORJAI, I. & ESCRIVA, H. 2015. Evolution of the Role of RA and FGF Signals in the Control of Somitogenesis in Chordates. *PLoS One,* 10**,** e0136587.

BERTRAND, S., CAMASSES, A., SOMORJAI, I., BELGACEM, M. R., CHABROL, O., ESCANDE, M. L., PONTAROTTI, P. & ESCRIVA, H. 2011. Amphioxus FGF signaling predicts the acquisition of vertebrate morphological traits. *Proc Natl Acad Sci U S A,* 108**,** 9160-5.

BESSHO, Y., HIRATA, H., MASAMIZU, Y. & KAGEYAMA, R. 2003. Periodic repression by the bHLH factor Hes7 is an essential mechanism for the somite segmentation clock. *Genes Dev,* 17**,** 1451-6.

BESSHO, Y., SAKATA, R., KOMATSU, S., SHIOTA, K., YAMADA, S. & KAGEYAMA, R. 2001. Dynamic expression and essential functions of Hes7 in somite segmentation. *Genes Dev,* 15**,** 2642-7.

BHAT, M., ROBICHAUD, N., HULEA, L., SONENBERG, N., PELLETIER, J. & TOPISIROVIC, I. 2015. Targeting the translation machinery in cancer. *Nat Rev Drug Discov,* 14**,** 261-78.

BINK, R. J., HABUCHI, H., LELE, Z., DOLK, E., JOORE, J., RAUCH, G. J., GEISLER, R., WILSON, S. W., DEN HERTOG, J., KIMATA, K. & ZIVKOVIC, D. 2003. Heparan sulfate 6-o-sulfotransferase is essential for muscle development in zebrafish. *J Biol Chem,* 278**,** 31118-27.

BONE, R. A., BAILEY, C. S. L., WIEDERMANN, G., FERJENTSIK, Z., APPLETON, P. L., MURRAY, P. J., MAROTO, M. & DALE, J. K. 2014. Spatiotemporal oscillations of Notch1, Dll1 and NICD are coordinated across the mouse PSM. *Development,* 141**,** 4806-4816.

BOROVIAK, T., LOOS, R., BERTONE, P., SMITH, A. & NICHOLS, J. 2014. The ability of inner-cell-mass cells to self-renew as embryonic stem cells is acquired following epiblast specification. *Nat Cell Biol,* 16**,** 516-28.

BOULET, A. M. & CAPECCHI, M. R. 2012. Signaling by FGF4 and FGF8 is required for axial elongation of the mouse embryo. *Dev Biol,* 371**,** 235-45.

BRENT, A. E. 2005. Somite formation: where left meets right. *Curr Biol,* 15**,** R468-70.

BRENT, A. E., SCHWEITZER, R. & TABIN, C. J. 2003. A somitic compartment of tendon progenitors. *Cell,* 113**,** 235-48.

BRISCOE, J. & SMALL, S. 2015. Morphogen rules: design principles of gradient-mediated embryo patterning. *Development,* 142**,** 3996-4009.

BROWN, D., YU, B. D., JOZA, N., BENIT, P., MENESES, J., FIRPO, M., RUSTIN, P., PENNINGER, J. M. & MARTIN, G. R. 2006. Loss of Aif function causes cell death in the mouse embryo, but the temporal progression of patterning is normal. *Proc Natl Acad Sci U S A,* 103**,** 9918-23.

BRUNET, T., BOUCLET, A., AHMADI, P., MITROSSILIS, D., DRIQUEZ, B., BRUNET, A.-C., HENRY, L., SERMAN, F., BÉALLE, G. & MÉNAGER, C. 2013. Evolutionary conservation of early mesoderm specification by mechanotransduction in Bilateria. *Nature communications,* 4.

BUCHBERGER, A., BONNEICK, S., KLEIN, C. & ARNOLD, H. H. 2002. Dynamic expression of chicken cMeso2 in segmental plate and somites. *Developmental dynamics,* 223**,** 108-118.

BURGESS, R., CSERJESI, P., LIGON, K. L. & OLSON, E. N. 1995. Paraxis: a basic helix-loop-helix protein expressed in paraxial mesoderm and developing somites. *Dev Biol,* 168**,** 296-306.

BURGESS, R., RAWLS, A., BROWN, D., BRADLEY, A. & OLSON, E. N. 1996. Requirement of the paraxis gene for somite formation and musculoskeletal patterning. *Nature,* 384**,** 570-573.

BURKE, A. C., NELSON, C. E., MORGAN, B. A. & TABIN, C. 1995. Hox genes and the evolution of vertebrate axial morphology. *Development,* 121**,** 333-346.

BURTSCHER, I. & LICKERT, H. 2009. Foxa2 regulates polarity and epithelialization in the endoderm germ layer of the mouse embryo. *Development,* 136**,** 1029-38.

BUSSEN, M., PETRY, M., SCHUSTER-GOSSLER, K., LEITGES, M., GOSSLER, A. & KISPERT, A. 2004. The T-box transcription factor Tbx18 maintains the separation of anterior and posterior somite compartments. *Genes Dev,* 18**,** 1209-21.

BUSZCZAK, M., SIGNER, R. A. & MORRISON, S. J. 2014. Cellular differences in protein synthesis regulate tissue homeostasis. *Cell,* 159**,** 242-251.

CAHAN, P., LI, H., MORRIS, S. A., DA ROCHA, E. L., DALEY, G. Q. & COLLINS, J. J. 2014. CellNet: network biology applied to stem cell engineering. *Cell,* 158**,** 903-915.

CAI, H., KATOH-KURASAWA, M., MURAMOTO, T., SANTHANAM, B., LONG, Y., LI, L., UEDA, M., IGLESIAS, P. A., SHAULSKY, G. & DEVREOTES, P. N. 2014. Nucleocytoplasmic shuttling of a GATA transcription factor functions as a development timer. *Science,* 343**,** 1249531.

CAMBRAY, N. & WILSON, V. 2007. Two distinct sources for a population of maturing axial progenitors. *Development,* 134**,** 2829-40.

CARAPUCO, M., NOVOA, A., BOBOLA, N. & MALLO, M. 2005. Hox genes specify vertebral types in the presomitic mesoderm. *Genes Dev,* 19**,** 2116-21.

CARPIO, A. 2005. Wave trains, self-oscillations and synchronization in discrete media. *Physica D: Nonlinear Phenomena,* 207**,** 117-136.

CARVER, E. A., JIANG, R., LAN, Y., ORAM, K. F. & GRIDLEY, T. 2001. The mouse snail gene encodes a key regulator of the epithelial-mesenchymal transition. *Mol Cell Biol,* 21**,** 8184-8.

CASS, C. E. 1972. Density-dependent resistance to puromycin in cell cultures. *Journal of cellular physiology,* 79**,** 139-146.

CATALA, M., TEILLET, M. A. & LE DOUARIN, N. M. 1995. Organization and development of the tail bud analyzed with the quail-chick chimaera system. *Mech Dev,* 51**,** 51-65.

CAYUSO, J., XU, Q. & WILKINSON, D. G. 2015. Mechanisms of boundary formation by Eph receptor and ephrin signaling. *Dev Biol,* 401**,** 122-31.

CHAL, J., OGINUMA, M., AL TANOURY, Z., GOBERT, B., SUMARA, O., HICK, A., BOUSSON, F., ZIDOUNI, Y., MURSCH, C., MONCUQUET, P., TASSY, O., VINCENT, S., MIYANARI, A., BERA, A., GARNIER, J. M., GUEVARA, G., HESTIN, M., KENNEDY, L., HAYASHI, S., DRAYTON, B., CHERRIER, T., GAYRAUD-MOREL, B., GUSSONI, E., RELAIX, F., TAJBAKHSH, S. & POURQUIE, O. 2015. Differentiation of pluripotent stem cells to muscle fiber to model Duchenne muscular dystrophy. *Nat Biotechnol,* 33**,** 962-9.

CHAL, J. & POURQUIE, O. 2009. Patterning and differentiation of the vertebrate spine. *In:* POURQUIE, O. (ed.) *The Skeletal System.* Cold Spring Harbor Laboratory Press.

CHALAMALASETTY, R. B., DUNTY, W. C., JR., BIRIS, K. K., AJIMA, R., IACOVINO, M., BEISAW, A., FEIGENBAUM, L., CHAPMAN, D. L., YOON, J. K., KYBA, M. & YAMAGUCHI, T. P. 2011. The Wnt3a/beta-catenin target gene Mesogenin1 controls the segmentation clock by activating a Notch signalling program. *Nat Commun,* 2**,** 390.

CHALAMALASETTY, R. B., GARRIOCK, R. J., DUNTY, W. C., JR., KENNEDY, M. W., JAILWALA, P., SI, H. & YAMAGUCHI, T. P. 2014. Mesogenin 1 is a master regulator of paraxial presomitic mesoderm differentiation. *Development,* 141**,** 4285-97.

CHANG, J. B. & FERRELL JR, J. E. 2013. Mitotic trigger waves and the spatial coordination of the Xenopus cell cycle. *Nature,* 500**,** 603-607.

CHAPMAN, D. L., AGULNIK, I., HANCOCK, S., SILVER, L. M. & PAPAIOANNOU, V. E. 1996. Tbx6, a mouse T-Box gene implicated in paraxial mesoderm formation at gastrulation. *Dev Biol,* 180**,** 534-42.

CHAPMAN, G., SPARROW, D. B., KREMMER, E. & DUNWOODIE, S. L. 2011. Notch inhibition by the ligand DELTA-LIKE 3 defines the mechanism of abnormal vertebral segmentation in spondylocostal dysostosis. *Hum Mol Genet,* 20**,** 905-16.

CHEN, G., GULBRANSON, D. R., YU, P., HOU, Z. & THOMSON, J. A. 2012a. Thermal stability of fibroblast growth factor protein is a determinant factor in regulating self-renewal, differentiation, and reprogramming in human pluripotent stem cells. *Stem Cells,* 30**,** 623-630.

CHEN, H., XU, Z., MEI, C., YU, D. & SMALL, S. 2012b. A system of repressor gradients spatially organizes the boundaries of Bicoid-dependent target genes. *Cell,* 149**,** 618-29.

CHEN, J., KANG, L. & ZHANG, N. 2005. Negative feedback loop formed by Lunatic fringe and Hes7 controls their oscillatory expression during somitogenesis. *Genesis,* 43**,** 196-204.

CHESEBRO, J. E., PUEYO, J. I. & COUSO, J. P. 2013. Interplay between a Wnt-dependent organiser and the Notch segmentation clock regulates posterior development in Periplaneta americana. *Biol Open,* 2**,** 227-37.

CHESLEY, P. 1935. Development of the short-tailed mutant in the house mouse. *J Exp Zool.,* 70**,** 429–435.

CHEUNG, D., MILES, C., KREITMAN, M. & MA, J. 2014. Adaptation of the length scale and amplitude of the Bicoid gradient profile to achieve robust patterning in abnormally large Drosophila melanogaster embryos. *Development,* 141**,** 124-35.

CHIPMAN, A. D. & AKAM, M. 2008. The segmentation cascade in the centipede Strigamia maritima: involvement of the Notch pathway and pair-rule gene homologues. *Developmental biology,* 319**,** 160-169.

CHIPMAN, A. D., ARTHUR, W. & AKAM, M. 2004. A double segment periodicity underlies segment generation in centipede development. *Curr Biol,* 14**,** 1250-5.

CHOE, C. P., MILLER, S. C. & BROWN, S. J. 2006. A pair-rule gene circuit defines segments sequentially in the short-germ insect Tribolium castaneum. *Proc Natl Acad Sci U S A,* 103**,** 6560-4.

CHRIST, B., HUANG, R. & SCAAL, M. 2007. Amniote somite derivatives. *Dev Dyn,* 236**,** 2382-96.

CHRIST, B., JACOB, H. & JACOB, M. 1974. Über den Ursprung der Flügelmuskulatur. Experimentelle Untersuchungen mit Wachtel-und Hühnerembryonen. *Experientia,* 30**,** 1446-1449.

CHRIST, B. & SCAAL, M. 2008. Formation and differentiation of avian somite derivatives. *Adv Exp Med Biol,* 638**,** 1-41.

CIRUNA, B. G., SCHWARTZ, L., HARPAL, K., YAMAGUCHI, T. P. & ROSSANT, J. 1997. Chimeric analysis of fibroblast growth factor receptor-1 (Fgfr1) function: a role for FGFR1 in morphogenetic movement through the primitive streak. *Development,* 124**,** 2829-41.

COLLIER, J. R., MCINERNEY, D., SCHNELL, S., MAINI, P. K., GAVAGHAN, D. J., HOUSTON, P. & STERN, C. D. 2000. A cell cycle model for somitogenesis: mathematical formulation and numerical simulation. *J Theor Biol,* 207**,** 305-16.

CONLON, F. L., WRIGHT, C. V. & ROBERTSON, E. J. 1995a. Effects of the TWis mutation on notochord formation and mesodermal patterning. *Mech Dev,* 49**,** 201-9.

CONLON, R. A., REAUME, A. G. & ROSSANT, J. 1995b. Notch1 is required for the coordinate segmentation of somites. *Development,* 121**,** 1533-45.

COOKE, J. 1975. Control of somite number during morphogenesis of a vertebrate, Xenopus laevis. *Nature,* 254**,** 196-9.

COOKE, J. & ZEEMAN, E. C. 1976. A clock and wavefront model for control of the number of repeated structures during animal morphogenesis. *J Theor Biol,* 58**,** 455-76.

COPF, T., SCHRODER, R. & AVEROF, M. 2004. Ancestral role of caudal genes in axis elongation and segmentation. *Proc Natl Acad Sci U S A,* 101**,** 17711-5.

COTTERELL, J., ROBERT-MORENO, A. & SHARPE, J. 2015. A Local, Self-Organizing Reaction-Diffusion Model Can Explain Somite Patterning in Embryos. *Cell Systems,* 1**,** 257-269.

CRAFT, A. M., AHMED, N., ROCKEL, J. S., BAHT, G. S., ALMAN, B. A., KANDEL, R. A., GRIGORIADIS, A. E. & KELLER, G. M. 2013. Specification of chondrocytes and cartilage tissues from embryonic stem cells. *Development,* 140**,** 2597-610.

CRAFT, A. M., ROCKEL, J. S., NARTISS, Y., KANDEL, R. A., ALMAN, B. A. & KELLER, G. M. 2015. Generation of articular chondrocytes from human pluripotent stem cells. *Nat Biotechnol,* 33**,** 638-45.

CRICK, F. 1970. Diffusion in embryogenesis. *Nature,* 225**,** 420-2.

CUNNINGHAM, T. J., BRADE, T., SANDELL, L. L., LEWANDOSKI, M., TRAINOR, P. A., COLAS, A., MERCOLA, M. & DUESTER, G. 2015. Retinoic acid activity in undifferentiated neural progenitors is sufficient to fulfill its role in restricting Fgf8 expression for somitogenesis. *PloS one,* 10**,** e0137894.

D'ALESSIO, A. C., FAN, Z. P., WERT, K. J., BARANOV, P., COHEN, M. A., SAINI, J. S., COHICK, E., CHARNIGA, C., DADON, D. & HANNETT, N. M. 2015. A Systematic Approach to Identify Candidate Transcription Factors that Control Cell Identity. *Stem cell reports,* 5**,** 763-775.

DALE, J. K., MALAPERT, P., CHAL, J., VILHAIS-NETO, G., MAROTO, M., JOHNSON, T., JAYASINGHE, S., TRAINOR, P., HERRMANN, B. & POURQUIE, O. 2006. Oscillations of the snail genes in the presomitic mesoderm coordinate segmental patterning and morphogenesis in vertebrate somitogenesis. *Dev Cell,* 10**,** 355-66.

DALE, J. K., MAROTO, M., DEQUEANT, M. L., MALAPERT, P., MCGREW, M. & POURQUIE, O. 2003. Periodic notch inhibition by lunatic fringe underlies the chick segmentation clock. *Nature,* 421**,** 275-8.

DAVIS, G. K. & PATEL, N. H. 1999. The origin and evolution of segmentation. *Trends Cell Biol,* 9**,** M68-72.

DE MONTE, S., D'OVIDIO, F., DANO, S. & SORENSEN, P. G. 2007. Dynamical quorum sensing: Population density encoded in cellular dynamics. *Proc Natl Acad Sci U S A,* 104**,** 18377-81.

DE ROBERTIS, E. M. 2008. The molecular ancestry of segmentation mechanisms. *Proceedings of the National Academy of Sciences of the United States of America,* 105**,** 16411-16412.

DE ROSA, R., PRUD'HOMME, B. & BALAVOINE, G. 2005. Caudal and even-skipped in the annelid Platynereis dumerilii and the ancestry of posterior growth. *Evol Dev,* 7**,** 574-87.

DELAUNE, E. A., FRANÇOIS, P., SHIH, N. P. & AMACHER, S. L. 2012. Single-cell-resolution imaging of the impact of Notch signaling and mitosis on segmentation clock dynamics. *Dev Cell,* 23**,** 995-1005.

DELFINI, M. C., DUBRULLE, J., MALAPERT, P., CHAL, J. & POURQUIE, O. 2005. Control of the segmentation process by graded MAPK/ERK activation in the chick embryo. *Proc Natl Acad Sci U S A,* 102**,** 11343-8.

DENANS, N., IIMURA, T. & POURQUIE, O. 2015. Hox genes control vertebrate body elongation by collinear Wnt repression. *Elife,* 4.

DENG, C. X., WYNSHAW-BORIS, A., SHEN, M. M., DAUGHERTY, C., ORNITZ, D. M. & LEDER, P. 1994. Murine FGFR-1 is required for early postimplantation growth and axial organization. *Genes Dev,* 8**,** 3045-57.

DEQUEANT, M. L., GLYNN, E., GAUDENZ, K., WAHL, M., CHEN, J., MUSHEGIAN, A. & POURQUIE, O. 2006. A complex oscillating network of signaling genes underlies the mouse segmentation clock. *Science,* 314**,** 1595-8.

DERTINGER, S. K., CHIU, D. T., JEON, N. L. & WHITESIDES, G. M. 2001. Generation of gradients having complex shapes using microfluidic networks. *Analytical Chemistry,* 73**,** 1240-1246.

DESCHAMPS, J. & VAN NES, J. 2005. Developmental regulation of the Hox genes during axial morphogenesis in the mouse. *Development,* 132**,** 2931-2942.

DESCHAMPS, J. & WIJGERDE, M. 1993. Two phases in the establishment of HOX expression domains. *Dev Biol,* 156**,** 473-80.

DESSAUD, E., RIBES, V., BALASKAS, N., YANG, L. L., PIERANI, A., KICHEVA, A., NOVITCH, B. G., BRISCOE, J. & SASAI, N. 2010. Dynamic assignment and maintenance of positional identity in the ventral neural tube by the morphogen sonic hedgehog. *PLoS Biol,* 8**,** e1000382.

DESSAUD, E., YANG, L. L., HILL, K., COX, B., ULLOA, F., RIBEIRO, A., MYNETT, A., NOVITCH, B. G. & BRISCOE, J. 2007. Interpretation of the sonic hedgehog morphogen gradient by a temporal adaptation mechanism. *Nature,* 450**,** 717-20.

DI-POI, N., MONTOYA-BURGOS, J. I., MILLER, H., POURQUIE, O., MILINKOVITCH, M. C. & DUBOULE, D. 2010. Changes in Hox genes' structure and function during the evolution of the squamate body plan. *Nature,* 464**,** 99-103.

DIAS, A. S., DE ALMEIDA, I., BELMONTE, J. M., GLAZIER, J. A. & STERN, C. D. 2014. Somites without a clock. *Science,* 343**,** 791-5.

DIEZ DEL CORRAL, R., OLIVERA-MARTINEZ, I., GORIELY, A., GALE, E., MADEN, M. & STOREY, K. 2003. Opposing FGF and retinoid pathways control ventral neural pattern, neuronal differentiation, and segmentation during body axis extension. *Neuron,* 40**,** 65-79.

DONOVAN, J., KORDYLEWSKA, A., JAN, Y. N. & UTSET, M. F. 2002. Tetralogy of fallot and other congenital heart defects in Hey2 mutant mice. *Curr Biol,* 12**,** 1605-10.

DONOVIEL, D. B., HADJANTONAKIS, A. K., IKEDA, M., ZHENG, H., HYSLOP, P. S. & BERNSTEIN, A. 1999. Mice lacking both presenilin genes exhibit early embryonic patterning defects. *Genes Dev,* 13**,** 2801-10.

DOREY, K. & AMAYA, E. 2010. FGF signalling: diverse roles during early vertebrate embryogenesis. *Development,* 137**,** 3731-42.

DOTTORI, M., HARTLEY, L., GALEA, M., PAXINOS, G., POLIZZOTTO, M., KILPATRICK, T., BARTLETT, P. F., MURPHY, M., KONTGEN, F. & BOYD, A. W. 1998. EphA4 (Sek1) receptor tyrosine kinase is required for the development of the corticospinal tract. *Proc Natl Acad Sci U S A,* 95**,** 13248-53.

DRIEVER, W. & NUSSLEIN-VOLHARD, C. 1988a. The bicoid protein determines position in the Drosophila embryo in a concentration-dependent manner. *Cell,* 54**,** 95-104.

DRIEVER, W. & NUSSLEIN-VOLHARD, C. 1988b. A gradient of bicoid protein in Drosophila embryos. *Cell,* 54**,** 83-93.

DUBRULLE, J., MCGREW, M. J. & POURQUIE, O. 2001. FGF signaling controls somite boundary position and regulates segmentation clock control of spatiotemporal Hox gene activation. *Cell,* 106**,** 219-32.

DUBRULLE, J. & POURQUIÉ, O. 2004. fgf8 mRNA decay establishes a gradient that couples axial elongation to patterning in the vertebrate embryo. *Nature,* 427**,** 419-422.

DUCHESNE, L., OCTEAU, V., BEARON, R. N., BECKETT, A., PRIOR, I. A., LOUNIS, B. & FERNIG, D. G. 2012. Transport of fibroblast growth factor 2 in the pericellular matrix is controlled by the spatial distribution of its binding sites in heparan sulfate. *PLoS Biol,* 10**,** e1001361.

DUNN, N. R., VINCENT, S. D., OXBURGH, L., ROBERTSON, E. J. & BIKOFF, E. K. 2004. Combinatorial activities of Smad2 and Smad3 regulate mesoderm formation and patterning in the mouse embryo. *Development,* 131**,** 1717-28.

DUNTY, W. C., JR., BIRIS, K. K., CHALAMALASETTY, R. B., TAKETO, M. M., LEWANDOSKI, M. & YAMAGUCHI, T. P. 2008. Wnt3a/beta-catenin signaling controls posterior body development by coordinating mesoderm formation and segmentation. *Development,* 135**,** 85-94.

DUNWOODIE, S. L., HENRIQUE, D., HARRISON, S. M. & BEDDINGTON, R. S. 1997. Mouse Dll3: a novel divergent Delta gene which may complement the function of other Delta homologues during early pattern formation in the mouse embryo. *Development,* 124**,** 3065-76.

DUPONT, S. 2015. Role of YAP/TAZ in cell-matrix adhesion-mediated signalling and mechanotransduction. *Experimental cell research*.

DUPONT, S., MORSUT, L., ARAGONA, M., ENZO, E., GIULITTI, S., CORDENONSI, M., ZANCONATO, F., LE DIGABEL, J., FORCATO, M. & BICCIATO, S. 2011. Role of YAP/TAZ in mechanotransduction. *Nature,* 474**,** 179-183.

DURBIN, L., SORDINO, P., BARRIOS, A., GERING, M., THISSE, C., THISSE, B., BRENNAN, C., GREEN, A., WILSON, S. & HOLDER, N. 2000. Anteroposterior patterning is required within segments for somite boundary formation in developing zebrafish. *Development,* 127**,** 1703-13.

ECHEVERRI, K. & OATES, A. C. 2007. Coordination of symmetric cyclic gene expression during somitogenesis by Suppressor of Hairless involves regulation of retinoic acid catabolism. *Dev Biol,* 301**,** 388-403.

ECONOMOU, A. D., OHAZAMA, A., PORNTAVEETUS, T., SHARPE, P. T., KONDO, S., BASSON, M. A., GRITLI-LINDE, A., COBOURNE, M. T. & GREEN, J. B. 2012. Periodic stripe formation by a Turing mechanism operating at growth zones in the mammalian palate. *Nature genetics,* 44**,** 348-351.

EIRAKU, M., TAKATA, N., ISHIBASHI, H., KAWADA, M., SAKAKURA, E., OKUDA, S., SEKIGUCHI, K., ADACHI, T. & SASAI, Y. 2011. Self-organizing optic-cup morphogenesis in three-dimensional culture. *Nature,* 472**,** 51-6.

ELBEDIWY, A., VINCENT-MISTIAEN, Z., SPENCER-DENE, B., STONE, R., BOEING, S., WCULEK, S., CORDERO, J., TAN, E., RIDGWAY, R. & BRUNTON, V. 2016. Integrin signalling regulates YAP/TAZ to control skin homeostasis. *Development***,** dev. 133728.

ENVER, T., PERA, M., PETERSON, C. & ANDREWS, P. W. 2009. Stem cell states, fates, and the rules of attraction. *Cell stem cell,* 4**,** 387-397.

ENZO, E., SANTINON, G., POCATERRA, A., ARAGONA, M., BRESOLIN, S., FORCATO, M., GRIFONI, D., PESSION, A., ZANCONATO, F. & GUZZO, G. 2015. Aerobic glycolysis tunes YAP/TAZ transcriptional activity. *The EMBO journal***,** e201490379.

ERIKSSON, B. J., UNGERER, P. & STOLLEWERK, A. 2013. The function of Notch signalling in segment formation in the crustacean Daphnia magna (Branchiopoda). *Developmental biology,* 383**,** 321-330.

ERMENTROUT, G. B. & KOPELL, N. 1986. Parabolic bursting in an excitable system coupled with a slow oscillation. *SIAM Journal on Applied Mathematics,* 46**,** 233-253.

EVRARD, Y. A., LUN, Y., AULEHLA, A., GAN, L. & JOHNSON, R. L. 1998. lunatic fringe is an essential mediator of somite segmentation and patterning. *Nature,* 394**,** 377-81.

FARIN, H. F., JORDENS, I., MOSA, M. H., BASAK, O., KORVING, J., TAURIELLO, D. V., DE PUNDER, K., ANGERS, S., PETERS, P. J., MAURICE, M. M. & CLEVERS, H. 2016. Visualization of a short-range Wnt gradient in the intestinal stem-cell niche. *Nature,* 530**,** 340-3.

FEHLING, H. J., LACAUD, G., KUBO, A., KENNEDY, M., ROBERTSON, S., KELLER, G. & KOUSKOFF, V. 2003. Tracking mesoderm induction and its specification to the hemangioblast during embryonic stem cell differentiation. *Development,* 130**,** 4217-4227.

FELLER, J., SCHNEIDER, A., SCHUSTER-GOSSLER, K. & GOSSLER, A. 2008. Noncyclic Notch activity in the presomitic mesoderm demonstrates uncoupling of somite compartmentalization and boundary formation. *Genes Dev,* 22**,** 2166-71.

FERJENTSIK, Z., HAYASHI, S., DALE, J. K., BESSHO, Y., HERREMAN, A., DE STROOPER, B., DEL MONTE, G., DE LA POMPA, J. L. & MAROTO, M. 2009. Notch Is a Critical Component of the Mouse Somitogenesis Oscillator and Is Essential for the Formation of the Somites. *PLoS Genet,* 5.

FERNANDEZ-SANCHEZ, M.-E., BRUNET, T., RÖPER, J.-C. & FARGE, E. 2015. Mechanotransduction's Impact on Animal Development, Evolution, and Tumorigenesis. *Annual Review of Cell and Developmental Biology,* 31**,** 373-397.

FIOR, R., MAXWELL, A. A., MA, T. P., VEZZARO, A., MOENS, C. B., AMACHER, S. L., LEWIS, J. & SAUDE, L. 2012. The differentiation and movement of presomitic mesoderm progenitor cells are controlled by Mesogenin 1. *Development,* 139**,** 4656-65.

FITZHUGH, R. 1961. Impulses and Physiological States in Theoretical Models of Nerve Membrane. *Biophys J,* 1**,** 445-66.

FLEMING, A., KEYNES, R. & TANNAHILL, D. 2004. A central role for the notochord in vertebral patterning. *Development,* 131**,** 873-80.

FLINT, O. P., EDE, D. A., WILBY, O. K. & PROCTOR, J. 1978. Control of somite number in normal and amputated mutant mouse embryos: an experimental and a theoretical analysis. *J Embryol Exp Morphol,* 45**,** 189-202.

FOLTZ, D. R., SANTIAGO, M. C., BERECHID, B. E. & NYE, J. S. 2002. Glycogen synthase kinase-3β modulates notch signaling and stability. *Current Biology,* 12**,** 1006-1011.

FONGANG, B. & KUDLICKI, A. 2013. The precise timeline of transcriptional regulation reveals causation in mouse somitogenesis network. *BMC Dev Biol,* 13**,** 42.

FOWLER, J. A. 1970. Control of vertebral number in teleosts-an embryological problem. *Quarterly Review of Biology***,** 148-167.

FRANCOIS, P., HAKIM, V. & SIGGIA, E. D. 2007. Deriving structure from evolution: metazoan segmentation. *Mol Syst Biol,* 3**,** 154.

FRANK, T. & TAY, S. 2013. Flow-switching allows independently programmable, extremely stable, high-throughput diffusion-based gradients. *Lab on a Chip,* 13**,** 1273-1281.

FUJIMOTO, K., ISHIHARA, S. & KANEKO, K. 2008. Network evolution of body plans. *PLoS One,* 3**,** e2772.

FUJINAGA, K., IRWIN, D., HUANG, Y., TAUBE, R., KUROSU, T. & PETERLIN, B. M. 2004. Dynamics of human immunodeficiency virus transcription: P-TEFb phosphorylates RD and dissociates negative effectors from the transactivation response element. *Mol Cell Biol,* 24**,** 787-95.

GADUE, P., HUBER, T. L., PADDISON, P. J. & KELLER, G. M. 2006. Wnt and TGF-beta signaling are required for the induction of an in vitro model of primitive streak formation using embryonic stem cells. *Proc Natl Acad Sci U S A,* 103**,** 16806-11.

GAERTNER, B. & ZEITLINGER, J. 2014. RNA polymerase II pausing during development. *Development,* 141**,** 1179-1183.

GAJEWSKI, M., ELMASRI, H., GIRSCHICK, M., SIEGER, D. & WINKLER, C. 2006. Comparative analysis of her genes during fish somitogenesis suggests a mouse/chick-like mode of oscillation in medaka. *Dev Genes Evol,* 216**,** 315-32.

GALCERAN, J., FARINAS, I., DEPEW, M. J., CLEVERS, H. & GROSSCHEDL, R. 1999. Wnt3a-/--like phenotype and limb deficiency in Lef1(-/-)Tcf1(-/-) mice. *Genes Dev,* 13**,** 709-17.

GALCERAN, J., HSU, S. C. & GROSSCHEDL, R. 2001. Rescue of a Wnt mutation by an activated form of LEF-1: regulation of maintenance but not initiation of Brachyury expression. *Proc Natl Acad Sci U S A,* 98**,** 8668-73.

GALLEGO, M. & VIRSHUP, D. M. 2007. Post-translational modifications regulate the ticking of the circadian clock. *Nat Rev Mol Cell Biol,* 8**,** 139-48.

GANGLOFF, Y.-G., MUELLER, M., DANN, S. G., SVOBODA, P., STICKER, M., SPETZ, J.-F., UM, S. H., BROWN, E. J., CEREGHINI, S. & THOMAS, G. 2004. Disruption of the mouse mTOR gene leads to early postimplantation lethality and prohibits embryonic stem cell development. *Molecular and cellular biology,* 24**,** 9508-9516.

GARCÍA-MARTÍNEZ, J. M., MORAN, J., CLARKE, R. G., GRAY, A., COSULICH, S. C., CHRESTA, C. M. & ALESSI, D. R. 2009. Ku-0063794 is a specific inhibitor of the mammalian target of rapamycin (mTOR). *Biochemical Journal,* 421**,** 29-42.

GARRIOCK, R. J., CHALAMALASETTY, R. B., KENNEDY, M. W., CANIZALES, L. C., LEWANDOSKI, M. & YAMAGUCHI, T. P. 2015. Lineage tracing of neuromesodermal progenitors reveals novel Wnt-dependent roles in trunk progenitor cell maintenance and differentiation. *Development,* 142**,** 1628-38.

GARSIDE, E. 1966. Developmental rate and vertebral number in salmonids. *Journal of the Fisheries Board of Canada,* 23**,** 1537-1551.

GARSIDE, E. & FRY, F. 1959. A possible relationship between yolk size and differentiation in trout embryos. *Canadian Journal of Zoology,* 37**,** 383-386.

GEE, S. T., MILGRAM, S. L., KRAMER, K. L., CONLON, F. L. & MOODY, S. A. 2011. Yes-associated protein 65 (YAP) expands neural progenitors and regulates Pax3 expression in the neural plate border zone. *PLoS One,* 6**,** e20309.

GEFFERS, I., SERTH, K., CHAPMAN, G., JAEKEL, R., SCHUSTER-GOSSLER, K., CORDES, R., SPARROW, D. B., KREMMER, E., DUNWOODIE, S. L. & KLEIN, T. 2007. Divergent functions and distinct localization of the Notch ligands DLL1 and DLL3 in vivo. *The Journal of cell biology,* 178**,** 465-476.

GESSLER, M., KNOBELOCH, K. P., HELISCH, A., AMANN, K., SCHUMACHER, N., ROHDE, E., FISCHER, A. & LEIMEISTER, C. 2002. Mouse gridlock: no aortic coarctation or deficiency, but fatal cardiac defects in Hey2 -/- mice. *Curr Biol,* 12**,** 1601-4.

GIBB, S., ZAGORSKA, A., MELTON, K., TENIN, G., VACCA, I., TRAINOR, P., MAROTO, M. & DALE, J. K. 2009. Interfering with Wnt signalling alters the periodicity of the segmentation clock. *Dev Biol,* 330**,** 21-31.

GIRALDEZ, A. J., CINALLI, R. M., GLASNER, M. E., ENRIGHT, A. J., THOMSON, J. M., BASKERVILLE, S., HAMMOND, S. M., BARTEL, D. P. & SCHIER, A. F. 2005. MicroRNAs regulate brain morphogenesis in zebrafish. *Science,* 308**,** 833-8.

GIRÓS, A., GRGUR, K., GOSSLER, A. & COSTELL, M. 2011. α5β1 integrin-mediated adhesion to fibronectin is required for axis elongation and somitogenesis in mice. *PloS one,* 6**,** e22002.

GIUDICELLI, F., OZBUDAK, E. M., WRIGHT, G. J. & LEWIS, J. 2007. Setting the tempo in development: an investigation of the zebrafish somite clock mechanism. *PLoS Biol,* 5**,** e150.

GLAZIER, J. A., ZHANG, Y., SWAT, M., ZAITLEN, B. & SCHNELL, S. 2008. Coordinated action of N-CAM, N-cadherin, EphA4, and ephrinB2 translates genetic prepatterns into structure during somitogenesis in chick. *Curr Top Dev Biol,* 81**,** 205-47.

GLIMM, T., ZHANG, J., SHEN, Y. Q. & NEWMAN, S. A. 2012. Reaction-diffusion systems and external morphogen gradients: the two-dimensional case, with an application to skeletal pattern formation. *Bull Math Biol,* 74**,** 666-87.

GOLDBETER, A. 2002. Computational approaches to cellular rhythms. *Nature,* 420**,** 238-45.

GOLDBETER, A., GONZE, D. & POURQUIÉ, O. 2007. Sharp developmental thresholds defined through bistability by antagonistic gradients of retinoic acid and FGF signaling. *Dev Dyn,* 236**,** 1495-508.

GOMEZ, C., OZBUDAK, E. M., WUNDERLICH, J., BAUMANN, D., LEWIS, J. & POURQUIÉ, O. 2008. Control of segment number in vertebrate embryos. *Nature,* 454**,** 335-9.

GONT, L. K., STEINBEISSER, H., BLUMBERG, B. & DE ROBERTIS, E. M. 1993. Tail formation as a continuation of gastrulation: the multiple cell populations of the Xenopus tailbud derive from the late blastopore lip. *Development,* 119**,** 991-1004.

GONZÁLEZ, A., MANOSALVA, I., LIU, T. & KAGEYAMA, R. 2013. Control of Hes7 expression by Tbx6, the Wnt pathway and the chemical Gsk3 inhibitor LiCl in the mouse segmentation clock. *PLoS One,* 8**,** e53323.

GOODWIN, B. C. & COHEN, M. H. 1969. A phase-shift model for the spatial and temporal organization of developing systems. *J Theor Biol,* 25**,** 49-107.

GOORDEN, S. M., HOOGEVEEN-WESTERVELD, M., CHENG, C., VAN WOERDEN, G. M., MOZAFFARI, M., POST, L., DUCKERS, H. J., NELLIST, M. & ELGERSMA, Y. 2011. Rheb is essential for murine development. *Molecular and cellular biology,* 31**,** 1672-1678.

GOUTI, M., TSAKIRIDIS, A., WYMEERSCH, F. J., HUANG, Y., KLEINJUNG, J., WILSON, V. & BRISCOE, J. 2014. In vitro generation of neuromesodermal progenitors reveals distinct roles for wnt signalling in the specification of spinal cord and paraxial mesoderm identity. *PLoS Biol,* 12**,** e1001937.

GRECO, T. L., TAKADA, S., NEWHOUSE, M. M., MCMAHON, J. A., MCMAHON, A. P. & CAMPER, S. A. 1996. Analysis of the vestigial tail mutation demonstrates that Wnt-3a gene dosage regulates mouse axial development. *Genes Dev,* 10**,** 313-24.

GRECO, V., HANNUS, M. & EATON, S. 2001. Argosomes: a potential vehicle for the spread of morphogens through epithelia. *Cell,* 106**,** 633-45.

GREEN, J. B. & SHARPE, J. 2015. Positional information and reaction-diffusion: two big ideas in developmental biology combine. *Development,* 142**,** 1203-11.

GREGOR, T., FUJIMOTO, K., MASAKI, N. & SAWAI, S. 2010. The onset of collective behavior in social amoebae. *Science,* 328**,** 1021-5.

GRIMA, R. & SCHNELL, S. 2007. Can tissue surface tension drive somite formation? *Dev Biol,* 307**,** 248-57.

HALDER, G., DUPONT, S. & PICCOLO, S. 2012. Transduction of mechanical and cytoskeletal cues by YAP and TAZ. *Nature reviews Molecular cell biology,* 13**,** 591-600.

HAMBURGER, V. & HAMILTON, H. L. 1951. A series of normal stages in the development of the chick embryo. *Journal of morphology,* 88**,** 49-92.

HAN, A. P., YU, C., LU, L., FUJIWARA, Y., BROWNE, C., CHIN, G., FLEMING, M., LEBOULCH, P., ORKIN, S. H. & CHEN, J. J. 2001. Heme-regulated eIF2α kinase (HRI) is required for translational regulation and survival of erythroid precursors in iron deficiency. *The EMBO journal,* 20**,** 6909-6918.

HANISCH, A., HOLDER, M. V., CHOORAPOIKAYIL, S., GAJEWSKI, M., ÖZBUDAK, E. M. & LEWIS, J. 2013. The elongation rate of RNA polymerase II in zebrafish and its significance in the somite segmentation clock. *Development,* 140**,** 444-53.

HANSEN, C. G., MOROISHI, T. & GUAN, K.-L. 2015. YAP and TAZ: a nexus for Hippo signaling and beyond. *Trends in cell biology,* 25**,** 499-513.

HARAGUCHI, S., KITAJIMA, S., TAKAGI, A., TAKEDA, H., INOUE, T. & SAGA, Y. 2001. Transcriptional regulation of Mesp1 and Mesp2 genes: differential usage of enhancers during development. *Mechanisms of development,* 108**,** 59-69.

HARFE, B. D., SCHERZ, P. J., NISSIM, S., TIAN, H., MCMAHON, A. P. & TABIN, C. J. 2004. Evidence for an expansion-based temporal Shh gradient in specifying vertebrate digit identities. *Cell,* 118**,** 517-28.

HARIMA, Y. & KAGEYAMA, R. 2013. Oscillatory links of Fgf signaling and Hes7 in the segmentation clock. *Curr Opin Genet Dev,* 23**,** 484-90.

HARIMA, Y., TAKASHIMA, Y., UEDA, Y., OHTSUKA, T. & KAGEYAMA, R. 2013. Accelerating the tempo of the segmentation clock by reducing the number of introns in the Hes7 gene. *Cell Rep,* 3**,** 1-7.

HARRIS, A. K., STOPAK, D. & WARNER, P. 1984. Generation of spatially periodic patterns by a mechanical instability: a mechanical alternative to the Turing model. *J Embryol Exp Morphol,* 80**,** 1-20.

HARRISON, S. M., HOUZELSTEIN, D., DUNWOODIE, S. L. & BEDDINGTON, R. S. 2000. Sp5, a new member of the Sp1 family, is dynamically expressed during development and genetically interacts with Brachyury. *Dev Biol,* 227**,** 358-72.

HARTMANN, D., DE STROOPER, B., SERNEELS, L., CRAESSAERTS, K., HERREMAN, A., ANNAERT, W., UMANS, L., LÜBKE, T., ILLERT, A. L. & VON FIGURA, K. 2002. The disintegrin/metalloprotease ADAM 10 is essential for Notch signalling but not for α-secretase activity in fibroblasts. *Human molecular genetics,* 11**,** 2615-2624.

HAYASHI, K., OHTA, H., KURIMOTO, K., ARAMAKI, S. & SAITOU, M. 2011. Reconstitution of the mouse germ cell specification pathway in culture by pluripotent stem cells. *Cell,* 146**,** 519-32.

HAYASHI, S., SHIMODA, T., NAKAJIMA, M., TSUKADA, Y., SAKUMURA, Y., DALE, J. K., MAROTO, M., KOHNO, K., MATSUI, T. & BESSHO, Y. 2009. Sprouty4, an FGF Inhibitor, Displays Cyclic Gene Expression under the Control of the Notch Segmentation Clock in the Mouse PSM. *PLoS ONE,* 4.

HENRIQUE, D., ABRANCHES, E., VERRIER, L. & STOREY, K. G. 2015. Neuromesodermal progenitors and the making of the spinal cord. *Development,* 142**,** 2864-75.

HENRIQUE, D., ADAM, J., MYAT, A., CHITNIS, A., LEWIS, J. & ISH-HOROWICZ, D. 1995. Expression of a Delta homologue in prospective neurons in the chick. *Nature,* 375**,** 787-790.

HERMITTE, S. & CHAZAUD, C. 2014. Primitive endoderm differentiation: from specification to epithelium formation. *Philos Trans R Soc Lond B Biol Sci,* 369.

HERRGEN, L., ARES, S., MORELLI, L. G., SCHRÖTER, C., JÜLICHER, F. & OATES, A. C. 2010. Intercellular coupling regulates the period of the segmentation clock. *Curr Biol,* 20**,** 1244-53.

HERRMANN, B. G. 1991. Expression pattern of the Brachyury gene in whole-mount TWis/TWis mutant embryos. *Development,* 113**,** 913-7.

HERRMANN, B. G., LABEIT, S., POUSTKA, A., KING, T. R. & LEHRACH, H. 1990. Cloning of the T gene required in mesoderm formation in the mouse. *Nature,* 343**,** 617-22.

HESTER, S. D., BELMONTE, J. M., GENS, J. S., CLENDENON, S. G. & GLAZIER, J. A. 2011. A multi-cell, multi-scale model of vertebrate segmentation and somite formation. *PLoS Comput Biol,* 7**,** e1002155.

HILGERS, V., POURQUIÉ, O. & DUBRULLE, J. 2005. In vivo analysis of mRNA stability using the Tet-Off system in the chicken embryo. *Dev Biol,* 284**,** 292-300.

HIRAMATSU, R., MATSUOKA, T., KIMURA-YOSHIDA, C., HAN, S. W., MOCHIDA, K., ADACHI, T., TAKAYAMA, S. & MATSUO, I. 2013. External mechanical cues trigger the establishment of the anterior-posterior axis in early mouse embryos. *Dev Cell,* 27**,** 131-44.

HIRATA, H., BESSHO, Y., KOKUBU, H., MASAMIZU, Y., YAMADA, S., LEWIS, J. & KAGEYAMA, R. 2004. Instability of Hes7 protein is crucial for the somite segmentation clock. *Nat Genet,* 36**,** 750-4.

HIRATA, H., YOSHIURA, S., OHTSUKA, T., BESSHO, Y., HARADA, T., YOSHIKAWA, K. & KAGEYAMA, R. 2002. Oscillatory expression of the bHLH factor Hes1 regulated by a negative feedback loop. *Science,* 298**,** 840-3.

HISCOCK, T. W. & MEGASON, S. G. 2015. Orientation of Turing-like Patterns by Morphogen Gradients and Tissue Anisotropies. *Cell Syst,* 1**,** 408-416.

HOLLEY, S. A., JULICH, D., RAUCH, G. J., GEISLER, R. & NUSSLEIN-VOLHARD, C. 2002. her1 and the notch pathway function within the oscillator mechanism that regulates zebrafish somitogenesis. *Development,* 129**,** 1175-83.

HORIKAWA, K., ISHIMATSU, K., YOSHIMOTO, E., KONDO, S. & TAKEDA, H. 2006. Noise-resistant and synchronized oscillation of the segmentation clock. *Nature,* 441**,** 719-23.

HORIKAWA, K., RADICE, G., TAKEICHI, M. & CHISAKA, O. 1999. Adhesive subdivisions intrinsic to the epithelial somites. *Dev Biol,* 215**,** 182-9.

HORNSTEIN, E. & TABIN, C. J. 2005. Developmental biology: asymmetrical threat averted. *Nature,* 435**,** 155-6.

HOSSAIN, Z., ALI, S. M., KO, H. L., XU, J., NG, C. P., GUO, K., QI, Z., PONNIAH, S., HONG, W. & HUNZIKER, W. 2007. Glomerulocystic kidney disease in mice with a targeted inactivation of Wwtr1. *Proceedings of the National Academy of Sciences,* 104**,** 1631-1636.

HOYLE, N. P. & ISH-HOROWICZ, D. 2013. Transcript processing and export kinetics are rate-limiting steps in expressing vertebrate segmentation clock genes. *Proc Natl Acad Sci U S A,* 110**,** E4316-24.

HRABE DE ANGELIS, M., MCINTYRE, J., 2ND & GOSSLER, A. 1997. Maintenance of somite borders in mice requires the Delta homologue DlI1. *Nature,* 386**,** 717-21.

HUANG, S., EICHLER, G., BAR-YAM, Y. & INGBER, D. E. 2005. Cell fates as high-dimensional attractor states of a complex gene regulatory network. *Physical review letters,* 94**,** 128701.

HUANG, Y., AINSLEY, J. A., REIJMERS, L. G. & JACKSON, F. R. 2013. Translational profiling of clock cells reveals circadianly synchronized protein synthesis. *PLoS Biol,* 11**,** e1001703.

HUBAUD, A. & POURQUIE, O. 2014. Signalling dynamics in vertebrate segmentation. *Nat Rev Mol Cell Biol,* 15**,** 709-21.

HUPPERT, S. S., ILAGAN, M. X., DE STROOPER, B. & KOPAN, R. 2005. Analysis of Notch function in presomitic mesoderm suggests a gamma-secretase-independent role for presenilins in somite differentiation. *Dev Cell,* 8**,** 677-88.

IMAYOSHI, I., ISOMURA, A., HARIMA, Y., KAWAGUCHI, K., KORI, H., MIYACHI, H., FUJIWARA, T., ISHIDATE, F. & KAGEYAMA, R. 2013. Oscillatory control of factors determining multipotency and fate in mouse neural progenitors. *Science,* 342**,** 1203-8.

ISHIBASHI, M., ANG, S. L., SHIOTA, K., NAKANISHI, S., KAGEYAMA, R. & GUILLEMOT, F. 1995. Targeted disruption of mammalian hairy and Enhancer of split homolog-1 (HES-1) leads to up-regulation of neural helix-loop-helix factors, premature neurogenesis, and severe neural tube defects. *Genes Dev,* 9**,** 3136-48.

ISHIKAWA, A., KITAJIMA, S., TAKAHASHI, Y., KOKUBO, H., KANNO, J., INOUE, T. & SAGA, Y. 2004. Mouse Nkd1, a Wnt antagonist, exhibits oscillatory gene expression in the PSM under the control of Notch signaling. *Mech Dev,* 121**,** 1443-53.

ISHIMATSU, K., TAKAMATSU, A. & TAKEDA, H. 2010. Emergence of traveling waves in the zebrafish segmentation clock. *Development,* 137**,** 1595-9.

ITOH, M., KIM, C.-H., PALARDY, G., ODA, T., JIANG, Y.-J., MAUST, D., YEO, S.-Y., LORICK, K., WRIGHT, G. J. & ARIZA-MCNAUGHTON, L. 2003. Mind bomb is a ubiquitin ligase that is essential for efficient activation of Notch signaling by Delta. *Developmental cell,* 4**,** 67-82.

ITOH, N. & ORNITZ, D. M. 2008. Functional evolutionary history of the mouse Fgf gene family. *Developmental Dynamics,* 237**,** 18-27.

JACKSON, S. A., SCHIESSER, J., STANLEY, E. G. & ELEFANTY, A. G. 2010. Differentiating embryonic stem cells pass through 'temporal windows' that mark responsiveness to exogenous and paracrine mesendoderm inducing signals. *PLoS One,* 5**,** e10706.

JAEGER, J. & GOODWIN, B. C. 2001. A cellular oscillator model for periodic pattern formation. *Journal of Theoretical Biology,* 213**,** 171-181.

JAEGER, J. & MONK, N. 2014. Bioattractors: dynamical systems theory and the evolution of regulatory processes. *The Journal of physiology,* 592**,** 2267-2281.

JAENISCH, R. & YOUNG, R. 2008. Stem cells, the molecular circuitry of pluripotency and nuclear reprogramming. *Cell,* 132**,** 567-82.

JAMES, R. G. & SCHULTHEISS, T. M. 2005. Bmp signaling promotes intermediate mesoderm gene expression in a dose-dependent, cell-autonomous and translation-dependent manner. *Dev Biol,* 288**,** 113-25.

JIANG, Y. J., AERNE, B. L., SMITHERS, L., HADDON, C., ISH-HOROWICZ, D. & LEWIS, J. 2000. Notch signalling and the synchronization of the somite segmentation clock. *Nature,* 408**,** 475-9.

JORG, D. J., MORELLI, L. G., ARES, S. & JULICHER, F. 2014. Synchronization dynamics in the presence of coupling delays and phase shifts. *Phys Rev Lett,* 112**,** 174101.

JOUFFE, C., CRETENET, G., SYMUL, L., MARTIN, E., ATGER, F., NAEF, F. & GACHON, F. 2013. The circadian clock coordinates ribosome biogenesis. *PLoS Biol,* 11**,** e1001455.

JOUVE, C., IIMURA, T. & POURQUIE, O. 2002. Onset of the segmentation clock in the chick embryo: evidence for oscillations in the somite precursors in the primitive streak. *Development,* 129**,** 1107-17.

JOUVE, C., PALMEIRIM, I., HENRIQUE, D., BECKERS, J., GOSSLER, A., ISH-HOROWICZ, D. & POURQUIE, O. 2000. Notch signalling is required for cyclic expression of the hairy-like gene HES1 in the presomitic mesoderm. *Development,* 127**,** 1421-9.

JULICH, D., COBB, G., MELO, A. M., MCMILLEN, P., LAWTON, A. K., MOCHRIE, S. G., RHOADES, E. & HOLLEY, S. A. 2015. Cross-Scale Integrin Regulation Organizes ECM and Tissue Topology. *Dev Cell,* 34**,** 33-44.

KAERN, M., MENZINGER, M. & HUNDING, A. 2000. Segmentation and somitogenesis derived from phase dynamics in growing oscillatory media. *Journal of Theoretical Biology,* 207**,** 473-493.

KAESTNER, K. H., BLECKMANN, S. C., MONAGHAN, A. P., SCHLONDORFF, J., MINCHEVA, A., LICHTER, P. & SCHUTZ, G. 1996. Clustered arrangement of winged helix genes fkh-6 and MFH-1: possible implications for mesoderm development. *Development,* 122**,** 1751-8.

KAGEYAMA, R., OHTSUKA, T. & KOBAYASHI, T. 2007. The Hes gene family: repressors and oscillators that orchestrate embryogenesis. *Development,* 134**,** 1243-51.

KAINZ, F., EWEN-CAMPEN, B., AKAM, M. & EXTAVOUR, C. G. 2011. Notch/Delta signalling is not required for segment generation in the basally branching insect Gryllus bimaculatus. *Development,* 138**,** 5015-5026.

KAMINO, K., FUJIMOTO, K. & SAWAI, S. 2011. Collective oscillations in developing cells: insights from simple systems. *Dev Growth Differ,* 53**,** 503-17.

KANKI, J. P. & HO, R. K. 1997. The development of the posterior body in zebrafish. *Development,* 124**,** 881-93.

KARABAGLI, H., KARABAGLI, P., LADHER, R. K. & SCHOENWOLF, G. C. 2002. Comparison of the expression patterns of several fibroblast growth factors during chick gastrulation and neurulation. *Anatomy and embryology,* 205**,** 365-370.

KAWAKAMI, Y., RAYA, A., RAYA, R. M., RODRIGUEZ-ESTEBAN, C. & IZPISUA BELMONTE, J. C. 2005. Retinoic acid signalling links left-right asymmetric patterning and bilaterally symmetric somitogenesis in the zebrafish embryo. *Nature,* 435**,** 165-71.

KENNEDY, M. W., CHALAMALASETTY, R. B., THOMAS, S., GARRIOCK, R. J., JAILWALA, P. & YAMAGUCHI, T. P. 2016. Sp5 and Sp8 recruit beta-catenin and Tcf1-Lef1 to select enhancers to activate Wnt target gene transcription. *Proc Natl Acad Sci U S A,* 113**,** 3545-50.

KERSZBERG, M. & WOLPERT, L. 2000. A clock and trail model for somite formation, specialization and polarization. *J Theor Biol,* 205**,** 505-10.

KEYTE, A. & SMITH, K. K. 2012. Heterochrony in somitogenesis rate in a model marsupial, Monodelphis domestica. *Evolution & development,* 14**,** 93-103.

KIM, N.-G. & GUMBINER, B. M. 2015. Adhesion to fibronectin regulates Hippo signaling via the FAK–Src–PI3K pathway. *The Journal of cell biology,* 210**,** 503-515.

KIM, S. H., JEN, W. C., DE ROBERTIS, E. M. & KINTNER, C. 2000. The protocadherin PAPC establishes segmental boundaries during somitogenesis in xenopus embryos. *Curr Biol,* 10**,** 821-30.

KIM, W., MATSUI, T., YAMAO, M., ISHIBASHI, M., TAMADA, K., TAKUMI, T., KOHNO, K., OBA, S., ISHII, S., SAKUMURA, Y. & BESSHO, Y. 2011. The period of the somite segmentation clock is sensitive to Notch activity. *Mol Biol Cell,* 22**,** 3541-9.

KIMELMAN, D. & MARTIN, B. L. 2012. Anterior–posterior patterning in early development: three strategies. *Wiley Interdisciplinary Reviews: Developmental Biology,* 1**,** 253-266.

KITAJIMA, S., TAKAGI, A., INOUE, T. & SAGA, Y. 2000. MesP1 and MesP2 are essential for the development of cardiac mesoderm. *Development,* 127**,** 3215-26.

KITANO, H. 2004. Biological robustness. *Nat Rev Genet,* 5**,** 826-37.

KLEIN, P. S. & MELTON, D. A. 1994. Induction of mesoderm in Xenopus laevis embryos by translation initiation factor 4E. *SCIENCE-NEW YORK THEN WASHINGTON-***,** 803-803.

KNEZEVIC, V., DE SANTO, R. & MACKEM, S. 1998. Continuing organizer function during chick tail development. *Development,* 125**,** 1791-801.

KOBAYASHI, T., MIZUNO, H., IMAYOSHI, I., FURUSAWA, C., SHIRAHIGE, K. & KAGEYAMA, R. 2009. The cyclic gene Hes1 contributes to diverse differentiation responses of embryonic stem cells. *Genes Dev,* 23**,** 1870-5.

KOIZUMI, K., NAKAJIMA, M., YUASA, S., SAGA, Y., SAKAI, T., KURIYAMA, T., SHIRASAWA, T. & KOSEKI, H. 2001. The role of presenilin 1 during somite segmentation. *Development,* 128**,** 1391-402.

KONDO, S. 2014. Developmental biology. Self-organizing somites. *Science,* 343**,** 736-7.

KONDO, S. & ASAI, R. 1995. A reaction-diffusion wave on the skin of the marine angelfish Pomacanthus. *Nature,* 376**,** 765-768.

KONDO, S. & MIURA, T. 2010. Reaction-diffusion model as a framework for understanding biological pattern formation. *Science,* 329**,** 1616-20.

KOO, B.-K., LIM, H.-S., SONG, R., YOON, M.-J., YOON, K.-J., MOON, J.-S., KIM, Y.-W., KWON, M.-C., YOO, K.-W. & KONG, M.-P. 2005. Mind bomb 1 is essential for generating functional Notch ligands to activate Notch. *Development,* 132**,** 3459-3470.

KROL, A. J., ROELLIG, D., DEQUÉANT, M. L., TASSY, O., GLYNN, E., HATTEM, G., MUSHEGIAN, A., OATES, A. C. & POURQUIÉ, O. 2011. Evolutionary plasticity of segmentation clock networks. *Development,* 138**,** 2783-92.

KUCHINA, A., ESPINAR, L., ÇAĞATAY, T., BALBIN, A. O., ZHANG, F., ALVARADO, A., GARCIA-OJALVO, J. & SÜEL, G. M. 2011. Temporal competition between differentiation programs determines cell fate choice. *Molecular systems biology,* 7**,** 557.

KUGLER, J. E., GAZDOIU, S., ODA-ISHII, I., PASSAMANECK, Y. J., ERIVES, A. J. & DI GREGORIO, A. 2010. Temporal regulation of the muscle gene cascade by Macho1 and Tbx6 transcription factors in Ciona intestinalis. *J Cell Sci,* 123**,** 2453-63.

KULESA, P. M. & FRASER, S. E. 2002. Cell dynamics during somite boundary formation revealed by time-lapse analysis. *Science,* 298**,** 991-5.

KUNATH, T., SABA-EL-LEIL, M. K., ALMOUSAILLEAKH, M., WRAY, J., MELOCHE, S. & SMITH, A. 2007. FGF stimulation of the Erk1/2 signalling cascade triggers transition of pluripotent embryonic stem cells from self-renewal to lineage commitment. *Development,* 134**,** 2895-902.

KURAMOTO, Y. 2012. *Chemical oscillations, waves, and turbulence*, Springer Science & Business Media.

KUSUMI, K., MAY, C. M. & ECKALBAR, W. L. 2013. A large-scale view of the evolution of amniote development: insights from somitogenesis in reptiles. *Current Opinion in Genetics & Development,* 23**,** 491-497.

KWIATKOWSKI, D. J., ZHANG, H., BANDURA, J. L., HEIBERGER, K. M., GLOGAUER, M., EL-HASHEMITE, N. & ONDA, H. 2002. A mouse model of TSC1 reveals sex-dependent lethality from liver hemangiomas, and up-regulation of p70S6 kinase activity in Tsc1 null cells. *Human molecular genetics,* 11**,** 525-534.

LAMAR, E., DEBLANDRE, G., WETTSTEIN, D., GAWANTKA, V., POLLET, N., NIEHRS, C. & KINTNER, C. 2001. Nrarp is a novel intracellular component of the Notch signaling pathway. *Genes & development,* 15**,** 1885-1899.

LANCASTER, M. A., RENNER, M., MARTIN, C. A., WENZEL, D., BICKNELL, L. S., HURLES, M. E., HOMFRAY, T., PENNINGER, J. M., JACKSON, A. P. & KNOBLICH, J. A. 2013. Cerebral organoids model human brain development and microcephaly. *Nature,* 501**,** 373-9.

LANG, A. H., LI, H., COLLINS, J. J. & MEHTA, P. 2014. Epigenetic landscapes explain partially reprogrammed cells and identify key reprogramming genes. *PLoS Comput Biol,* 10**,** e1003734.

LAPLANTE, M. & SABATINI, D. M. 2012. mTOR signaling in growth control and disease. *Cell,* 149**,** 274-293.

LAUSCHKE, V. M. 2013. Scaling of embryonic patterning based on phase-gradient encoding. *Dissertation - University of Heidelberg*.

LAUSCHKE, V. M., TSIAIRIS, C. D., FRANCOIS, P. & AULEHLA, A. 2013. Scaling of embryonic patterning based on phase-gradient encoding. *Nature,* 493**,** 101-5.

LEE, M. T., BONNEAU, A. R. & GIRALDEZ, A. J. 2013. Zygotic genome activation during the maternal-to-zygotic transition. *Annual review of cell and developmental biology,* 30**,** 581-613.

LEIMEISTER, C., EXTERNBRINK, A., KLAMT, B. & GESSLER, M. 1999. Hey genes: a novel subfamily of hairy-and Enhancer of split related genes specifically expressed during mouse embryogenesis. *Mech Dev,* 85**,** 173-7.

LEITGES, M., NEIDHARDT, L., HAENIG, B., HERRMANN, B. G. & KISPERT, A. 2000. The paired homeobox gene Uncx4.1 specifies pedicles, transverse processes and proximal ribs of the vertebral column. *Development,* 127**,** 2259-67.

LEVINE, J. H. & ELOWITZ, M. B. 2014. Polyphasic feedback enables tunable cellular timers. *Current Biology,* 24**,** R994-R995.

LEVINE, J. H., FONTES, M. E., DWORKIN, J. & ELOWITZ, M. B. 2012. Pulsed feedback defers cellular differentiation. *PLoS Biol,* 10**,** e1001252.

LEVINE, J. H., LIN, Y. & ELOWITZ, M. B. 2013. Functional roles of pulsing in genetic circuits. *Science,* 342**,** 1193-1200.

LEWIS, J. 2003. Autoinhibition with transcriptional delay: a simple mechanism for the zebrafish somitogenesis oscillator. *Curr Biol,* 13**,** 1398-408.

LI, C., SCOTT, D. A., HATCH, E., TIAN, X. & MANSOUR, S. L. 2007. Dusp6 (Mkp3) is a negative feedback regulator of FGF-stimulated ERK signaling during mouse development. *Development,* 134**,** 167-76.

LI, T., MA, G., CAI, H., PRICE, D. L. & WONG, P. C. 2003. Nicastrin is required for assembly of presenilin/γ-secretase complexes to mediate Notch signaling and for processing and trafficking of β-amyloid precursor protein in mammals. *The Journal of neuroscience,* 23**,** 3272-3277.

LINASK, K. K., LUDWIG, C., HAN, M. D., LIU, X., RADICE, G. L. & KNUDSEN, K. A. 1998. N-cadherin/catenin-mediated morphoregulation of somite formation. *Dev Biol,* 202**,** 85-102.

LINDNER, B., GARCιA-OJALVO, J., NEIMAN, A. & SCHIMANSKY-GEIER, L. 2004. Effects of noise in excitable systems. *Physics Reports,* 392**,** 321-424.

LIPPMANN, E. S., WILLIAMS, C. E., RUHL, D. A., ESTEVEZ-SILVA, M. C., CHAPMAN, E. R., COON, J. J. & ASHTON, R. S. 2015. Deterministic HOX patterning in human pluripotent stem cell-derived neuroectoderm. *Stem cell reports,* 4**,** 632-644.

LIU, J., PRINDLE, A., HUMPHRIES, J., GABALDA-SAGARRA, M., ASALLY, M., LEE, D. Y., LY, S., GARCIA-OJALVO, J. & SUEL, G. M. 2015. Metabolic co-dependence gives rise to collective oscillations within biofilms. *Nature,* 523**,** 550-4.

LOHMUELLER, J. J., ARMEL, T. Z. & SILVER, P. A. 2012. A tunable zinc finger-based framework for Boolean logic computation in mammalian cells. *Nucleic acids research***,** gks142.

LOMBERK, G., BENSI, D., FERNANDEZ-ZAPICO, M. E. & URRUTIA, R. 2006. Evidence for the existence of an HP1-mediated subcode within the histone code. *Nat Cell Biol,* 8**,** 407-15.

LOPEZ, T. P. & FAN, C. M. 2013. Dynamic CREB family activity drives segmentation and posterior polarity specification in mammalian somitogenesis. *Proc Natl Acad Sci U S A,* 110**,** E2019-27.

LU, C. & THOMPSON, C. B. 2012. Metabolic regulation of epigenetics. *Cell metabolism,* 16**,** 9-17.

LU, R., YANG, A. & JIN, Y. 2011. Dual functions of T-box 3 (Tbx3) in the control of self-renewal and extraembryonic endoderm differentiation in mouse embryonic stem cells. *Journal of Biological Chemistry,* 286**,** 8425-8436.

MA, L., CHEN, Z., ERDJUMENT-BROMAGE, H., TEMPST, P. & PANDOLFI, P. P. 2005. Phosphorylation and functional inactivation of TSC2 by Erk: implications for tuberous sclerosisand cancer pathogenesis. *Cell,* 121**,** 179-193.

MACDONALD, B. T., ADAMSKA, M. & MEISLER, M. H. 2004. Hypomorphic expression of Dkk1 in the doubleridge mouse: dose dependence and compensatory interactions with Lrp6. *Development,* 131**,** 2543-52.

MALLO, M. 2015. Revisiting the involvement of signaling gradients in somitogenesis. *FEBS J.*

MALLO, M., WELLIK, D. M. & DESCHAMPS, J. 2010. Hox genes and regional patterning of the vertebrate body plan. *Developmental biology,* 344**,** 7-15.

MANSOURI, A., VOSS, A. K., THOMAS, T., YOKOTA, Y. & GRUSS, P. 2000. Uncx4.1 is required for the formation of the pedicles and proximal ribs and acts upstream of Pax9. *Development,* 127**,** 2251-8.

MARA, A. & HOLLEY, S. A. 2007. Oscillators and the emergence of tissue organization during zebrafish somitogenesis. *Trends Cell Biol,* 17**,** 593-9.

MARR, C., ZHOU, J. X. & HUANG, S. 2016. Single-Cell Gene Expression Profi ling and Cell State Dynamics: Collecting Data, Correlating Data Points and Connecting the Dots. *bioRxiv***,** 044743.

MARTIN, B. L. & KIMELMAN, D. 2009. Wnt signaling and the evolution of embryonic posterior development. *Curr Biol,* 19**,** R215-9.

MARTINS, G. G., RIFES, P., AMANDIO, R., RODRIGUES, G., PALMEIRIM, I. & THORSTEINSDOTTIR, S. 2009. Dynamic 3D cell rearrangements guided by a fibronectin matrix underlie somitogenesis. *PLoS One,* 4**,** e7429.

MARUHASHI, M., VAN DE PUTTE, T., HUYLEBROECK, D., KONDOH, H. & HIGASHI, Y. 2005. Involvement of SIP1 in positioning of somite boundaries in the mouse embryo. *Dev Dyn,* 234**,** 332-8.

MASAMIZU, Y., OHTSUKA, T., TAKASHIMA, Y., NAGAHARA, H., TAKENAKA, Y., YOSHIKAWA, K., OKAMURA, H. & KAGEYAMA, R. 2006. Real-time imaging of the somite segmentation clock: revelation of unstable oscillators in the individual presomitic mesoderm cells. *Proc Natl Acad Sci U S A,* 103**,** 1313-8.

MAURY, Y., CÔME, J., PISKOROWSKI, R. A., SALAH-MOHELLIBI, N., CHEVALEYRE, V., PESCHANSKI, M., MARTINAT, C. & NEDELEC, S. 2015. Combinatorial analysis of developmental cues efficiently converts human pluripotent stem cells into multiple neuronal subtypes. *Nature biotechnology,* 33**,** 89-96.

MCGREGOR, A. P., PECHMANN, M., SCHWAGER, E. E. & DAMEN, W. G. 2009. An ancestral regulatory network for posterior development in arthropods. *Communicative & integrative biology,* 2**,** 174-176.

MCGREW, M. J., SHERMAN, A., LILLICO, S. G., ELLARD, F. M., RADCLIFFE, P. A., GILHOOLEY, H. J., MITROPHANOUS, K. A., CAMBRAY, N., WILSON, V. & SANG, H. 2008. Localised axial progenitor cell populations in the avian tail bud are not committed to a posterior Hox identity. *Development,* 135**,** 2289-99.

MCMILLEN, P., CHATTI, V., JULICH, D. & HOLLEY, S. A. 2016. A Sawtooth Pattern of Cadherin 2 Stability Mechanically Regulates Somite Morphogenesis. *Curr Biol,* 26**,** 542-9.

MEHTA, P. & GREGOR, T. 2010. Approaching the molecular origins of collective dynamics in oscillating cell populations. *Curr Opin Genet Dev,* 20**,** 574-80.

MEINHARDT, A., EBERLE, D., TAZAKI, A., RANGA, A., NIESCHE, M., WILSCH-BRAUNINGER, M., STEC, A., SCHACKERT, G., LUTOLF, M. & TANAKA, E. M. 2014. 3D reconstitution of the patterned neural tube from embryonic stem cells. *Stem Cell Reports,* 3**,** 987-99.

MEINHARDT, H. 1986. Models of segmentation. *Somites in developing embryos.* Springer.

MEINHARDT, H. 2004. Out-of-phase oscillations and traveling waves with unusual properties: the use of three-component systems in biology. *Physica D: Nonlinear Phenomena,* 199**,** 264-277.

MIKELS, A. J. & NUSSE, R. 2006. Wnts as ligands: processing, secretion and reception. *Oncogene,* 25**,** 7461-8.

MIKKELSEN, T. S., KU, M., JAFFE, D. B., ISSAC, B., LIEBERMAN, E., GIANNOUKOS, G., ALVAREZ, P., BROCKMAN, W., KIM, T.-K. & KOCHE, R. P. 2007. Genome-wide maps of chromatin state in pluripotent and lineage-committed cells. *Nature,* 448**,** 553-560.

MILEV, N. B. & REDDY, A. B. 2015. Circadian redox oscillations and metabolism. *Trends Endocrinol Metab,* 26**,** 430-7.

MILLER, S. A., HUANG, A. C., MIAZGOWICZ, M. M., BRASSIL, M. M. & WEINMANN, A. S. 2008. Coordinated but physically separable interaction with H3K27-demethylase and H3K4-methyltransferase activities are required for T-box protein-mediated activation of developmental gene expression. *Genes Dev,* 22**,** 2980-93.

MILLER, S. A., MOHN, S. E. & WEINMANN, A. S. 2010. Jmjd3 and UTX play a demethylase-independent role in chromatin remodeling to regulate T-box family member-dependent gene expression. *Mol Cell,* 40**,** 594-605.

MIURA, S., DAVIS, S., KLINGENSMITH, J. & MISHINA, Y. 2006. BMP signaling in the epiblast is required for proper recruitment of the prospective paraxial mesoderm and development of the somites. *Development,* 133**,** 3767-75.

MONK, N. A. 2003. Oscillatory expression of Hes1, p53, and NF-kappaB driven by transcriptional time delays. *Curr Biol,* 13**,** 1409-13.

MORELLI, L. G., ARES, S., HERRGEN, L., SCHROTER, C., JULICHER, F. & OATES, A. C. 2009. Delayed coupling theory of vertebrate segmentation. *HFSP J,* 3**,** 55-66.

MORENO-RISUENO, M. A., VAN NORMAN, J. M., MORENO, A., ZHANG, J. Y., AHNERT, S. E. & BENFEY, P. N. 2010. Oscillating Gene Expression Determines Competence for Periodic Arabidopsis Root Branching. *Science,* 329**,** 1306-1311.

MORENO, T. A., JAPPELLI, R., BELMONTE, J. C. I. & KINTNER, C. 2008. Retinoic acid regulation of the Mesp–Ripply feedback loop during vertebrate segmental patterning. *Developmental biology,* 315**,** 317-330.

MORENO, T. A. & KINTNER, C. 2004. Regulation of segmental patterning by retinoic acid signaling during Xenopus somitogenesis. *Dev Cell,* 6**,** 205-18.

MORIMOTO, M., KISO, M., SASAKI, N. & SAGA, Y. 2006. Cooperative Mesp activity is required for normal somitogenesis along the anterior-posterior axis. *Dev Biol,* 300**,** 687-98.

MORIMOTO, M., SASAKI, N., OGINUMA, M., KISO, M., IGARASHI, K., AIZAKI, K., KANNO, J. & SAGA, Y. 2007. The negative regulation of Mesp2 by mouse Ripply2 is required to establish the rostro-caudal patterning within a somite. *Development,* 134**,** 1561-9.

MORIMOTO, M., TAKAHASHI, Y., ENDO, M. & SAGA, Y. 2005. The Mesp2 transcription factor establishes segmental borders by suppressing Notch activity. *Nature,* 435**,** 354-9.

MORIN-KENSICKI, E. M., BOONE, B. N., HOWELL, M., STONEBRAKER, J. R., TEED, J., ALB, J. G., MAGNUSON, T. R., O'NEAL, W. & MILGRAM, S. L. 2006. Defects in yolk sac vasculogenesis, chorioallantoic fusion, and embryonic axis elongation in mice with targeted disruption of Yap65. *Molecular and cellular biology,* 26**,** 77-87.

MORRIS, S. A., CAHAN, P., LI, H., ZHAO, A. M., SAN ROMAN, A. K., SHIVDASANI, R. A., COLLINS, J. J. & DALEY, G. Q. 2014. Dissecting engineered cell types and enhancing cell fate conversion via CellNet. *Cell,* 158**,** 889-902.

MOURIKIS, P., LAKE, R. J., FIRNHABER, C. B. & DEDECKER, B. S. 2010. Modifiers of notch transcriptional activity identified by genome-wide RNAi. *BMC developmental biology,* 10**,** 1.

MULLER, P., ROGERS, K. W., YU, S. R., BRAND, M. & SCHIER, A. F. 2013. Morphogen transport. *Development,* 140**,** 1621-38.

MURAKAMI, M., ICHISAKA, T., MAEDA, M., OSHIRO, N., HARA, K., EDENHOFER, F., KIYAMA, H., YONEZAWA, K. & YAMANAKA, S. 2004. mTOR is essential for growth and proliferation in early mouse embryos and embryonic stem cells. *Molecular and cellular biology,* 24**,** 6710-6718.

MURRAY, P. J., MAINI, P. K. & BAKER, R. E. 2011. The clock and wavefront model revisited. *J Theor Biol,* 283**,** 227-38.

MURTAUGH, L. C., STANGER, B. Z., KWAN, K. M. & MELTON, D. A. 2003. Notch signaling controls multiple steps of pancreatic differentiation. *Proceedings of the National Academy of Sciences,* 100**,** 14920-14925.

NAGAHARA, H., MA, Y., TAKENAKA, Y., KAGEYAMA, R. & YOSHIKAWA, K. 2009. Spatiotemporal pattern in somitogenesis: A non-Turing scenario with wave propagation. *Physical Review E,* 80**,** 021906.

NAGUMO, J., ARIMOTO, S. & YOSHIZAWA, S. 1962. An Active Pulse Transmission Line Simulating Nerve Axon. *Proceedings of the IRE,* 50**,** 2061-2070.

NAHMAD, M. & STATHOPOULOS, A. 2009. Dynamic interpretation of hedgehog signaling in the Drosophila wing disc. *PLoS Biol,* 7**,** e1000202.

NAICHE, L. A., HOLDER, N. & LEWANDOSKI, M. 2011. FGF4 and FGF8 comprise the wavefront activity that controls somitogenesis. *Proc Natl Acad Sci U S A,* 108**,** 4018-23.

NAKAJIMA, Y., MORIMOTO, M., TAKAHASHI, Y., KOSEKI, H. & SAGA, Y. 2006. Identification of Epha4 enhancer required for segmental expression and the regulation by Mesp2. *Development,* 133**,** 2517-25.

NAKAMOTO, A., HESTER, S., CONSTANTINOU, S., BLAINE, W., TEWKSBURY, A., MATEI, M., NAGY, L. M. & WILLIAMS, T. 2015. Changing cell behaviours during beetle embryogenesis correlates with slowing of segmentation. *Nature communications,* 6.

NEDA, Z., RAVASZ, E., VICSEK, T., BRECHET, Y. & BARABASI, A. L. 2000. Physics of the rhythmic applause. *Phys Rev E Stat Phys Plasmas Fluids Relat Interdiscip Topics,* 61**,** 6987-92.

NELSON, D., IHEKWABA, A., ELLIOTT, M., JOHNSON, J., GIBNEY, C., FOREMAN, B., NELSON, G., SEE, V., HORTON, C. & SPILLER, D. 2004. Oscillations in NF-κB signaling control the dynamics of gene expression. *Science,* 306**,** 704-708.

NGUYEN, P. D., HOLLWAY, G. E., SONNTAG, C., MILES, L. B., HALL, T. E., BERGER, S., FERNANDEZ, K. J., GUREVICH, D. B., COLE, N. J., ALAEI, S., RAMIALISON, M., SUTHERLAND, R. L., POLO, J. M., LIESCHKE, G. J. & CURRIE, P. D. 2014. Haematopoietic stem cell induction by somite-derived endothelial cells controlled by meox1. *Nature,* 512**,** 314-8.

NICHOLS, J., SILVA, J., ROODE, M. & SMITH, A. 2009. Suppression of Erk signalling promotes ground state pluripotency in the mouse embryo. *Development,* 136**,** 3215-22.

NICHOLS, J. & SMITH, A. 2012. Pluripotency in the embryo and in culture. *Cold Spring Harb Perspect Biol,* 4**,** a008128.

NIEDERREITHER, K., ABU-ABED, S., SCHUHBAUR, B., PETKOVICH, M., CHAMBON, P. & DOLLÉ, P. 2002. Genetic evidence that oxidative derivatives of retinoic acid are not involved in retinoid signaling during mouse development. *Nat Genet,* 31**,** 84-8.

NIEDERREITHER, K., MCCAFFERY, P., DRÄGER, U. C., CHAMBON, P. & DOLLÉ, P. 1997. Restricted expression and retinoic acid-induced downregulation of the retinaldehyde dehydrogenase type 2 (RALDH-2) gene during mouse development. *Mech Dev,* 62**,** 67-78.

NITANDA, Y., MATSUI, T., MATTA, T., HIGAMI, A., KOHNO, K., NAKAHATA, Y. & BESSHO, Y. 2013. 3'-UTR-dependent regulation of mRNA turnover is critical for differential distribution patterns of cyclic gene mRNAs. *FEBS J*.

NIWA, H. 2011. Wnt: what's needed to maintain pluripotency? *Nat Cell Biol,* 13**,** 1024-6.

NIWA, Y., MASAMIZU, Y., LIU, T., NAKAYAMA, R., DENG, C. X. & KAGEYAMA, R. 2007. The initiation and propagation of Hes7 oscillation are cooperatively regulated by Fgf and notch signaling in the somite segmentation clock. *Dev Cell,* 13**,** 298-304.

NIWA, Y., SHIMOJO, H., ISOMURA, A., GONZALEZ, A., MIYACHI, H. & KAGEYAMA, R. 2011. Different types of oscillations in Notch and Fgf signaling regulate the spatiotemporal periodicity of somitogenesis. *Genes Dev,* 25**,** 1115-20.

NOVAK, B. & TYSON, J. J. 2008. Design principles of biochemical oscillators. *Nat Rev Mol Cell Biol,* 9**,** 981-91.

NOWOTSCHIN, S., FERRER-VAQUER, A., CONCEPCION, D., PAPAIOANNOU, V. E. & HADJANTONAKIS, A. K. 2012. Interaction of Wnt3a, Msgn1 and Tbx6 in neural versus paraxial mesoderm lineage commitment and paraxial mesoderm differentiation in the mouse embryo. *Dev Biol,* 367**,** 1-14.

O'NEILL, J. S. & REDDY, A. B. 2011. Circadian clocks in human red blood cells. *Nature,* 469**,** 498-503.

O'NEILL, J. S., VAN OOIJEN, G., DIXON, L. E., TROEIN, C., CORELLOU, F., BOUGET, F. Y., REDDY, A. B. & MILLAR, A. J. 2011. Circadian rhythms persist without transcription in a eukaryote. *Nature,* 469**,** 554-8.

O'NEILL, K. & THORPE, C. 2013. BMP signaling and spadetail regulate exit of muscle precursors from the zebrafish tailbud. *Developmental biology,* 375**,** 117-127.

OATES, A. C. & HO, R. K. 2002. Hairy/E(spl)-related (Her) genes are central components of the segmentation oscillator and display redundancy with the Delta/Notch signaling pathway in the formation of anterior segmental boundaries in the zebrafish. *Development,* 129**,** 2929-46.

OATES, A. C., MORELLI, L. G. & ARES, S. 2012. Patterning embryos with oscillations: structure, function and dynamics of the vertebrate segmentation clock. *Development,* 139**,** 625-39.

OGAWA, H., ISHIGURO, K., GAUBATZ, S., LIVINGSTON, D. M. & NAKATANI, Y. 2002. A complex with chromatin modifiers that occupies E2F- and Myc-responsive genes in G0 cells. *Science,* 296**,** 1132-6.

OGINUMA, M., HIRATA, T. & SAGA, Y. 2008a. Identification of presomitic mesoderm (PSM)-specific Mesp1 enhancer and generation of a PSM-specific Mesp1/Mesp2-null mouse using BAC-based rescue technology. *Mech Dev,* 125**,** 432-40.

OGINUMA, M., NIWA, Y., CHAPMAN, D. L. & SAGA, Y. 2008b. Mesp2 and Tbx6 cooperatively create periodic patterns coupled with the clock machinery during mouse somitogenesis. *Development,* 135**,** 2555-62.

OGINUMA, M., TAKAHASHI, Y., KITAJIMA, S., KISO, M., KANNO, J., KIMURA, A. & SAGA, Y. 2010. The oscillation of Notch activation, but not its boundary, is required for somite border formation and rostral-caudal patterning within a somite. *Development,* 137**,** 1515-22.

OHTSUKA, T., ISHIBASHI, M., GRADWOHL, G., NAKANISHI, S., GUILLEMOT, F. & KAGEYAMA, R. 1999. Hes1 and Hes5 as notch effectors in mammalian neuronal differentiation. *EMBO J,* 18**,** 2196-207.

OHUCHI, H., KIMURA, S., WATAMOTO, M. & ITOH, N. 2000. Involvement of fibroblast growth factor (FGF) 18-FGF8 signaling in specification of left-right asymmetry and brain and limb development of the chick embryo. *Mechanisms of development,* 95**,** 55-66.

OKA, C., NAKANO, T., WAKEHAM, A., DE LA POMPA, J. L., MORI, C., SAKAI, T., OKAZAKI, S., KAWAICHI, M., SHIOTA, K., MAK, T. W. & HONJO, T. 1995. Disruption of the mouse RBP-J kappa gene results in early embryonic death. *Development,* 121**,** 3291-301.

OKUBO, Y., SUGAWARA, T., ABE-KODUKA, N., KANNO, J., KIMURA, A. & SAGA, Y. 2012. Lfng regulates the synchronized oscillation of the mouse segmentation clock via trans-repression of Notch signalling. *Nat Commun,* 3**,** 1141.

OLIVERA-MARTINEZ, I., HARADA, H., HALLEY, P. A. & STOREY, K. G. 2012. Loss of FGF-dependent mesoderm identity and rise of endogenous retinoid signalling determine cessation of body axis elongation. *PLoS Biol,* 10**,** e1001415.

OLIVERA-MARTINEZ, I., SCHURCH, N., LI, R. A., SONG, J., HALLEY, P. A., DAS, R. M., BURT, D. W., BARTON, G. J. & STOREY, K. G. 2014. Major transcriptome re-organisation and abrupt changes in signalling, cell cycle and chromatin regulation at neural differentiation in vivo. *Development,* 141**,** 3266-3276.

OSTER, G. F., MURRAY, J. D. & HARRIS, A. K. 1983. Mechanical aspects of mesenchymal morphogenesis. *J Embryol Exp Morphol,* 78**,** 83-125.

OYAMA, T., HARIGAYA, K., SASAKI, N., OKAMURA, Y., KOKUBO, H., SAGA, Y., HOZUMI, K., SUGANAMI, A., TAMURA, Y. & NAGASE, T. 2011. Mastermind-like 1 (MamL1) and mastermind-like 3 (MamL3) are essential for Notch signaling in vivo. *Development,* 138**,** 5235-5246.

OZBUDAK, E. M. & LEWIS, J. 2008. Notch signalling synchronizes the zebrafish segmentation clock but is not needed to create somite boundaries. *PLoS Genet,* 4**,** e15.

OZBUDAK, E. M., TASSY, O. & POURQUIE, O. 2010. Spatiotemporal compartmentalization of key physiological processes during muscle precursor differentiation. *Proc Natl Acad Sci U S A,* 107**,** 4224-9.

PACKHAM, E. A. & BROOK, J. D. 2003. T-box genes in human disorders. *Human Molecular Genetics,* 12**,** R37-R44.

PAGLIUCA, F. W., MILLMAN, J. R., GÜRTLER, M., SEGEL, M., VAN DERVORT, A., RYU, J. H., PETERSON, Q. P., GREINER, D. & MELTON, D. A. 2014. Generation of functional human pancreatic β cells in vitro. *Cell,* 159**,** 428-439.

PAIGE, J. S., WU, K. Y. & JAFFREY, S. R. 2011. RNA mimics of green fluorescent protein. *Science,* 333**,** 642-646.

PALMEIRIM, I., DUBRULLE, J., HENRIQUE, D., ISH-HOROWICZ, D. & POURQUIE, O. 1998. Uncoupling segmentation and somitogenesis in the chick presomitic mesoderm. *Dev Genet,* 23**,** 77-85.

PALMEIRIM, I., HENRIQUE, D., ISH-HOROWICZ, D. & POURQUIÉ, O. 1997. Avian hairy gene expression identifies a molecular clock linked to vertebrate segmentation and somitogenesis. *Cell,* 91**,** 639-48.

PANOVSKA-GRIFFITHS, J., PAGE, K. M. & BRISCOE, J. 2013. A gene regulatory motif that generates oscillatory or multiway switch outputs. *Journal of The Royal Society Interface,* 10**,** 20120826.

PARK, H. W., KIM, Y. C., YU, B., MOROISHI, T., MO, J.-S., PLOUFFE, S. W., MENG, Z., LIN, K. C., YU, F.-X. & ALEXANDER, C. M. 2015. Alternative Wnt signaling activates YAP/TAZ. *Cell,* 162**,** 780-794.

PASINI, A., MANENTI, R., ROTHBACHER, U. & LEMAIRE, P. 2012. Antagonizing retinoic acid and FGF/MAPK pathways control posterior body patterning in the invertebrate chordate Ciona intestinalis. *PLoS One,* 7**,** e46193.

PAULL, D., SEVILLA, A., ZHOU, H., HAHN, A. K., KIM, H., NAPOLITANO, C., TSANKOV, A., SHANG, L., KRUMHOLZ, K. & JAGADEESAN, P. 2015. Automated, high-throughput derivation, characterization and differentiation of induced pluripotent stem cells. *Nature methods,* 12**,** 885-892.

PEEL, A. D., CHIPMAN, A. D. & AKAM, M. 2005. Arthropod segmentation: Beyond the Drosophila paradigm. *Nature Reviews Genetics,* 6**,** 905-916.

PERANTONI, A. O., TIMOFEEVA, O., NAILLAT, F., RICHMAN, C., PAJNI-UNDERWOOD, S., WILSON, C., VAINIO, S., DOVE, L. F. & LEWANDOSKI, M. 2005. Inactivation of FGF8 in early mesoderm reveals an essential role in kidney development. *Development,* 132**,** 3859-71.

PESHKIN, L., WUHR, M., PEARL, E., HAAS, W., FREEMAN, R. M., JR., GERHART, J. C., KLEIN, A. M., HORB, M., GYGI, S. P. & KIRSCHNER, M. W. 2015. On the Relationship of Protein and mRNA Dynamics in Vertebrate Embryonic Development. *Dev Cell,* 35**,** 383-94.

PETER LOPEZ, T. & FAN, C. M. 2012. A transgenic Tbx6;CreERT2 line for inducible gene manipulation in the presomitic mesoderm. *Genesis,* 50**,** 490-5.

PETERSEN, C. P. & REDDIEN, P. W. 2009. Wnt signaling and the polarity of the primary body axis. *Cell,* 139**,** 1056-1068.

PFEUTY, B. & KANEKO, K. 2014. Reliable binary cell-fate decisions based on oscillations. *Physical Review E,* 89**,** 022707.

PIERSMA, B., BANK, R. A. & BOERSEMA, M. 2015. Signaling in fibrosis: TGF-β, wNT, and YAP/TAZ converge. *Frontiers in medicine,* 2.

PRIMMETT, D. R., NORRIS, W. E., CARLSON, G. J., KEYNES, R. J. & STERN, C. D. 1989. Periodic segmental anomalies induced by heat shock in the chick embryo are associated with the cell cycle. *Development,* 105**,** 119-30.

PRIMMETT, D. R., STERN, C. D. & KEYNES, R. J. 1988. Heat shock causes repeated segmental anomalies in the chick embryo. *Development,* 104**,** 331-9.

PUEYO, J. I., LANFEAR, R. & COUSO, J. P. 2008. Ancestral Notch-mediated segmentation revealed in the cockroach Periplaneta americana. *Proceedings of the National Academy of Sciences of the United States of America,* 105**,** 16614-16619.

QUACKENBUSH, J. 2001. Computational analysis of microarray data. *Nat Rev Genet,* 2**,** 418-427.

RACKHAM, O. J., FIRAS, J., FANG, H., OATES, M. E., HOLMES, M. L., KNAUPP, A. S., SUZUKI, H., NEFZGER, C. M., DAUB, C. O. & SHIN, J. W. 2016. A predictive computational framework for direct reprogramming between human cell types. *Nature genetics*.

RADICE, G. L., RAYBURN, H., MATSUNAMI, H., KNUDSEN, K. A., TAKEICHI, M. & HYNES, R. O. 1997. Developmental defects in mouse embryos lacking N-cadherin. *Dev Biol,* 181**,** 64-78.

RAFF, M. Intracellular developmental timers. Cold Spring Harbor symposia on quantitative biology, 2007. Cold Spring Harbor Laboratory Press, 431-435.

RAJ, A., VAN DEN BOGAARD, P., RIFKIN, S. A., VAN OUDENAARDEN, A. & TYAGI, S. 2008. Imaging individual mRNA molecules using multiple singly labeled probes. *Nature methods,* 5**,** 877.

RALLIS, C., PINCHIN, S. M. & ISH-HOROWICZ, D. 2010. Cell-autonomous integrin control of Wnt and Notch signalling during somitogenesis. *Development,* 137**,** 3591-3601.

RAN, F. A., HSU, P. D., LIN, C.-Y., GOOTENBERG, J. S., KONERMANN, S., TREVINO, A. E., SCOTT, D. A., INOUE, A., MATOBA, S. & ZHANG, Y. 2013. Double nicking by RNA-guided CRISPR Cas9 for enhanced genome editing specificity. *Cell,* 154**,** 1380-1389.

RANGEL, M. C., KARASAWA, H., CASTRO, N. P., NAGAOKA, T., SALOMON, D. S. & BIANCO, C. 2012. Role of Cripto-1 during epithelial-to-mesenchymal transition in development and cancer. *The American journal of pathology,* 180**,** 2188-2200.

RASPOPOVIC, J., MARCON, L., RUSSO, L. & SHARPE, J. 2014. Modeling digits. Digit patterning is controlled by a Bmp-Sox9-Wnt Turing network modulated by morphogen gradients. *Science,* 345**,** 566-70.

RESENDE, T. P., FERREIRA, M., TEILLET, M.-A., TAVARES, A. T., ANDRADE, R. P. & PALMEIRIM, I. 2010. Sonic hedgehog in temporal control of somite formation. *Proceedings of the National Academy of Sciences,* 107**,** 12907-12912.

RETNOAJI, B., AKIYAMA, R., MATTA, T., BESSHO, Y. & MATSUI, T. 2014. Retinoic acid controls proper head-to-trunk linkage in zebrafish by regulating an anteroposterior somitogenetic rate difference. *Development,* 141**,** 158-165.

RHEE, J., TAKAHASHI, Y., SAGA, Y., WILSON-RAWLS, J. & RAWLS, A. 2003. The protocadherin papc is involved in the organization of the epithelium along the segmental border during mouse somitogenesis. *Dev Biol,* 254**,** 248-61.

RICHARDSON, M. K., ALLEN, S. P., WRIGHT, G. M., RAYNAUD, A. & HANKEN, J. 1998. Somite number and vertebrate evolution. *Development,* 125**,** 151-160.

RIEDEL-KRUSE, I. H., MÜLLER, C. & OATES, A. C. 2007. Synchrony dynamics during initiation, failure, and rescue of the segmentation clock. *Science,* 317**,** 1911-5.

RILEY, M. F., BOCHTER, M. S., WAHI, K., NUOVO, G. J. & COLE, S. E. 2013. Mir-125a-5p-mediated regulation of Lfng is essential for the avian segmentation clock. *Dev Cell,* 24**,** 554-61.

ROGERS, K. W. & SCHIER, A. F. 2011. Morphogen gradients: from generation to interpretation. *Annu Rev Cell Dev Biol,* 27**,** 377-407.

RON, D. & HARDING, H. P. 2007. 13 eIF2α Phosphorylation in Cellular Stress Responses and Disease. *Cold Spring Harbor Monograph Archive,* 48**,** 345-368.

ROSENBLUH, J., NIJHAWAN, D., COX, A. G., LI, X., NEAL, J. T., SCHAFER, E. J., ZACK, T. I., WANG, X., TSHERNIAK, A. & SCHINZEL, A. C. 2012. β-Catenin-driven cancers require a YAP1 transcriptional complex for survival and tumorigenesis. *Cell,* 151**,** 1457-1473.

ROSSANT, J., ZIRNGIBL, R., CADO, D., SHAGO, M. & GIGUÈRE, V. 1991. Expression of a retinoic acid response element-hsplacZ transgene defines specific domains of transcriptional activity during mouse embryogenesis. *Genes Dev,* 5**,** 1333-44.

ROW, R. H. & KIMELMAN, D. 2009. Bmp inhibition is necessary for post-gastrulation patterning and morphogenesis of the zebrafish tailbud. *Developmental biology,* 329**,** 55-63.

ROWTON, M., RAMOS, P., ANDERSON, D. M., RHEE, J. M., CUNLIFFE, H. E. & RAWLS, A. 2013. Regulation of mesenchymal-to-epithelial transition by PARAXIS during somitogenesis. *Dev Dyn,* 242**,** 1332-44.

ROY, M. N., PRINCE, V. E. & HO, R. K. 1999. Heat shock produces periodic somitic disturbances in the zebrafish embryo. *Mech Dev,* 85**,** 27-34.

SAGA, Y. 2012. The mechanism of somite formation in mice. *Curr Opin Genet Dev,* 22**,** 331-8.

SAGA, Y., HATA, N., KOSEKI, H. & TAKETO, M. M. 1997. Mesp2: a novel mouse gene expressed in the presegmented mesoderm and essential for segmentation initiation. *Genes Dev,* 11**,** 1827-39.

SAGA, Y. & TAKEDA, H. 2001. The making of the somite: molecular events in vertebrate segmentation. *Nat Rev Genet,* 2**,** 835-45.

SAGER, B. M. 1996. Propagation of traveling waves in excitable media. *Genes Dev,* 10**,** 2237-50.

SAKAI, Y., MENO, C., FUJII, H., NISHINO, J., SHIRATORI, H., SAIJOH, Y., ROSSANT, J. & HAMADA, H. 2001. The retinoic acid-inactivating enzyme CYP26 is essential for establishing an uneven distribution of retinoic acid along the anterio-posterior axis within the mouse embryo. *Genes Dev,* 15**,** 213-25.

SANCHEZ, C. G., TEIXEIRA, F. K., CZECH, B., PREALL, J. B., ZAMPARINI, A. L., SEIFERT, J. R., MALONE, C. D., HANNON, G. J. & LEHMANN, R. 2015. Regulation of Ribosome Biogenesis and Protein Synthesis Controls Germline Stem Cell Differentiation. *Cell stem cell*.

SARRAZIN, A. F., PEEL, A. D. & AVEROF, M. 2012. A segmentation clock with two-segment periodicity in insects. *Science,* 336**,** 338-41.

SASAI, Y., KAGEYAMA, R., TAGAWA, Y., SHIGEMOTO, R. & NAKANISHI, S. 1992. Two mammalian helix-loop-helix factors structurally related to Drosophila hairy and Enhancer of split. *Genes Dev,* 6**,** 2620-34.

SASAKI, N., KISO, M., KITAGAWA, M. & SAGA, Y. 2011. The repression of Notch signaling occurs via the destabilization of mastermind-like 1 by Mesp2 and is essential for somitogenesis. *Development,* 138**,** 55-64.

SATOU, Y., IMAI, K. S. & SATOH, N. 2004. The ascidian Mesp gene specifies heart precursor cells. *Development,* 131**,** 2533-41.

SAWADA, A., KIYONARI, H., UKITA, K., NISHIOKA, N., IMUTA, Y. & SASAKI, H. 2008. Redundant roles of Tead1 and Tead2 in notochord development and the regulation of cell proliferation and survival. *Molecular and cellular biology,* 28**,** 3177-3189.

SAWADA, A., SAGA, Y. & TAKEDA, H. 2000. [Zebrafish somitogenesis-roles of mesp- and hairy-related genes]. *Tanpakushitsu Kakusan Koso,* 45**,** 2738-44.

SAWADA, A., SHINYA, M., JIANG, Y. J., KAWAKAMI, A., KUROIWA, A. & TAKEDA, H. 2001. Fgf/MAPK signalling is a crucial positional cue in somite boundary formation. *Development,* 128**,** 4873-80.

SCHIER, A. F. & TALBOT, W. S. 2005. Molecular genetics of axis formation in zebrafish. *Annu Rev Genet,* 39**,** 561-613.

SCHMIDT, E. K., CLAVARINO, G., CEPPI, M. & PIERRE, P. 2009. SUnSET, a nonradioactive method to monitor protein synthesis. *Nature methods,* 6**,** 275-277.

SCHNELL, S. & MAINI, P. K. 2000. Clock and induction model for somitogenesis. *Developmental Dynamics,* 217**,** 415-420.

SCHRÖTER, C., ARES, S., MORELLI, L. G., ISAKOVA, A., HENS, K., SOROLDONI, D., GAJEWSKI, M., JÜLICHER, F., MAERKL, S. J., DEPLANCKE, B. & OATES, A. C. 2012. Topology and dynamics of the zebrafish segmentation clock core circuit. *PLoS Biol,* 10**,** e1001364.

SCHRÖTER, C., HERRGEN, L., CARDONA, A., BROUHARD, G. J., FELDMAN, B. & OATES, A. C. 2008. Dynamics of zebrafish somitogenesis. *Dev Dyn,* 237**,** 545-53.

SCHROTER, C. & OATES, A. C. 2010. Segment number and axial identity in a segmentation clock period mutant. *Curr Biol,* 20**,** 1254-8.

SCHULTZ, D., LU, M., STAVROPOULOS, T. & BEN-JACOB, E. 2013. Turning oscillations into opportunities: lessons from a bacterial decision gate. *Scientific reports,* 3.

SCHULTZ, J. 1929. The Minute reaction in the development of Drosophila melanogaster. *Genetics,* 14**,** 366-419.

SCHUSTER-GOSSLER, K., HARRIS, B., JOHNSON, K. R., SERTH, J. & GOSSLER, A. 2009. Notch signalling in the paraxial mesoderm is most sensitive to reduced Pofut1 levels during early mouse development. *BMC developmental biology,* 9**,** 6.

SCHWAB, D. J., BAETICA, A. & MEHTA, P. 2012. Dynamical quorum-sensing in oscillators coupled through an external medium. *Physica D: Nonlinear Phenomena,* 241**,** 1782-1788.

SCHWENDINGER-SCHRECK, J., KANG, Y. & HOLLEY, S. A. 2014. Modeling the zebrafish segmentation clock's gene regulatory network constrained by expression data suggests evolutionary transitions between oscillating and nonoscillating transcription. *Genetics,* 197**,** 725-38.

SEBE-PEDROS, A., ARIZA-COSANO, A., WEIRAUCH, M. T., LEININGER, S., YANG, A., TORRUELLA, G., ADAMSKI, M., ADAMSKA, M., HUGHES, T. R., GOMEZ-SKARMETA, J. L. & RUIZ-TRILLO, I. 2013. Early evolution of the T-box transcription factor family. *Proc Natl Acad Sci U S A,* 110**,** 16050-5.

SEMRAU, S. & VAN OUDENAARDEN, A. 2015. Studying Lineage Decision-Making In Vitro: Emerging Concepts and Novel Tools. *Annual review of cell and developmental biology,* 31**,** 317-345.

SERNEELS, L., DEJAEGERE, T., CRAESSAERTS, K., HORRÉ, K., JORISSEN, E., TOUSSEYN, T., HÉBERT, S., COOLEN, M., MARTENS, G. & ZWIJSEN, A. 2005. Differential contribution of the three Aph1 genes to γ-secretase activity in vivo. *Proceedings of the National Academy of Sciences of the United States of America,* 102**,** 1719-1724.

SERRANO, I., MCDONALD, P. C., LOCK, F., MULLER, W. J. & DEDHAR, S. 2013. Inactivation of the Hippo tumour suppressor pathway by integrin-linked kinase. *Nature communications,* 4.

SGRO, A. E., SCHWAB, D. J., NOORBAKHSH, J., MESTLER, T., MEHTA, P. & GREGOR, T. 2015. From intracellular signaling to population oscillations: bridging size- and time-scales in collective behavior. *Mol Syst Biol,* 11**,** 779.

SHANKARAN, S. S., SIEGER, D., SCHROTER, C., CZEPE, C., PAULY, M. C., LAPLANTE, M. A., BECKER, T. S., OATES, A. C. & GAJEWSKI, M. 2007. Completing the set of h/E(spl) cyclic genes in zebrafish: her12 and her15 reveal novel modes of expression and contribute to the segmentation clock. *Dev Biol,* 304**,** 615-32.

SHARMA, R., TREMBLAY M., SHAFER M., BAREKE E., MAJEWSKI J., BOUCHARD,M. 2015. Molecular mechanisms of Presomitic mesoderm specification. *McGill Graduate Research Day*.

SHETH, R., MARCON, L., BASTIDA, M. F., JUNCO, M., QUINTANA, L., DAHN, R., KMITA, M., SHARPE, J. & ROS, M. A. 2012. Hox genes regulate digit patterning by controlling the wavelength of a Turing-type mechanism. *Science,* 338**,** 1476-80.

SHI, S. & STANLEY, P. 2003. Protein O-fucosyltransferase 1 is an essential component of Notch signaling pathways. *Proceedings of the National Academy of Sciences,* 100**,** 5234-5239.

SHI, Z. & BARNA, M. 2015. Translating the genome in time and space: specialized ribosomes, RNA regulons, and RNA-binding proteins. *Annual review of cell and developmental biology,* 31**,** 31-54.

SHIFLEY, E. T., VANHORN, K. M., PEREZ-BALAGUER, A., FRANKLIN, J. D., WEINSTEIN, M. & COLE, S. E. 2008. Oscillatory lunatic fringe activity is crucial for segmentation of the anterior but not posterior skeleton. *Development,* 135**,** 899-908.

SHIH, N. P., FRANÇOIS, P., DELAUNE, E. A. & AMACHER, S. L. 2015. Dynamics of the slowing segmentation clock reveal alternating two-segment periodicity. *Development,* 142**,** 1785-1793.

SHIMADA, A., DOHKE, K., SADAIE, M., SHINMYOZU, K., NAKAYAMA, J., URANO, T. & MURAKAMI, Y. 2009. Phosphorylation of Swi6/HP1 regulates transcriptional gene silencing at heterochromatin. *Genes Dev,* 23**,** 18-23.

SHIMOJO, H., ISOMURA, A., OHTSUKA, T., KORI, H., MIYACHI, H. & KAGEYAMA, R. 2016. Oscillatory control of Delta-like1 in cell interactions regulates dynamic gene expression and tissue morphogenesis. *Genes Dev,* 30**,** 102-16.

SHIMOJO, H. & KAGEYAMA, R. 2016. Oscillatory control of Delta-like1 in somitogenesis and neurogenesis: A unified model for different oscillatory dynamics. *Semin Cell Dev Biol,* 49**,** 76-82.

SHIMOJO, H., OHTSUKA, T. & KAGEYAMA, R. 2008. Oscillations in notch signaling regulate maintenance of neural progenitors. *Neuron,* 58**,** 52-64.

SHIMOZONO, S., IIMURA, T., KITAGUCHI, T., HIGASHIJIMA, S. & MIYAWAKI, A. 2013. Visualization of an endogenous retinoic acid gradient across embryonic development. *Nature,* 496**,** 363-6.

SHIOGAI, Y. & KURAMOTO, Y. 2003. Wave propagation in nonlocally coupled oscillators with noise. *Progress of Theoretical Physics Supplement,* 150**,** 435-438.

SICK, S., REINKER, S., TIMMER, J. & SCHLAKE, T. 2006. WNT and DKK determine hair follicle spacing through a reaction-diffusion mechanism. *Science,* 314**,** 1447-50.

SIGNER, R. A., MAGEE, J. A., SALIC, A. & MORRISON, S. J. 2014. Haematopoietic stem cells require a highly regulated protein synthesis rate. *Nature,* 509**,** 49-54.

SILVA, J., BARRANDON, O., NICHOLS, J., KAWAGUCHI, J., THEUNISSEN, T. W. & SMITH, A. 2008. Promotion of reprogramming to ground state pluripotency by signal inhibition. *PLoS Biol,* 6**,** e253.

SIRBU, I. O. & DUESTER, G. 2006. Retinoic-acid signalling in node ectoderm and posterior neural plate directs left-right patterning of somitic mesoderm. *Nat Cell Biol,* 8**,** 271-7.

SONNEN, K. F. & AULEHLA, A. 2014. Dynamic signal encoding-From cells to organisms. *Semin Cell Dev Biol.*

SOROLDONI, D., JORG, D. J., MORELLI, L. G., RICHMOND, D. L., SCHINDELIN, J., JULICHER, F. & OATES, A. C. 2014. Genetic oscillations. A Doppler effect in embryonic pattern formation. *Science,* 345**,** 222-5.

SORRE, B., WARMFLASH, A., BRIVANLOU, A. H. & SIGGIA, E. D. 2014. Encoding of temporal signals by the TGF-β pathway and implications for embryonic patterning. *Developmental cell,* 30**,** 334-342.

SORRENTINO, G., RUGGERI, N., SPECCHIA, V., CORDENONSI, M., MANO, M., DUPONT, S., MANFRIN, A., INGALLINA, E., SOMMAGGIO, R. & PIAZZA, S. 2014. Metabolic control of YAP and TAZ by the mevalonate pathway. *Nature cell biology,* 16**,** 357-366.

SOZA-RIED, C., OZTURK, E., ISH-HOROWICZ, D. & LEWIS, J. 2014. Pulses of Notch activation synchronise oscillating somite cells and entrain the zebrafish segmentation clock. *Development,* 141**,** 1780-1788.

SPARROW, D. B., CHAPMAN, G., TURNPENNY, P. D. & DUNWOODIE, S. L. 2007. Disruption of the somitic molecular clock causes abnormal vertebral segmentation. *Birth Defects Res C Embryo Today,* 81**,** 93-110.

STAFFORD, D. A., MONICA, S. D. & HARLAND, R. M. 2014. Follistatin interacts with Noggin in the development of the axial skeleton. *Mech Dev,* 131**,** 78-85.

STAUBER, M., LACLEF, C., VEZZARO, A., PAGE, M. E. & ISH-HOROWICZ, D. 2012. Modifying transcript lengths of cycling mouse segmentation genes. *Mech Dev,* 129**,** 61-72.

STAUBER, M., SACHIDANANDAN, C., MORGENSTERN, C. & ISH-HOROWICZ, D. 2009. Differential axial requirements for lunatic fringe and Hes7 transcription during mouse somitogenesis. *PLoS One,* 4**,** e7996.

STEPHENSON, R. O., ROSSANT, J. & TAM, P. P. 2012. Intercellular interactions, position, and polarity in establishing blastocyst cell lineages and embryonic axes. *Cold Spring Harb Perspect Biol,* 4.

STERN, C. D., FRASER, S. E., KEYNES, R. J. & PRIMMETT, D. R. 1988. A cell lineage analysis of segmentation in the chick embryo. *Development,* 104**,** 231-244.

STERN, C. D. & PIATKOWSKA, A. M. 2015. Multiple roles of timing in somite formation. *Semin Cell Dev Biol,* 42**,** 134-9.

STICH, M. 2003. *Target patterns and pacemakers in reaction-diffusion systems.* Technische Universität Berlin.

STICH, M. & MIKHAILOV, A. S. 2006. Target patterns in two-dimensional heterogeneous oscillatory reaction–diffusion systems. *Physica D: Nonlinear Phenomena,* 215**,** 38-45.

STICH, M., MIKHAILOV, A. S. & KURAMOTO, Y. 2009. Self-organized pacemakers and bistability of pulses in an excitable medium. *Physical Review E,* 79**,** 026110.

STOLLEWERK, A., SCHOPPMEIER, M. & DAMEN, W. G. 2003. Involvement of Notch and Delta genes in spider segmentation. *Nature,* 423**,** 863-865.

STROGATZ, S. H. 2003. *Sync : the emerging science of spontaneous order,* New York, Hyperion.

SUDHEER, S., LIU, J., MARKS, M., KOCH, F., ANURIN, A., SCHOLZE, M., DOROTHEA SENFT, A., WITTLER, L., MACURA, K., GROTE, P. & HERRMANN, B. G. 2016. Different Concentrations of FGF Ligands, FGF2 or FGF8 Determine Distinct States of WNT-Induced Presomitic Mesoderm. *Stem Cells.*

SUN, X., MEYERS, E. N., LEWANDOSKI, M. & MARTIN, G. R. 1999. Targeted disruption of Fgf8 causes failure of cell migration in the gastrulating mouse embryo. *Genes Dev,* 13**,** 1834-46.

SURIBEN, R., FISHER, D. A. & CHEYETTE, B. N. 2006. Dact1 presomitic mesoderm expression oscillates in phase with Axin2 in the somitogenesis clock of mice. *Dev Dyn,* 235**,** 3177-83.

SURIBEN, R., KIVIMAE, S., FISHER, D. A., MOON, R. T. & CHEYETTE, B. N. 2009. Posterior malformations in Dact1 mutant mice arise through misregulated Vangl2 at the primitive streak. *Nat Genet,* 41**,** 977-85.

SWIATEK, P. J., LINDSELL, C. E., DEL AMO, F. F., WEINMASTER, G. & GRIDLEY, T. 1994. Notch1 is essential for postimplantation development in mice. *Genes Dev,* 8**,** 707-19.

SWIECICKI, J. M., BARTSCH, A., TAILHADES, J., DI PISA, M., HELLER, B., CHASSAING, G., MANSUY, C., BURLINA, F. & LAVIELLE, S. 2014. The Efficacies of Cell-Penetrating Peptides in Accumulating in Large Unilamellar Vesicles Depend on their Ability To Form Inverted Micelles. *ChemBioChem,* 15**,** 884-891.

TAKADA, S., STARK, K. L., SHEA, M. J., VASSILEVA, G., MCMAHON, J. A. & MCMAHON, A. P. 1994. Wnt-3a regulates somite and tailbud formation in the mouse embryo. *Genes Dev,* 8**,** 174-89.

TAKAHASHI, J., OHBAYASHI, A., OGINUMA, M., SAITO, D., MOCHIZUKI, A., SAGA, Y. & TAKADA, S. 2010. Analysis of Ripply1/2-deficient mouse embryos reveals a mechanism underlying the rostro-caudal patterning within a somite. *Dev Biol,* 342**,** 134-45.

TAKAHASHI, Y., HIRAOKA, S., KITAJIMA, S., INOUE, T., KANNO, J. & SAGA, Y. 2005. Differential contributions of Mesp1 and Mesp2 to the epithelialization and rostro-caudal patterning of somites. *Development,* 132**,** 787-96.

TAKAHASHI, Y., INOUE, T., GOSSLER, A. & SAGA, Y. 2003. Feedback loops comprising Dll1, Dll3 and Mesp2, and differential involvement of Psen1 are essential for rostrocaudal patterning of somites. *Development,* 130**,** 4259-68.

TAKAHASHI, Y., KOIZUMI, K., TAKAGI, A., KITAJIMA, S., INOUE, T., KOSEKI, H. & SAGA, Y. 2000. Mesp2 initiates somite segmentation through the Notch signalling pathway. *Nat Genet,* 25**,** 390-6.

TAKAHASHI, Y., TAKAGI, A., HIRAOKA, S., KOSEKI, H., KANNO, J., RAWLS, A. & SAGA, Y. 2007. Transcription factors Mesp2 and Paraxis have critical roles in axial musculoskeletal formation. *Dev Dyn,* 236**,** 1484-94.

TAKAHASHI, Y., YASUHIKO, Y., TAKAHASHI, J., TAKADA, S., JOHNSON, R. L., SAGA, Y. & KANNO, J. 2013. Metameric pattern of intervertebral disc/vertebral body is generated independently of Mesp2/Ripply-mediated rostro-caudal patterning of somites in the mouse embryo. *Dev Biol,* 380**,** 172-84.

TAKAOKA, K., YAMAMOTO, M. & HAMADA, H. 2011. Origin and role of distal visceral endoderm, a group of cells that determines anterior-posterior polarity of the mouse embryo. *Nat Cell Biol,* 13**,** 743-52.

TAKASHIMA, Y., OHTSUKA, T., GONZALEZ, A., MIYACHI, H. & KAGEYAMA, R. 2011. Intronic delay is essential for oscillatory expression in the segmentation clock. *Proc Natl Acad Sci U S A,* 108**,** 3300-5.

TAKEBAYASHI, K., SASAI, Y., SAKAI, Y., WATANABE, T., NAKANISHI, S. & KAGEYAMA, R. 1994. Structure, chromosomal locus, and promoter analysis of the gene encoding the mouse helix-loop-helix factor HES-1. Negative autoregulation through the multiple N box elements. *J Biol Chem,* 269**,** 5150-6.

TAKEMOTO, T., UCHIKAWA, M., KAMACHI, Y. & KONDOH, H. 2006. Convergence of Wnt and FGF signals in the genesis of posterior neural plate through activation of the Sox2 enhancer N-1. *Development,* 133**,** 297-306.

TAKEMOTO, T., UCHIKAWA, M., YOSHIDA, M., BELL, D. M., LOVELL-BADGE, R., PAPAIOANNOU, V. E. & KONDOH, H. 2011. Tbx6-dependent Sox2 regulation determines neural or mesodermal fate in axial stem cells. *Nature,* 470**,** 394-8.

TAKETOMI, T., YOSHIGA, D., TANIGUCHI, K., KOBAYASHI, T., NONAMI, A., KATO, R., SASAKI, M., SASAKI, A., ISHIBASHI, H., MORIYAMA, M., NAKAMURA, K., NISHIMURA, J. & YOSHIMURA, A. 2005. Loss of mammalian Sprouty2 leads to enteric neuronal hyperplasia and esophageal achalasia. *Nat Neurosci,* 8**,** 855-7.

TAM, P. P. 1981. The control of somitogenesis in mouse embryos. *J Embryol Exp Morphol,* 65 Suppl**,** 103-28.

TANAKA, M., JOKUBAITIS, V., WOOD, C., WANG, Y., BROUARD, N., PERA, M., HEARN, M., SIMMONS, P. & NAKAYAMA, N. 2009. BMP inhibition stimulates WNT-dependent generation of chondrogenic mesoderm from embryonic stem cells. *Stem Cell Res,* 3**,** 126-41.

TANIGUCHI, K., AYADA, T., ICHIYAMA, K., KOHNO, R., YONEMITSU, Y., MINAMI, Y., KIKUCHI, A., MAEHARA, Y. & YOSHIMURA, A. 2007. Sprouty2 and Sprouty4 are essential for embryonic morphogenesis and regulation of FGF signaling. *Biochem Biophys Res Commun,* 352**,** 896-902.

TASSY, O. & POURQUIÉ, O. 2013. Manteia, a predictive data mining system for vertebrate genes and its applications to human genetic diseases. *Nucleic acids research***,** gkt807.

TEN TUSSCHER, K. 2013. Mechanisms and constraints shaping the evolution of body plan segmentation. *The European Physical Journal E,* 36**,** 1-12.

TEN TUSSCHER, K. H. & HOGEWEG, P. 2011. Evolution of networks for body plan patterning; interplay of modularity, robustness and evolvability. *PLoS Comput Biol,* 7**,** e1002208.

TENIN, G., WRIGHT, D., FERJENTSIK, Z., BONE, R., MCGREW, M. J. & MAROTO, M. 2010. The chick somitogenesis oscillator is arrested before all paraxial mesoderm is segmented into somites. *BMC Dev Biol,* 10**,** 24.

THOMSON, M., LIU, S. J., ZOU, L. N., SMITH, Z., MEISSNER, A. & RAMANATHAN, S. 2011. Pluripotency factors in embryonic stem cells regulate differentiation into germ layers. *Cell,* 145**,** 875-89.

TIEDEMANN, H. B., SCHNELTZER, E., ZEISER, S., WURST, W., BECKERS, J., PRZEMECK, G. K. & HRABE DE ANGELIS, M. 2014. Fast synchronization of ultradian oscillators controlled by delta-notch signaling with cis-inhibition. *PLoS Comput Biol,* 10**,** e1003843.

TITMARSH, D. M., CHEN, H., WOLVETANG, E. J. & COOPER-WHITE, J. J. 2013. Arrayed cellular environments for stem cells and regenerative medicine. *Biotechnology journal,* 8**,** 167-179.

TONEGAWA, A., FUNAYAMA, N., UENO, N. & TAKAHASHI, Y. 1997. Mesodermal subdivision along the mediolateral axis in chicken controlled by different concentrations of BMP-4. *Development,* 124**,** 1975-84.

TONEGAWA, A. & TAKAHASHI, Y. 1998. Somitogenesis controlled by Noggin. *Dev Biol,* 202**,** 172-82.

TOYODA, R., ASSIMACOPOULOS, S., WILCOXON, J., TAYLOR, A., FELDMAN, P., SUZUKI-HIRANO, A., SHIMOGORI, T. & GROVE, E. A. 2010. FGF8 acts as a classic diffusible morphogen to pattern the neocortex. *Development,* 137**,** 3439-3448.

TROFKA, A., SCHWENDINGER-SCHRECK, J., BREND, T., PONTIUS, W., EMONET, T. & HOLLEY, S. A. 2012. The Her7 node modulates the network topology of the zebrafish segmentation clock via sequestration of the Hes6 hub. *Development,* 139**,** 940-7.

TSIAIRIS, C. D. & AULEHLA, A. 2016. Self-Organization of Embryonic Genetic Oscillators into Spatiotemporal Wave Patterns. *Cell,* 164**,** 656-67.

TU, B. P. & MCKNIGHT, S. L. 2006. Metabolic cycles as an underlying basis of biological oscillations. *Nature reviews Molecular cell biology,* 7**,** 696-701.

TUFCEA, D. E. & FRANÇOIS, P. 2015. Critical Timing without a Timer for Embryonic Development. *Biophysical journal,* 109**,** 1724-1734.

TURING, A. M. 1952. The Chemical Basis of Morphogenesis. *Philosophical Transactions of the Royal Society of London,* 641**,** 37-72.

TURNER, D. A., BAILLIE-JOHNSON, P. & MARTINEZ ARIAS, A. 2016. Organoids and the genetically encoded self-assembly of embryonic stem cells. *Bioessays,* 38**,** 181-91.

TURNER, D. A., HAYWARD, P. C., BAILLIE-JOHNSON, P., RUE, P., BROOME, R., FAUNES, F. & MARTINEZ ARIAS, A. 2014a. Wnt/beta-catenin and FGF signalling direct the specification and maintenance of a neuromesodermal axial progenitor in ensembles of mouse embryonic stem cells. *Development,* 141**,** 4243-53.

TURNER, D. A., TROTT, J., HAYWARD, P., RUE, P. & MARTINEZ ARIAS, A. 2014b. An interplay between extracellular signalling and the dynamics of the exit from pluripotency drives cell fate decisions in mouse ES cells. *Biol Open,* 3**,** 614-26.

TZOUANACOU, E., WEGENER, A., WYMEERSCH, F. J., WILSON, V. & NICOLAS, J. F. 2009. Redefining the progression of lineage segregations during mammalian embryogenesis by clonal analysis. *Dev Cell,* 17**,** 365-76.

UEDA, T., WATANABE-FUKUNAGA, R., FUKUYAMA, H., NAGATA, S. & FUKUNAGA, R. 2004. Mnk2 and Mnk1 are essential for constitutive and inducible phosphorylation of eukaryotic initiation factor 4E but not for cell growth or development. *Molecular and cellular biology,* 24**,** 6539-6549.

UMEDA, K., ZHAO, J., SIMMONS, P., STANLEY, E., ELEFANTY, A. & NAKAYAMA, N. 2012. Human chondrogenic paraxial mesoderm, directed specification and prospective isolation from pluripotent stem cells. *Sci Rep,* 2**,** 455.

UOSAKI, H., CAHAN, P., LEE, D. I., WANG, S., MIYAMOTO, M., FERNANDEZ, L., KASS, D. A. & KWON, C. 2015. Transcriptional Landscape of Cardiomyocyte Maturation. *Cell reports,* 13**,** 1705-1716.

URIU, K., MORISHITA, Y. & IWASA, Y. 2010. Random cell movement promotes synchronization of the segmentation clock. *Proc Natl Acad Sci U S A,* 107**,** 4979-84.

VALENTIN, G. & OATES, A. C. 2013. Opening a can of centipedes: new insights into mechanisms of body segmentation. *BMC Biol,* 11**,** 116.

VAN DEN BRINK, S. C., BAILLIE-JOHNSON, P., BALAYO, T., HADJANTONAKIS, A.-K., NOWOTSCHIN, S., TURNER, D. A. & ARIAS, A. M. 2014. Symmetry breaking, germ layer specification and axial organisation in aggregates of mouse embryonic stem cells. *Development,* 141**,** 4231-4242.

VARELAS, X., SAMAVARCHI-TEHRANI, P., NARIMATSU, M., WEISS, A., COCKBURN, K., LARSEN, B. G., ROSSANT, J. & WRANA, J. L. 2010. The Crumbs complex couples cell density sensing to Hippo-dependent control of the TGF-β-SMAD pathway. *Developmental cell,* 19**,** 831-844.

VERMOT, J., GALLEGO LLAMAS, J., FRAULOB, V., NIEDERREITHER, K., CHAMBON, P. & DOLLE, P. 2005. Retinoic acid controls the bilateral symmetry of somite formation in the mouse embryo. *Science,* 308**,** 563-6.

VERMOT, J. & POURQUIÉ, O. 2005. Retinoic acid coordinates somitogenesis and left-right patterning in vertebrate embryos. *Nature,* 435**,** 215-20.

VILHAIS-NETO, G. C., MARUHASHI, M., SMITH, K. T., VASSEUR-COGNET, M., PETERSON, A. S., WORKMAN, J. L. & POURQUIE, O. 2010. Rere controls retinoic acid signalling and somite bilateral symmetry. *Nature,* 463**,** 953-7.

VINCENT, S. D., DUNN, N. R., HAYASHI, S., NORRIS, D. P. & ROBERTSON, E. J. 2003. Cell fate decisions within the mouse organizer are governed by graded Nodal signals. *Genes Dev,* 17**,** 1646-62.

VOON, D. C., SUBRATA, L. S., BALTIC, S., LEU, M. P., WHITEWAY, J. M., WONG, A., KNIGHT, S. A., CHRISTIANSEN, F. T. & DALY, J. M. 2005. Use of mRNA-and protein-destabilizing elements to develop a highly responsive reporter system. *Nucleic acids research,* 33**,** e27-e27.

WAHL, M. B., DENG, C., LEWANDOSKI, M. & POURQUIÉ, O. 2007. FGF signaling acts upstream of the NOTCH and WNT signaling pathways to control segmentation clock oscillations in mouse somitogenesis. *Development,* 134**,** 4033-41.

WANG, H., YANG, H., SHIVALILA, C. S., DAWLATY, M. M., CHENG, A. W., ZHANG, F. & JAENISCH, R. 2013. One-step generation of mice carrying mutations in multiple genes by CRISPR/Cas-mediated genome engineering. *Cell,* 153**,** 910-918.

WANG, J. H. & DING, X. Y. 2006. Cloning and analyzing of Xenopus Mespo promoter in retinoic acid regulated Mespo expression. *Acta biochimica et biophysica Sinica,* 38**,** 759-764.

WANGLAR, C., TAKAHASHI, J., YABE, T. & TAKADA, S. 2014. Tbx protein level critical for clock-mediated somite positioning is regulated through interaction between Tbx and Ripply. *PLoS One,* 9**,** e107928.

WARD, A. B. & MEHTA, R. S. 2010. Axial elongation in fishes: using morphological approaches to elucidate developmental mechanisms in studying body shape. *Integr Comp Biol,* 50**,** 1106-19.

WARTLICK, O., KICHEVA, A. & GONZALEZ-GAITAN, M. 2009. Morphogen gradient formation. *Cold Spring Harb Perspect Biol,* 1**,** a001255.

WARTLICK, O., MUMCU, P., KICHEVA, A., BITTIG, T., SEUM, C., JULICHER, F. & GONZALEZ-GAITAN, M. 2011. Dynamics of Dpp signaling and proliferation control. *Science,* 331**,** 1154-9.

WATANABE, T., SATO, Y., SAITO, D., TADOKORO, R. & TAKAHASHI, Y. 2009. EphrinB2 coordinates the formation of a morphological boundary and cell epithelialization during somite segmentation. *Proc Natl Acad Sci U S A,* 106**,** 7467-72.

WEBB, A. B., LENGYEL, I. M., JORG, D. J., VALENTIN, G., JULICHER, F., MORELLI, L. G. & OATES, A. C. 2016. Persistence, period and precision of autonomous cellular oscillators from the zebrafish segmentation clock. *Elife,* 5.

WEBB, A. B. & OATES, A. C. 2016. Timing by rhythms: Daily clocks and developmental rulers. *Dev Growth Differ,* 58**,** 43-58.

WEBB, A. B., SOROLDONI, D., OSWALD, A., SCHINDELIN, J. & OATES, A. C. 2014. Generation of dispersed presomitic mesoderm cell cultures for imaging of the zebrafish segmentation clock in single cells. *J Vis Exp*.

WEHN, A. K. & CHAPMAN, D. L. 2010. Tbx18 and Tbx15 null-like phenotypes in mouse embryos expressing Tbx6 in somitic and lateral plate mesoderm. *Dev Biol,* 347**,** 404-13.

WENNEKAMP, S., MESECKE, S., NEDELEC, F. & HIIRAGI, T. 2013. A self-organization framework for symmetry breaking in the mammalian embryo. *Nat Rev Mol Cell Biol,* 14**,** 452-9.

WIEDERMANN, G., BONE, R. A., SILVA, J. C., BJORKLUND, M., MURRAY, P. J. & DALE, J. K. 2015. A balance of positive and negative regulators determines the pace of the segmentation clock. *Elife,* 4**,** e05842.

WILLIAM, D. A., SAITTA, B., GIBSON, J. D., TRAAS, J., MARKOV, V., GONZALEZ, D. M., SEWELL, W., ANDERSON, D. M., PRATT, S. C., RAPPAPORT, E. F. & KUSUMI, K. 2007. Identification of oscillatory genes in somitogenesis from functional genomic analysis of a human mesenchymal stem cell model. *Dev Biol,* 305**,** 172-86.

WILLIAMS, D. R., SHIFLEY, E. T., BRAUNREITER, K. M. & COLE, S. E. 2016. A novel targeted Lunatic fringe allele predicted to reduce protein secretion is dominant and disrupts somitogenesis. *Development***,** dev. 128538.

WILLIAMS, L. H., FROMM, G., GOKEY, N. G., HENRIQUES, T., MUSE, G. W., BURKHOLDER, A., FARGO, D. C., HU, G. & ADELMAN, K. 2015. Pausing of RNA polymerase II regulates mammalian developmental potential through control of signaling networks. *Molecular cell,* 58**,** 311-322.

WILSON, V. & BEDDINGTON, R. 1997. Expression of T protein in the primitive streak is necessary and sufficient for posterior mesoderm movement and somite differentiation. *Dev Biol,* 192**,** 45-58.

WILSON, V. & BEDDINGTON, R. S. 1996. Cell fate and morphogenetic movement in the late mouse primitive streak. *Mech Dev,* 55**,** 79-89.

WILSON, V., RASHBASS, P. & BEDDINGTON, R. S. 1993. Chimeric analysis of T (Brachyury) gene function. *Development,* 117**,** 1321-31.

WINDNER, S. E., DORIS, R. A., FERGUSON, C. M., NELSON, A. C., VALENTIN, G., TAN, H., OATES, A. C., WARDLE, F. C. & DEVOTO, S. H. 2015. Tbx6, Mesp-b and Ripply1 regulate the onset of skeletal myogenesis in zebrafish. *Development,* 142**,** 1159-68.

WINFREE, A. T. 2001. *The geometry of biological time,* New York, Springer.

WITTLER, L., SHIN, E. H., GROTE, P., KISPERT, A., BECKERS, A., GOSSLER, A., WERBER, M. & HERRMANN, B. G. 2007. Expression of Msgn1 in the presomitic mesoderm is controlled by synergism of WNT signalling and Tbx6. *EMBO Rep,* 8**,** 784-9.

WOLPERT, L. 1969. Positional information and the spatial pattern of cellular differentiation. *J Theor Biol,* 25**,** 1-47.

WRIGHT, D., FERJENTSIK, Z., CHONG, S. W., QIU, X., JIANG, Y. J., MALAPERT, P., POURQUIE, O., VAN HATEREN, N., WILSON, S. A., FRANCO, C., GERHARDT, H., DALE, J. K. & MAROTO, M. 2009. Cyclic Nrarp mRNA expression is regulated by the somitic oscillator but Nrarp protein levels do not oscillate. *Dev Dyn,* 238**,** 3043-55.

WYMEERSCH, F. J., HUANG, Y., BLIN, G., CAMBRAY, N., WILKIE, R., WONG, F. C. & WILSON, V. 2016. Position-dependent plasticity of distinct progenitor types in the primitive streak. *Elife,* 5.

XUE, Y., GAO, X., LINDSELL, C. E., NORTON, C. R., CHANG, B., HICKS, C., GENDRON-MAGUIRE, M., RAND, E. B., WEINMASTER, G. & GRIDLEY, T. 1999. Embryonic lethality and vascular defects in mice lacking the Notch ligand Jagged1. *Human molecular genetics,* 8**,** 723-730.

YABE, T. & TAKADA, S. 2012. Mesogenin causes embryonic mesoderm progenitors to differentiate during development of zebrafish tail somites. *Dev Biol,* 370**,** 213-22.

YAMAGUCHI, T. P., TAKADA, S., YOSHIKAWA, Y., WU, N. & MCMAHON, A. P. 1999. T (Brachyury) is a direct target of Wnt3a during paraxial mesoderm specification. *Genes Dev,* 13**,** 3185-90.

YAMAMOTO, A., AMACHER, S. L., KIM, S. H., GEISSERT, D., KIMMEL, C. B. & DE ROBERTIS, E. M. 1998. Zebrafish paraxial protocadherin is a downstream target of spadetail involved in morphogenesis of gastrula mesoderm. *Development,* 125**,** 3389-97.

YAMAMOTO, A., KEMP, C., BACHILLER, D., GEISSERT, D. & DE ROBERTIS, E. M. 2000. Mouse paraxial protocadherin is expressed in trunk mesoderm and is not essential for mouse development. *Genesis,* 27**,** 49-57.

YANAGISAWA, K. O., FUJIMOTO, H. & URUSHIHARA, H. 1981. Effects of the brachyury (T) mutation on morphogenetic movement in the mouse embryo. *Dev Biol,* 87**,** 242-8.

YASUHIKO, Y., HARAGUCHI, S., KITAJIMA, S., TAKAHASHI, Y., KANNO, J. & SAGA, Y. 2006. Tbx6-mediated Notch signaling controls somite-specific Mesp2 expression. *Proc Natl Acad Sci U S A,* 103, 3651-6.

YASUHIKO, Y., KITAJIMA, S., TAKAHASHI, Y., OGINUMA, M., KAGIWADA, H., KANNO, J. & SAGA, Y. 2008. Functional importance of evolutionarily conserved Tbx6 binding sites in the presomitic mesoderm-specific enhancer of Mesp2. *Development,* 135, 3511-9.

YASUO, H., KOBAYASHI, M., SHIMAUCHI, Y. & SATOH, N. 1996. The ascidian genome contains another T-domain gene that is expressed in differentiating muscle and the tip of the tail of the embryo. *Dev Biol,* 180, 773-9.

YING, Q. L., WRAY, J., NICHOLS, J., BATLLE-MORERA, L., DOBLE, B., WOODGETT, J., COHEN, P. & SMITH, A. 2008. The ground state of embryonic stem cell self-renewal. *Nature,* 453, 519-23.

YOON, J. K. & WOLD, B. 2000. The bHLH regulator pMesogenin1 is required for maturation and segmentation of paraxial mesoderm. *Genes Dev,* 14, 3204-14.

YOSHIKAWA, Y., FUJIMORI, T., MCMAHON, A. P. & TAKADA, S. 1997. Evidence that absence of Wnt-3a signaling promotes neuralization instead of paraxial mesoderm development in the mouse. *Dev Biol,* 183, 234-42.

YOUNG, T., ROWLAND, J. E., VAN DE VEN, C., BIALECKA, M., NOVOA, A., CARAPUCO, M., VAN NES, J., DE GRAAFF, W., DULUC, I., FREUND, J. N., BECK, F., MALLO, M. & DESCHAMPS, J. 2009. Cdx and Hox genes differentially regulate posterior axial growth in mammalian embryos. *Dev Cell,* 17, 516-26.

YU, H. M., JERCHOW, B., SHEU, T. J., LIU, B., COSTANTINI, F., PUZAS, J. E., BIRCHMEIER, W. & HSU, W. 2005. The role of Axin2 in calvarial morphogenesis and craniosynostosis. *Development,* 132, 1995-2005.

YU, S. R., BURKHARDT, M., NOWAK, M., RIES, J., PETRASEK, Z., SCHOLPP, S., SCHWILLE, P. & BRAND, M. 2009. Fgf8 morphogen gradient forms by a source-sink mechanism with freely diffusing molecules. *Nature,* 461, 533-6.

ZÁKÁNY, J., KMITA, M., ALARCON, P., DE LA POMPA, J.-L. & DUBOULE, D. 2001. Localized and transient transcription of Hox genes suggests a link between patterning and the segmentation clock. *Cell,* 106, 207-217.

ZHANG, L., KENDRICK, C., JULICH, D. & HOLLEY, S. A. 2008. Cell cycle progression is required for zebrafish somite morphogenesis but not segmentation clock function. *Development,* 135, 2065-70.

ZHANG, N. & GRIDLEY, T. 1998. Defects in somite formation in lunatic fringe-deficient mice. *Nature,* 394, 374-7.

ZHANG, P., MCGRATH, B., LI, S. A., FRANK, A., ZAMBITO, F., REINERT, J., GANNON, M., MA, K., MCNAUGHTON, K. & CAVENER, D. R. 2002a. The PERK eukaryotic initiation factor 2α kinase is required for the development of the skeletal system, postnatal growth, and the function and viability of the pancreas. *Molecular and cellular biology,* 22, 3864-3874.

ZHANG, P., MCGRATH, B. C., REINERT, J., OLSEN, D. S., LEI, L., GILL, S., WEK, S. A., VATTEM, K. M., WEK, R. C. & KIMBALL, S. R. 2002b. The GCN2 eIF2α kinase is required for adaptation to amino acid deprivation in mice. *Molecular and Cellular Biology,* 22, 6681-6688.

ZHANG, Z., O'ROURKE, J. R., MCMANUS, M. T., LEWANDOSKI, M., HARFE, B. D. & SUN, X. 2011. The microRNA-processing enzyme Dicer is dispensable for somite segmentation but essential for limb bud positioning. *Dev Biol,* 351, 254-65.

ZHAO, B., LI, L., LEI, Q. & GUAN, K.-L. 2010. The Hippo–YAP pathway in organ size control and tumorigenesis: An updated version. *Genes & development,* 24, 862-874.

ZHAO, B., LI, L., WANG, L., WANG, C.-Y., YU, J. & GUAN, K.-L. 2012. Cell detachment activates the Hippo pathway via cytoskeleton reorganization to induce anoikis. *Genes & development,* 26, 54-68.

ZISMANOV, V., CHICHKOV, V., COLANGELO, V., JAMET, S., WANG, S., SYME, A., KOROMILAS, A. E. & CRIST, C. 2016. Phosphorylation of eIF2α Is a Translational Control Mechanism Regulating Muscle Stem Cell Quiescence and Self-Renewal. *Cell stem cell,* 18, 79-90.

Alexis HUBAUD

Dynamique de la signalisation cellulaire au cours de la segmentation des Vertébrés

Résumé

Une caractéristique majeure des Vertébrés est leur segmentation le long de l'axe antéro-postérieur, comme le montre la colonne vertébrale. Cette disposition sériée a d'importantes conséquences sur l'organisation du corps adulte et sa locomotion. Elle est la conséquence de la somitogénèse, un processus embryonnaire par lequel le mésoderme paraxial devient progressivement segmenté en blocs épithéliaux appelés somites. En effet, une nouvelle paire de somites est formée à intervalle de temps régulier et se différencie ultérieurement en plusieurs types cellulaires. De fait, la segmentation du mésoderme présomitique sert de plan pour l'organisation finale du squelette axial. Ce processus est basé sur un oscillateur moléculaire, appelée l' « horloge de segmentation », qui consiste en une activation périodique d'un ensemble de gènes et de voies de signalisation cellulaire. Cet oscillateur sous-tend la périodicité de la somitogénèse, alors que des gradients de signalisation le long du mésoderme présomitique confinent spatialement la détermination en segments.

Au cours de cette thèse, nous avons cherché à comprendre le contrôle moléculaire et la dynamique de signalisation qui régulent la segmentation des Vertébrés. Dans un premier temps, nous avons étudié la régulation transcriptionnelle de *Mesp2*, un facteur central du programme de segmentation et nous avons montré que le facteur de transcription Tbx6 contrôle son expression chez le poulet. Par la suite, nous présentons un système d'étude *ex vivo* de l'horloge de segmentation chez la souris basée sur un rapporteur fluorescent pour le gène cyclique *Lunatic Fringe*. Ce système d'explants présente des oscillations stables du rapporteur, qui nous permet de mieux visualiser et contrôler ce processus oscillatoire. En nous appuyant sur cet outil, nous avons pu identifier des conditions requises pour l'émergence d'oscillations chez la souris. En particulier, nous avons mis en évidence une nécessité de contacts intercellulaires et de la voie Notch, que l'on peut interpréter dans le cadre d'un système excitable. Nous montrons par la suite que des facteurs mécaniques peuvent contrôler cette transition vers un état oscillant et peut changer le système dans un état auto-entretenu, où la signalisation Notch n'est plus requise. Nous comparons nos résultats à d'autres systèmes expérimentaux et proposons de synthétiser ces observations dans le cadre d'un système excitable. De plus, nous avons été en mesure de contrôler la différenciation de notre système par répression de la voie Fgf. Nous avons observé un effet dose-dépendant qui est difficilement interprétable dans le cadre du modèle actuel de segmentation (« horloge et front de détermination »). Nous discutons les implications de ces résultats à la lumière de modèles alternatifs de segmentation. Par ailleurs, ce système d'étude *ex vivo* nous a permis d'identifier un rôle du taux de traduction protéique dans le contrôle de la période de l'horloge de segmentation. Enfin, nous présentons des travaux en cours, où nous cherchons à reconstituer l'horloge de segmentation *in vitro* à partir de cellules souches murines différenciées. Cela nous permettrait de disposer d'un outil puissant pour l'étude ce processus *in vitro*, mais également de mieux comprendre l'établissement de l'horloge de segmentation en la recréant.

Mots-clés : segmentation des Vertébrés ; somitogénèse ; oscillations ; horloge de segmentation et front de détermination ; régionalisation embryonnaire

Alexis HUBAUD

Signaling dynamics during Vertebrate segmentation

Summary

A fundamental feature of the Vertebrate body is its segmentation along the antero-posterior axis, as evidenced by the vertebral column. Such serial arrangement has important consequences on the adult body organization and its locomotion. It originates from somitogenesis, an embryonic process by which the paraxial mesoderm becomes progressively subdivided into epithelial blocks, called somites. A new pair of segments is formed at a regular time interval and later differentiates into various cell types. Thus, the segmentation of the presomitic mesoderm serves as a blueprint to the final organization of the axial skeleton. Such process relies on a molecular oscillator, named the "segmentation clock", which consists in the periodic activation of a subset of genes and signaling pathways. This oscillator underlies the periodicity of somitogenesis, while signaling gradients along the presomitic mesoderm spatially gate the determination into segments.

Here, we aim to understand the molecular control and the signaling dynamics underlying the segmentation in Vertebrates. First, we studied the transcriptional regulation of *Mesp2*, a master regulator of the segmental program, and we show that the transcription factor Tbx6 controls the onset of its expression in chicken. Then, we present a new *ex vivo* system to study the segmentation clock in mouse based on a fluorescent reporter for the cyclic gene *Lunatic Fringe*. This explants system displays stable oscillations of the reporter, and thus enables us to better visualize and manipulate this oscillatory process. We took advantage of this tool to identify conditions necessary to the emergence of oscillations in mouse. Notably, we found that there is a requirement for intercellular contact and Notch signaling, which could be interpreted in terms of an excitable system. We further show that mechanical factors control this oscillatory transition and can switch the system in a self-oscillatory system, where Notch signaling is no longer required. We compare our results to other experimental systems and discuss how an excitable framework can encapsulate these different findings. Moreover, we could induce the differentiation of our system by inhibiting Fgf signaling. We observed a dose-dependent effect that is not explained by the current model of segmentation in the field ("clock-and-wavefront"). We discuss the implications of these results in the light of alternative segmentation models. Furthermore, this *ex vivo* system enabled us to identify a role of the translation rate in setting the period of the segmentation clock. Last, we present ongoing efforts to reconstitute the segmentation clock *in vitro* from differentiated mouse embryonic stem cells. This would provide a powerful tool to study this oscillatory process *in vitro*, but also a better understanding of the segmentation clock by building it.

Keywords: Vertebrate segmentation; somitogenesis; oscillations; clock-and-wavefront; embryonic patterning